# The Soralux Daylighting System: Passive Solar Illumination for Deep-Plan Building Spaces



by

Kevin W. Thuot

B.S. Mechanical Engineering
The University of Texas at Austin, 2006

SUBMITTED TO THE DEPARTMENT OF MECHANICAL ENGINEERING IN PARTIAL FULFILLMENT OF THE REQUIREMENTS FOR THE DEGREE OF

MASTER OF SCIENCE IN MECHANICAL ENGINEERING
AT THE
MASSACHUSETTS INSTITUTE OF TECHNOLOGY

JUNE 2011



Signature of Author: _____
Department of Mechanical Engineering
May 6, 2011

Certified by: _____
Marilyne Andersen
Associate Professor of Sustainable Construction Technologies
École Polytechnique Fédérale de Lausanne
Thesis Supervisor

Certified by: _____
Leon Glicksman
Professor of Building Technology & Mechanical Engineering
Thesis Supervisor

Accepted by: _____
David E. Hardt
Ralph E. and Eloise F. Cross Professor of Mechanical Engineering
Chairman, Committee on Graduate Students

# The Soralux Daylighting System: Passive Solar Illumination for Deep-Plan Building Spaces

by

Kevin W. Thuot

Submitted to the Department of Mechanical Engineering
on May 6, 2011 in Partial Fulfillment of the
Requirements for the Degree of Master of Science in
Mechanical Engineering

ABSTRACT

Daylight is a valuable resource for both energy and human health. However, this resource is often underutilized in buildings due to the difficulty of controlling the changing qualities of daylight. Deep-plan building spaces pose an especially challenging problem because traditional sidelighting strategies are only effective for workplanes adjacent to the facade. Infrequently adjusted shading systems can also limit the availability of daylight. A number of advanced daylighting systems have been developed that attempt to address these challenges with varying priorities and success.

This thesis proposes a new technology named the Soralux Daylighting System. The system is passive, requires no shading adjustments, even under direct sunlight, and works well with deep-plan spaces on the order of 8 to 15 m deep. The Soralux system presents itself as a double-glazing window unit, allowing it to be easily integrated into curtain wall facades typical of deep-plan offices in large cities. Computer simulations using the ray tracing programs Radiance and TracePro were conducted to estimate the annual performance of the system. Variables such as facade orientation, sky obstruction, and climate were evaluated for their effect on system performance. The system was found to increase light levels by a factor of 2 to 10 compared to an unshaded window at depths between 8 and 15 m from the facade.

Two physical mockups of the Soralux system were fabricated for testing. The first mockup tested was a small proof-of-concept prototype, while the second was a full-scale mockup which was installed in a Tokyo office building. The physical mockups were used to evaluate visual comfort and appearance. A monitoring campaign was also conducted for the Tokyo mockup and the measured data were compared with a Radiance model of the building space to validate the accuracy of the simulation results. The average error between simulated and measured illuminance values was 16%. Based on these results, recommendations are provided identifying which scenarios are well-suited for the system. The Soralux Daylighting System is scheduled to be permanently installed into a Tokyo office building in 2012.

Thesis Supervisor: Marilyne Andersen
Title: Associate Professor of Sustainable Construction Technologies, ÉPFL

Thesis Supervisor: Leon Glicksman
Title: Professor of Building Technology & Mechanical Engineering, MIT

# Acknowledgements

One of the things I was continually impressed by during my time at MIT was that, despite busy schedules, the faculty and students were graciously willing to lend a hand when it was requested. First, thank you to my two advisors, Marilyne Andersen and Leon Glicksman. As an advisor, Marilyne always struck the right balance between supporting me and pushing me to go further. She also continued to serve as my advisor after transferring to a new university, even though she was under no obligation to do so. Leon provided excellent overall guidance on the project and had a knack for asking penetrating questions that would uncover unexplored areas.

This work would not have been possible without the financial support and feedback from Hulic Co., Ltd. Thank you to Hulic for being willing to invest in the research process, where outcomes can be uncertain. Thanks specifically to Masashi Fukuda of Hulic who put in long hours and was a tireless advocate for this project within the company. Thanks also to Hikalu Kobayashi of Taisei Co. whose work was instrumental in constructing the Tokyo mockup on a tight schedule.

Greg Ward, creator of Radiance, and Axel Jacobs of London Metropolitan University provided guidance in developing my Radiance simulation process and helped me troubleshoot when I found puzzling results. Mark Belanger of the MIT Edgerton Center sat down with me and explained how the 3D printing process worked, turning a project I thought would take several weeks into one that took a few days.

I also relied on the support of my research lab, the Building Technology Group. Kathleen Ross made me feel at home in the group and helped me navigate the administrative hurdles of MIT. Thanks also to my fellow Building Technology students for their constructive ideas and friendship. Two that I should single out are Siân Kleindienst, who helped me get started with Radiance, and Shreya Dave, who provided the methodology and simulation results for the Relative Energy Impact calculation.

A big thank you goes to all my friends and family who provided support and encouragement throughout the process. Thank you to my father, Cliff Thuot, who taught me by example to forge my own path. Thank you to my mother, Janet Thuot, who always made sure I knew I had her support, no matter what. And finally, thank you most of all to my beautiful bride-to-be, Dominique Melissinos. She is the love of my life and my best friend and I become a better person every day I am around her. She helped at every stage of the project and this thesis would not exist without her.

# Table of Contents

# 1 Introduction

The rhythms of life in preindustrial societies used to be governed by the sun's rise and fall. The ancient Greeks designed houses and entire cities with access to the sun as a primary design consideration. A medical authority of the time, Oribasius, encouraged Greeks to spend their time in south-facing rooms because of the perceived health benefits of daylight (Butti & Perlin, 1980). The Roman Empire went so far as to pass sun-rights laws, which prevented new construction from blocking existing structures' access to the sun (Butti & Perlin, 1980).

As the centuries passed, daylight remained the only form of light available with sufficient intensity to allow a range of necessary activities. In the 1600s in Europe and North America, the most widespread form of artificial illumination was the tallow candle, consisting of a wick suspended in a shaft of solid animal fat. The list of shortcomings of this luminaire was long: they were expensive; the emitted light was not very bright; the burning fat gave off a rancid smell; the wick had to be trimmed every 15 minutes; charred pieces of wick posed a fire hazard; and the candles had to be stored securely so they would not be eaten by rats (Ekirch, 2005). With features like these, it is no wonder that daylight was the preferred method of illumination, when it was available. The preference for daylight was so strong that using candlelight during the day was known as "burning daylight" and was seen as a mark on one's moral character (Ekirch, 2005).

As technology improved the performance of artificial lighting, society's preferences swung in the opposite direction. By the 1930s, electric lighting was seen by many as the way of the future (Ander, 2003; Talman & Keally, 1930). Electric lighting offered a level of control not possible with daylight. People began to ask why they should bother with daylight when all they had to do was flip a switch. In 1930, this point of view was taken to the extreme in a *New York Times* article titled "Now the Windowless Building with its Own Climate," which advocated for eliminating windows entirely because, among other reasons, windows waste precious wall space (Talman & Keally, 1930). In recent decades, the pendulum has been swinging back in the direction of daylight for two main reasons: energy consumption and occupant well-being.

## 1.1 Benefits of Daylight

Electric lighting typically accounts for between 20% and 40% of primary energy consumption in commercial buildings (U.S. Department of Energy, 2009; Ihm et al., 2009). As both energy prices and awareness of the environmental impact of energy generation rise, more attention is being paid to minimizing the amount of energy consumed in buildings. Daylighting studies have shown that proper daylighting design can result in reductions of 50% to 80% of the energy needed for artificial lighting (Bodart & De Herde, 2002; Ihm et al., 2009). When the illuminance contribution from daylight is sufficient, artificial lights can be dimmed or turned off.

Daylight has a higher luminous efficacy than all but the most efficient forms of electric lighting (Kristensen, 1991). Luminous efficacy is the ratio of the number of lumens emitted by a light source per watt of thermal dissipation, so a higher luminous efficacy means that less heat is produced for the same amount of light. When visible light is absorbed by a surface it is remitted as heat in the form of long-wave infrared radiation. Glass is opaque to long-wave infrared radiation, so the majority of the heat resulting from both daylight and artificial light must be removed from a building through its climate control system. Daylight's higher luminous efficacy has the potential to reduce building cooling requirements, but the admission of daylight must be controlled so that solar heat gains resulting from excessive amounts of direct sunlight do not negate the energy savings from reduced artificial light use. Daylight availability also tends to be well aligned with times of peak energy demand when electricity prices can be elevated, further increasing the potential cost savings.

The effect of daylight on the health and performance of building occupants is another positive benefit. It is well established that light received by the eye regulates the circadian rhythms of the human body (Rea et al., 2002). A concern with current minimum recommendations for indoor illuminance is that these levels may not be high enough for circadian regulation (Rea et al., 2002). A study by Lambert et al. found that the prevailing amount of sunlight observed by the eye affects the rate of serotonin turnover in the brain (2002). Low serotonin turnover has an impact on mood and can lead to Seasonal Affective Disorder (SAD) (Lambert et al., 2002). SAD affects up to 9% of the population in high latitudes during the short days of winter (Rea et al., 2002). Additionally, workers in daylit spaces report fewer problems with common ailments such as headaches and eye strain (Edwards & Torcellini, 2002; Rashid & Zimring, 2008). Other studies have shown a relationship between better daylight availability and higher productivity and reduced absenteeism for office workers (Edwards & Torcellini, 2002; Rashid & Zimring,

2008). Similar performance improvements have also been reported for elementary students learning in daylit spaces (Heschong et al., 2002). Although causation has not been proven in many of these cases, at the very least it is generally accepted that people prefer natural light over artificial light. In one study, 96% of respondents expressed this preference (Markus, 1967). Daylight provides a range of benefits, but also presents challenges that must be addressed.

## 1.2 Challenges of Working with Daylight

The more desirable aspects of daylight from sidelight windows, such as workplane illuminance and a pleasant view of the outdoors, have to be balanced against the need to control glare and unwanted solar heat gains. The evaluation of glare in a building space is a complex problem. The most severe type of glare is disability glare, which occurs when the eye is exposed to light sources that are far outside of its adaptation range (Ruck et al., 2000). For example, disability glare can occur when staring at the sun or immediately after turning on a bright light after the eye has adjusted to darkness. Disability glare is a painful sensation and someone experiencing disability glare will immediately take action to avoid it.

A less serious form of glare is discomfort glare. Discomfort glare is characterized by a feeling of annoyance, rather than pain (Ruck et al., 2000). Although there are several glare metrics that have been proposed, none has achieved widespread acceptance for the evaluation of daylight. However, the existing metrics do share common variables, which help explain the factors that contribute to the perception of glare. The four factors are 1) the luminance of the glare source, 2) the perceived size of the glare source, 3) the position of the glare source relative to the center of the subject's field of view, and 4) the background, or average, luminance of the subject's full field of view (Wienold & Christoffersen, 2006). These variables indicate that glare is a function of both the glare source and the viewing position of the subject. They also show that glare is not just based on the brightness of a particular light source, rather it is also dependent on the ratio luminance values in the field of view. Studies have shown that people are somewhat more tolerant of limited levels of glare resulting from daylight as opposed to artificial light, which further complicates glare assessment (Wienold & Christoffersen, 2006).

Maintaining comfortable and effective lighting conditions using daylight is also a challenge because of the wide variety of possible sky conditions. The sun is constantly changing position in the sky over the course of each day and throughout the year. The sky can be fully clear, fully overcast, and anywhere in

between. The sky condition, as it is observed inside a building space, is also dependent on other factors including orientation, sky obstructions, geographic location, and local weather patterns. The problem becomes even more complicated as a floor plan is made deeper because the lighting conditions at a given instant can vary widely in different locations within the space. Sidelit spaces with a depth of more than one to two times the ceiling height generally cannot be lit by daylight alone (this problem is discussed further in Section 2.1). All this complexity has to be understood and managed in order for daylight to benefit a building space.

Many readers will be familiar with the following scenario outlining a fundamental problem with sidelight daylighting in a shared office space. Inevitably, in a multi-person office some desks will be closer to the facade than others. Since light levels drop exponentially with increasing distance from the window, the desks nearest the windows are often brightly lit, while desks farther into the room receive much lower levels of illumination. Light levels on the desks nearest the window are often so high that those occupants are obliged to shut the window blinds, thereby blocking out almost all incoming daylight. Now desks in the front and back of the room have inadequate light levels and the electric lights are switched on. As the day progresses the illumination incident on the window changes such that it would be acceptable and even welcome to let the daylight back in again. However, the occupants have more pressing issues to deal with and no one thinks about or wants the responsibility for adjusting the blinds on a regular basis. And so things remain, often day after day, with sunlight beating down on the window blinds to no avail while workers toil under artificial lighting.

This situation describes a unilaterally sidelit space, the most common type of building space (Ruck et al., 2000). This type of space allows daylight in from a single facade and does not admit toplight from the ceiling. The reason unilateral sidelighting is so common is that, in a multi-room multi-story building, there is often only a single exterior wall available in the room. As seen in the scenario above, unilateral sidelighting leads to uneven light distribution in deep spaces. Only light that enters with an elevation angle near horizontal is able to travel to the back of the room before hitting a surface. As a result, low-level sky obstructions, such as neighboring buildings, have a severe impact on light levels at the back of the room. Unilaterally sidelit spaces also have difficulty striking a balance between providing illuminance and an exterior view with controlling glare and solar heat gains.

A number of innovative sidelight daylighting systems have tried to solve these basic problems by redirecting or controlling incoming daylight in order to enhance the visual performance of the building space. However, most require some combination of active tracking systems and active shading systems.

The requirement for a daylighting system to be actively adjusted based on sky conditions can be a serious drawback (see Section 2.3 for further discussion). If the active system is manually controlled, the daylighting system can suffer from infrequent adjustment. If automatically controlled, initial cost and maintenance become increased concerns. What is needed is a system which can effectively illuminate deep spaces over the entire year without requiring active control.

## 1.3 Thesis Overview

The overall design problem can be reduced to the following problem statement: develop a passive system for use in deep-plan building spaces, which effectively redistributes daylight incident on a building's facade onto the workplane for a wide range of sky conditions, without causing visual discomfort or impeding normal use of the space.

The new system proposed here, named the Soralux Daylighting System, accomplishes these goals. The system consists of three sets of light redirecting elements:

1) Reflective louvers which collect the external light and collimate it into a range of elevation angles near horizontal.
2) Cylindrical lenses which spread the collimated light in the azimuth direction to prevent glare. (The convention used throughout this paper for azimuth and elevation is shown in Figure 4.12 on page 45.)
3) Ceiling tiles with a spread-specular reflectance to push light deeper into the space.

The first permanent installation of the Soralux system will be in the project sponsor's new headquarters building in Tokyo, Japan. The system will be installed on the building's southwest facade on multiple floors. The installation site is representative of the design context studied throughout this thesis: a deep-plan office space with sky obstructions due to urban surroundings. The new building is scheduled for completion in 2012.

This thesis will document the design and validation of the Soralux Daylighting System. The next chapter focuses on the design goals and constraints. Chapter 3 presents a literature review of related existing daylighting systems. Chapter 4 provides a detailed description of the design of the Soralux system. Chapter 5 presents the results of computer-based performance simulations and Chapter 6 reviews experimental results from two different physical mockups of the system. Chapter 7 discusses the results

and puts forth recommendations for which scenarios are best suited for the Soralux Daylighting System. Finally, Chapter 8 concludes with a summary of the research effort and a description of future work.

# 2 Design Context

Before embarking on a new development effort, it is important to fully understand the design context. The design context includes all the operating conditions, requirements, and constraints that will be imposed on the design. Different types of building spaces can have very different lighting needs, so at the outset of this research effort, several decisions were made to define and limit the scope of the daylighting problem to be solved. First, it was decided that the space to be daylit would be a deep, unilaterally sidelit (as opposed to multilaterally sidelit or toplit) open-plan space. This type of space was chosen because unilateral sidelighting is the most common daylighting situation. The template for this type of space is a large office building with an open-plan layout. The design and performance evaluations were conducted with an open-plan office in mind. However, this template can also apply to other spaces such as libraries, lobbies, factories, laboratories, classrooms, and any other large open space where people congregate during the day. Second, the effort was to focus on solutions that would work well for a wide variety of sky conditions, even with partially obstructed sky views. The final decision was to consider only passive, rather than active, daylighting systems. This decision was motivated by the reluctance of some potential users of daylighting systems to invest in active systems due to their perceived complication, cost, and recurring maintenance (Littlefair et al., 1994). With these conditions in mind, we evaluated solutions based on their ability to provide workplane illuminance, while controlling glare and solar thermal gains.

## 2.1 Building Space

Open-plan office spaces are often found in dense cities, where real estate is at a premium. They allow more workers per square meter of floor space, can be reconfigured more easily, and cost less to construct compared to private offices (National Research Council Canada, 2010). Figure 2.1 shows an example of a deep-plan office.

From a daylighting perspective, an open-plan office space in a large building is problematic. The distance from the facade to the back of the room can be 15 m or more, which is much greater than the depth for which a conventional sidelight window is able to provide adequate levels of daylight. Maximum ceiling heights are often limited in this type of office space, due to the need to maximize usable space in the building.

Figure 2.1: A Typical Open-Plan Office

Windows are generally able to provide adequate daylight to a distance between one and two times the distance from the top of the window to the floor when the blinds are operated regularly (Reinhart, 2005). Thus, for a room with a 2.8 m high ceiling, adequate daylight levels could be expected up to a distance between 2.8 and 5.6 m from the facade. This range is only a rule of thumb because the actual limit depends on a number of factors including sky condition, glazing transmittance, blind position, and required illuminance. Another complication when working with large office buildings is that since the building is many stories tall, conventional toplighting strategies such as skylights are not useful as they cannot be utilized effectively below the top floor.

In addition to constraints imposed by the building itself, the urban surroundings of a large office building affect the design of the daylighting system as well. In large cities, many tall buildings cluster together in the same area. As a result, views of the sky, especially near the horizon, are often obstructed by the surrounding buildings. This reduces the amount of daylight available at the facade for use inside the space. The reduction in illumination is more pronounced during times when direct sunlight, in addition to skylight, is blocked by the urban surroundings.

## 2.2 Geographic Location

Tokyo, Japan was chosen as the main location to study the Soralux system. Tokyo's urban environment matches the conditions described above with densely packed tall buildings, including many open-plan office buildings. In addition, Tokyo will be the site of the first permanent installation of the Soralux Daylighting System. Tokyo's latitude (35.7°) also places it approximately in the middle of the band of densely populated latitudes between 18°N and 56°N, making the city a good intermediate testing point.

Figure 2.2 illustrates how the path of the sun changes over the course of the day and the year as a function of latitude. The four cities shown are Austin, USA (latitude: 30.3°); Tokyo, Japan (latitude: 35.7°); Boston, USA (latitude: 42.4°); and Stockholm, Sweden (latitude: 59.4°). All times are legal standard time, not solar time. As latitude increases (for the Northern Hemisphere), the peak solar elevation angle drops and the range of possible solar azimuth angles increases. For Tokyo, the peak solar elevation angle ranges from 31° at the winter solstice to 78° at the summer solstice.

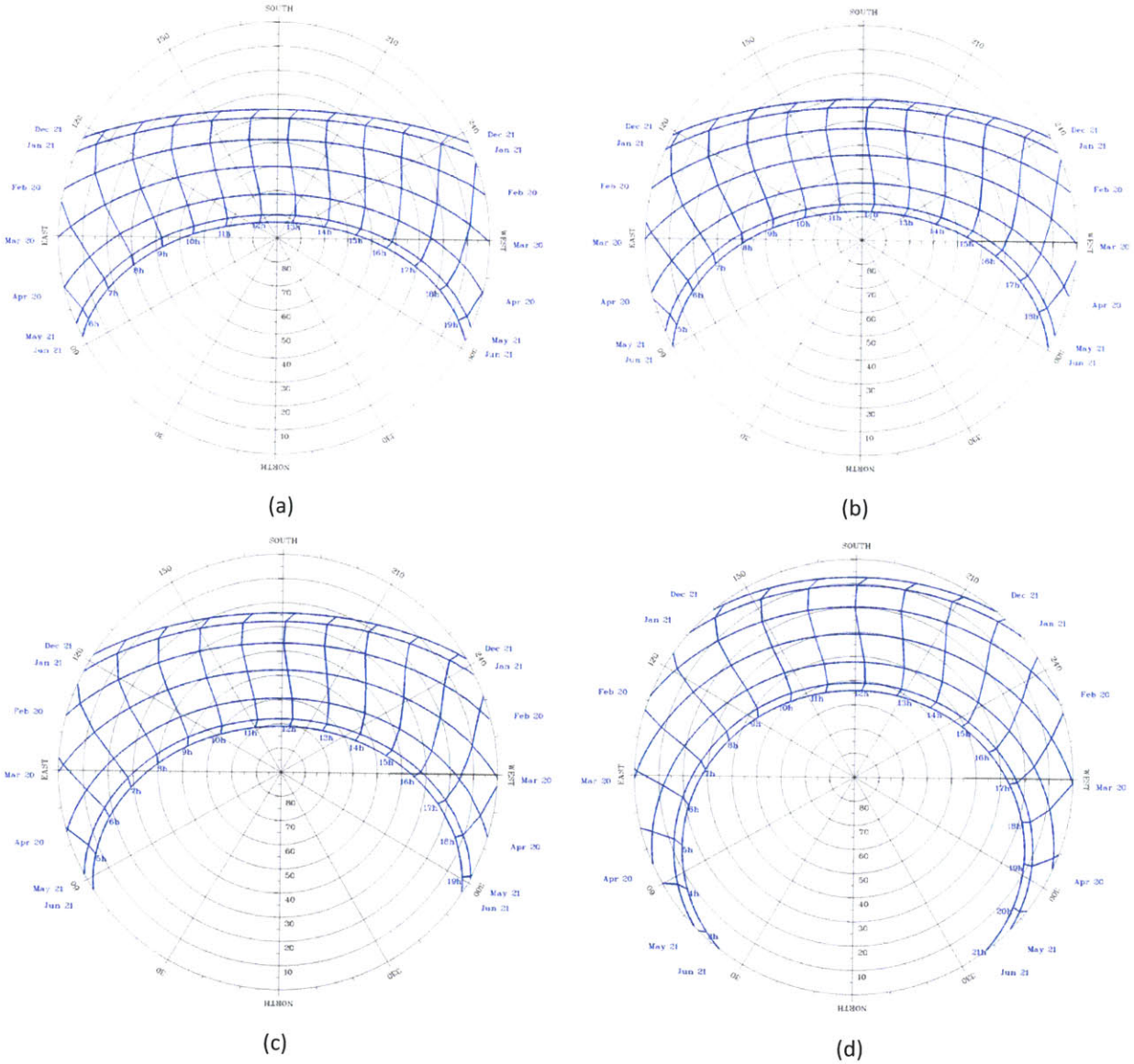


Figure 2.2: Sun Course Charts for Austin (a), Tokyo (b), Boston (c), and Stockholm (d) (Adapted from The University of Oregon, Solar Radiation Monitoring Laboratory, 2008)

## 2.3 Common Issues with Existing Systems

Before trying to improve on existing daylighting systems, a review of recurring daylighting problems is necessary. The most common issue is ineffectiveness due to sky conditions, resulting from either under-illumination or over-illumination.

Passive daylighting systems are often only effective for a limited range of incoming light directions and, as a result, have difficulty providing elevated levels of workplane illuminance for significant parts of the year. The transmissive properties of these systems are such that they redirect some incoming angles of light favorably, but others unfavorably. Aizlewood conducted a study of four different advanced passive daylighting systems: a light shelf, Okasolar louvers, a prismatic glazing, and a prismatic film (1993). All four of these systems were found to significantly reduce workplane illuminance compared to an unshaded window for overcast conditions. Under the variety of sunny conditions found over the course of the day and year, no system was able to consistently provide increased workplane illumination in the rear part of the room. A review of the pros and cons of additional relevant advanced daylighting systems is found in Chapter 3.

Not only do these systems have problems with under-illumination, they also suffer from over-illumination. Most existing systems allow direct sun to enter the room at a downward angle, either totally unimpeded or as a specular reflection, and so they are likely to cause glare for certain times of the day and year (Ruck et al., 2000). In order to mitigate these glare problems, the typical solution is to couple the daylighting system with a shading system. While this may solve the glare problem, the daylighting system is often ineffective during these sunny periods because the emitted light is blocked by the shading system.

Control of the shading system leads to a third major problem with existing daylighting systems. Most office buildings are equipped with manually controlled venetian blinds to regulate the amount of daylight entering the workspace. Multiple studies have shown that occupants are much more likely to close their blinds in response to excessive daylight levels than to reopen their blinds after natural lighting conditions have improved (Rea, 1984; Reinhart & Voss, 2003). The blinds get "stuck" in the closed position for long periods of time because occupants do not think about or are uninterested in altering them based on exterior conditions. The effect is even more apparent in shared office spaces because of social norms about asking others for permission before making a lighting change (Reinhart & Voss, 2003). This problem with shading systems can negatively affect installed daylighting systems if a

solution is not found because a daylighting system cannot be effective if it is always blocked by an unresponsive shading system. Consequently, daylighting systems which allow glary conditions even for short periods can find themselves totally blocked for days, or even permanently. One solution to this problem is to automate the movement of the blinds, and thus eliminate the need for active occupant involvement. However, automated shading systems are more expensive in both upfront and recurring costs than their passive counterparts because they require moving machinery, an accurate control system, and some level of skilled human monitoring and maintenance (Ruck et al., 2000). The motion of automated systems can also be distracting to building occupants.

In summary, for the daylighting application considered in this thesis, there are four crucial challenges to be addressed. First, using only sidelight, the system must boost light levels in deep spaces beyond what can be accomplished with a basic glazed facade, while maintaining visual comfort. Second, the system must be effective over a wide range of sky conditions, including time of day, time of year, and degree of sky clearness. Third, the performance of the system must not be greatly diminished by the presence of low-level sky obstructions, commonly found in urban situations. Finally, the system must fulfill these objectives while remaining passive (ie. without any moving parts). Adjustments to the system itself or to a separate shading system are prohibited. The next chapter will take a closer look at existing daylighting systems that have attempted to meet these challenges.

# 3 State of the Art

Since they do not create light themselves, daylighting systems are effectively light redistribution systems. Sidelit spaces often have an exponential illuminance profile, with much higher light levels adjacent to the facade. The common objective of most of the daylighting systems considered here is to take a portion of the light that would fall near the facade and redirect it, by means of reflection, refraction, or diffraction, so that the light is pushed farther into the room. A collection of representative passive sidelighting technologies were evaluated with the performance objectives of this research effort in mind:

a) Effectively operates over a wide range of sky conditions.
b) Prevents glare and thermal discomfort from undiffused direct sunlight.
c) Pushes light deep into the space.

The major daylighting system categories evaluated are light shelves, prismatic systems, holographic systems, anidolic systems, and louver systems. For each category, representative examples are described and their performance characteristics are discussed.

## 3.1 Light Shelves

The light shelf is perhaps the simplest light redirecting technology. It consists of a horizontal plane affixed to the facade that reflects incoming light onto the ceiling and deeper into the space. The upper surface of the shelf can either be specular or diffuse. A specular surface will result in better performance but will also require more frequent cleaning (Aizlewood, 1993). The shelf can be mounted on the interior or exterior side of the facade. The exterior version is able to gather more light because of reduced shading from the building itself, but the frequency of cleaning required to keep an exterior light shelf functioning effectively may be prohibitive (Ruck et al., 2000). The basic geometry of an interior light shelf is shown in Figure 3.1.

The performance of the light shelf is not impressive compared to some of the other existing technologies. For overcast conditions, the light shelf causes a reduction in light levels throughout the room. Although the overall reduction is undesirable, a positive aspect is that the reduction is greater near the front of the room, resulting in a more even light distribution profile (Littlefair et al., 1994).

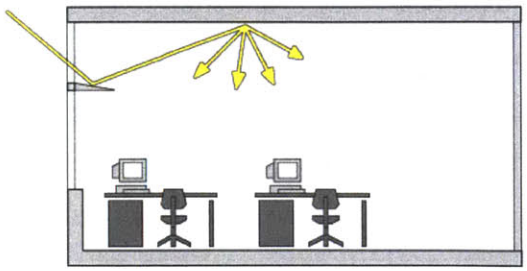

Figure 3.1: Operation of an Interior Light Shelf (Reprinted from Maunder, n.d.)

The geometry of the light shelf also limits its effectiveness under sunny conditions. For high angle (summer) sun, the horizontal shelf redirects light up at a high angle, meaning the light does not travel very far into the room before hitting the ceiling (Aizlewood, 1993). For low-angle (winter, early morning, late afternoon, etc.) sun, although the light is redirected at a favorable angle deep into the room, the projected angle of the shelf is significantly reduced, meaning it intercepts and redirects a smaller amount of light (Aizlewood, 1993). Another major drawback is that the light shelf allows large amounts of direct sunlight to pass through unimpeded, requiring an adjustable shading system to protect occupants from glare (Aizlewood, 1993).

Although the specular surface of the light shelf is not sophisticated enough to perform well over a wide range of sky conditions, the basic principle of using a specular surface to direct incoming light onto the ceiling of a space is useful for further concept generation.

## 3.2 Prismatic Systems

Another innovative daylighting technology is the prismatic panel. Prismatic panels are typically made of acrylic or glass and incorporate a sawtooth profile on one or both of their outer surfaces. As a result, incoming light is refracted, and sometimes reflected through total internal reflection, into a different outgoing angle, as shown in Figure 3.2 (Ruck et al., 2000).

Although the prismatic panel is able to redirect light, as a passive system it is not able to adequately control the output direction of light for the full range of incident sun angles. Its greatest effect is to provide some glare protection near the facade, but the prismatic panel does not markedly improve illumination levels in the rear part of a room (Lorenz, 2001). One limitation to the efficiency of the system is that, due to the geometry of the prism, some of the light will undergo total internal reflection

inside the prism and be rejected (Lorenz, 2001). In one study conducted of a prismatic panel, the system was found to increase light levels in the back of a space only near the equinoxes (Aizlewood, 1993). Under overcast skies and in the winter and summer, the system reduced light levels away from the facade (Aizlewood, 1993). Furthermore, prismatic panels allow direct sunlight through at a downward angle, at least for some times of the day and year, potentially causing glare. There are many different possible prismatic panel geometries, but the performance described here is typical.

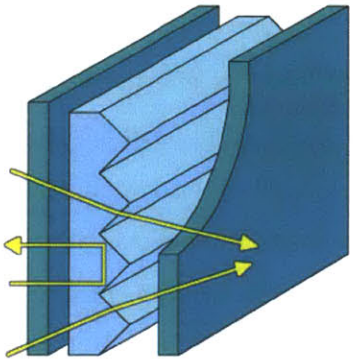

Figure 3.2: Effect of a Prismatic Panel on Incident Light (Reprinted from Maunder, n.d.)

The utility of prismatic panels as stand-alone daylighting systems is limited due to their tendency to send light in a wide range of directions. However, this weakness can be turned into a strength when prisms are used for a different purpose. Given the appropriate shape, prisms have the ability to spread out the direction of collimated sunlight by means of refraction, and thus decrease the intensity of sunlight in any one direction. Prisms can be used as an effective and highly transmissive glare control device.

The Laser Cut Panel (LCP) is another application of the prism to daylight redirection. LCPs can be made by, as the name implies, using a laser to cut a series of parallel lines into a clear acrylic panel. The cut surfaces act as mirrors. Light first passes through the outer surface into the prism. It is then redirected off the cut surface through total internal reflection and passes out the other side of the panel traveling upwards, as shown in Figure 3.3. The system has some strong advantages in that it is simple to produce and can be used in the main view window because it maintains a relatively clear view to the outdoors at viewing angles near horizontal (Edmonds, 1993).

However, the LCP has some significant shortcomings. First, in a vertical orientation the system is useful only under direct sun, as it has almost no impact under overcast or clear but sunless conditions (Ruck et al., 2000). However, an LCP tilted out from the facade at a 30° was shown to increase light levels at a

depth of 8 to 12 meters by about 200% compared to a clear window (Edmonds, 1993). Although this increase is notable, especially given the tendency for other daylighting systems to reduce illumination under overcast skies, in absolute terms the increase is modest. Using the daylight factors provided in Edmonds (1993), for a 20 klux overcast sky, a 200% increase at the back of the room would correspond to increasing the workplane illuminance from about 40 lux to about 80 lux. Daylight factor is defined as the ratio of illuminance inside a space to the exterior global horizontal illuminance under totally overcast conditions (Ruck et al., 2000).

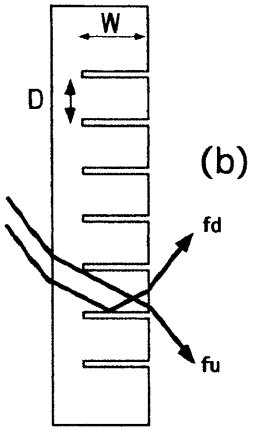


Figure 3.3: Effect of an LCP on Incident Light (Reprinted from Edmonds, 2005, p. 75, Fig. 2)

Another limitation of the system is that it only redirects sunlight onto the ceiling at a favorably shallow angle for a limited range of sun positions. If the sun is too high in the sky, the light is internally reflected twice and exits downwards at the same angle it entered the LCP. If the sun is too low in the sky, light passes through the panel without being reflected at all. Both of these situations can result in glare for room occupants and a separate shading system is required as a result.

A useful concept introduced by the LCP is using a repeating array of vertical elements to redirect incoming light. The LCP can be thought of as a stack of very small light shelves. By replacing a light shelf which can be .5 m long with an LCP that is on the order of .01 m thick, the system is more easily integrated into the facade and the need for cleaning can be eliminated by placing it inside a double-glazing.

Another prismatic system, known as both sun directing glass and ADO-Toplight, makes clever use of total internal reflection in a manner similar to the LCP. As shown in Figure 3.4, acrylic profiles stack on top of each other inside a double-glazing (Laar & Grimme, 2002).

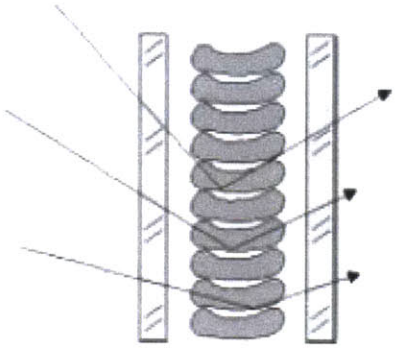

Figure 3.4: Sun Directing Glass (Reprinted from Ruck et al., 2000, p. 4-67)

The rounded section at the inlet of the profile acts to converge the rays into the rest of the channel. The rays then bounce off the lower surface via total internal reflection and exit the other side of the profile. This system is impressive in its simplicity, but it is not without limitations. First, the system allows descending sun rays for effective incoming elevation angles less than 15° and greater than 65°, so the system will have to be shaded for particular times of the day and year to prevent glare (Ruck et al., 2000). Also, because the light is bent away from the surface normal as it leaves the profile, the light is not collimated near horizontal. This prevents a large portion of the light from traveling deep into the space before it hits the diffusing ceiling. Testing found that sun directing glass outperformed a 6 m control space equipped with partially closed venetian blinds but the system was not compared with a clear unshaded window (Ruck et al., 2000).

Sun directing glass takes the concept found in the LCP one step further by shaping the prism in such a way that the emitted light is better controlled than with the flat surfaces of the LCP.

## 3.3 Holographic Optical Elements

Holographic optical elements embedded in a double-glazing offer a more exotic approach to daylight redirection. The system relies on diffraction of light resulting from a "polymeric film with holographic diffraction gratings" (Ruck et al., 2000, p.4-77). The holographic film redirects light from a particular area of the sky onto the ceiling of a room. However, because it causes severe color dispersion it cannot be used under direct sunlight (Ruck et al., 2000). This technology has not undergone rigorous testing as of yet.

## 3.4 Anidolic Systems

Anidolic systems offer some key advantages over other systems. They are able to precisely limit the angular range of the emitted light and can be effective in redirecting diffuse light. These systems are defined using the principles of nonimaging optics and generally incorporate highly reflective parabolic surfaces. For a more detailed discussion of the workings of an anidolic system, see Section 4.2.1.

The Zenithal Anidolic Collector, shown in Figure 3.5, is one example of an anidolic system. Its great strength lies in the fact that it is able to effectively redirect diffuse skylight to the back of a room. Most other systems perform either on par with or worse than an unshaded window under overcast skies, but the Zenithal Anidolic Collector significantly outperforms the uncovered window (Scartezzini & Courret, 2004). A prototype that was tested was found to increase the daylight factor of the test space from 1.75% to 3.5% at a distance of 6 m from the facade. For an overcast sky with a global horizontal illuminance of 20,000 lux, this corresponds to increasing workplane illuminance from 350 to 700 lux (Scartezzini & Courret, 2002).

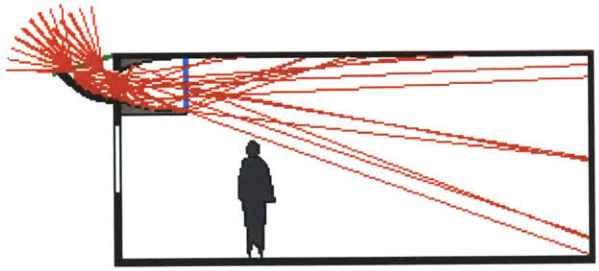

Figure 3.5: The Zenithal Anidolic Collector (Reprinted from Scartezzini, 2010)

In spite of this unique ability, this system has some limitations. Since it allows specular descending rays, the system must be shaded under sunny conditions to protect from glare. The physical dimensions of the system are also quite large, around 1 to 2 m long and .5 to 1 m tall. This size reduces the ceiling height near the facade and makes using the space underneath awkward. Integrating the exterior light scoop can also be an architectural challenge.

Although the particular configuration used in the Zenithal Anidolic Collector does not lend itself to use under direct sunlight, the light redirecting principles it embodies are valuable. Through the use of parabolic curves, the system is able to efficiently pass light from a large area through a smaller opening and control the angular range of emitted light.

An attempt to better integrate the Zenithal Anidolic Collector into building spaces resulted in the Anidolic Ceiling (Figure 3.6). The Anidolic Ceiling incorporates the same type of parabolic geometry but adds a horizontal light duct at the outlet of the anidolic collector (Courret et al., 1998). Similar to the Zenithal Anidolic Collector, the Anidolic Ceiling was shown to double daylight factors at a depth of 6 m from the facade (Courret et al., 1998).

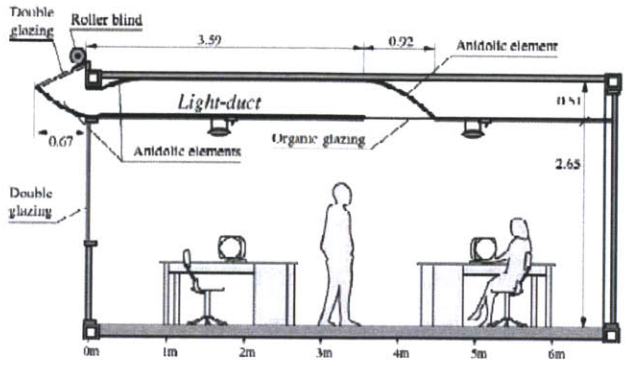


Figure 3.6: Anidolic Ceiling System (Reprinted from Courret et al., 1998)

The reflective duct transports the light deeper into the room where it is released through an overhead glazing. This approach reduces glare concerns, but the system still has to be shaded under sunny conditions. In addition, the Anidolic Ceiling takes up a large volume of space in the building, requiring either lower ceiling heights or increased floor spacing (Courret et al., 1998). Another drawback is that the amount of reflective surface required is substantially more than for the simpler Zenithal Anidolic Collector. As the length of the duct increases, the total amount of light emitted decreases, due to the increasing percentage of light absorbed by the walls of the duct.

The Anidolic Ceiling system introduces the idea of using a secondary reflector, located inside of the building space, in addition to the anidolic collector installed on the facade. The combination of these two elements allows light to penetrate farther into the space.

A third type of anidolic system, known as Anidolic Solar Blinds, makes use of a 3D anidolic profile. However, the main purpose of this system it to provide shading by rejecting high angle sunlight so it is not useful for increasing illuminance in deep spaces (Scartezzini & Courret, 2002).

## 3.5 Louver Systems

Reflective louvers form another relevant group of daylighting systems. Louver systems are often designed to be located between two panes of glass, making the task of integration into the facade much easier than with larger systems such as the Zenithal Anidolic Collector. Conceptually, louver systems generally consist of a vertical array of identically-shaped curved slats, with a profile that redirects daylight onto the ceiling (Ruck et al., 2000).

Some louver systems are designed explicitly for sun shading. Examples include the micro-light guiding shade, Okasolar louvers, and Retrolux louvers (Figure 3.7). The intent of these systems is to control glare and heating loads by rejecting sunlight over a wide range of angles, while still allowing through some light. Although these concerns may be preeminent in tropical climates, these systems do not lead to significantly improved daylighting conditions in deep spaces, as a result of the large fraction of incident light rejected (Aizlewood, 1993; Greenup & Edmonds, 2003; Laar & Grimme, 2002).

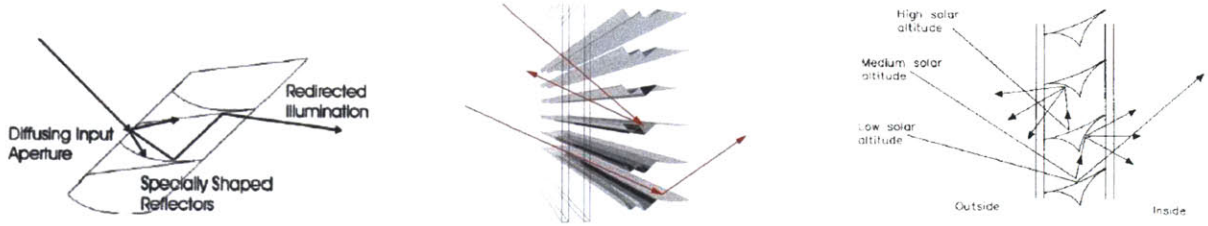


(a) (b) (c)

Figure 3.7: Micro-Light Guiding Shade (a), Retrolux Louvers (b), and Okasolar Louvers (c) (Reprinted from Greenup & Edmonds, 2003, p. 100, Fig. 1; Köster Lichtplanung, n.d.; Ruck et al., 2000, p. 4-24, Fig. 4-4.2)

These systems introduce the idea of using an array of light reflecting elements, rather than the light refracting elements seen in Section 3.2. There are several advantages of using reflective elements instead of refractive elements, including no losses due to total internal reflection and light is not spread at the outlet of the array due to the transition to a medium (air) with a lower index of refraction.

Bartenbach et al. proposed another potentially useful louver system (1987). One embodiment of their design is known as the Fish Louver (shown in Figure 3.8), which uses reflective slats to redirect light onto the ceiling (Ruck et al., 2000).

A major advantage of this design is that light from above the horizon cannot be reflected downwards from the surface of the louver (Bartenbach et al., 1987). As a result, glare due to direct sunlight is not an issue. The louver allows all ray directions from above the horizon to pass through successfully, resulting

in a relatively high overall transmittance (Ruck et al., 2000). The flat and curved sections of the outer half of the Fish Louver also illustrate an efficient way to concentrate light from a larger area to a smaller one in the context of a louver array.

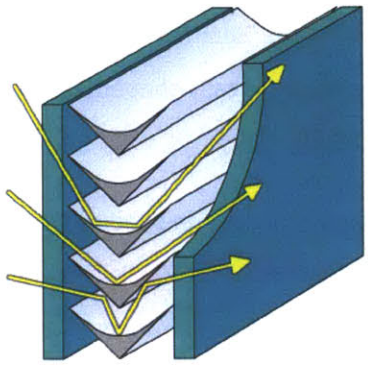

Figure 3.8: Fish Louvers (Reprinted from Maunder, n.d.)

The main drawback to this system is that the shape of the louver does not effectively collimate the light near horizontal at the outlet. Consequently, much of the light hits the ceiling immediately adjacent to the facade and is not able to illuminate the deeper parts of a space. Using a very shallow (3.4 m) and heavily obstructed test room the system was found to increase light levels over a closed venetian blind for some sky conditions, but not for others (Ruck et al., 2000). Scartezzini and Courret investigated a closed related louver design and came to similar conclusions: the system did not perform better than the reference case under overcast conditions but showed promise under sunny conditions (2004). Quantitative illuminance values for this evaluation were not reported.

Compagnon evaluated a reflector system comprised of anidolic profiles, as shown in Figure 3.9 below (1994). The inner anidolic curves are tilted upwards so that light exiting the reflectors would be directed onto the ceiling, to protect from glare. The idea of using anidolic profiles to compose a louver array is an attractive one. However, in this configuration the design of the outer half of the louver results in the rejection of all light above a projected elevation angle of 60° (see Section 4.2.4 for a definition of projected elevation angle). Light enters the room at a maximum of 60° above horizontal, which is a lower maximum elevation angle than that of the Fish Louver. However, the output elevation range is still fairly wide and the amount of light traveling deeply into the space will be limited as a result. The lower curve of the CPC profile is truncated in this design, meaning that the louvers will spill light below horizontal, potentially causing glare. Also, although it is more compact than the Zenithal Anidolic Collector, the size of the assembly is still rather bulky at .48 m depth (Compagnon, 1994).

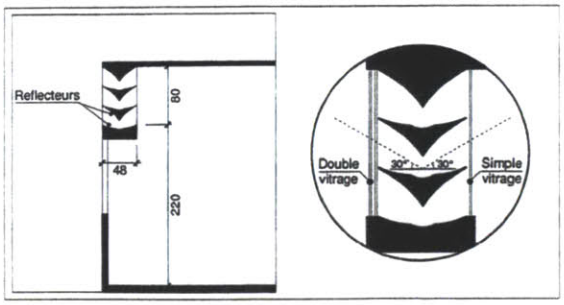


Figure 3.9: Anidolic Louvers (Reprinted from Compagnon, 1994, p. 138, Fig. 5.47)

The CPC was incorporated into another louver system developed by Eames and Norton (1994). As with Compagnon's design, light enters the louver array through a skyward tilted CPC, as shown in Figure 3.10. However, in Eames and Norton's design the inner half of the louver is composed of a flat section and a circular section, rather than another CPC. These inner surfaces cause several problems that make this design problematic.

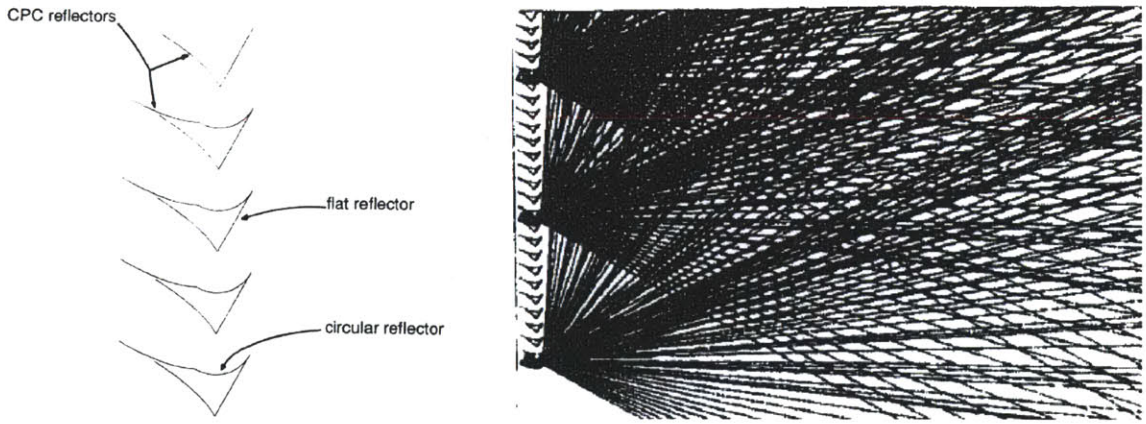


Figure 3.10: Asymmetric Anidolic Louver Profile (a) and Ray Tracing Through the Profile (b) (Reprinted from Eames & Norton, 1994, pp. 74-75, Figs. 1 & 2)

The louvers are spaced such that sunlight can pass directly through without being redirected. Also, light is able to reflect off the outer CPC and enter the room at a downward angle. Both of these effects have the potential to cause glare under direct sunlight. The output elevation angle ranges up to 90°, which means that a large portion of the light hits the ceiling immediately adjacent to the facade without travelling very far into the space. The inner flat surface of this louver is diffuse, so light hitting it will be scattered in all directions, further limiting the louver's ability to guide light to the back of the space. Finally, the CPC inlet section rejects light with an elevation angle above 65°, for light normal to the

facade in azimuth. As the azimuth angle of the light increases, this cut-off angle drops from 65° down to 0°, for light nearly parallel to the facade. As a result, the system is not able to transmit light from a large portion of the sky. The lower portion of the sky from which the system does successfully pass light is also the first to be blocked by surrounding sky obstructions. Although this design suffers from some major shortcomings, the concept of coupling a CPC with additional flat, circular, or parabolic surfaces leads to additional configurations that potentially have superior performance qualities.

Additional attempts were made by Courret et al. to incorporate anidolic geometry into a louver array, as shown in Figure 3.11 below (1994). These designs have some intriguing features but, ultimately, are not suitable for a deep-plan space. The first two images show the same design at different scales. These louvers are similar in structure to Eames and Norton's design, except that their orientation with respect to incoming light is reversed. The CPC in these designs is located on the inner side of the louver, which generally leads to better performance compared with Eames and Norton's louver design.

The Courret et al. louvers collimate light into a very narrow range around horizontal, but since the anidolic curves are not tilted towards the ceiling, approximately half of the light will exit below horizontal. This might be acceptable for a shallow office with a depth 3 or 4 m, but it would cause disturbing glare in deeper spaces. Another drawback with this design is that a large fraction of the incoming light is rejected by the steeply inclined plane at the louver's inlet. Finally, the very long and slender shape of the louver would be difficult to produce accurately, especially at the scale shown in the middle image. The system in the rightmost image is similar in form and function to the Okasolar louvers discussed above. The intent is to reject high-angle light while admitting low-angle light. This design allows light to exit at a downward angle as well, meaning that all the variants shown in Figure 3.11 would likely require an additional shading system if exposed to direct sun.

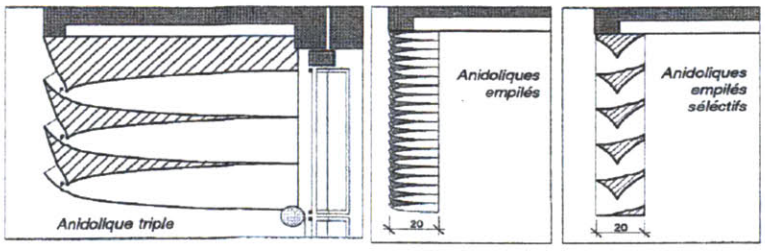


Figure 3.11: Additional Anidolic Louver Designs (Reprinted from Courret et al., 1994, p. 3, Fig. 3)

A recent entry into the reflective louver category is the LightLouver system, shown in Figure 3.12 (Rogers et al., 2004). This advanced daylighting system offers a significant advantage compared with the

other louver systems. Light exiting the LightLouver array has a maximum elevation angle of around 40°, which means that light is able to penetrate the space more deeply before hitting the ceiling. Once again, there are several downsides worth noting. First, the LightLouver system allows low-angle sunlight (5° or less) to enter the room at a downward angle (Rogers et al., 2004). This may or may not be a problem depending on the circumstance of a particular installation site. Second, the entire exterior-facing surface of the louver is a diffusing surface, which rejects a large fraction of the total incoming daylight, leaving less to distribute into the room (Rogers et al., 2004). This exemplifies a recurring trade-off seen in louver systems between the amount of light rejected by the louver and the extent of the emitted light's angular range. Finally, the aspect ratio (width/pitch) of the LightLouver is rather large at 2.75 (Rogers et al., 2004). More louvers would be required to fill an equivalent window opening compared to a design with a smaller aspect ratio.

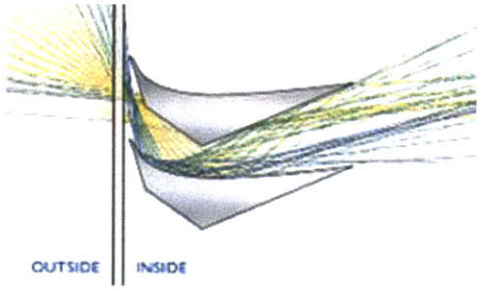


Figure 3.12: Ray Tracing Through LightLouvers (Reprinted from LightLouver, 2010)

A final limitation common to most of the daylighting systems discussed here is that, although they may emit light at an angle near horizontal, light penetration depth is limited because the systems are designed to direct light onto a diffusing white ceiling, which scatters light uniformly in all directions. The diffusing ceiling wastes much of the effort that went into collimating the light near horizontal and limits how well the back of a deep space can be lit using daylight.

Although some are more effective than others, none of the existing systems evaluated were able to passively control daylight in order to consistently provide elevated illuminance levels in deep spaces, while controlling glare. Even though none provided a complete solution, some of the better performing systems had qualities that we could improve upon to create a better daylighting system for the given design context. Based on the apparent need for a new solution, the Soralux Daylighting System was developed.

# 4 Soralux Daylighting System Description

The details of the Soralux Daylighting System's design and operation are laid out in this chapter. A description of the system was originally published in "A Novel Louver System for Increasing Daylight Usage in Buildings" (Thuot & Andersen, 2011).

The basic function of the Soralux Daylighting System is to take both diffuse skylight and direct sunlight from a wide range of incoming angles and pass them into the building space at a shallow upward angle. The system intercepts light that would otherwise land in the front of the room and redirects it towards the rear, thereby increasing workplane illuminance in the back of the space and evening out the illuminance distribution. To assist the light in penetrating deeply, light that hits the ceiling near the facade is specularly reflected down onto the workplane, rather than being diffusely scattered. The system accomplishes these tasks passively, without any adjustments for sun tracking or shading.

The Soralux Daylighting System is comprised of three major subassemblies. Two of these subassemblies, the reflective louvers and refractive rods, are housed in a window unit installed at the top of the daylit facade. The other subassembly consists of reflective ceiling panels which extend from the daylit facade to a distance of 4 m inboard (the distance required will vary based on room size and performance goals). Figure 4.1 shows a schematic of the overall system.

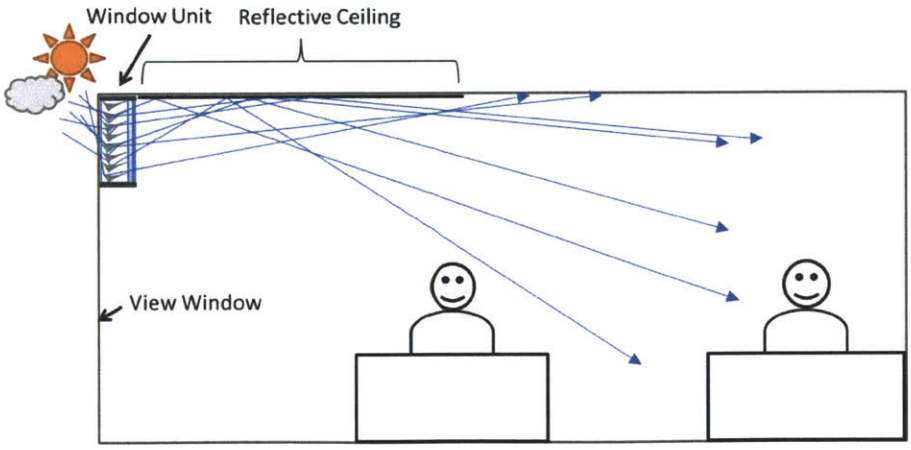


Figure 4.1: Cross-Sectional Diagram of the Soralux Daylighting System

After entering the window unit through the outer glazing, light first passes through an array of reflective louvers, which collimate the light into a narrow elevation angle range between 0° and 40°. Then the light

passes through an array of refractive rods which act as lenses and diffuse the light in the azimuthal direction in order to prevent glare resulting from direct sunlight. After traveling at an upward angle into the room, the reflective ceiling redirects the light deeper into the space at a shallow angle.

## 4.1 Window Unit

Figures 4.2 and 4.3 show close-up views of the window unit's cross-section. The unit contains two glass panes, similar to a standard double-glazed window unit. The louver and rod assemblies are located between the outer and inner glass panes. Both the louvers and the rods are sensitive to dust and scratching, so placing them inside the window unit provides protection and eliminates maintenance.

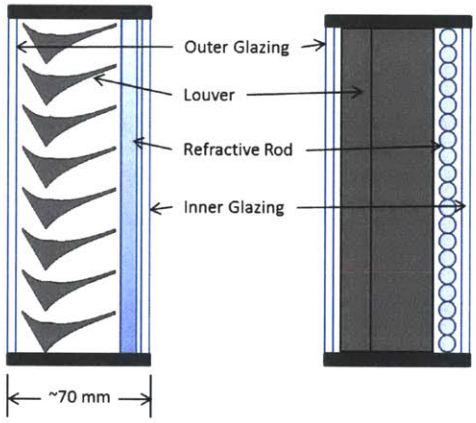


Figure 4.2: Window Unit Section View (Left) and Plan View (Right)

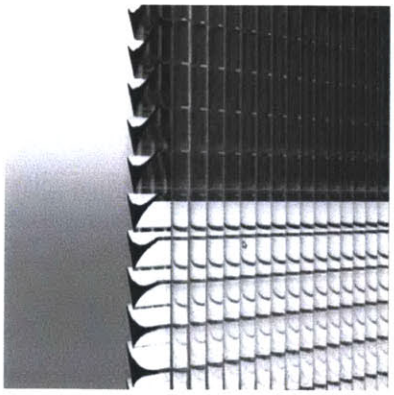

Figure 4.3: Radiance Rendering of Window Unit Cross-Section. The Louvers Above Eye Level Appear Dark Because They Do Not Emit Light Below Horizontal.

To protect occupants from glare, there is no view through the window unit to the outdoors. The bottom of the unit should be no lower than approximately 2.1 m off the ground to allow for a view window on the lower portion of the facade.

## 4.2 Louver Assembly

The core of the system is a vertical array of reflective louvers, which redirects incoming light in a controlled manner deep into the space. To understand how the louvers work to redirect light, it is first necessary to cover some background information on optics.

### 4.2.1 Background on the Compound Parabolic Concentrator

The search for a passive system that could redirect light deeply into a room, while also preventing direct sunlight from entering at a downward angle, led to the science of nonimaging, or anidolic, optics and a technology called the Compound Parabolic Collector (CPC). The CPC is key to the functioning of the Soralux Daylighting System, so an overview of its design and function is in order.

The CPC was developed in the 1960s and one of its first applications was as a solar concentrator. The main advantage of the technology is that it accepts all light rays from a defined angular extent and concentrates them on a smaller area with a minimum number of bounces and without the need for precise sun tracking. Both of these features are favorable for a concentrating solar energy system. The CPC, when used for daylighting applications, uses the same type of reflector profile, but light moves through it in the opposite direction. Light enters from all directions through a small inlet aperture and is aligned into a controlled angular range at the outlet (Winston et al., 2005). This type of system is able to exert tighter control over the direction of emitted light than many of the other systems discussed in Chapter 3. This thesis focuses exclusively on two-dimensional (2D) CPC (trough-like) profiles, but there are three-dimensional (3D) CPC (cone-like) designs as well, such as the one used in the anidolic solar blinds discussed in Section 3.4.

Four variables define the CPC profile: length (L), entry aperture half-width (a'), exit aperture half-width (a), and maximum output angle ($\theta_{max}$) (Winston et al., 2005). Setting any two of the four is sufficient to fully define the CPC profile. Figure 4.4 identifies these variables on the CPC profile.

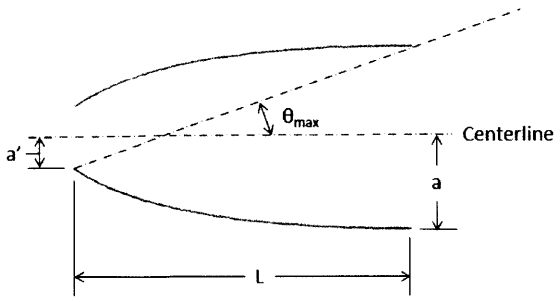


Figure 4.4: Defining Variables of the CPC

With two of the four variables given, the following two equations allow the remaining variables to be determined:

$$L = \frac{a'(1+\sin\theta_{\max})\cos\theta_{max}}{\sin^2\theta_{max}} \qquad \text{Equation 4.1}$$

$$a = \frac{a'}{\sin\theta_{max}} \qquad \text{Equation 4.2}$$

Figure 4.5 illustrates the relationship between the four parameters. As the maximum outlet angle is decreased, the length of the CPC increases. For $\theta_{max}$ of about 20° or less the required length increases dramatically. In addition, decreasing the maximum output angle increases the ratio of outlet aperture width to inlet aperture width, which can reduce the amount of light collected. Once the four variables are determined, the parametric equations shown in Equations 4.3 through 4.5 can be used to define the 2D CPC (Winston et al., 2005).

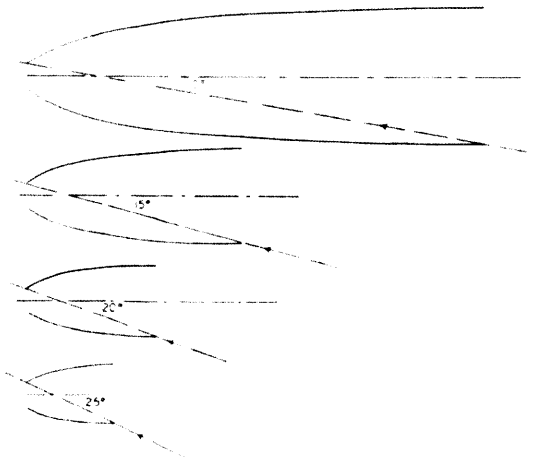

Figure 4.5: A Smaller Maximum Output Angle Results in an Increased Length for the CPC (Adapted from Winston et al., 2005, p. 52, Fig. 4.11)

$$r = \pm\left[\frac{2f\sin(\phi-\theta_{max})}{1-\cos\phi} - a'\right] \qquad \text{Equation 4.3}$$

$$z = \frac{2f\cos(\phi-\theta_{max})}{1-\cos\phi} \qquad \text{Equation 4.4}$$

Where, $f = a'(1+\sin\theta_{max})$ Equation 4.5

And $\phi$ varies from $2\theta_{max}$ to $90+\theta_{max}$

### 4.2.2 Louver Profile Description

A key insight gained during the review process of existing systems was that the principles of the Compound Parabolic Collector could be used to create a new louver system, which would improve on some of the drawbacks of both the anidolic and louver systems described in Chapter 3. These drawbacks include ineffectiveness for some sun positions, glare resulting from direct sunlight, large volumetric requirements, and the need for actively controlled shading systems. The resulting design is an original louver system that incorporates a CPC profile. The louvers, when combined with the refractive rods and ceiling elements, form an effective daylighting system which meets the goals laid out in Section 1.3.

The steps below outline the profile definition process for the Soralux louver. Figure 4.6 illustrates these steps.

a) Create the basic CPC profile, using Equations 4.1 through 4.5 (Figure 4.6(a)).
b) Rotate CPC counterclockwise (for the CPC orientation shown in the picture) by $\theta_{max}$ (Figure 4.6(b)).
c) Add a parabola with a vertical axis of symmetry using the left end of the upper CPC section as the focus and the left end of the lower CPC section as a point on the parabola (Figure 4.6(c)).
d) Move upper CPC section vertically downwards far enough so that there is a small gap between the right ends of the two CPC sections (Figure 4.6(d)).
e) Add a straight line connecting the right ends of the upper and lower CPC sections. The angle of this line with respect to horizontal must be equal to or greater than $\theta_{max}$ to prevent downward reflected rays (Figure 4.6(e)).
f) Add a line starting at the left end of the new lower CPC profile and connect it to the parabola created in step (c). The closer this line is to 45° from horizontal the better, but the point where

the line intersects the parabola can be freely chosen. This completes the louver outline (Figure 4.6(f)).

g) To locate the louvers with respect to one another, copy and move the completed louver outline vertically upwards or downwards from the original's location by the same amount as the CPC section was moved in step (d) (Figure 4.6(g)).

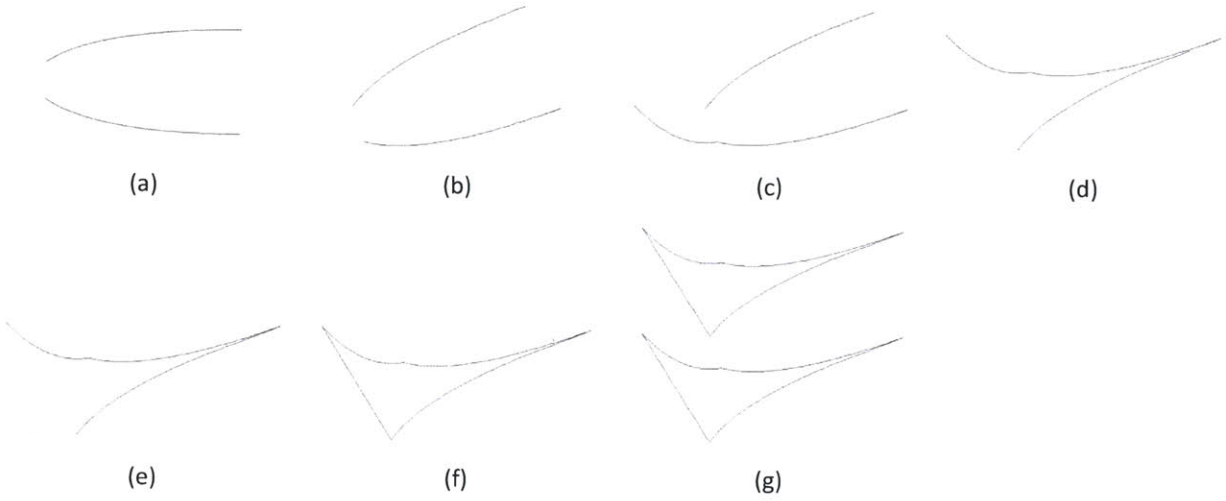


Figure 4.6: Steps to Create the Soralux Louver Profile

The profile shown here and in the following section is the ideal shape, with the profile coming to a sharp point at either end. Manufacturing capabilities will likely require a larger minimum thickness. In that case, the distance in step (d) can be increased accordingly.

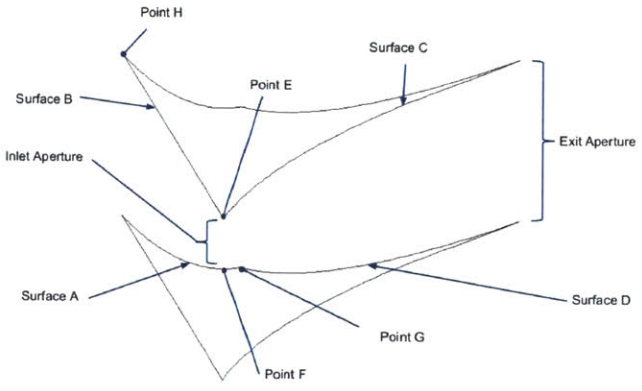


Figure 4.7: Important Features of the Soralux Louver

To understand how the louver array works, it helps to think in terms of the geometry of the channel created between two louvers, rather than the geometry of the louver itself. There are four surfaces that

make up this channel, as shown in Figure 4.7. It can be seen that, viewed together, Surfaces A, C, and D form a profile similar to the Zenithal Anidolic Collector. All outer surfaces of the louver have a specular mirror-like finish.

### a) Surface A

Surface A is a parabolic curve, used to collect incident light and redirect it through the small Inlet Aperture. The nature of the parabolic profile ensures that any light ray which strikes the parabola with an elevation angle less than or equal to 90° will successfully pass through the inlet. In other words, the ray must be moving toward, rather than away from, the louver Exit Aperture when it hits Surface A. This effect occurs because the vertex of the parabola (Point F) is located directly underneath the focus (Point E) at the proper distance so that the curve of the parabola intersects the end of Surface D (Point G). Figure 4.8(a) shows the definition of the elevation angle and an example of a ray with an elevation angle of 90°, after it reflects off Surface B, which barely makes it through the inlet.

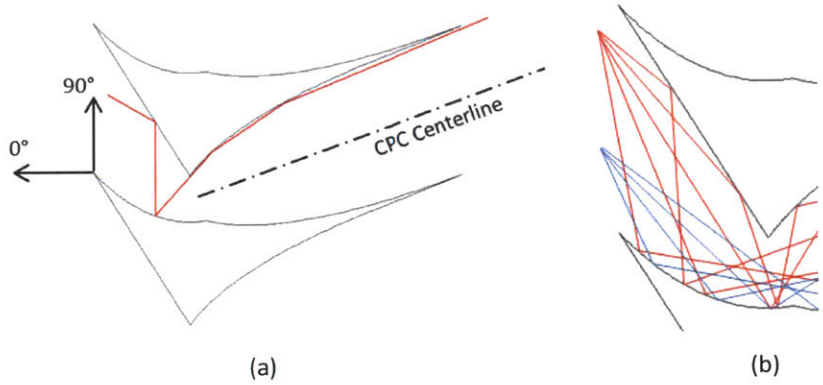


Figure 4.8: Example of a Ray that Barely Passes Through Inlet (a); Rays Reflecting Off Surface A Through Inlet (b)

The design differs in this regard from the Zenithal Anidolic Collector. With the Zenithal Anidolic Collector, the CPC (Surfaces C and D) is not tilted upward as it is in this louver design. With the Zenithal Anidolic Collector design, the end of the Surface D is located directly underneath the end of Surface C. For the Zenithal Anidolic Collector, the vertex of the parabolic light scoop (Surface A) is simply located at Point F, and the resulting profile for Surface A is exactly half of a full parabola. However, in the case of the Soralux louver, the end of Surface D (Point G) does not fall directly underneath the end of Surface C (Point E). The choice was made to keep the vertex of Surface A (Point F) directly underneath the end of Surface C (Point E). The parabolic profile of Surface A was defined so that its focus was located at the end of Surface C (Point E) and so that it also intersected the end of Surface D (Point G). This choice of

profile maximizes the distance from the parabola's vertex to its focus, which minimizes how steeply the parabola curves upwards. This is important because the steeper the curve of the parabola, the more low-angle light will be rejected, since Surface B would have to be tilted at a steeper angle for it to intersect with the steeper parabola.

### b) Surface B

Surface B is the simplest of the four louver surfaces, as it is planar, rather than parabolic. Its purpose is analogous to that of the backboard of a basketball goal. Incoming light that bounces off Surface B is redirected toward Surface A, as shown in Figure 4.9. As long as a reflected ray leaves Surface B at an elevation angle less than or equal to 90°, it will strike the parabola of Surface A and enter the Inlet Aperture (refer back to Figure 4.8(a) for an example of such a ray). Without surfaces A and B, only a small fraction of the light hitting the facade would enter the Inlet Aperture, as the rest would be lost in the interstitial space between adjacent Inlet Apertures.

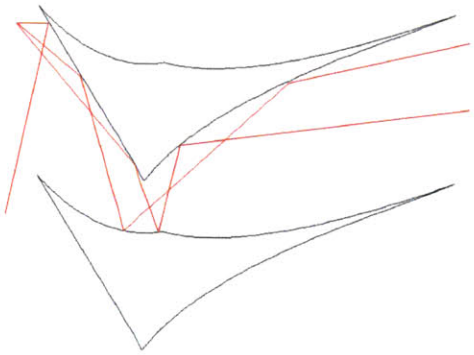

Figure 4.9: Example Rays Reflecting Off Surface B

As mentioned above, the angle of Surface B with respect to horizontal controls how efficiently low-angle light passes through the louvers. Ideally, the angle of Surface B with respect to horizontal would be 45° so that horizontal light would be reflected off Surface B directly downwards onto Surface A. In that case, any incoming light with an elevation angle of 0° or greater would be successfully passed into the Inlet Aperture.

In the louver design proposed here, the angle of Surface B with respect to horizontal is 58.9°, rather than 45°. This increase in angle is necessary to make Surfaces A and B of the same louver intersect at Point H. As a result, the majority of light rays normal to the facade in the azimuth direction and incoming at an elevation angle less than a 27.8°, referred to as the cut-off angle, are rejected by the outer half of

the louver. With this type of louver design, there is a direct connection between the maximum output angle and the cut-off angle. The tighter the output light's angular range is the higher the cut-off angle will be. For an urban setting, the impact of losing light from near the horizon is less significant than it otherwise would be because the urban surroundings will often block the view to the bottom portion of the sky. It should also be noted that for light rays that are not perpendicular to the facade, the projected elevation angle is increased, meaning that a significant portion of light coming in at less than a 27.8° elevation angle also passes through the louvers successfully. This effect is explored further in Section 4.2.4.

### c) Surfaces C and D

The profiles of Surfaces C and D are governed by the equations in Section 4.2.1. The maximum output angle for the chosen design was 20°. All light exiting the louvers will be within plus or minus 20° of the centerline of the CPC, as shown in Figure 4.10. Twenty degrees was chosen as a compromise between the competing factors of the angular range of exiting light and the cut-off angle. The CPC surfaces are tilted upwards by 20° to prevent them from allowing downward traveling rays which would cause glare when exposed to direct sun. Consequently, the output range for light emitted from the louvers is between 0° and 40° above horizontal, regardless of the incoming direction of the light.

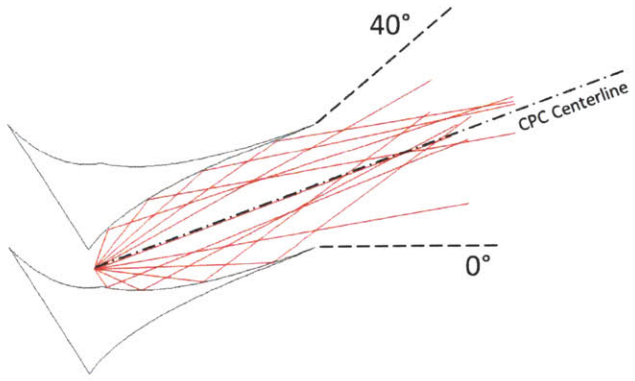


Figure 4.10: Example Rays Reflecting Off Surfaces C and D

## 4.2.3 Ray Paths Through the Louvers

Figure 4.11 also shows how incoming rays at different positions and elevation angles will be redirected by the louvers. Light travels from left to right in the images. Notice that of all the ray paths traced in the images, none exits the louver channel at an angle less than 0° above horizontal. The images also illustrate how some low-angle incoming light is rejected by the louver inlet and bounces back outside.

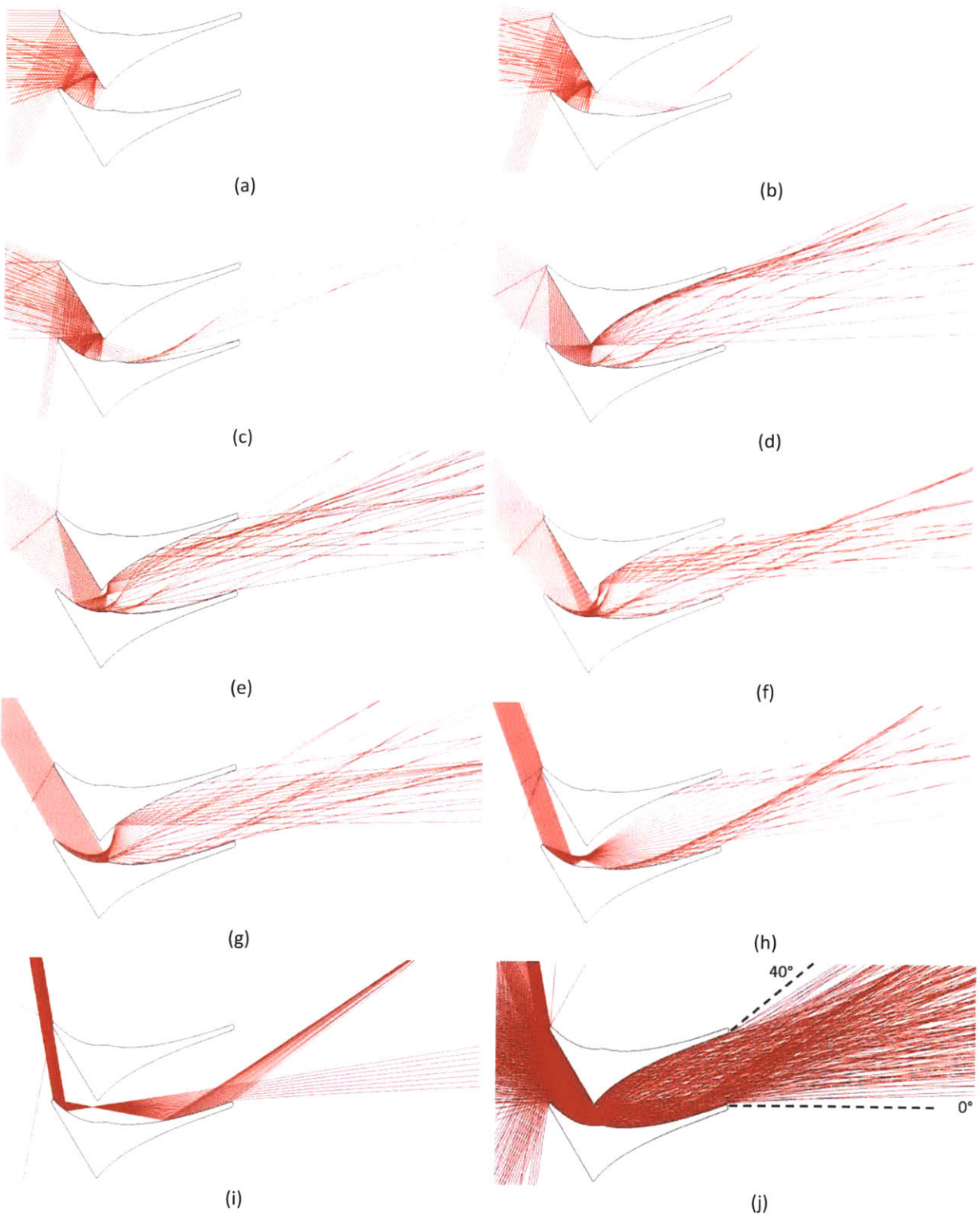


Figure 4.11: Ray Tracing Through Louvers for Varying Elevation Angles: 0° (a), 10° (b), 20° (c), 30° (d), 40° (e), 50° (f), 60° (g), 70° (h), 80° (i), Superposition of All Angles (j)

A question arises when looking at the images in Figure 4.11: what happens to rays that are out of plane, rather than in plane, with the louvers' cross-section? On this matter, Winston et al. explain that

> the ray tracing in any 2D trough-like reflector is simple even for rays not in a plane perpendicular to the length of the trough. This is because the normal to the surface has no component parallel to the length of the trough, and thus the law of reflection can be applied in two dimensions only. The ray direction cosine in the third dimension is constant. Thus, if [a diagram] shows a 2D CPC with the length of the trough perpendicular to the plane of the diagram, all rays can be traced using only their projections on this plane (2005, pp.53-54).

Based on this understanding, if the 2D ray path diagrams show that for any incoming ray direction no rays are directed downward at the outlet, the same will be true for any incoming ray direction in 3D as well.

### 4.2.4 Effect of Azimuth Angle on Cut-Off Angle

As seen in Figure 4.11 above, the inlet of the louver channel rejects a large portion of incoming light with a low elevation angle. For light that is normal to the facade ($\alpha = 0$), the cut-off elevation angle below which light reflecting off of Surface B will be rejected is 27.8°. As mentioned previously, for an urban setting such as Tokyo, the impact of losing light from near the horizon is less significant than it otherwise would be because the urban surroundings will often obstruct the view to the lower portion of the sky.

The importance of this limitation is further reduced by the fact that the cut-off angle is at its maximum when light is normal to the facade and reduces in magnitude as the azimuth angle of the light increases. As discussed in Section 4.2.3, rays that are not normal to the facade can be accurately ray traced by projecting their path onto a plane normal to the facade. However, as the azimuth angle ($\alpha$) between the facade and the light increases, the projected elevation angle ($\phi$) will also increase. Figure 4.12 illustrates the relevant geometry. Notice how, for a constant elevation angle ($\eta$), increasing the azimuth angle ($\alpha$) will result in an increase in the projected elevation angle ($\phi$). If a ray's projected elevation angle ($\phi$) is greater than the cut-off angle ($\eta_c$) then it will successfully pass through the louver.

The derivation of the relationship between $\eta$, $\phi$, and $\alpha$ is shown in Equations 4.6 through 4.10 below. Figure 4.12 provides the definition of the variables found in these equations. The cut-off elevation angle ($\eta_c$) as a function of $\alpha$ can be found from Equation 4.10. For this particular design, $\phi$ equals 27.8°.

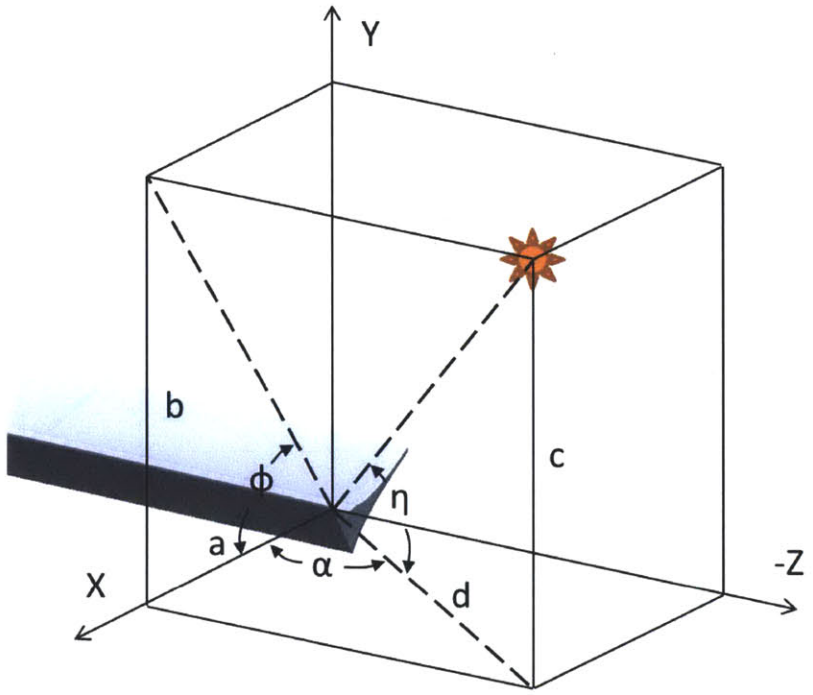


Figure 4.12: Geometry of Elevation Angle (η), Projected Elevation Angle (ϕ), and Azimuth Angle (α)

$$\tan\phi = \frac{b}{a} \qquad \text{Equation 4.6}$$

$$b = c \qquad \text{Equation 4.7}$$

$$\cos\alpha = \frac{a}{d} \qquad \text{Equation 4.8}$$

$$\tan\eta = \frac{c}{d} = \frac{b}{d} = \frac{a\tan\phi}{\frac{a}{\cos\alpha}} = \tan\phi\cos\alpha \qquad \text{Equation 4.9}$$

$$\eta = \tan^{-1}(\tan\phi\cos\alpha) \qquad \text{Equation 4.10}$$

A review of Figure 4.13 shows that the cut-off angle declines slowly at first but continues to fall faster as α increases from 0 to 90°. Figure 4.14 shows the cut-off angle plotted on the Tokyo sun chart for a south-facing facade. This figure highlights the importance of determining the behavior of light in 3D rather than only 2D. The solid black line represents the cut-off angle as it has been defined in this section and the dashed black line represents what the cut-off angle would have been incorrectly thought to be if it had been assumed that the simple 2D case where α = 0 applied to all azimuth angles. This effect is especially useful for south-facing facades because the sun will be lower in the sky at high azimuth angles.

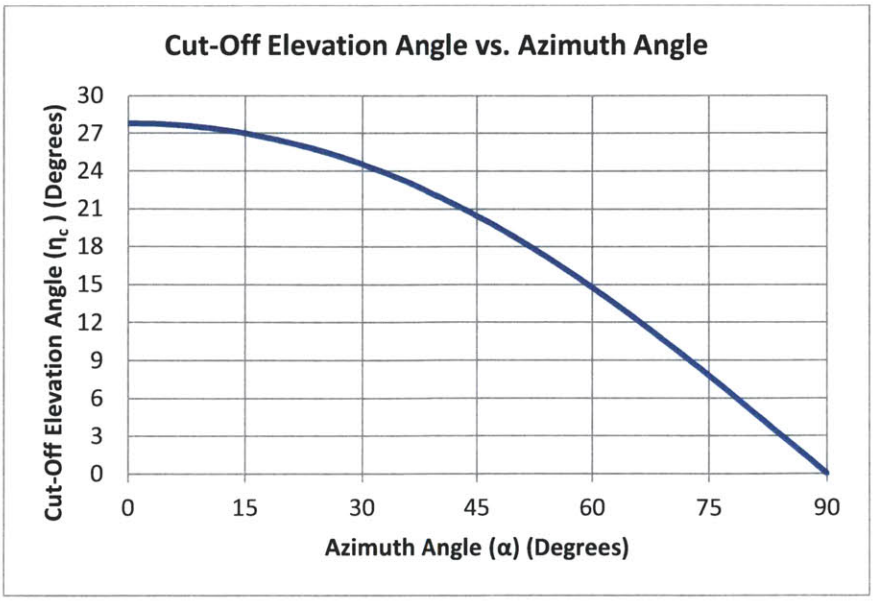


Figure 4.13: Cut-Off Elevation Angle as a Function of Azimuth Angle

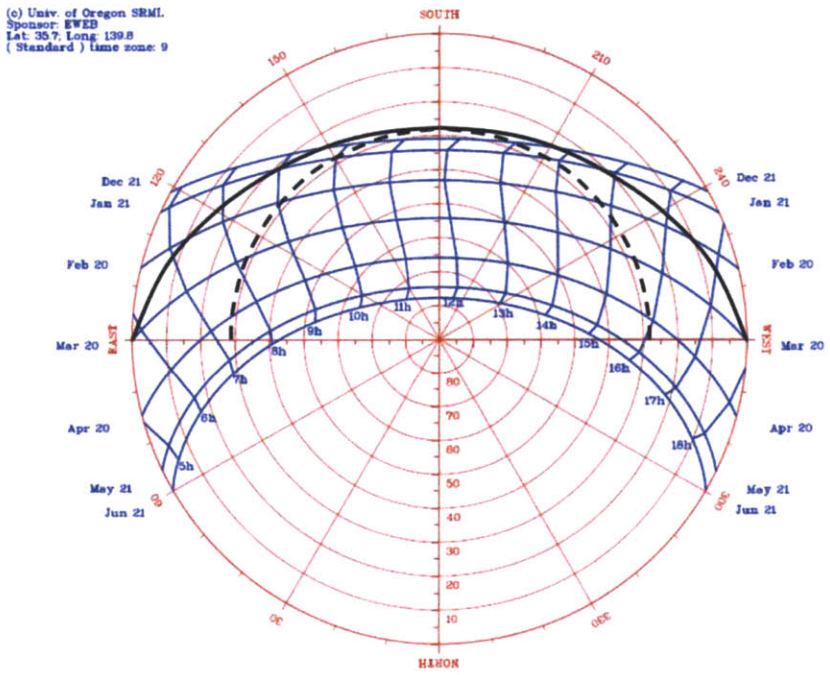


Figure 4.14: Actual Cut-Off Angle (Solid) and Constant Elevation Angle of 27° (Dashed) for a South-Facing System Using Tokyo Sun Course Chart (Adapted from UO Solar Radiation Monitoring Laboratory, 2008)

As latitude increases, the average position of the sun in the sky decreases. Consequently, the cut-off angle begins to become more of a problem, as direct sunlight is rejected over a larger portion of annual daylit hours. However, the use of direct sunlight for daylighting an urban setting far from the equator is

problematic to begin with because the low rising sun will frequently be occluded by the urban surroundings. If, in a northerly city such as Stockholm, Sweden (latitude: 59.4°), sky obstructions were not the limiting factor for direct sunlight access, a different variant of the louver design might be more appropriate. Figure 4.16(a) shows another variant of the louver with a cut-off angle of 19.6°. This lower cut-off angle will allow more low-angle sunlight to be used. However, reduction in cut-off angle comes at the expense of an increase maximum output angle, which would reduce the light's average depth of penetration into the room.

Globally, most large cities are located between 30°N and 60°N latitude. Tokyo, Japan is an example of a major city within this range of latitudes at 35.7°N. For a south-facing facade with Tokyo's latitude, the standard Soralux louver's 27.8° cut-off angle does not present much of a problem, as the sun remains above the cut-off angle for the large majority of daylit hours. The same logic applies to north-facing facades in the Southern Hemisphere.

When the sun is below the cut-off angle, near sunrise or sunset, the system will reflect sunlight back into the building's surroundings. This reflected sunlight has the potential to cause uncomfortable glare for people outside the building. This problem is expected to be minor for several reasons.

1. Outwardly reflected light can only occur near sunrise or sunset and, depending on the orientation, only for certain times of the year.
2. The brightness of the sun is much lower near sunrise and sunset than it is at mid-day.
3. The size of the bright area on the louver array as seen from any single location will be limited because light is reflected in many different directions.
4. The frequency and duration of these periods will be further limited by the presence of surrounding sky obstructions.

### 4.2.5 Additional Louver Details

Figure 4.15 shows the relative positions of two louvers in the vertical array with their major dimensions. The absolute size of the louver cross-section can be increased or decreased, but the ratio of the dimensions must remain the same for the device to function properly. The louvers have a constant cross-section in the direction normal to the page.

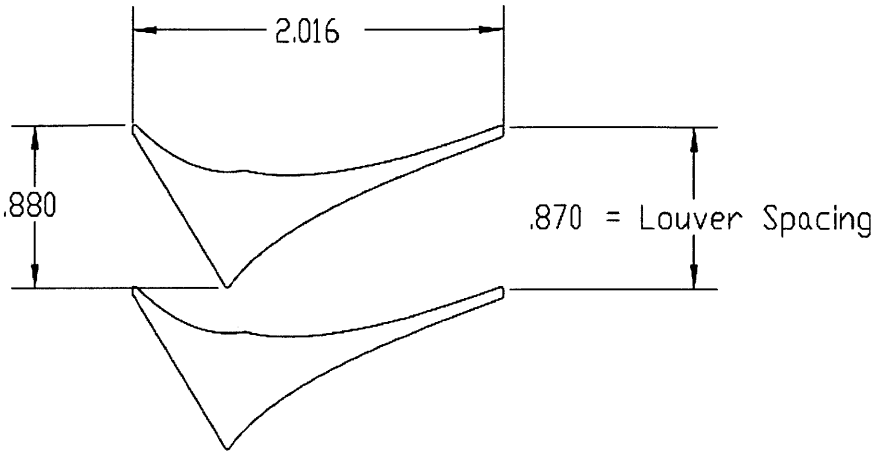


Figure 4.15: Major Soralux Louver Dimensions (Units in Inches)

The width of the louvers was targeted for approximately 2 inches to minimize the number of individual louvers required to fill a clerestory window, while also keeping the window unit relatively thin. Also, as the louver's size is decreased minimum material thicknesses and dimensional tolerances become more problematic. Although the ideal louver shape would have both ends of the cross-section come to sharp points, this shape is not easily producible. To improve the manufacturability of the louver the minimum thickness was set to 1.5 mm. The aspect ratio (width/pitch) of this variant of the Soralux louver is 2.32, which compares favorably to the 2.75 aspect ratio of the LightLouver (described in Section 3.5). To fill the same volume of window area, 19% more individual LightLouvers would be required compared to Soralux louvers.

### 4.2.6 Variations on the Design

In choosing between different louver variants, there is a tradeoff which must be decided based on the needs of the user. As the maximum output angle is reduced (which is desirable in order to push light deeper into the space) the amount of light rejected at the inlet increases and the spacing, or pitch, between louvers decreases, as shown in Figure 4.16. Louver-to-louver pitch is important because it determines how many louvers are required to fill a given facade height, which in turn will affect the production costs of the system. For this thesis, the design shown in Figure 4.16(b), with a maximum output angle of 40°, was chosen for detailed analysis and prototyping because it presented a good balance between maximum output angle and cut-off angle.

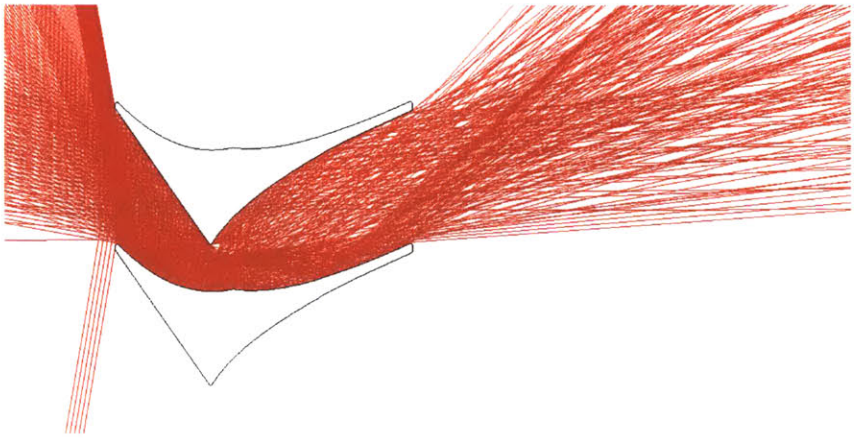

(a)

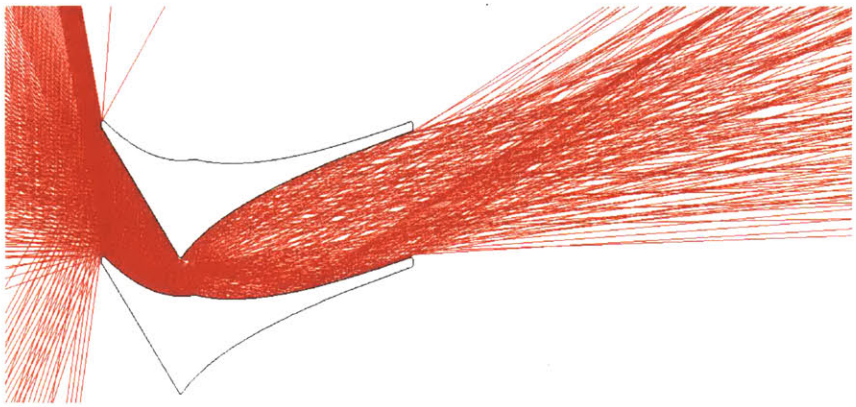

(b)

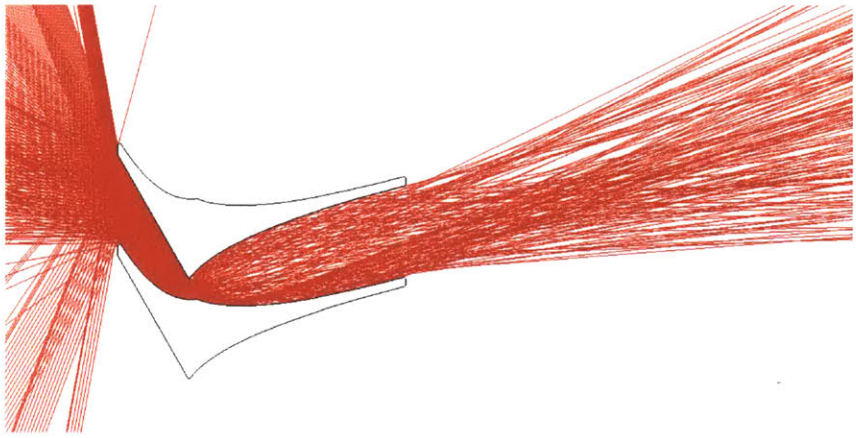

(c)

Figure 4.16: 50° (a), 40° (b), and 30° (c) Maximum Output Angle Louver Variants

### 4.2.7 Louver Production

The two classes of engineering materials that are potentially suited to make up the louver body are metals and polymers. The choice of material and manufacturing processes are coupled because the selection of one limits the options for the other. Metals have high stiffnesses, high melting points, and are very durable under sunlight. Polymers have lower densities and potentially enable lower cost production. Aluminum was identified as the leading candidate of the metal materials, due to its low density relative to other metals, ease of manufacturing, and ready availability. No attempt was made to identify the most promising polymer.

Both material types have potential issues that need to be investigated. Aluminum has a high coefficient of thermal expansion for metals of approximately $2.2 \times 10^{-5}$ m/mK. The coefficient of thermal expansion for polymers is even higher than aluminum. Depending on the range of temperatures seen inside the window unit, the louver could distort enough from thermal stresses to cause glare from stray light rays. The durability of polymers under sunlight over an extended period of years would have to be evaluated. Also, in a sealed window unit, there is the potential for molecules outgassed by the polymer to collect on the glazing surfaces over time, potentially fogging the glass.

The MIT mockup louvers, described in Section 6.1, were made of ABS plastic. This was the material used by the 3D printing machine used to produce the louvers so there was no choice of material involved. For the Tokyo mockup, described in Section 6.2, the louvers were made from Aluminum alloy 6063-T5, a good material for extrusion.

Extrusion is the manufacturing process that is likely to result in the lowest cost to produce large quantities of the louvers. With extrusion, molten material is pushed through a specially shaped die which determines the part's final shape. Because the louvers have a constant cross-section, a continuous process like extrusion can make very long louver sections rapidly which can then be cut to size. The biggest question around using extrusion is the difficultly of achieving tight tolerances on the produced parts (Kalpakjian & Schmid, 2001). An accurate louver profile is critical to ensuring that light is reflected in the proper directions.

Other major manufacturing methods that could be used include injection molding (for polymers) or die casting (for metals). In these processes, molten material is injected into a closed die. The die is shaped such that when the material fills the cavity and cools, it has the desired final shape. These are batch,

rather than continuous processes, so the production rate is lower. A significant drawback to this approach is that the louvers would have to be made in smaller spans which would then be joined together. However, these processes can achieve tighter tolerances than with extrusion, resulting in a more accurate final profile (Kalpakjian & Schmid, 2001).

The surfaces of the louver should be both highly reflective and highly specular to maximize the overall transmittance of the light redirecting system. The importance of a high reflectance value is amplified by the fact that most light rays reflect multiple times on their way through the louver channel. Figure 4.17 shows the impact on effective reflectance for light that bounces off the louvers multiple times. A seemingly small increase, or decrease, in reflectance can have a large effect on the total percentage of incident light transmitted through the system.

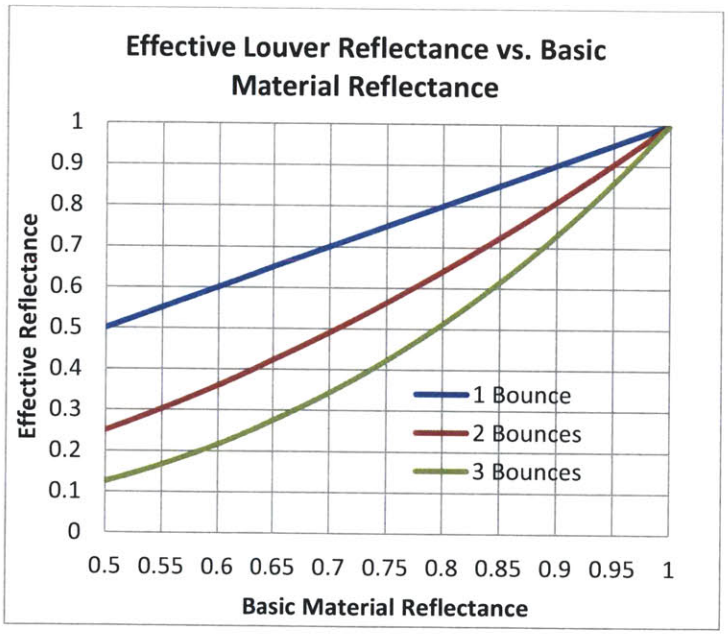


Figure 4.17: Effective Reflectance for Multiple Bounces Off Louver Surface

Although a higher reflectance is better purely in terms of total daylight transmitted, there are two other considerations which counterbalance this factor. First is cost. Generally speaking, a higher surface reflectance requires a more expensive production process. Second, since the Soralux system operates under a wide range of input illuminances, care must be taken so that the reflective ceiling, at its brightest, does not cause disturbing glare. It is possible that increasing the reflectance above a certain level is not warranted because it will lead to increased glare under direct sun.

There are several options available to make the outer surfaces of the louver reflective:

a) Finely polish the louvers to make their outer surfaces highly reflective. This can only be done if a metal such as aluminum is used as the base material. Several techniques exist including mechanical polishing, chemical mechanical polishing, and electropolishing (Kalpakjian & Schmid, 2001).

b) Use a particle vapor deposition process to coat the louver in a reflective material, possibly aluminum or silver. Metals or polymers could be used as the base material. This process is expensive relative to the others considered.

c) Apply an adhesive backed-reflective film to the outer surfaces of the louver. The formation of small air bubbles under the film during application is a concern, as is the film's durability over the lifetime of the system.

Final determination of materials and production process will depend on the volume of systems to be produced and a detailed producibility analysis is beyond the scope of this work.

## 4.3 Refractive Rods

The louvers spread the elevation angle of the incoming light but they do not spread the light's azimuth angle. Without the inclusion of the refractive rods, under direct sun, the reflective ceiling will exhibit a bright streak located on a line between the occupant's eyes and the sun (see Appendix C). The visual effect is similar in appearance to the reflection of sunlight off the surface of a moving body of water, such as a river. During testing of the MIT mockup (discussed in Section 6.1.2) a maximum brightness of about 350,000 candelas/$m^2$ (or .02% of the luminance of the sun at mid-day) was observed on the ceiling when using the louvers without the refractive rods. While not debilitating if not at the center of the field of vision, this level of luminance was deemed to be much too high for an office environment.

### 4.3.1 Operation of Rods

To mitigate glare concerns, a horizontal array of optically clear rods, made of either highly transmissive acrylic or glass are placed at the outlet of the louvers. These elements act as cylindrical lenses which spread the light in the azimuth direction, without affecting the light's elevation angle. Under direct

sunlight conditions, the bright streak on the ceiling seen without the rods is replaced with a much larger area of lower brightness. Diffusing direct sunlight in this manner helps prevent glare from being an issue. The total amount of light in the room is modestly reduced by adding the rods, but the glare protection they provide justifies their inclusion in the design. An evaluation of the rods' location in the window unit is provided in Section 5.4.2.

The recommended material for the rods is acrylic because it does not yellow from exposure to direct sunlight. It is also less brittle than glass and has a relatively low density. Acrylic is used in applications such as airplane windows, where the material is exposed to sunlight for an extended period of years. However, additional investigation is needed to confirm the suitability of acrylic for the proposed daylighting application.

Figure 4.18 provides an illustration of how the rods affect light passing through them. The images show a top view looking down the length of the rods. The light rays traced have a 0° elevation angle. Light with a different elevation angle will travel a somewhat different path through the system, but these images give an idea of the effect of the rods. Figure 6.5 on page 105 demonstrates the effect of the rods on a physical mockup of the daylighting system.

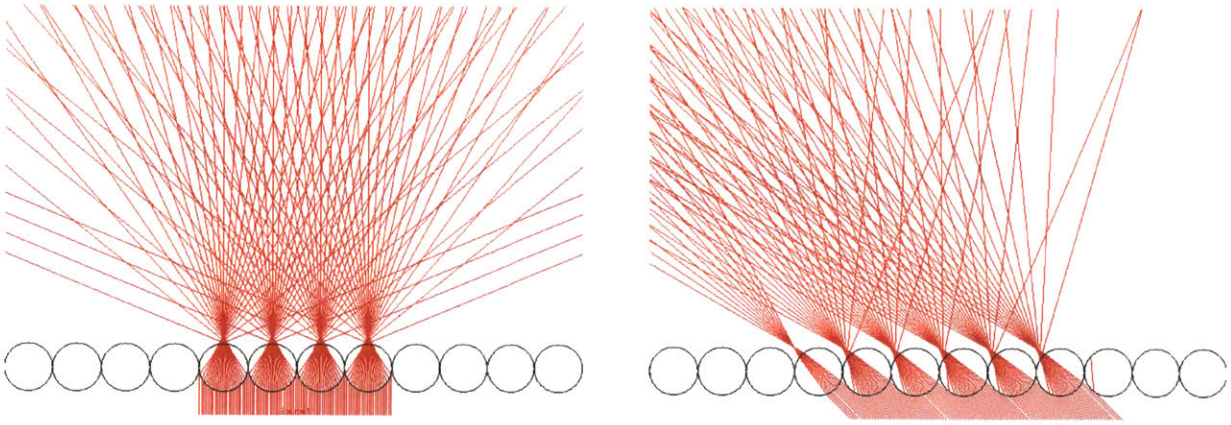

Figure 4.18: Ray Tracing Through Transparent Rods

The main advantage to using refractive rods over other light diffusing technologies is that the rods spread light out in the azimuth direction, without impacting the light's elevation angle. This is important because the light exiting the louvers has been collimated in the elevation direction. Other technologies, such as translucent glass, diffuse light in all directions and have a lower overall transmittance than the clear rods. If the cylinders could be made into a structurally sound inner glazing that prevented air

infiltration, the design would be further improved because it would eliminate the transmission losses associated with the inner pane of glass. However, for this design effort, the choice was made to use discrete rods and a separate inner glazing for ease of manufacture, ease of cleaning, and to protect the rods from scratching and dust. Additional refractive shapes considered are discussed in Section 4.3.2.

The diameter of the rods can be chosen based on project constraints. Thinner rods will generally be better because they will weigh less and allow the window unit to be thinner. However, they must not be so thin that breakage is an issue during assembly and installation. Regarding cost, an economic analysis must be conducted based on prevailing product pricing because, although thinner rods are less expensive than thicker ones, more total feet of rod will be required to cover the same length of facade. It is expected that a rod diameter of approximately 10 mm will work well for most applications.

### 4.3.2 Selecting the Shape

Once the idea of using a horizontal array of repeating refractive shapes to provide glare protection was settled upon, the next step was to determine the cross-section of the refractive shapes. A round of brainstorming resulted in a group of different cross-sections for testing using the ray tracing program TracePro. Figure 4.19 shows plan view cross-sections of each of the variants. In each figure, three of the repeating elements are shown to illustrate the pattern formed by the array.

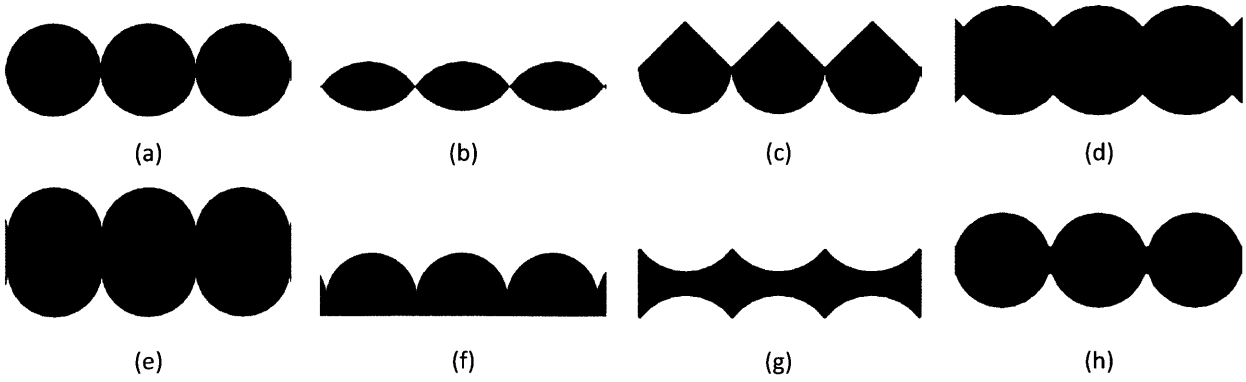


Figure 4.19: Cross-Sectional Profiles for Refractive Element Variants Circle (a), Lens (b), Baseball (c), Smush (d), Stretch (e), Half (f), Concave (g), and Hourglass (h)

The main design objectives evaluated were a) the ability to disperse light in the azimuth direction while b) maintaining a high effective transmittance over a wide range of incoming light angles. Additional considerations were the ease of manufacturing the refractive elements and whether they could eliminate the need for one of the window unit glazings.

The shapes were modeled in SolidWorks and exported to TracePro for analysis. The following list contains the relevant details of the simulation.

- Wavelength used for ray tracing: 555 nm (monochromatic green light).
- Ray trace threshold: for effective transmittance results: .01; for ray trace images: .49. During the ray trace, when rays are broken into multiple subrays, all subrays with an intensity less than the ray trace threshold are terminated. This value was set to .49 for the ray trace images to keep them uncluttered by multitudes of minor rays.
- Effective transmittance was calculated by creating a plane parallel and adjacent to the outlet surface of the refractor and measuring the total flux intersecting this plane as a fraction of the total flux emitted by the source. This was done using the Illuminance Map tool in TracePro. Effective transmittance includes the effects of the separate window glazing, if included in the design.
- For cases which include a separate pane of glass, the glass used has a normal transmittance of 93%.
- For all the variants, the material chosen was acrylic, with an index of refraction of 1.49.
- Total number of rays traced: 997. A prime number was chosen so that the rays would not hit at the exact same places for each instance of the refractor shape.
- The model did not account for losses due to absorption in the material, only reflection and refraction were considered. Absorption losses will be very small for the material thicknesses considered.

### a) Effective Transmittance

Figures 4.20 through 4.22 show effective transmittance results for each refractor variant for a set of incoming light angles. Ideally, the chosen variant would exhibit a high transmittance over the entire range of possible angles.

Because they are composed of an array of discrete entities the Circle, Lens, and Baseball variants require a separate interior glazing to close out the window unit. As a result, the effective transmittance of these variants with and without an additional pane of clear glass is provided in the figures. The remaining variants can potentially function as the interior glazing because they have continuous cross-sections.

The results show that the Circle variant performs the best over the range of angles tested. It maintains a consistently high effective transmittance over all twelve angles tested. However, the Circle design requires a separate pane of glass, which lowers its performance. Lens and Half are dominated by all three variants of Circle, because they perform worse for all twelve angles. Baseball, Smush, and Half Flip outperform Circle by a small amount for some angles, but perform much worse for others. Concave performs similarly to Circle at 0° and 30° azimuth, but worse at 60°. Stretch and Hourglass have transmittances near Circle, but they have other problems which will be described in the next section.

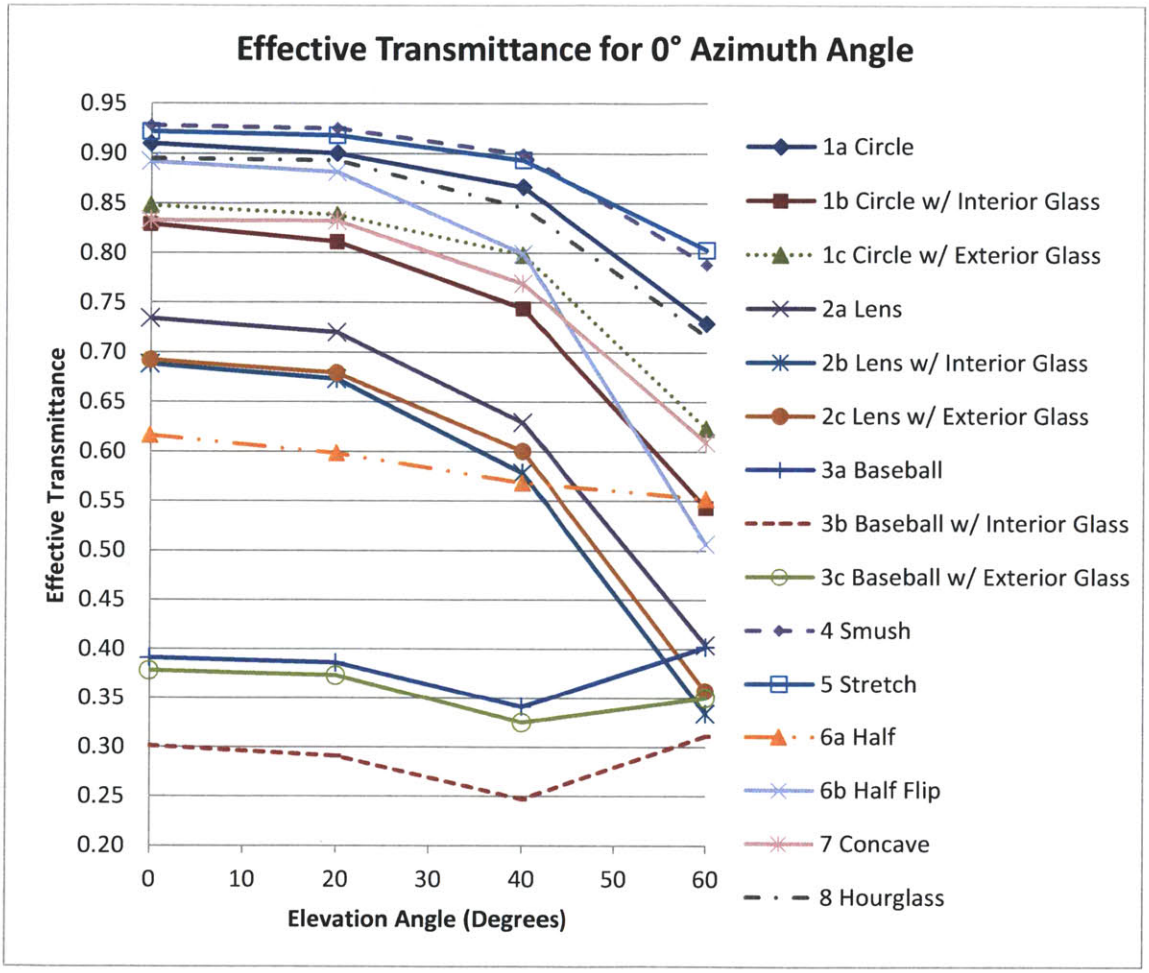


Figure 4.20: Refractive Element Effective Transmittance for 0° Azimuth Angle

### b) Refracted Light Pattern

In addition to the effective transmittance, the pattern of light created by the refractor is important to consider. The following pairs of images show how a beam of collimated light is refracted through each variant for two different incoming light directions.

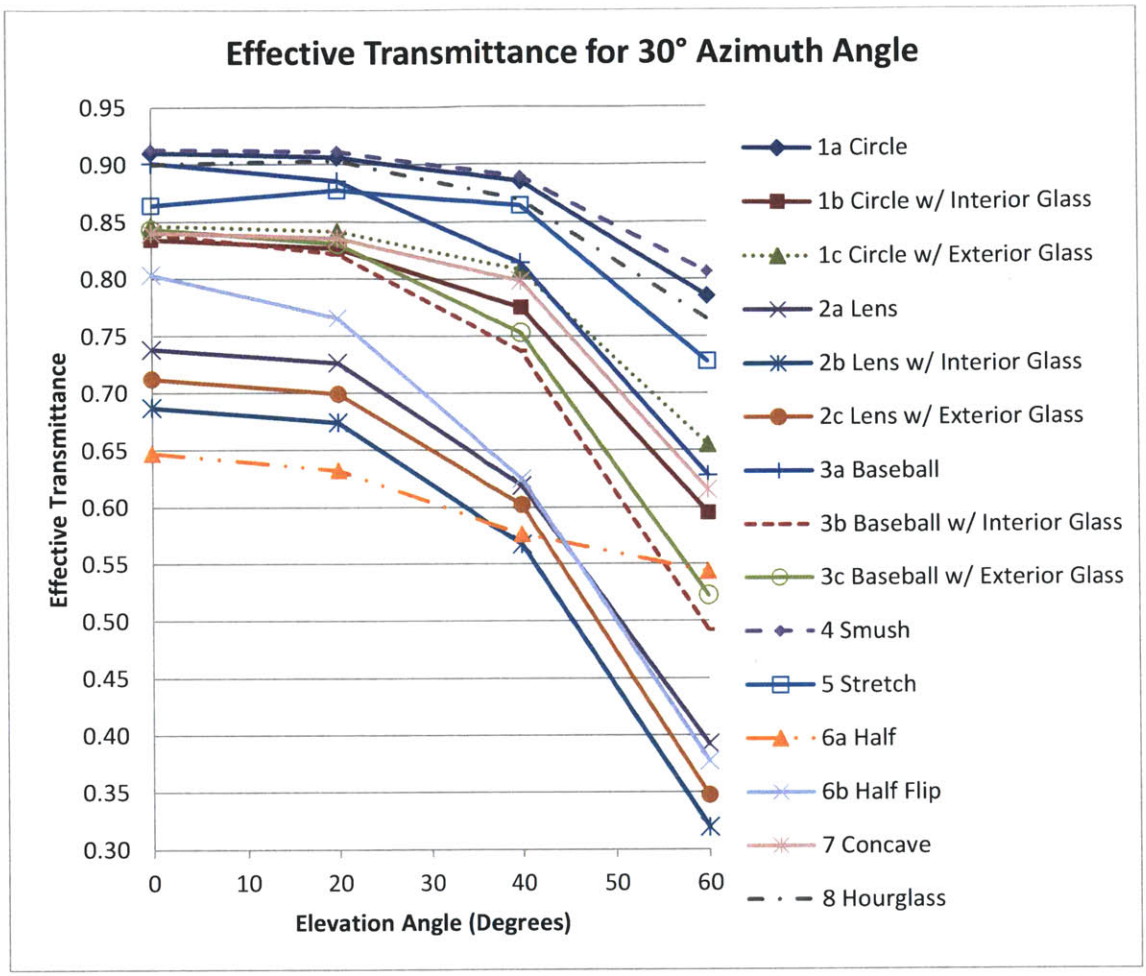


Figure 4.21: Refractive Element Effective Transmittance for 30° Azimuth Angle

There is no single ideal shape for the refracted light pattern, but for this design application the preferred system is one that fans most of the light over an azimuth angle between ±60° from the facade normal. If the azimuth range is too small then the peak brightness on the ceiling associated with direct sun will not be adequately attenuated. If the azimuth range is too large then the amount of light that penetrates deeply into the space will be excessively reduced due to the large light component which is bent close to parallel with the facade.

The Circle refractor shows good light distribution properties. It spreads the light out over a wide angle, as shown in Figure 4.23(a,b), while maintaining a high effective transmittance. An additional beneficial feature is that, when incoming light is at a non-zero azimuthal angle, the Circle design bends the incoming rays so that they are, on average, closer to normal to the facade. This effect allows the light to

penetrate the space more deeply because the direction component parallel to the facade is reduced. A third advantage is that acrylic and glass rods of circular cross-section are widely available for purchase and are relatively inexpensive, eliminating the need for custom part or process development.

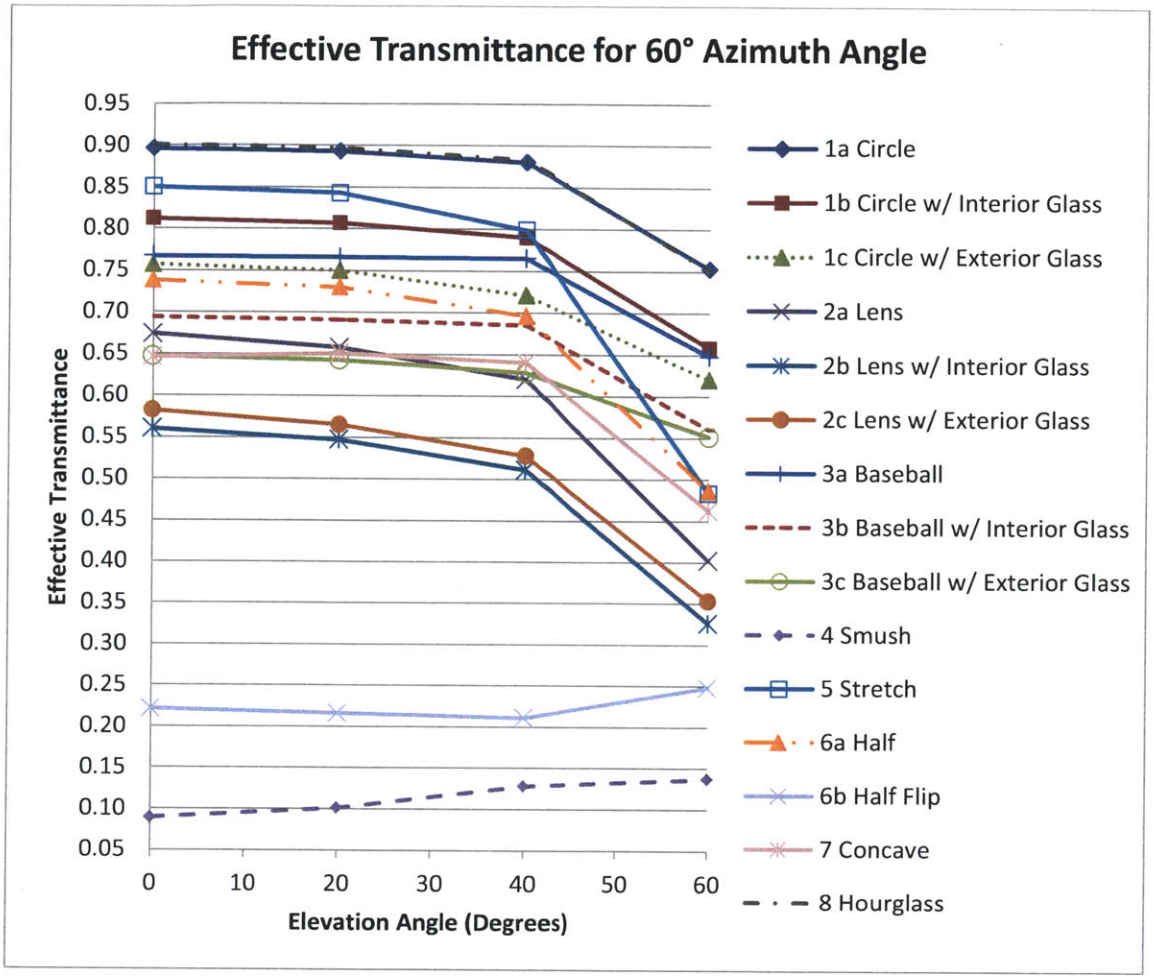


Figure 4.22: Refractive Element Effective Transmittance for 60° Azimuth Angle

The Lens variant, shown in Figure 4.23(c,d), does an adequate job of dispersing the light. However, at high azimuth angles, the design tends to bend light closer to parallel, rather than normal to, the facade. The Baseball design (see Figure 4.23(e,f)) spreads light evenly at high azimuth angles, but at angles near normal to the facade, most of the light is rejected via total internal reflection. The Smush variant, shown in Figure 4.24(a,b), does an excellent job of fanning light out at angles near horizontal, but rejects almost all of the light at high azimuth angles. Similarly, the Stretch design performs well for angles near normal but performs very poorly for high azimuth cases (Figure 4.24(c,d)).

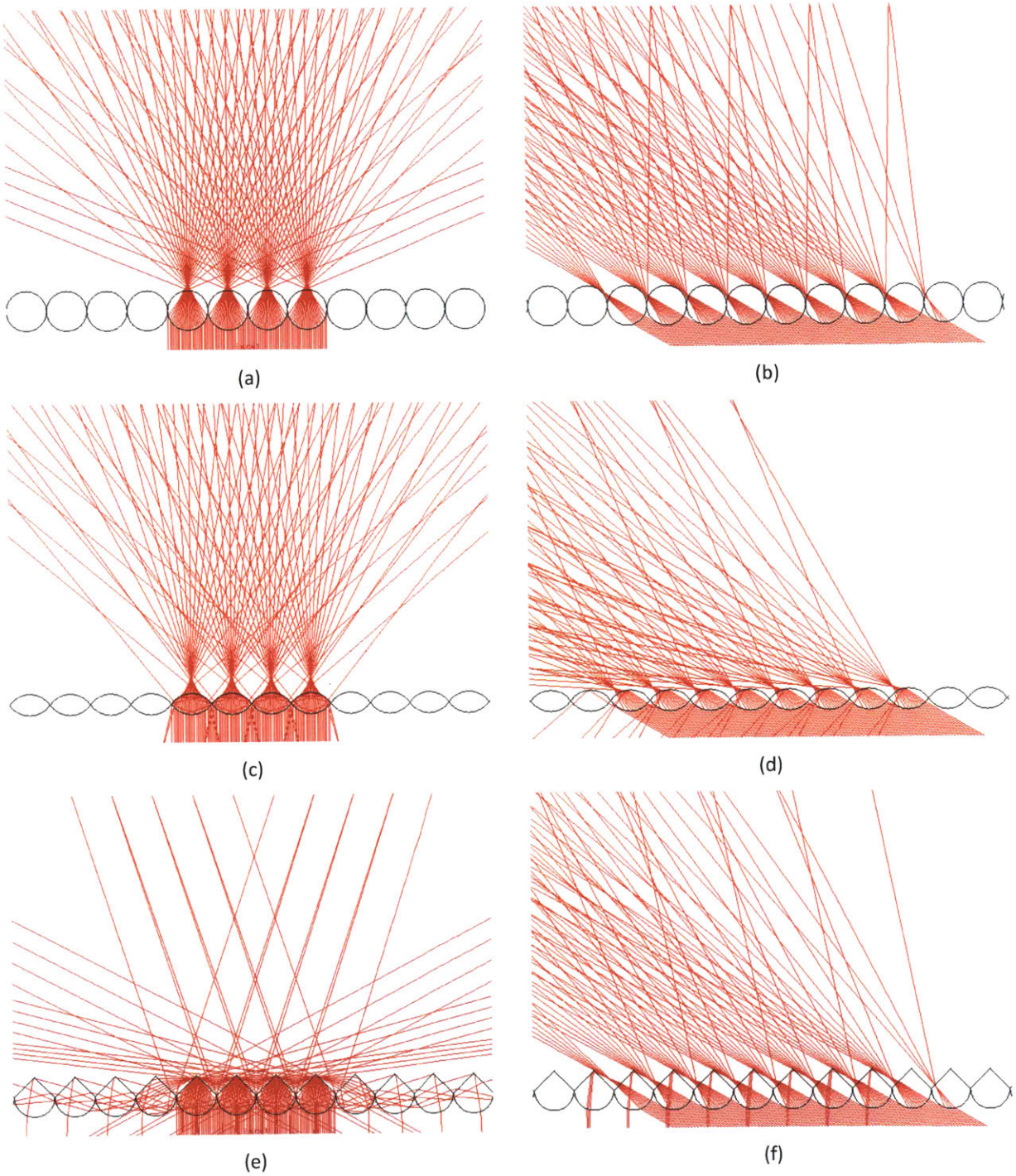


Figure 4.23: Circle (a,b), Lens (c,d), and Baseball (e,f) Variant Transmission Patterns at 0° (Left) and 60° (Right) Azimuth Angles

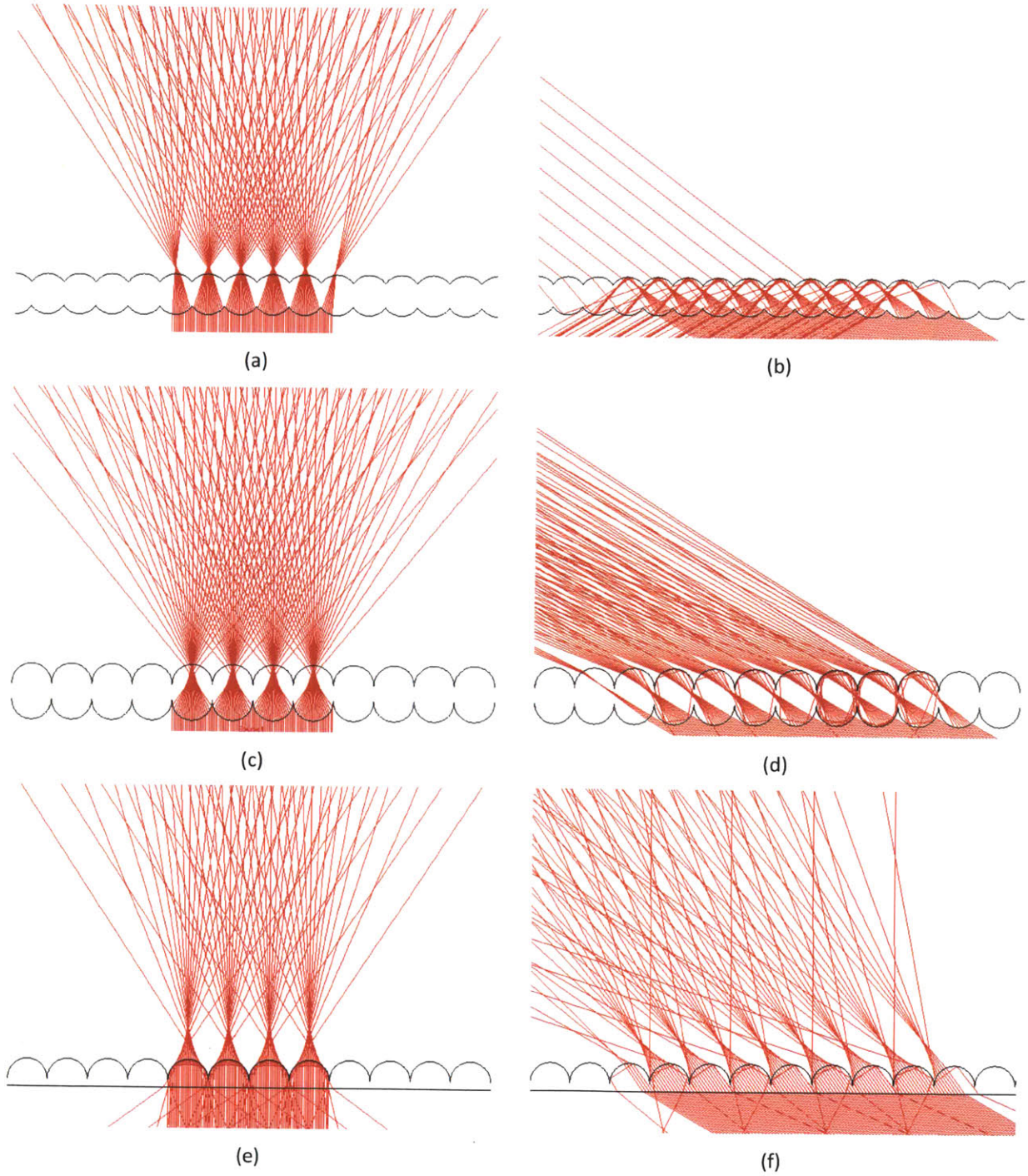


Figure 4.24: Smush (a,b), Stretch (c,d), and Half (e,f) Variant Transmission Patterns at 0° (Left) and 60° (Right) Azimuth Angles

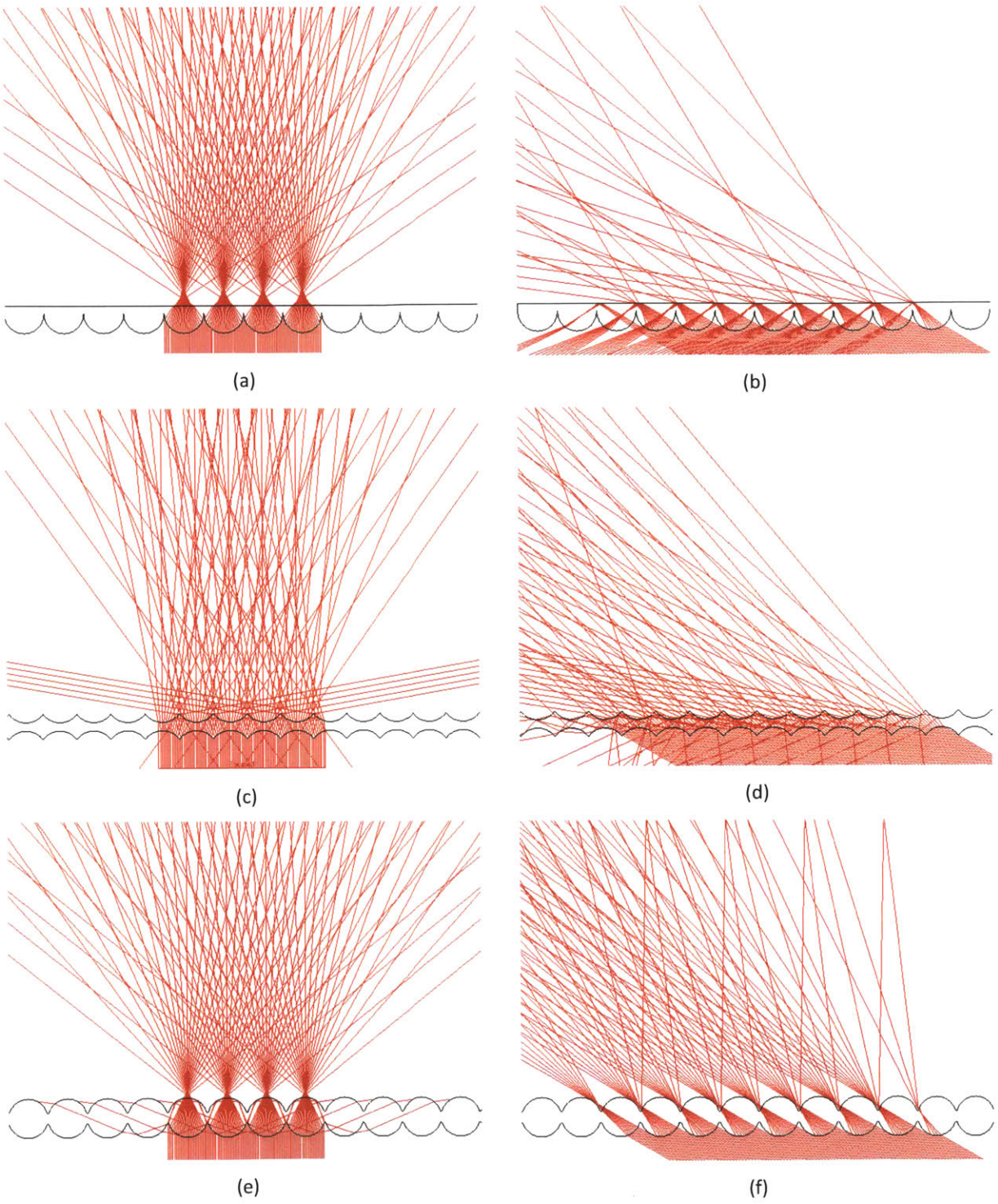


Figure 4.25: Half Flip (a,b), Concave (c,d), and Hourglass (e,f) Variant Transmission Patterns at 0° (Left) and 60° (Right) Azimuth Angles

The Half design has a relatively good output distribution pattern across the range of azimuth angles, as shown in Figure 4.24(e,f). Its main drawback compared to the Circle design is that it consistently transmitted less light due to higher reflectance losses. However, the overall transmittance is high enough that further work on this variant may make it a viable alternative to the Circle design. The major benefit of the Half design is that it could be made as a single piece, rather than an array of separate rods. This would allow the refractor to replace one of the two glazings in the window assembly, which would increase the overall transmittance of the system. One additional concern is that this design does not spread light as widely as the Circle design, which would result in higher peak luminance values on the ceiling. The Half Flip design (Figure 4.25(a,b)) is not a viable alternative as it performs well for low azimuth angles, but poorly for high azimuth angles.

Although the Concave variant does spread out incoming light, it does so in a haphazard manner, as shown in Figure 4.25(c,d). A significant portion of the light is bent nearly parallel with the facade, which prevents the light from passing deeply into the space.

The final variant considered is the Hourglass design (Figure 4.25(e,f)). This design is very similar to the Circle design, except that instead of discrete circles, the circles are merged by forming a thin neck between them. The performance of this design is comparable to that of the Circle variant, but it offers the possibility of being formed as a single piece, rather than as dozens of discrete rods. This single piece could replace the inner pane of flat glass, thereby increasing the transmittance of the system, decreasing its thickness and weight, and offsetting some of the element's cost. However, the difficulty of cleaning in the narrow neck spaces was deemed to be a major problem. Also, the thinness of the neck region, while necessary to maintain the high overall transmittance, might make the pane too fragile during handling and installation.

## 4.4 Reflections Within the Window Unit

Some of the light that is emitted by the louvers is reflected off the refractive layer and the interior pane of glass, rather than being transmitted. This rogue light bounces through the system at all angles and some of it emerges at a downward angle into the room. This effect's potential to cause glare was tested using TracePro. The amount of light exiting the system at a downward angle as a fraction of incident light varied between 3% and 4%, depending on the incident light's elevation angle, as shown in Figure 4.26.

This percentage should also be an upper bound on the actual amount seen, because the louvers' surfaces were assumed to be perfect mirrors with a reflectance of one. The fact that the louvers will absorb a portion of the light means that the actual amount of descending light will be reduced.

During the Tokyo mockup testing, discussed in Section 6.2, this effect was observed and confirmed not to be a glare source. This small portion of light emitted by the system at a downward angle produces, in visual effect, a soft glow, which is aesthetically pleasing.

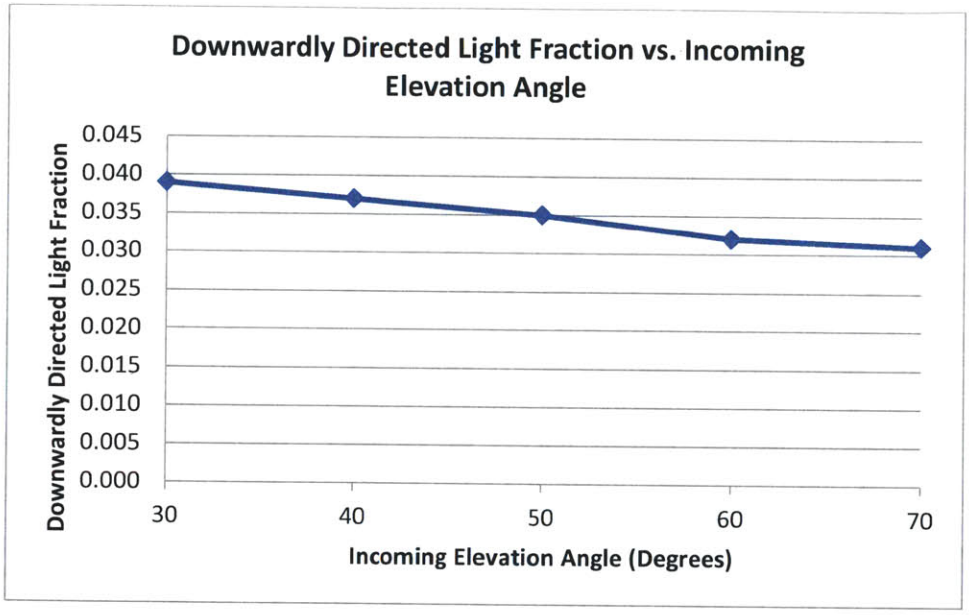


Figure 4.26: Fraction of Incident Light Directed Downward Due to Reflections Within the Window Unit

## 4.5 Reflective Ceiling

The final element of the proposed daylighting system is the reflective ceiling. The greater the distance between a given louver and the ceiling, the deeper the light from that louver will be able to penetrate into the room. However, for most office buildings the ceiling height is limited by the need to maximize rentable space. In light of this constraint, a reflective ceiling can be used to redirect light emitted by the window unit deeper into the space. To limit glare and distracting mirrored reflections on the ceiling that would result from a purely specular surface, the reflective surface has a bumpy texture, which helps to scatter the light without eliminating its directionality (see the spread reflection shown in Figure 4.27).

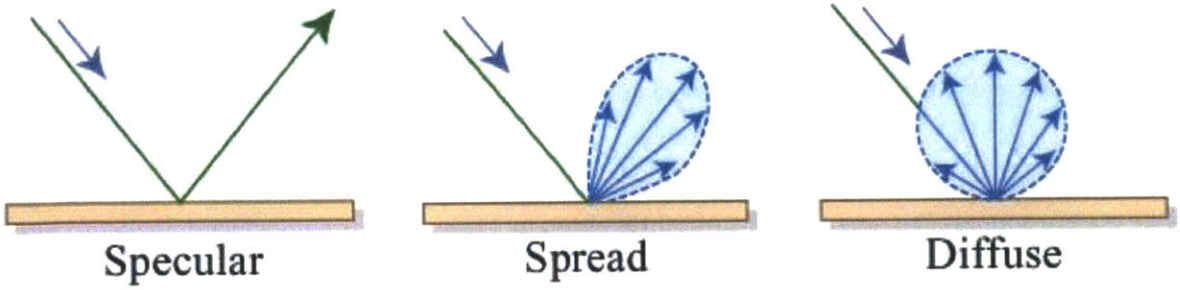


Figure 4.27: Specular, Spread, and Diffuse Reflections (Adapted from MIT OpenCourseWare, 2004)

If the surface of the ceiling had a typical matte or diffuse finish then most of the light exiting the window unit would hit the ceiling near the front of the room and be scattered onto the workplane immediately below. With a diffuse surface, impinging light is scattered in all directions evenly so only a small portion would be reflected off the ceiling deeply into the space. This is true even of light that exits the louvers near horizontal. A diffuse ceiling wastes much of the benefit of the louvers, because the ceiling cannot take advantage of the fact that the light impinges on it at a shallow angle. Using a ceiling with a specular, rather than a diffuse, surface makes the overall system much more effective. Light hitting the ceiling at a shallow angle bounces off at a shallow angle. All the light is directed deeper into the space at a favorable angle, rather than being diffusely scattered. The spreading effect of ceiling material is explored further in Section 6.2.2.

The bumpy ceiling texture, when coupled with the refractive rods, prevents the specular reflection off the ceiling from causing glare by reducing the peak brightness associated with direct sunlight. A practical benefit of the bumpy ceiling texture is that potentially distracting mirror images on the ceiling will not be discernible to the office's occupants. Figures 4.28 and 4.29 illustrate the difference between the ceiling material's spread reflection and a mirrored specular reflection. A pink highlighter is placed on each sample in Figure 4.28. Figure 4.29 shows the reflection of an overhead light fixture for the spread and specular materials.

The deeper the reflective ceiling extends from the daylit facade, the better the performance at the back of the room. However, each additional unit of length provides diminishing returns. The effect of the reflective ceiling's length is evaluated further in Section 5.4.2. The rest of the ceiling beyond the end of the reflective section can use the standard acoustical tile layout.

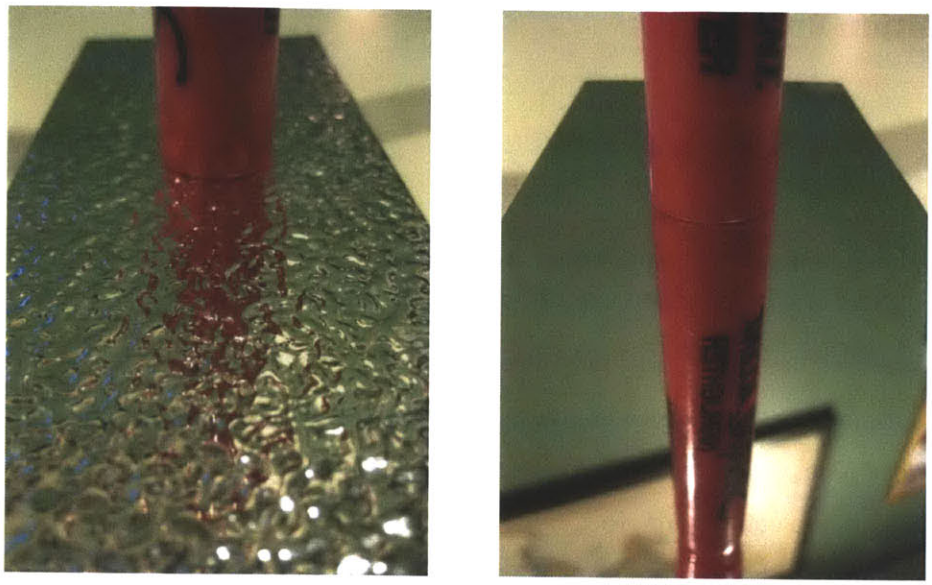

(a) (b)

Figure 4.28: Reflection of a Pink Highlighter off of Ceiling Material (a) and Specular Mirror (b)

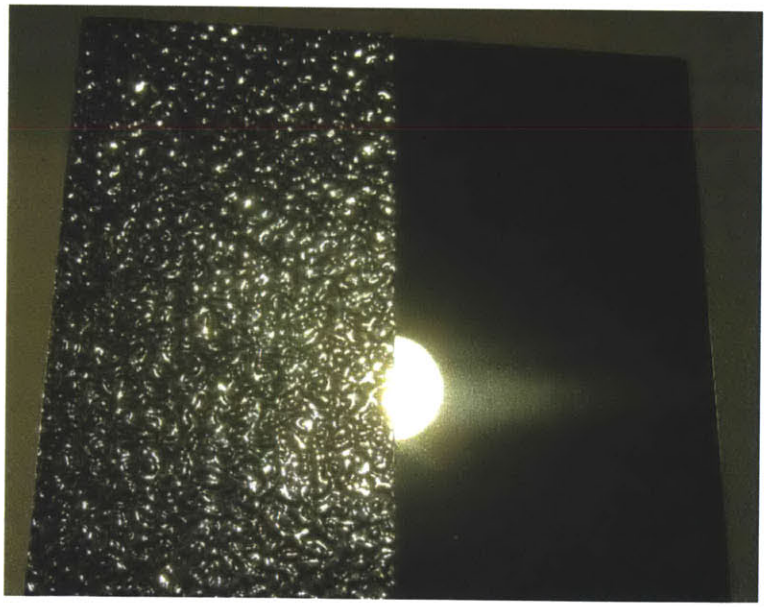

Figure 4.29: Reflection of a Light Source Off of Ceiling Material (Left) and Specular Mirror (Right)

# 5 Simulation Results

## 5.1 Simulation Method

Traditionally, daylighting situations were only evaluated for a few key times of year under generic sky conditions. Although the traditional approach provides useful information, it is not sufficient on its own because the approach does not characterize the behavior of the space over the full year. For example, a set of simulations might be performed at 9am, 12pm, and 3pm on one equinox and both solstices under completely clear skies, with one additional simulation done under a completely overcast sky (Mardaljevic, 2000). Evaluations are often limited to this small set, both because the results are easy to understand and because the time to simulate a full year's worth of weather data at hourly (or more frequent) intervals can be time prohibitive (Reinhart & Herkel, 2000). There are about 4400 daylit hours in the course of a year and generating 4400 renderings or illuminance readings is very computation intensive. An additional drawback to the traditional approach is that, because it uses generic skies, it does not provide any insight into how the weather patterns of a particular location will affect performance.

The needs of this project dictated that a more comprehensive simulation approach be identified. The ideal approach would be able to simulate and report a full year's worth of results in a few minutes to a few hours. In addition, the approach would need to be able to account for site-specific weather patterns in the annual calculations. The ray tracing program Radiance has the capability to meet these requirements. Results are generated quickly using the Daylight Coefficient Method of illuminance calculation. The Daylight Coefficient Method breaks the annual illuminance calculation into two parts, and in doing so, sharply reduces the total calculation time required. The details of the Radiance simulation method are provided in Appendix A and the scripts used to run the simulations are provided in Appendix B.

## 5.2 Initial Feasibility Study

As an initial feasibly study of both the Soralux Daylighting System and the simulation method, a case study building was modeled in Radiance (shown in Figure 5.1). The site chosen is the future location for

the research sponsor's new headquarters building. The sponsor, Hulic Co. Ltd., will install the Soralux system into this building during its construction in 2012.

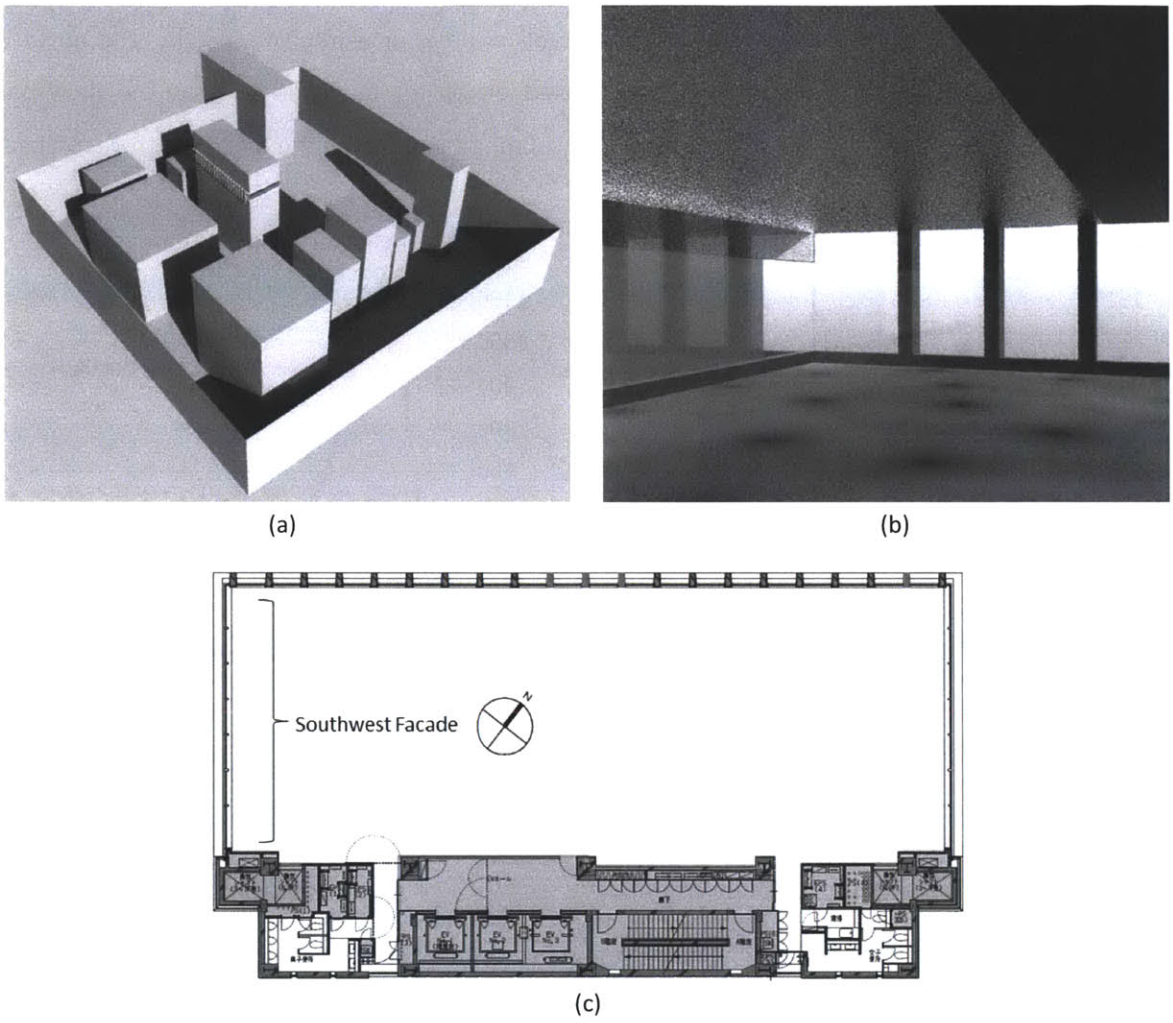


Figure 5.1: Hulic Headquarters Building and Its Surroundings (a), View from Inside the Office Space (b), and Floorplan of Office Space (c)

Figure 5.2 shows the performance of the Soralux system versus a shaded and unshaded window for two different representative sky conditions. In the Hulic headquarters feasibility study model, the facade below 2.2 m from the floor was unchanged for all cases: the interior blinds were closed at a 65° angle to keep out all direct sunlight but still allow through some diffuse daylight. Daylight diffused in this manner is unlikely to cause glare, however, the amount and depth of light penetration is limited with closed blinds. The shaded case extended these closed blinds up to the ceiling, whereas the unshaded case left the top .6 m of the glazed facade uncovered. These cases provide points of comparison with the performance of the daylighting system. The Soralux system was installed on the building's southwest

facade and filled the same .6 m at the top of the facade as the uncovered window case. Illuminance values were measured along the centerline of the room moving away from the southwest facade to determine how the illuminance profile changed with increasing depth. The measurement points were .75 m off the floor in order to capture illuminance levels at desk, or workplane, height. The northwest and northeast facades were fully shaded with closed blinds for all cases so that the illuminance contribution from these facades would be negligible, isolating the effect of the daylit southwest facade.

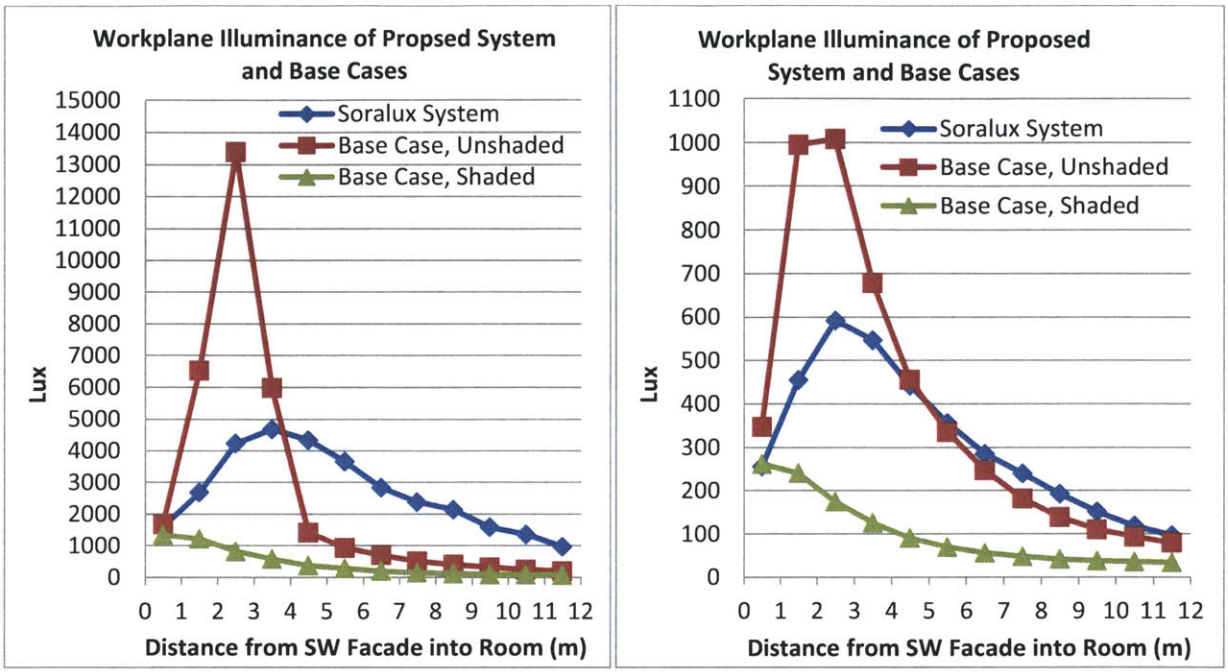


(a) (b)

Figure 5.2: Illuminance Results for Sunny (a) and Overcast (b) Conditions for Hulic Case Study

Under sunny conditions, the louver system outperforms both the unshaded and shaded window sections by about 300% in the back two-thirds of the space, as shown in Figure 5.2(a). The louver system also avoids the extremely high peak illuminance seen in the unshaded case resulting from direct sunlight transmission, which would likely cause glare and thermal discomfort for occupants.

Under overcast conditions, the overall illuminance levels shown in Figure 5.2(b) are much lower for all cases. The louver system still outperforms the uncovered window at distances greater than 5 m from the facade by about 20% to 30% and outperforms the shaded window at all positions by several hundred percent.

These initial results showed that the system did have the potential to improve lighting conditions in deep-plan spaces. Although the effect was expected, the feasibly revealed the stark difference in lighting levels between sunny and overcast conditions. Because the study included some simplifying assumptions (no minimum louver section thickness, no window frame or mullions, etc.) that would tend to increase the reported illuminance, light levels for overcast conditions were identified as a potential performance problem. These suspicions would be confirmed by later testing, discussed in Section 5.4.

The study also indicated that the simulation method outlined in Appendix A was a feasible approach to annual simulation. The simulations were completed in a reasonable amount of time and the results appeared to be internally consistent (ie. changes that would be expected to reduce light levels actually did decrease light levels). However, to verify the Radiance model's accuracy on an absolute basis, it would have to be compared with measurements from an actual building space. This comparison was carried out for a physical prototype of the Soralux system and is covered in Section 6.2.5.

It should be noted that the design of the system modeled in the feasibility study was different from that of the final design. The refractive rods had not been included yet, so the system consisted of the louvers and the reflective ceiling only. Additional differences between this model and the generic model discussed in Section 5.3 include louver minimum cross-sectional thickness, surface reflectance values, facade orientation, reflective ceiling length, and mullion and frame transmission losses. As a result, the illuminance values shown here are higher than those of the final generic simulations.

## 5.3 Radiance Model Description of Generic Space

In order to gain a complete picture of how the Soralux Daylighting System performs, it must be studied under a variety of conditions. How well the system functions will be dependent on the specifics of its configuration, the space to be daylit, and the space's surroundings. A generic office space model was constructed in Radiance to develop an understanding of how the Soralux system performs under a range of conditions. The space was sidelit only from a single facade and the floor plan was very deep at 15 m. This depth is worth highlighting because, in many daylighting system evaluations, the depth of the test room is no more than 6 or 8 m (Aizlewood, 1993; Ruck et al., 2000; Scartezzini & Courret, 2002). The Soralux system was tested to this greater depth because illuminating deep-plan spaces was a specific goal of the project, as was the requirement to use sidelight only. The space was also tested with varying levels of sky obstruction to account for the urban obstructions the system is expected to encounter.

The space was modified as needed to test the full range of conditions listed in Section 5.4. For each condition, both the full Soralux system and the base case were tested. A clear unshaded clerestory window of equal area to the daylighting system and a diffuse white ceiling was used as the base case. The unshaded window is a common point of comparison for daylighting system evaluations and is one of two standard reference cases defined by the International Energy Agency's Solar Heating and Cooling Task 21 (Ruck et al., 2000). A generic unshaded window provides a simple reference case that is easily modeled and understood.

Workplane illuminance .75 m off the floor was recorded for each of these conditions, representing the amount of light falling at desk height throughout the room. The space was modeled as an empty room, without interior furniture. The clerestory window was .71 m high. This height and the floor to ceiling height of 2.8 m were chosen to match the dimensions of the first permanent installation site (the Hulic headquarters building, discussed in Section 1.3). The bottom of the Soralux window unit is located 2.09 m off the floor to keep horizontal light emitted from the unit above standing height. The facade below 2.09 m from the floor was modeled as a view window with venetian blinds closed at a 65° angle: this angle prevents beam sunlight from entering the building space, while also allowing some diffuse light into the front of the room. Additional model details are provided in Figures 5.3 and 5.4 and Table 5.1.

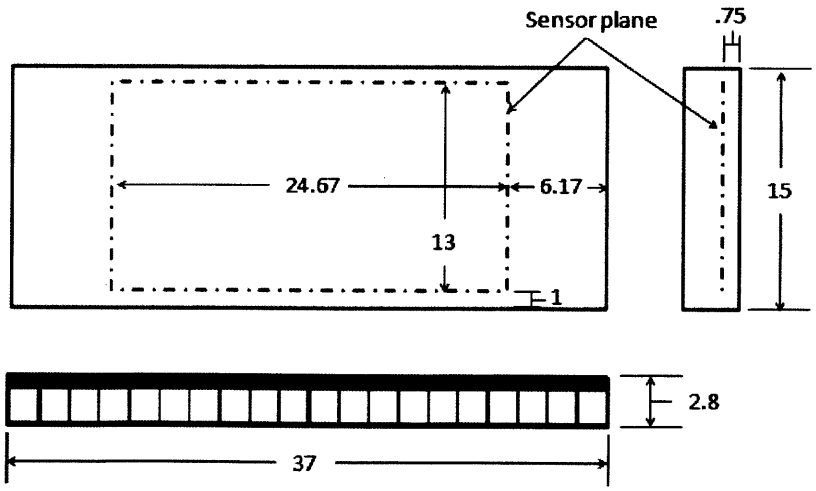


Figure 5.3: 3-View Drawing of Generic Model with Dimensions (Meters)

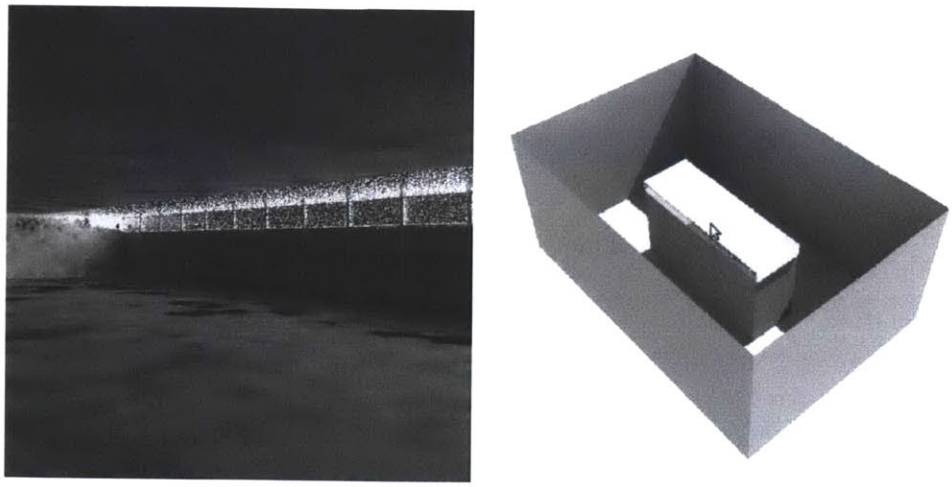

(a) (b)

Figure 5.4: Generic Model Space Interior (a) and Exterior with Surroundings (b)

Table 5.1: Generic Radiance Model Parameters

| Name | Value | Notes |
|---|---|---|
| Refractive Rod Absorbtance over 1 m | 0.146 | .004 over 1 inch |
| Refractive Rod Index of Refraction | 1.49 | |
| Louver Reflectance | 0.87 | |
| Louver Specularity | 1.00 | Mirror material type |
| Louver Roughness | 0.00 | |
| Reflective Ceiling Reflectance | 0.856 | |
| Reflective Ceiling Specularity | 0.95 | |
| Reflective Ceiling Roughness | 0.125 | |
| Wall Reflectance | 0.50 | |
| Floor Reflectance | 0.15 | |
| Standard Ceiling Reflectance | 0.70 | |
| Window Unit Frame Reflectance | 0.60 | |
| Mullion Reflectance | 0.50 | |
| Venetian Blind Reflectance | 0.40 | |
| Glass Transmittance (for each pane) | 0.859 | Transmissivity = .935 |
| Exterior Ground Reflectance | 0.08 | |
| Surrounding Building Reflectance | 0.10 | |

As explained in Appendix A, Radiance's ambient settings need to be increased to very high levels in order to ensure repeatable results. The following settings were used in the Rtcontrib calculation. Setting

the –ab value to 30 did not alter the results or calculation time by a noticeable amount over the other –ab value tested of 12, so the higher value was utilized.

Table 5.2: Generic Radiance Model Ambient Settings

| Setting | Value Used | Recommended Very Accurate Settings (Jacobs, 2008) | Setting Description (Ward Larson & Shakespeare, 1997) |
|---|---|---|---|
| -ab | 30 | 5 | Sets number of diffuse bounces |
| -ad | 4,194,304 | 2048 | Sets number of hemisphere divisions for sampling |
| -as | 16,384 | 512 | Sets number of additional samples sent to divisions showing large variation |
| -ar | 157,480 | 512 | Sets the minimum spacing between surfaces required to prevent interpolation |
| -aa | 0.02 | 0.08 | Sets the maximum allowable error |
| -lw | 0.00000003 | N/A | Sets the minimum contribution of a ray to the final result required for the ray to be traced |

## 5.4 Simulation Results

A large set of design cases was simulated using the generic Radiance model described in Section 5.3. The results shown here are a representative cross-section of the full data set. The full data set consists of 128 annual simulations for four different climates.

The bulk of the simulations resulted from an experiment with the variables described below. All possible combinations of these variables lead to 120 separate cases (3 x 4 x 5 x 2 = 120).

- Facade condition, 3 conditions. The facade condition states were chosen so that the Soralux system could be compared with the uncovered window base case, with and without the lower window included.
    - Clerestory window: Soralux Daylighting System; view window: opaque
    - Clerestory window: uncovered clear glazing; view window: opaque
    - Clerestory window: opaque; view window: partially closed interior blinds
- Facade orientation, 4 conditions.
    - North

    - South
    - East
    - West
- Exterior sky obstructions, 5 conditions. These obstruction angles were chosen to represent increasing levels of sky obstruction due to urban surroundings.
    - 0° above horizon
    - 15° above horizon
    - 30° above horizon
    - 45° above horizon
    - 60° above horizon
- Space width, 2 conditions. Two widths were chosen to represent different sized spaces. The particular dimensions chosen were multiples of the width of the Soralux window unit and mullion width. The window unit including the frame was modeled as 1.8 m wide and the interstitial mullions were .053 m wide. The mullion width was set for convenience so that the resulting width of the wide space would be a whole number. The wide space included 20 window units and the narrow space had four.
    - Wide (37 m wide x 15 m deep)
    - Narrow (7.4 m wide x 15 m deep)

A single representative case was chosen to illustrate the results in detail. The parameters under consideration were varied from their reference levels to show their influence on the reference case. The range of results found throughout the full data set is discussed as well. The reference case chosen was the wide (37 m wide) room with a south-facing facade and a 15° sky obstruction. This case was chosen because it has a favorable room size and orientation for the system, while still including some sky obstructions.

Except where noted, the following conditions apply:

- Simulations use Tokyo weather data obtained from the *Energy Plus* Tokyo weather file (U.S. Department of Energy, 2010).
- All times are in local legal time, not solar time.
- Illuminance values are reported on a workplane .75 m from the floor.

- Simulations combine the results of the upper clerestory windows and lower view windows so that the lighting contribution from the partially closed blinds in the lower window is included.
- Annual lux thresholds are presented as a fraction of daytime working hours. Daytime working hours are defined for this evaluation as hours between 8am and 7pm where the exterior unobstructed diffuse horizontal illuminance was at least 1000 lux. This eliminated working hours when the sun had already set or was about to set, without eliminating daytime overcast time steps. For the Tokyo weather file, daytime working hours represent 82% of all working hours between 8am and 7pm.

### 5.4.1 Detailed Reference Case Results

This section evaluates the reference case (wide room, south facade, 15° sky obstruction) for a range of specific sky conditions. Figures 5.5 through 5.7 present the conditions for the Soralux system and for the base case. The intent is to illustrate the behavior and dynamics of the system and base case over the course of the year. The results shown here are similar to those of the traditional approach discussed in Section 5.1. Contour lines corresponding to 700, 500, and 300 lux are marked. Seven hundred lux is the standard recommended workplane illuminance in the Japanese office buildings constructed by Hulic, the research sponsor. In the US and Europe, 300 to 500 lux is typically recommended (Mardaljevic et al., 2009).

For Figures 5.5 through 5.7, south is located at the bottom edge and west is located at the left edge. The sensor plane's location in the room is shown in Figure 5.3. In comparing the system with the base case, it is important to keep in mind that the base case is not a truly realistic alternative since the glare resulting from direct sunlight would be unacceptable. However, the base case is still useful because it provides an easily understandable comparison to the results for the Soralux system.

Figure 5.5 shows results for sunny conditions at the spring/fall equinox and summer solstice for the Soralux system and the base case. At 11:30am on the spring/fall equinox, the system is working in an ideal manner. Light levels are 500 lux or more to a depth of 12 m. The base case shows very high light levels in the first 2 m, resulting from direct sunlight transmission, that then quickly fall below 300 lux at 6 m. By 2:30pm, light levels are somewhat lower, but the system still produces 500 lux at 10 m from the facade. For a south-facing facade under the same sky conditions, the performance of the Soralux system will be symmetric about solar noon. Therefore, the results for 2:30pm legal time will be similar to results

for times around 9:30am legal time. The profile for the base case at 2:30pm is similar to its result at mid-day, except that light levels fall even more sharply from high to low. For both spring/fall equinox time steps, the ratio of workplane illuminance between the Soralux system and the base case is similar. As shown in Figure 5.8, the Soralux system reaches parity with the unshaded window by 2 m from the facade. Illuminance levels continue to increase relative to the base case until about 8 m from the facade, where the ratio stabilizes at approximately 900 to 1000% over the base case levels. To be clear, a ratio of 100% would mean that the system and the base case had the same light levels.

The behavior of the curves shown in Figure 5.8 seem to change at 8 m for a number of the conditions. After increasing from the front of the room to 8 m, the illuminance ratio tends to stabilize at this point to the back of the room. This appears to be an effect caused by the external sky obstructions. With the geometry used in the model, the workplane sensor's view of the sky is completely obstructed by the exterior surroundings at 7.75 m from the facade. From 8 m to the back of the space, all the sensors can see is indirect light reflected off internal or external surfaces, resulting in less variation from one point to the next. This transition point will vary for different sites because of different sky obstruction situations and room geometries. As the angle of sky obstruction increases, the transition point will move closer to the facade, as the sky will be occluded at a shallower depth into the room.

The results for the summer solstice, shown in Figure 5.5, are at first somewhat counterintuitive. Light levels are lower near the summer solstice than they are for the spring and fall equinoxes and winter solstice. The sun's elevation angle is high (maximum 77°) near the summer solstice. When the sun is very high in the sky, two effects limit the amount of sunlight incident on the louvers. First, the amount of sun rays intercepted by the window unit drops because the unit's projected area normal to the sun's rays decreases. Second, the reflectance of the outer pane of glass increases at high incident angles, meaning less light is transmitted into the system. These two effects are illustrated in Figure 5.9.

Although these effects are well known, seeing them in graph form assists in understanding their impact on daylight availability. A benefit of this behavior is that the solar gains associated with admitted sunlight are limited during the summer, the hottest part of the year, which will help prevent the system from introducing excessive thermal loads during this time.

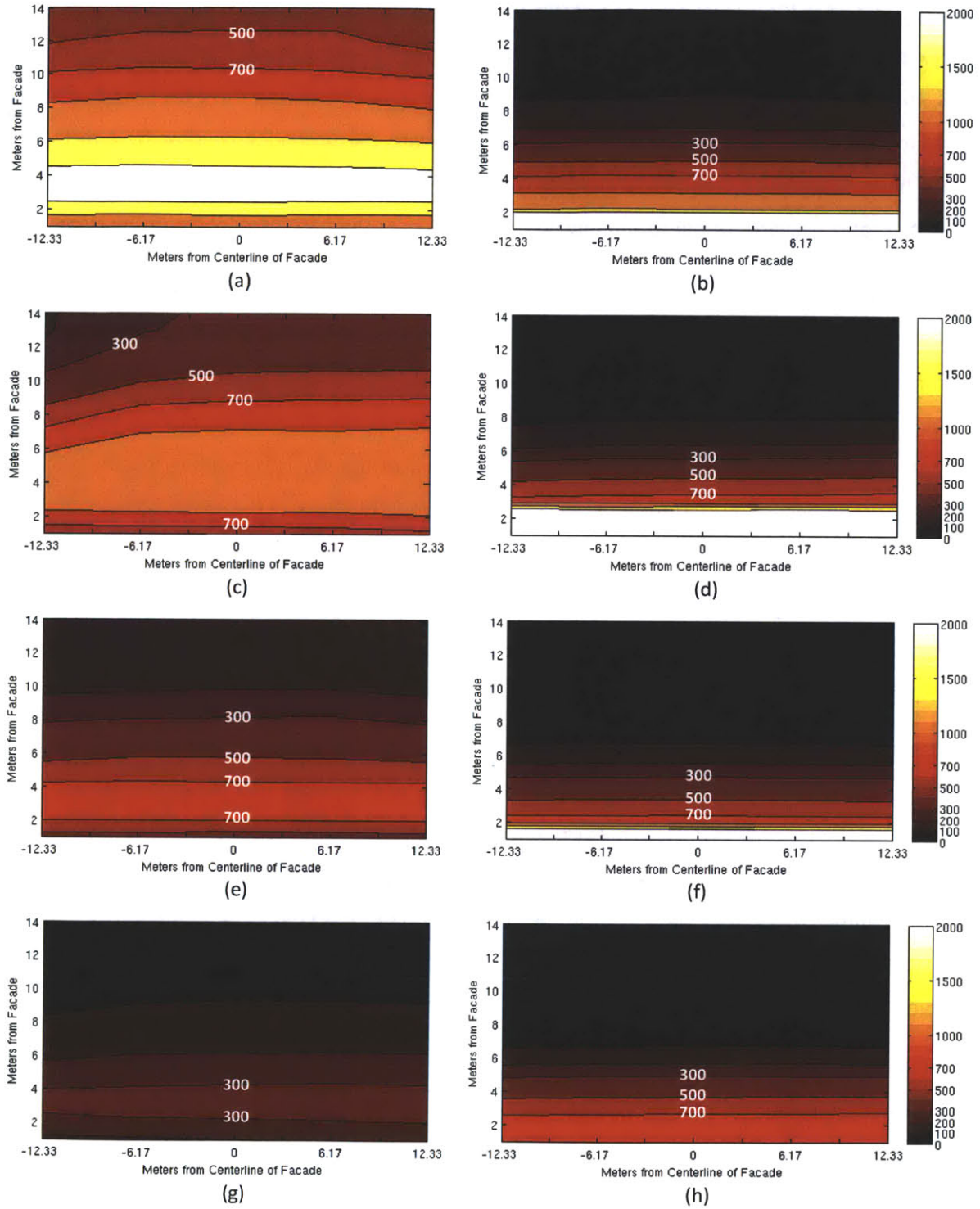


Figure 5.5: Workplane Illuminance: Sunny 11:30am Spring/Fall Equinox, System (a), Base Case (b); Sunny 2:30pm Spring/Fall Equinox, System (c), Base Case (d); Sunny 11:30am Summer Solstice, System (e), Base Case (f); Sunny 2:30pm Summer Solstice, System (g), Base Case (h)

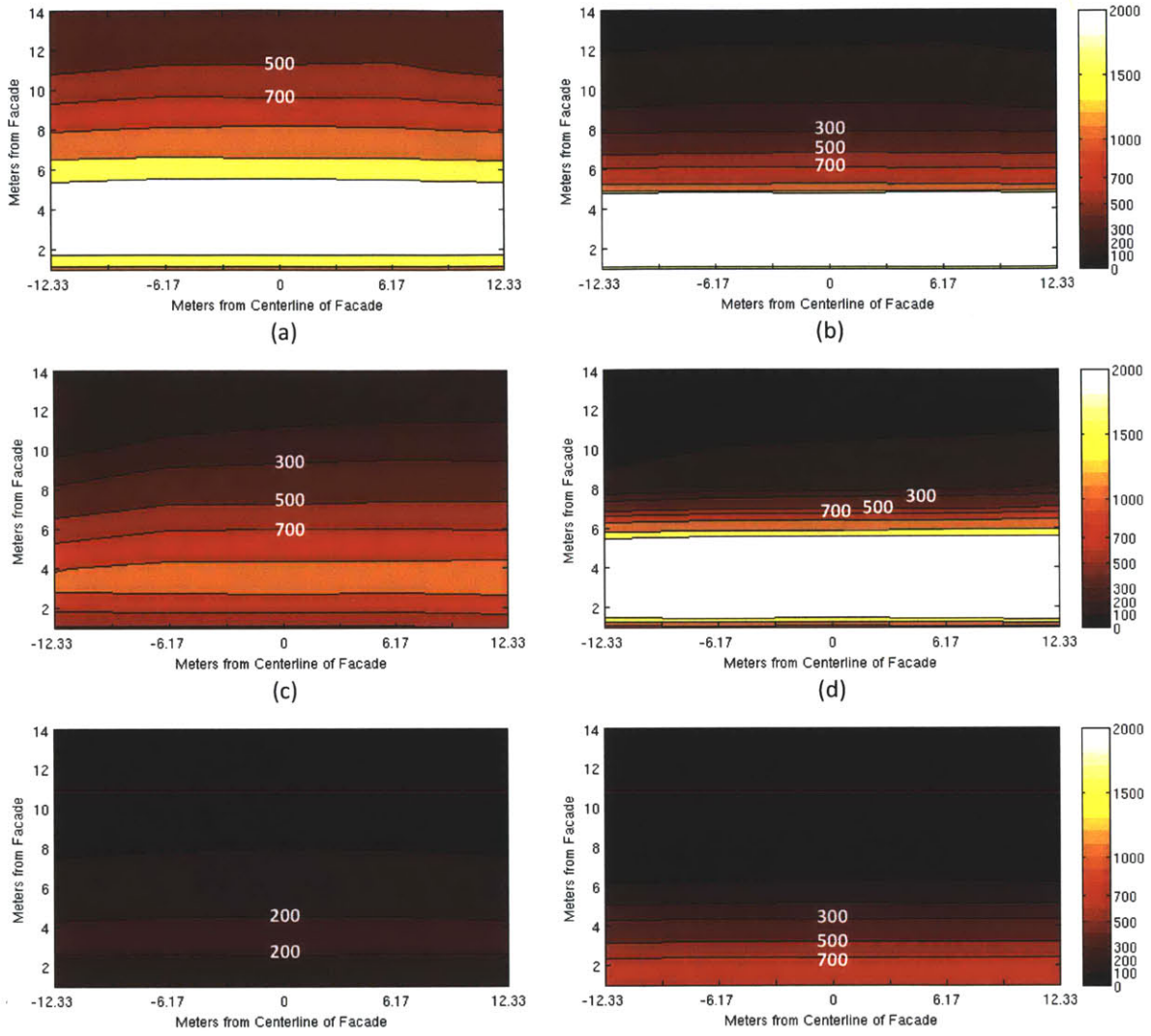


Figure 5.6: Workplane Illuminance: Sunny 11:30am Winter Solstice, System (a), Base Case (b); Sunny 2:30pm Winter Solstice, System (c), Base Case (d); Overcast, 20 klux Global Horizontal, System (e), Base Case (f)

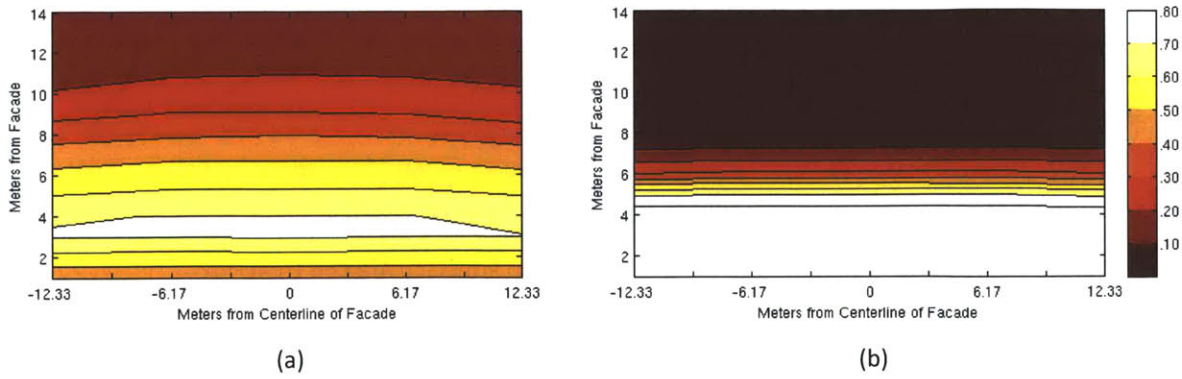


Figure 5.7: Daytime Daylight Autonomy with a 300 Lux Threshold, System (a), Base Case (b)

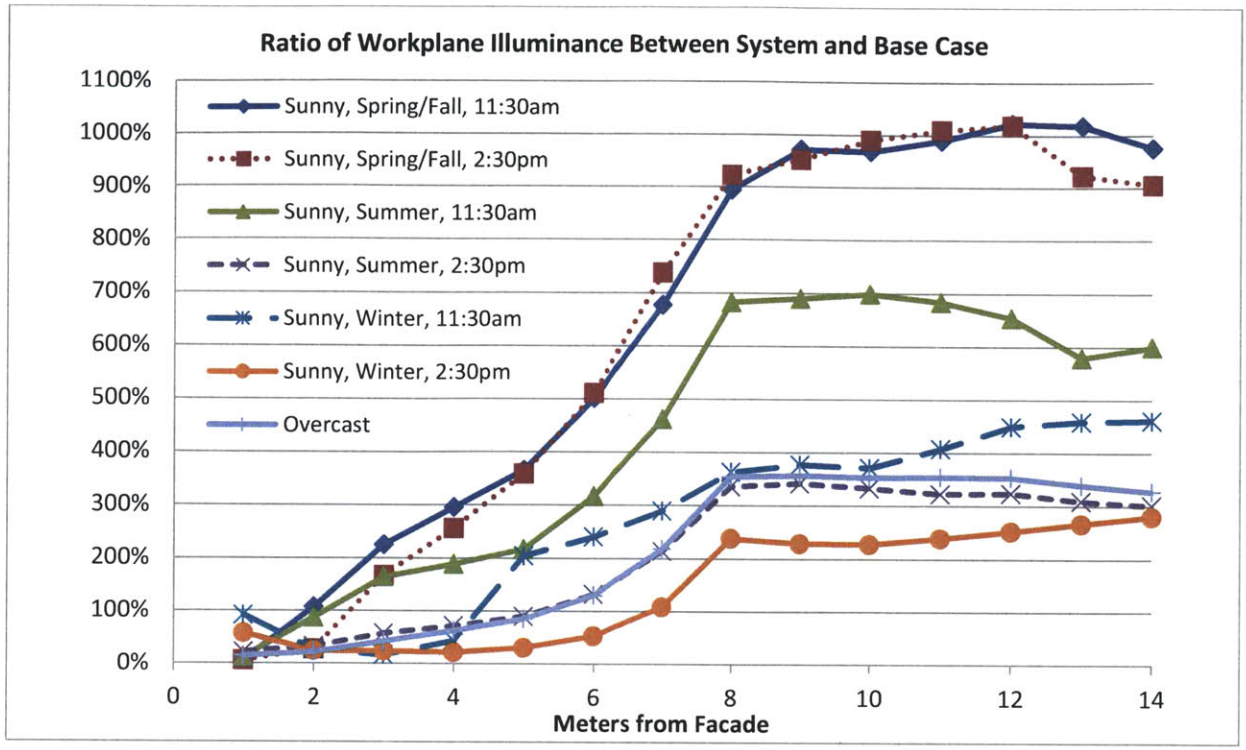


Figure 5.8: Ratio of Workplane Illuminance Between System Case and Base Case Along Room Centerline (>100% Means Higher Light Levels for System Case Than Base Case)

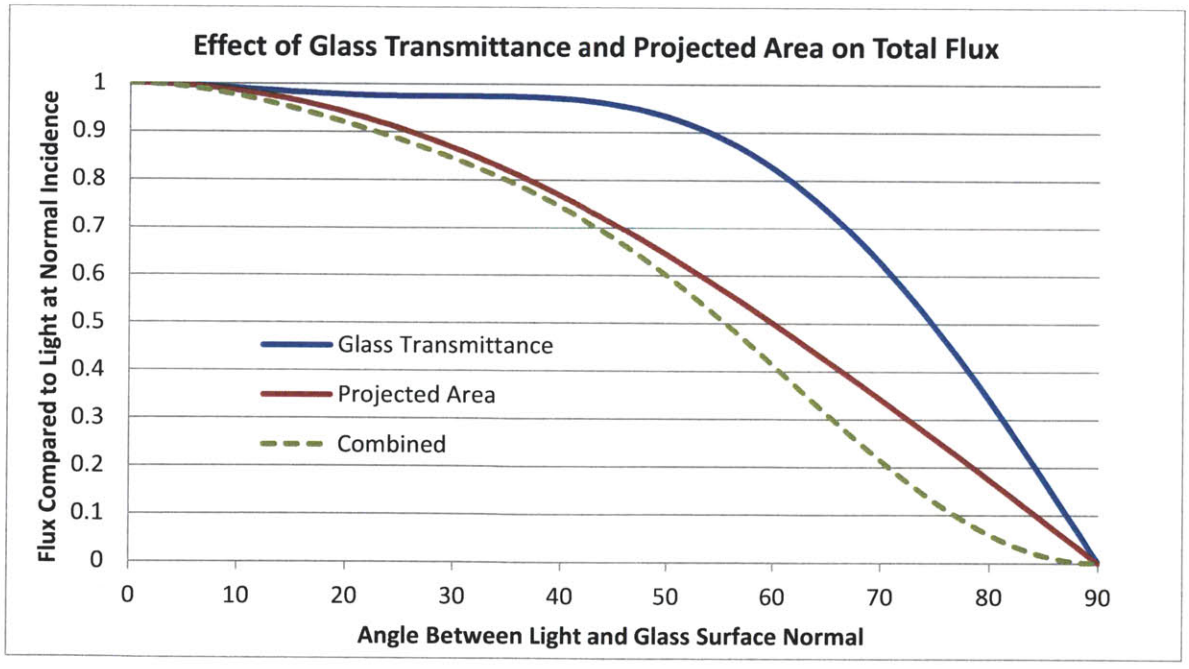


Figure 5.9: Effect of Glass Transmittance and Projected Area on Total Flux

At mid-day during the summer solstice, the system can provide about 300 lux to a depth of about 8 m, whereas the base case drops below 300 lux at about 5 m. The ratio of workplane illuminance between the system and the base case increases over the first 8 m to a maximum of 700% and the ratio remains in the 600 to 700% range from 8 m to the back of the space at 15 m (as shown in Figure 5.8). At 2:30pm, the direction of direct sunlight is nearly parallel to facade so there is almost no direct solar contribution. Under this condition, the system is not greatly different from base case. The system's illuminance ratio is less than 100% (meaning it provides less light than the base case) from the facade to 5 m. From 5 m to the back of the space, the system workplane illuminance levels are approximately 300% to 350% of the base case levels. Although this is a substantial increase in relative terms, the absolute illuminance levels are rather low, as shown in Figure 5.5. Interestingly, the illuminance ratio curve shown in Figure 5.8 for sunny conditions on the summer solstice at 2:30pm is very similar to the curve for the overcast case. This makes sense, as neither condition has significant exposure to direct sunlight.

Near the winter solstice, the system is observed to be working to its full potential once again, as shown in Figure 5.6. At 11:30am, the full 15 m space has at least 300 lux; 500 lux is provided to a depth of 11 m. Illuminance levels are higher for the system than for the base case starting at 5 m from the facade, and the ratio of system to base case increases from 200% at 5 m to 460% at 15 m. At 2:30pm, the system provides at least 300 lux to a depth of 8 m. From 8 m to the back of the room at 15 m, the ratio between the system and the base case ranges from 240% to 280%. Even though light levels are quite high for these winter cases, the illuminance ratio between the system and base case is lower than what was seen in fall/spring (200% to 500% instead of 900% to 1000%) in part because the sun's lower elevation angle in the winter allows light to penetrate more deeply through the unobstructed window of the base case.

Due to the limited amount of light available under an overcast sky and the light losses associated with the Soralux system, results for the overcast case are very modest, as shown in Figure 5.6. Although this result is disappointing, the desires for the system to remain passive and integrate easily with the rest of the facade conflict with the ability to provide significantly improved workplane illuminance under overcast skies. By locating the system behind a vertical piece of glass, the system intercepts a relatively small amount of light from the top of the sky dome and much of the light from above 60° elevation is reflected away from the building off the outer pane of glass. Light levels resulting from the system are greater than the base case starting at a depth of 5.5 m and stabilize at about 350% of the base case levels from 8 m to the back of the room. However, even though the Soralux system provides a

substantial relative increase over the base case for the back half of the space, absolute illuminance levels are still low, peaking at 220 lux and falling to 40 lux at the back of the room.

To actually achieve the base case results in a room with manual venetian blinds, someone would have to walk around and pull up 20 or 30 sets of blinds when the sky became overcast and then lower them all again when the sun came out: an unlikely prospect in most office environments. The overcast light levels achieved by the Soralux system occur without any system adjustment.

By raising the overall transmittance of the system (louver reflectance, ceiling reflectance, glass transmittance, etc.), light levels for overcast conditions could be boosted by as much as 50%. However, this would also boost the light levels under sunny conditions by a similar amount. Increasing 200 lux to 300 lux under overcast conditions would mean increasing 2000 lux to roughly 3000 lux for sunny conditions. By maximizing the overall transmittance, the risk increases that the reflective ceiling would be excessively bright under sunny conditions. Additionally, the system would become more expensive to produce. Consequently, raising the system's overall transmittance was not considered a viable path to increasing performance for overcast conditions.

Finally, Figure 5.7 compares the annual Daytime Daylight Autonomy (defined as the percentage of daytime working hours when 300 lux is achieved at a particular point) for the system and base cases. The Soralux system provides a clear improvement over the base case for this annual metric. The system causes a higher daytime daylight autonomy compared to the base case beginning at 6 m from the facade (54% versus 32% on the centerline of the room). The base case's daytime daylight autonomy falls to zero at 8 m, while the system's ranges from 40% at 8 m to 14% at 14 m along the centerline of the room.

Figure 5.10 provides workplane illuminance for selected time steps along the centerline of the room for the system and base cases. Dashed lines demarking 300, 500, and 700 lux are included as they are common minimum illuminance requirements for office spaces.

Not only does the Soralux system provide increased illumination in the back of the space, lighting levels are also more uniform from the front to the back than with the base case. For the Soralux system under the seven sky conditions described in Figures 5.5 and 5.6, the ratio of the maximum to the minimum workplane illuminance for an individual sky condition varied from a high of 8.1 (sunny, summer solstice, 11:30am) to a low of 4.5 (sunny, spring/fall equinox, 2:30pm). For the base case, the same ratio varied from a high of 440 (sunny, spring/fall equinox, 11:30am) to 53.9 (sunny, summer solstice, 2:30pm).

Uniformity is increased because the Soralux system reduces illuminance levels at the front of the room while increasing them at the back. A more evenly lit space may appear brighter to the eye than one with a higher ratio of illuminance levels because the eye has a smaller brightness range to accommodate.

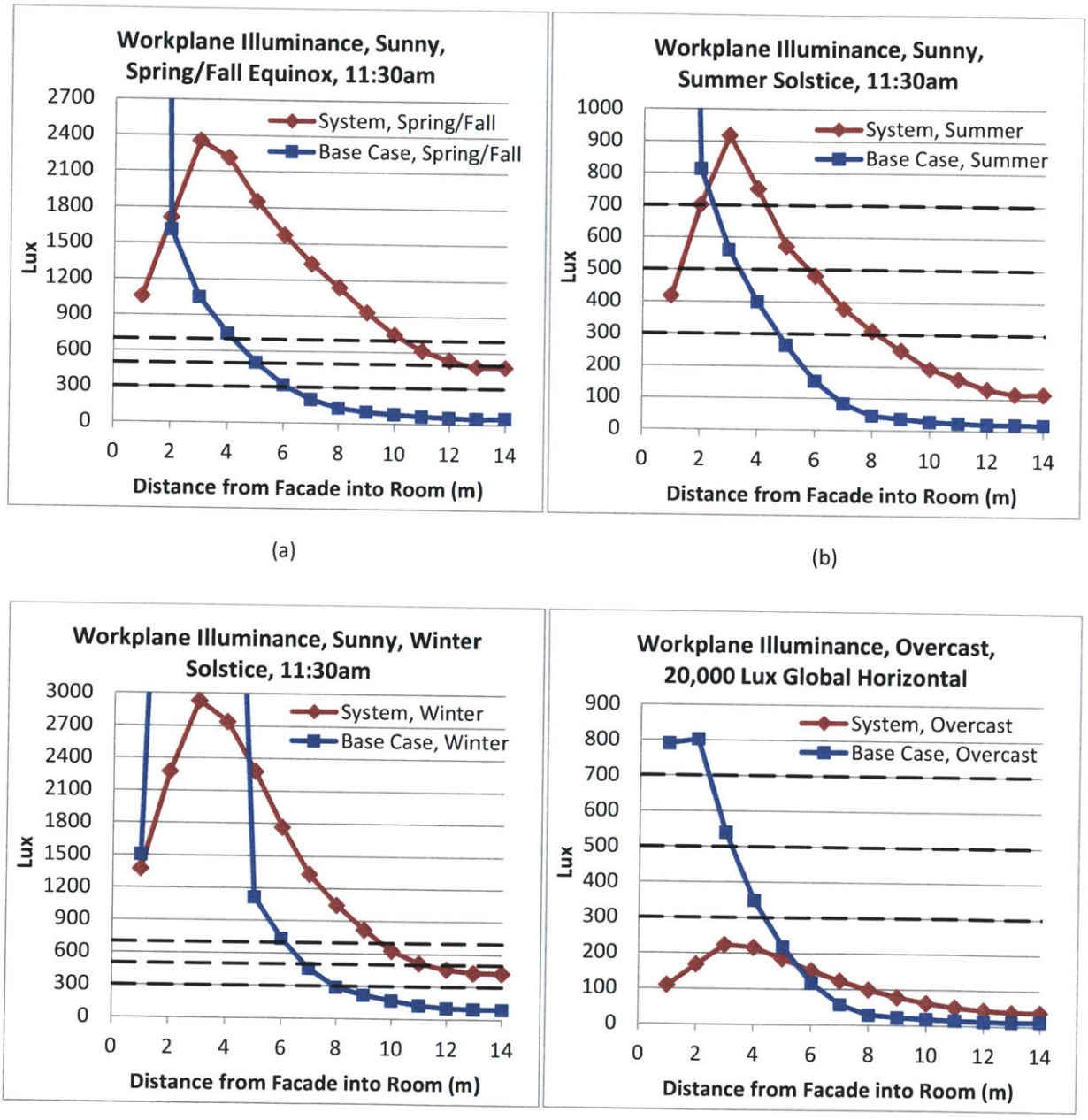


Figure 5.10: Centerline Workplane Illuminance: Sunny, Spring/Fall, 11:30am (Base Case Peak: 20,638 Lux) (a); Sunny, Summer, 11:30am (Base Case Peak: 3665 lux) (b); Sunny, Winter, 11:30am (Base Case Peak: 19,009 Lux) (c); Overcast, 20,000 Lux Global Horizontal Illuminance (d)

Figure 5.11 shows the annual median workplane illuminance at each sensor point for each hour of the workday for the Soralux system. Per the definition of the median, half of the hourly results are above these values, and half are below. These results show all working hours, rather than only daytime working hours. The sensors shown are on the centerline of the room. The figure shows that the performance of the system peaks in the middle of the day between 10am and 1pm, with illuminance dropping slowly around these peak hours.

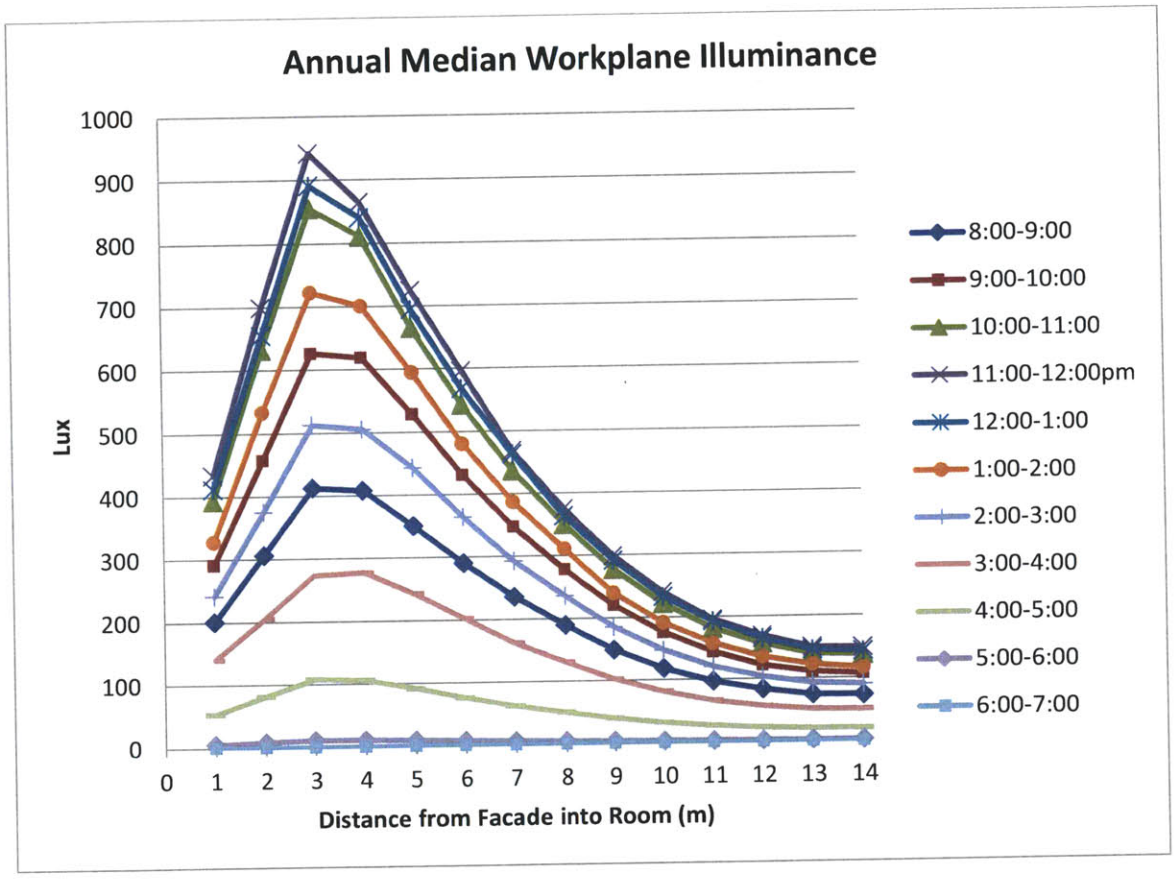


Figure 5.11: Centerline Annual Median Workplane Illuminance for All Working Hours as a Function of Distance from the Facade

The curves in Figure 5.12, representing workplane illuminance at a particular location as a function of time of day, have the appearance of sine waves. For a south-facing facade, illuminance levels will be highest in the middle of the day because the system will be exposed to the highest amount of direct sunlight during this period. From 5 to 7pm, the median values are near zero because the sun has usually set by this time of day.

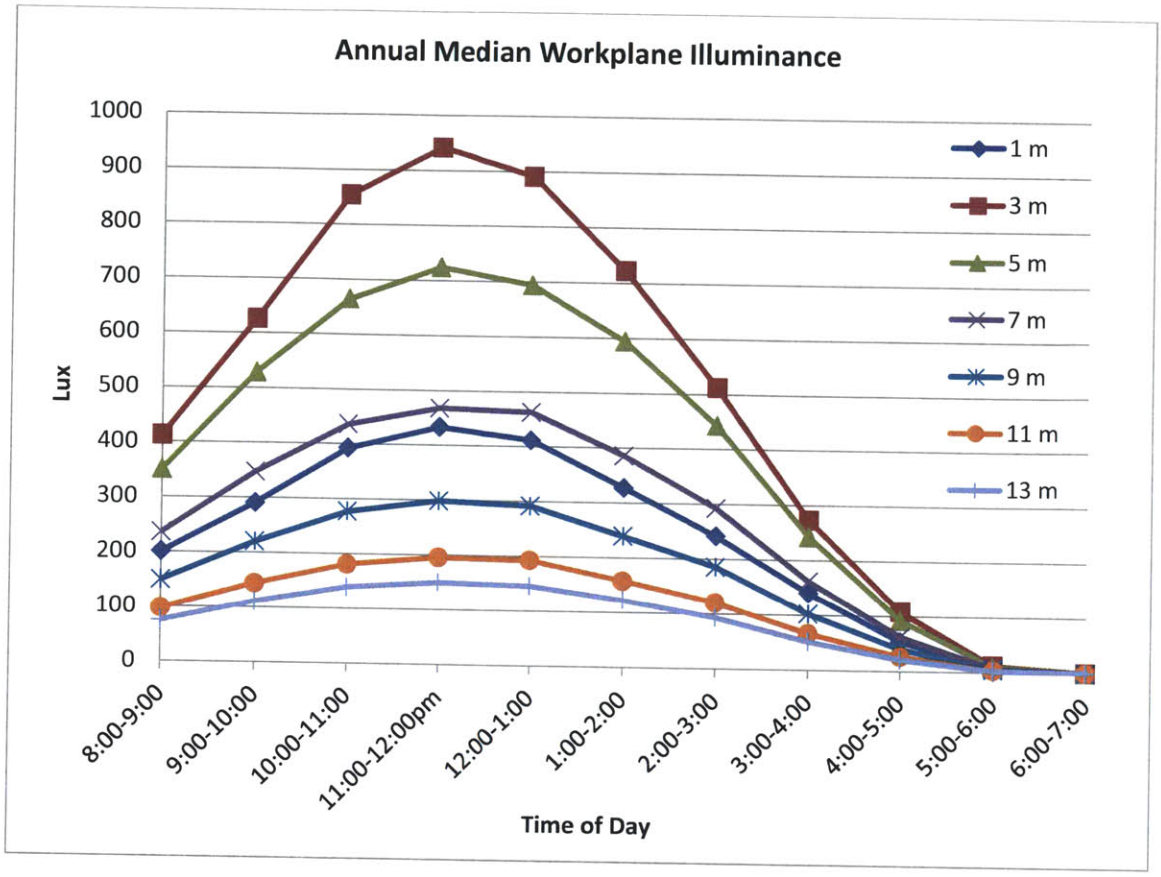


Figure 5.12: Centerline Annual Median Workplane Illuminance for All Working Hours as a Function of Time of Day

A seasonal effect is also seen in the annual illuminance results. Figure 5.13 shows median workplane illuminance at mid-day by season. The median values vary by a factor of 2 to 3 between seasons. The differences are driven by both the sun course and the prevailing weather patterns in the Tokyo weather file. Because of the symmetry of the sun course about the solstices, the spring and summer time periods will experience the same range of sun positions. The same is true for the fall and winter time periods. If the weather conditions were similar for the pair of time periods then their median illuminance profile would be expected to be similar as well. This is true of the spring and summer in the figure below. However, fall and winter do not exhibit the same illuminance pattern. This difference is attributable to an increase in sky clearness during the winter months, compared to the fall months. As discussed above, the Soralux system performs better at mid-day near the winter solstice compared to the summer solstice because the system intercepts more sunlight when the sun is lower in the sky.

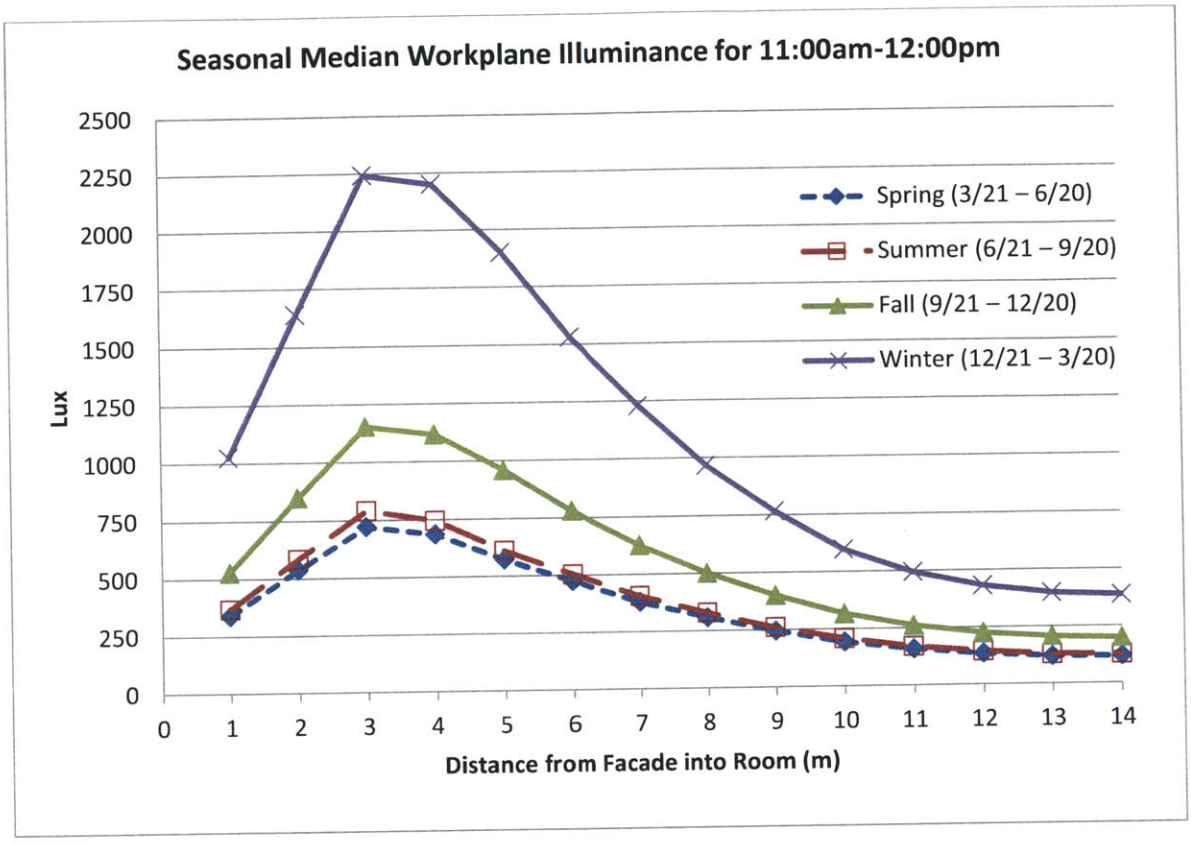


Figure 5.13: Centerline Seasonal Median Workplane Illuminance for 11:00am-12:00pm

### 5.4.2 Annual Results for All Cases

The following set of simulations were run to provide a more complete understanding of how relevant variables affect the performance of the system. In each instance, the variable being studied was varied from the conditions of the reference case characterized above (wide room, south facade, 15° sky obstruction). The results are presented for the entire year, rather than at individual time steps to condense the data and encapsulate the annual performance for a particular site. All of the following illuminance results are based on measurements along the centerline of the room.

#### a) Effect of Sky Obstructions

In an urban setting, the level of sky obstruction resulting from the surroundings has a major impact on the effectiveness of the Soralux system. The magnitude of sky obstructions varies from one street to another and also for different floors in the same building. In this study, the sky obstruction angle was defined as the angle from the ceiling at the facade of the test space to the top of the building across the street, in a plane normal to the test building's facade, as shown in Figure 5.14.

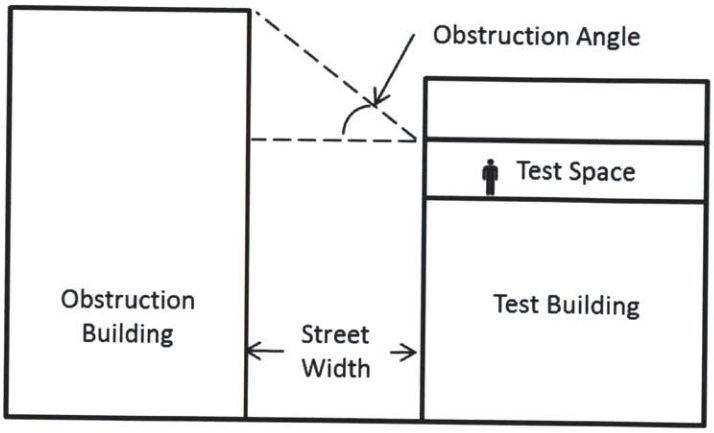


Figure 5.14: Definition of Sky Obstruction Angle

The ceiling was chosen as the reference plane for measuring the obstruction angle for two reasons. First, the Soralux window unit will usually abut the ceiling and extend downward, meaning that the obstruction angle for any individual louver will be equal to or greater than the defined obstruction angle. Second, the distance from street level to the test space ceiling height will generally be easier to determine than some other arbitrary plane such as the mid-plane height of the test space. This simplicity should aid engineers and architects in evaluating their particular building site during the initial design process.

In the Radiance model, the obstruction was defined as an opaque wall 20 m from the daylit facade at the appropriate height. As a reference, for a 25 m street-to-street spacing and a 4 m floor-to-floor height, the obstruction angles 15°, 30°, 45°, and 60° correspond to buildings across the street that are about 2, 4, 6, and 11 floors taller than the test floor. The 0° obstruction case would apply where the test space is higher than its immediate surroundings.

Figure 5.15(a) shows that the performance of the Soralux system is only modestly reduced for obstruction angles up to 30°. For example, at 8 m from the facade the percent of daytime working hours where illuminance is at least 300 lux falls from 42% with no sky obstructions, to 40% and 33% for 15° and 30° obstruction angles, respectively. Light levels fall sharply for 45° and 60° sky obstructions. Three hundred lux is achieved at 8 m for 12% of daytime working hours with a 45° obstruction and only 3% with a 60° obstruction. This result makes intuitive sense, because more and more of the sky as well as the solar window (the full section of sky where the sun appears at any point during the year) is blocked with an increasing obstruction angle. The loss of direct sunlight due to obstructions has a major impact on the annual performance of the system.

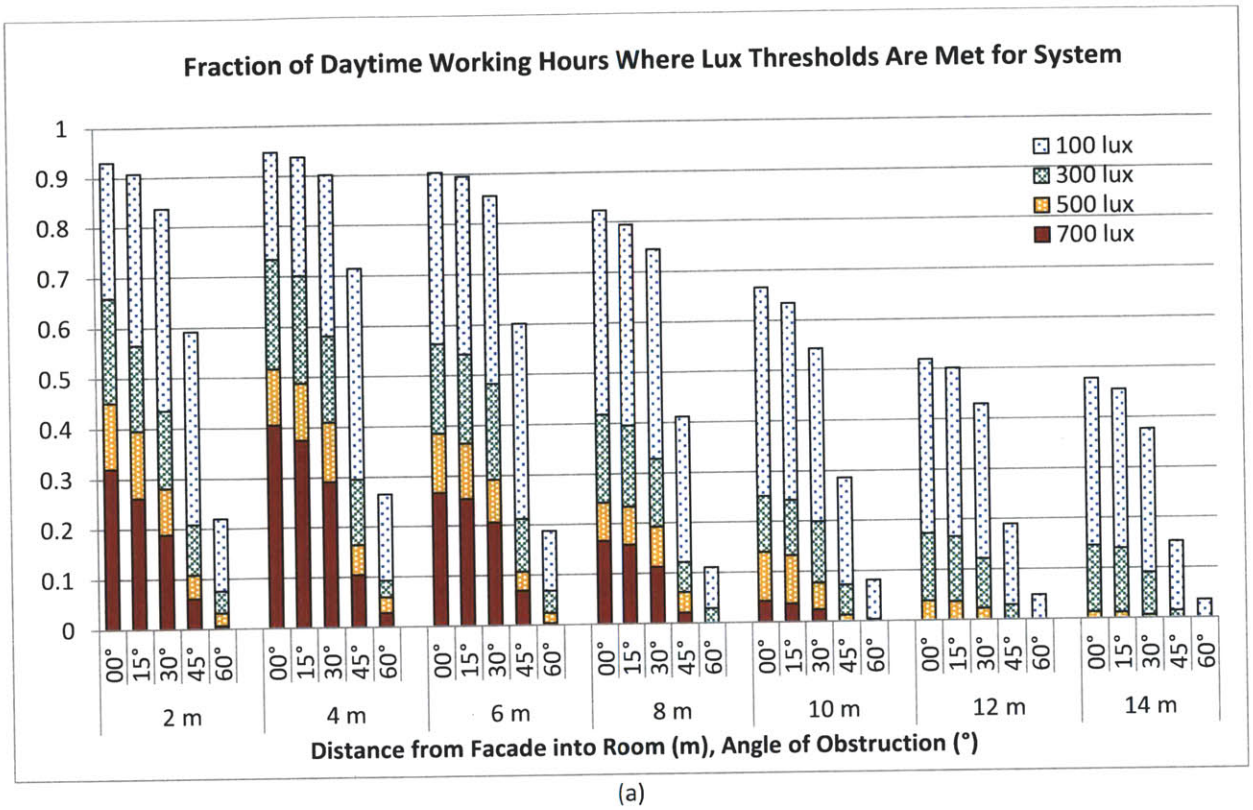


(a)

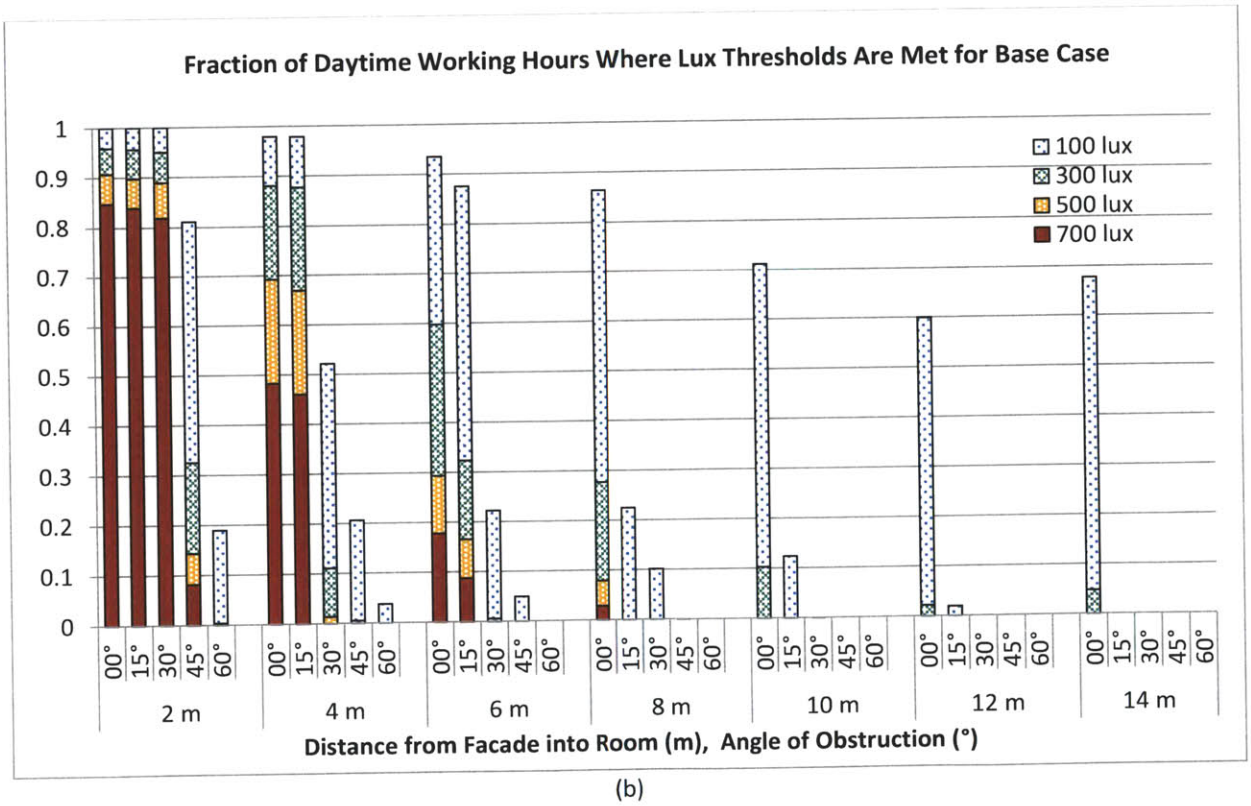


(b)

Figure 5.15: Effect of Sky Obstruction Angle on Daytime Daylight Autonomy: Soralux System (a) and Base Case (b)

The results for the base case (Figure 5.15(b)) fall much more severely beginning with a 15° obstruction angle. At 4 m from the facade, still relatively close to the window, the base case transitions from providing over 700 lux for 48% of daytime working hours with a 0° obstruction angle to providing 300 lux or more for less than 1% of daytime working hours for an obstruction angle of 30°. The base case relies on low-angle light near the horizon to illuminate the rear of the space and this light is the first to be cut off by increasingly tall obstructions. Because the Soralux system obtains light primarily from the upper two-thirds of the sky, it is less affected by sky obstructions due to the surrounding environment. Although absolute light levels fall with increasing obstruction angle, the relative performance of the Soralux system compared to the base case improves.

### b) Effect of Orientation

The orientation of the facade also has to be taken into account when placing the daylighting system. The generic office model was rotated in Radiance, along with the surrounding obstructions, to obtain results for the four different cardinal directions (shown in Figure 5.16).

As the Soralux system relies on exposure to direct sun to operate most effectively, south is the best orientation for the facade. For example, at 8 m from the facade the system provides at least 300 lux for 40% of daytime working hours. West and east produce largely similar results, with west consistently at slightly higher levels. At 8 m from the facade, west and east produce at least 300 lux for 22% and 18% of daytime working hours, respectively. West has slightly better results than east because the working hours considered (8am to 7pm) are skewed toward the afternoon. Consequently, the west facade receives more hours of direct sunlight and, therefore, has better overall performance. Since they do not receive as much direct sun, the east and west cases reach 300 lux approximately half as often as the south case.

The system performs poorly on northern facades because it rarely sees direct sun, and when it does, the sun is at very high incidence angles. As a result, the north-facing system never provides 300 lux at 8 m from the facade and provides 300 lux for less than 1% of daytime working hours at 6 m from the facade. As with the Soralux system, the best orientation for the base case is south, then west, then east, and then north. The base case does not ever provide 300 lux at 8 m from the facade for any orientation.

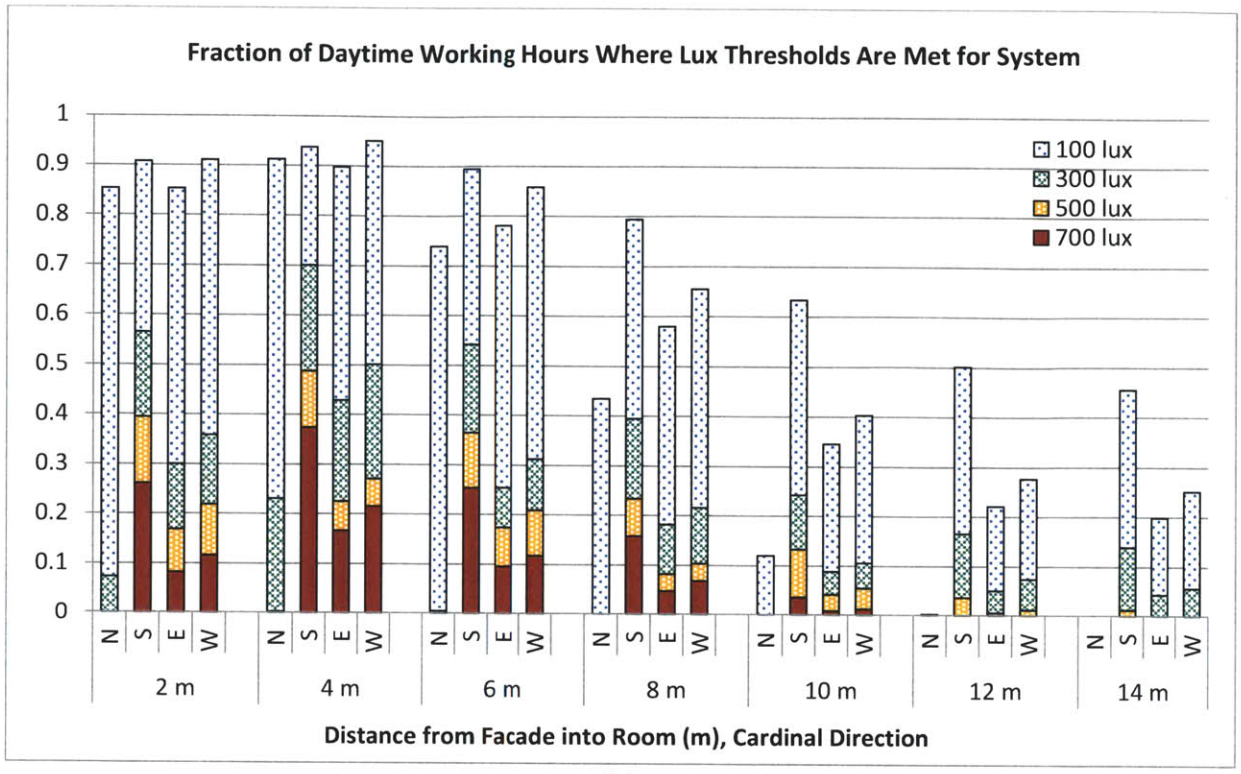


(a)

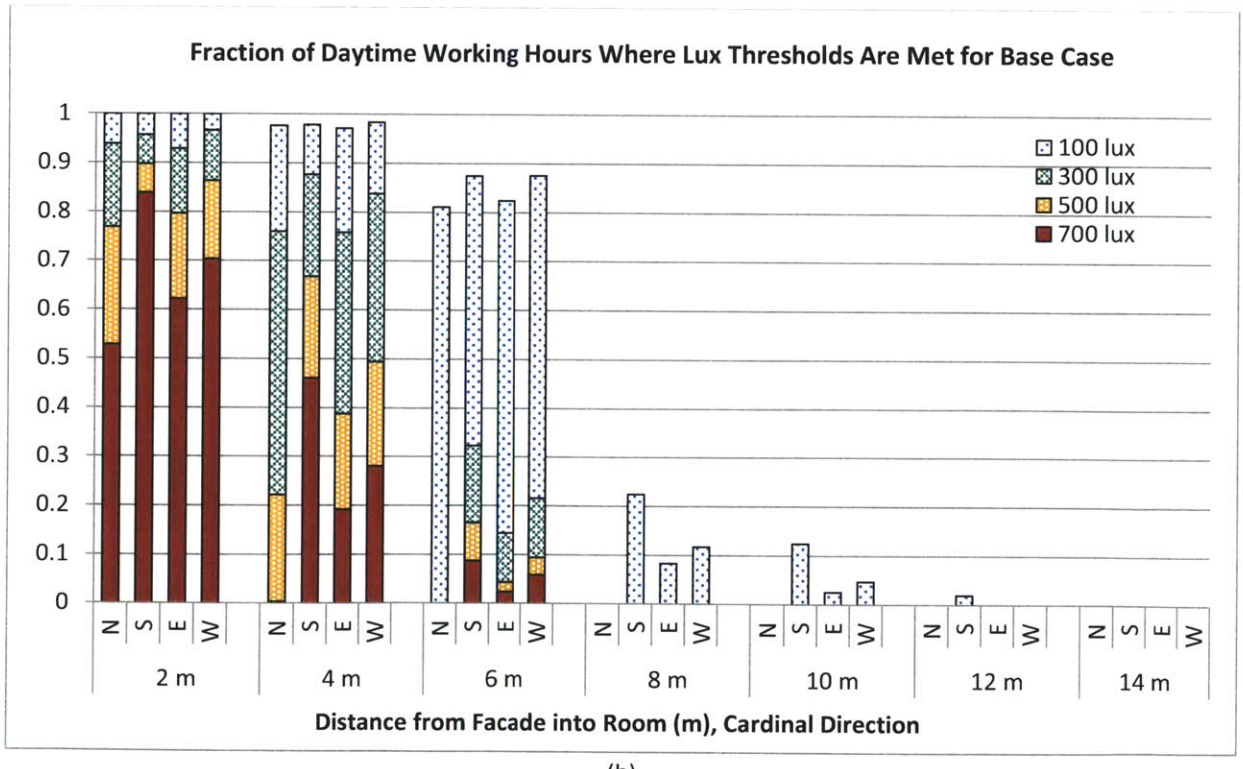


(b)

Figure 5.16: Effect of Facade Orientation on Daytime Daylight Autonomy: Soralux System (a) and Base Case (b)

### c) Effect of Room Width

The width of the room to be daylit has an impact on the performance of the system. In the generic model, a narrow room (7.4 m wide) was created within the wide room (37 m wide) by adding interior walls to the large space. The depth of the room remained at 15 m. A wide room is better for daylighting than a narrow room because in a narrow room, more light emitted by the system hits the side walls before descending to the workplane. Around half of this light is absorbed, depending on the wall reflectance (50% in the case evaluated), and most of the remaining light is diffusely reflected back into the front of the room. This restriction reduces the amount of light that travels deeply into the space.

The simulated results shown in Figure 5.17 bear this effect out. The narrow room reduces light levels only slightly at the front of the narrow room, but the reduction continues to increase at increasingly deeper points in the room. As an example, the fraction of daytime working hours where the Soralux system provides at least 100 lux at 4 m from the facade is 94% for the 37 m wide room and 91% for the 7.4 m wide room. Farther back in the space at 12 m from the facade, the difference in these two values becomes much larger: 50% for the wide room and 23% for the narrow room. The same effect is seen in the base case except, as typical, the light levels fall much faster than for the Soralux system at points deeper into the space. For the example described above, the values for the base case wide room are 100% at 4 m and 2% at 12 m. For the narrow room the base case values are 100% at 4 m and 0% at 12 m.

### d) Effect of Geographic Location and Climate

In order to ensure the system is effective for locations other than Tokyo (latitude 35.7°), simulations were run for three additional major cities: Austin (latitude 30.3°), Boston (latitude 42.4°), and Stockholm (latitude 59.4°), as shown in Figure 5.18. These cities are examples of locations where large deep-plan offices might be located and their range of latitudes provide coverage of the most populated latitudes on the globe. The differences between the cities were their latitude and local weather patterns. Because the results were calculated using the Daylight Coefficient Method, the geometry model of the test space did not have to be altered. For each city, a separate Sky Matrix was computed and combined with the Daylight Coefficient Matrix to arrive at the final result (as described in Appendix A).

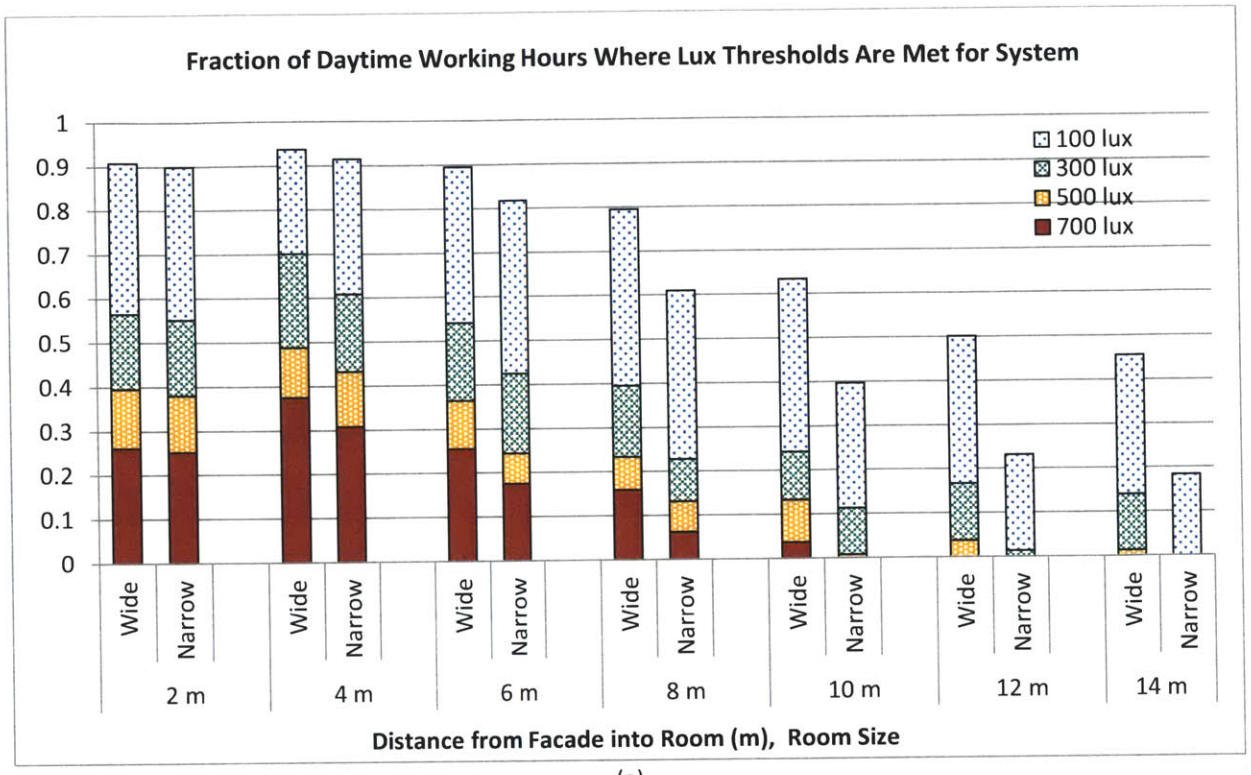


(a)

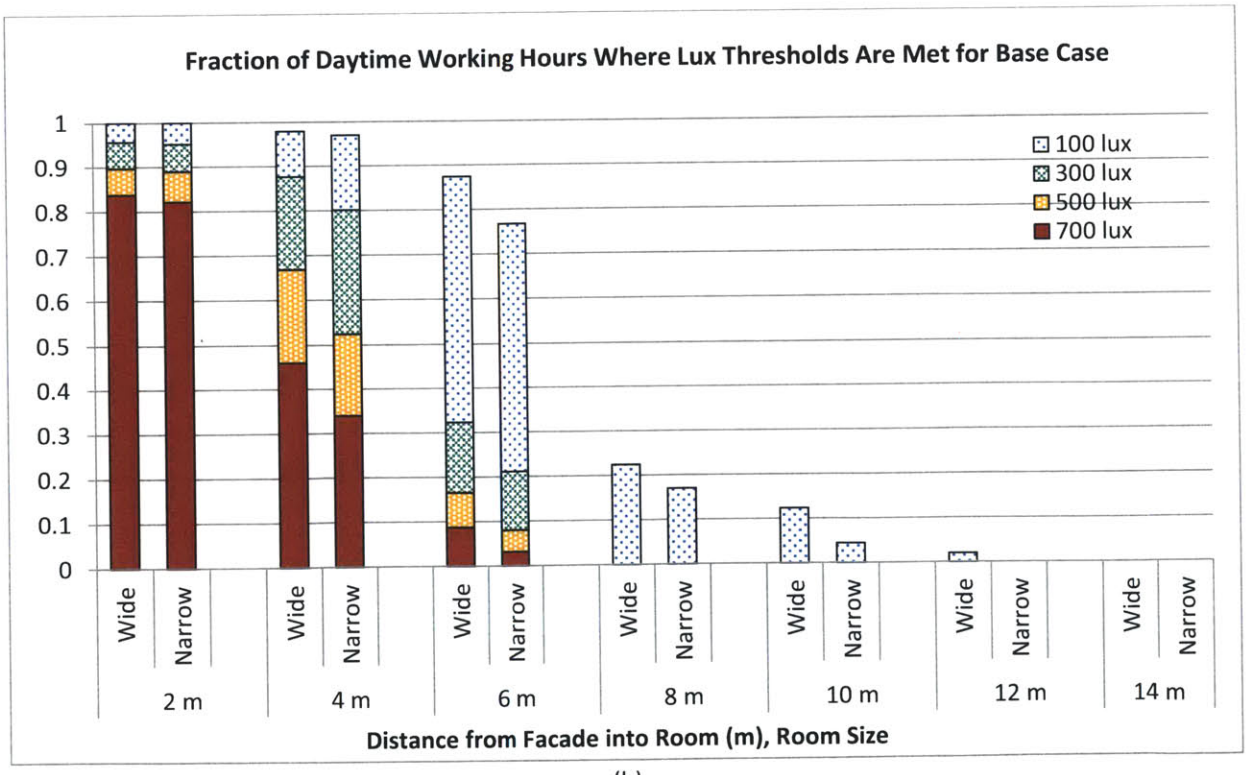


(b)

Figure 5.17: Effect of Room Width on Daytime Daylight Autonomy: Soralux System (a) and Base Case (b)

For this set of results, total working hours (8am-7pm) were used, rather than daytime working hours. The different locations have different numbers of daytime working hours, so to fairly compare them, total working hours (4015 for all cases) were used. For the remainder of the experiments, no base case results are included because the intent is to compare the Soralux system to itself under different conditions.

Between Austin, Boston, and Tokyo there was a surprisingly small difference in annual performance at the 300 lux level or higher. The percentage of all working hours where the system provides at least 300 lux at 8 m from the facade was 36% for Austin, 32% for Tokyo, 39% for Boston, and 29% for Stockholm. For example, Austin has a sunnier climate than Tokyo so one might expect a bigger difference in the results. However, part of the advantage Austin has from its sunny climate is offset by its sun course in the summer. As discussed in Section 5.4.1, the system is not particularly effective when the sun elevation angle moves above approximately 70°. This happens for a larger portion of the year in Austin than in Tokyo. For any particular location, weather patterns and sun course will combine in a unique way to affect performance so it is not sufficient to simply look at one factor or the other in isolation when evaluating a site.

The performance in Stockholm is noticeably lower than the other cities primarily because in the winter the sun does not rise very high in the sky. As a result, sun is blocked for a large number of time steps by the 15° sky obstruction or rejected at the inlet of the louver. The difference is especially apparent for lower light conditions inside the room. At 8 m from the facade, the system provides at least 100 lux for 44% of all working hours for Stockholm, whereas these values for Austin, Tokyo, and Boston are 73%, 65%, and 65%, respectively. For locations with very high latitudes, such as Stockholm, a louver design with a cut-off angle less than the main Soralux louver variant's 27.8° (the variant shown in Figure 4.16(a) on page 49 has a cut-off angle of 19.6°) may be more effective, even though it has a higher maximum output angle. The lower cut-off angle would allow the system to make use of more hours of direct sunlight, provided the sun was not blocked by the surroundings. A higher maximum output angle would mean that the light, on average, would not penetrate the space as deeply, reducing its efficacy in deep spaces.

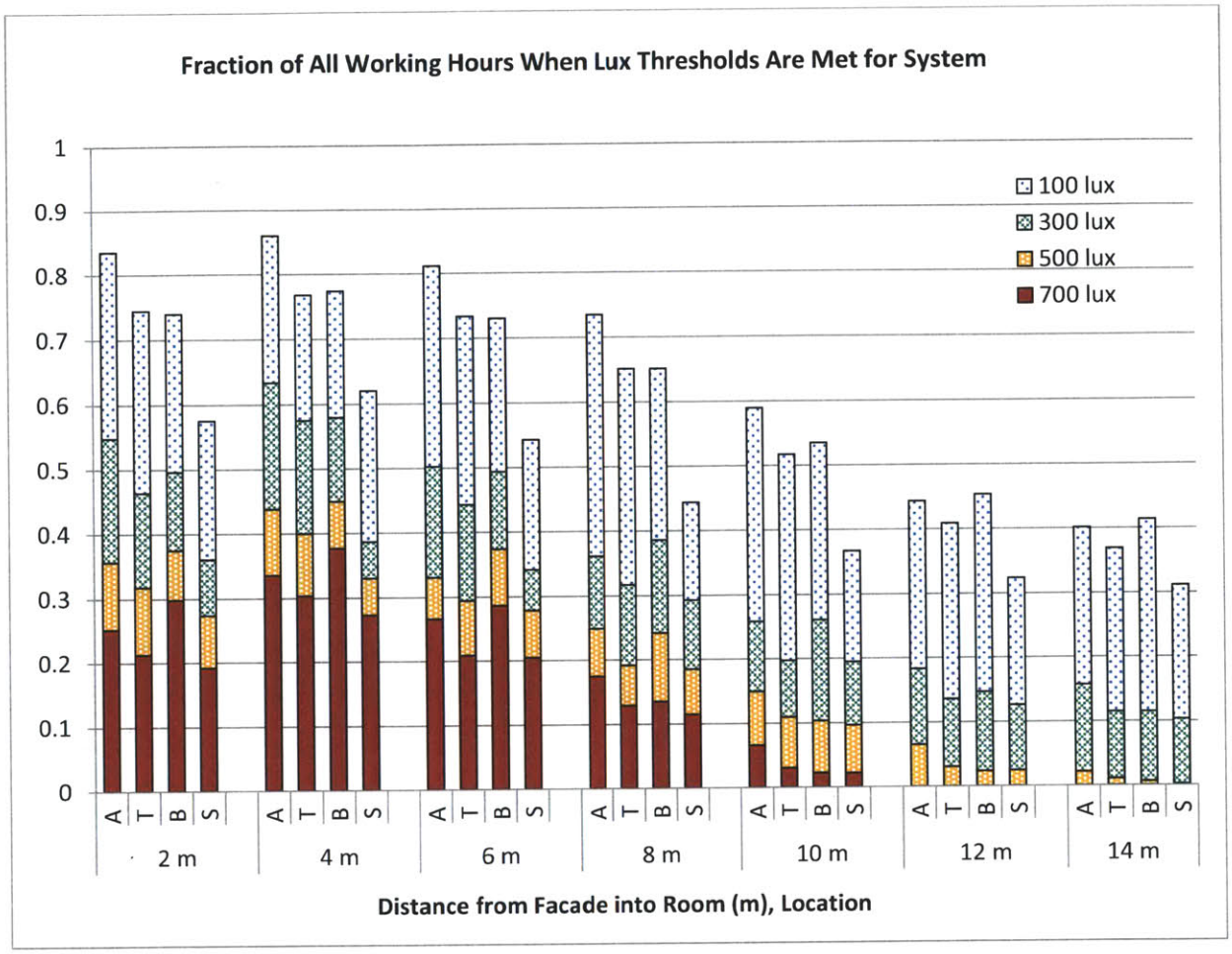


Figure 5.18: Effect of Geographic Location and Local Climate on System Daytime Daylight Autonomy (A: Austin, T: Tokyo, B: Boston, S: Stockholm)

### e) Effect of View Window Contribution

To clarify the effect of the lower view window with partially closed blinds on the results, Figure 5.19 shows the reference case with and without the lower window contribution. The lower window makes a relatively small difference in lighting levels. The difference is largest at the front of the room and diminishes with increasing depth. The inclusion of the lower window increases the percentage of daytime working hours with an illuminance of at least 300 lux from 45% to 57% at 2 m from the facade. At 14 m from the facade the addition of the lower window only increases the value from 12% to 14%.

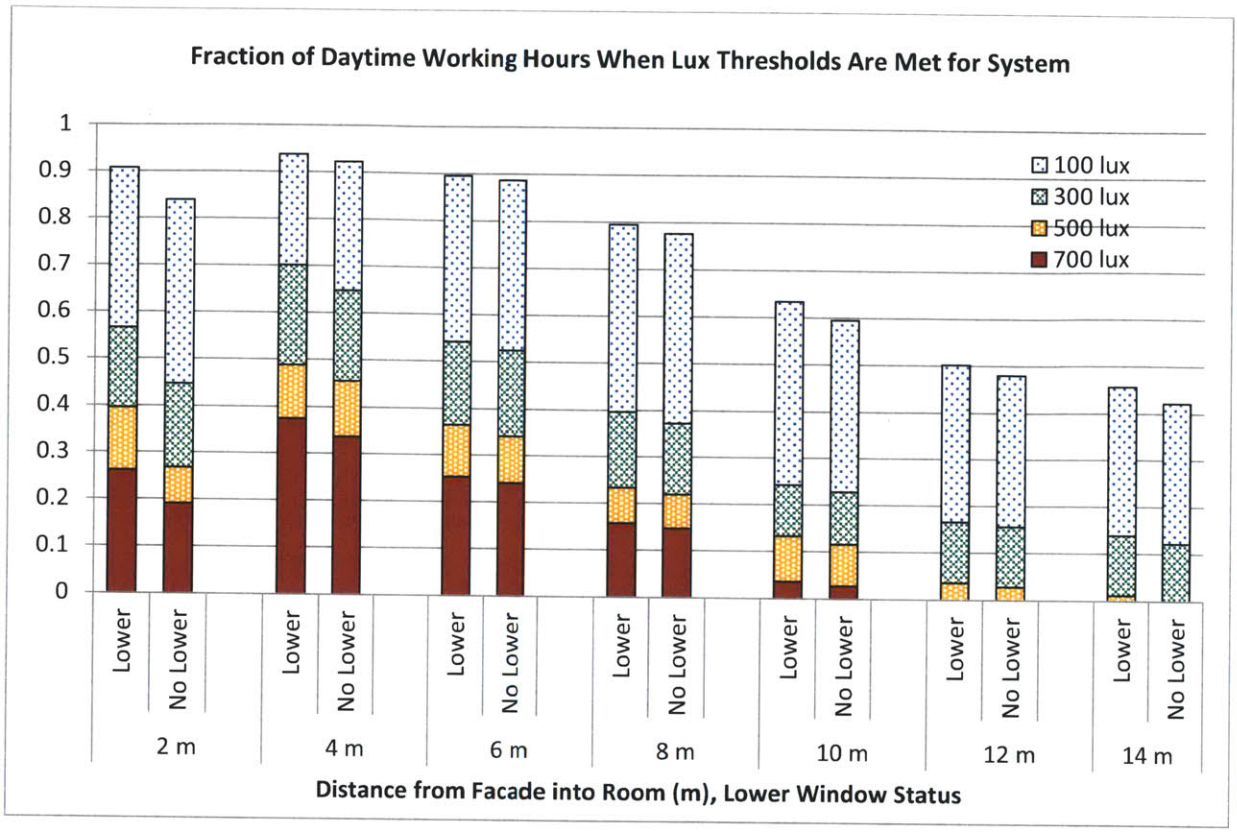


Figure 5.19: Effect of View Window with Partially Closed Venetian Blinds on System Daytime Daylight Autonomy

### f) Effect of Reflective Ceiling Length

The final two experiments consist of design trades conducted early in the development of the system to determine its configuration. First is the length of the reflective ceiling, as measured from the facade. The first column in each group shown in Figure 5.20 presents the performance of the system with a diffuse white ceiling (reflectance = .70, specularity = 0), rather than the reflective ceiling (reflectance = .856, specularity = .95). Without a reflective ceiling, light levels fall rapidly to much lower levels than for the rest of the variants. At 4 m from the facade, the variant without the reflective ceiling is only able to provide 300 lux or more for 40% of daytime working hours, whereas all the variants with reflective ceilings are in the 69% to 73% range. Deeper into the space at 8 m, the variant without a reflective ceiling is never able to produce 500 lux on the workplane, while the variants which include a reflective ceiling produce 500 lux for between 17% and 24% of daytime working hours.

When the reflective ceiling is included, the trend shows that a longer ceiling section results in higher illuminance levels in the back half of the space, while the levels in the front of the space are slightly

reduced. Very deep in the space at 12 m from the facade, the 2 m, 4 m, 6 m, and 15 m reflective ceilings are able to provide 300 lux or more for 8%, 17%, 20%, and 25% of daytime working hours, respectively. Near the facade at 2 m, the percentage of daytime working hours with an illuminance of 300 lux or more falls from 70% with no reflective ceiling, to 63%, 57%, 56%, and 56% for reflective ceiling lengths of 2 m, 4 m, 6 m, and 15 m, respectively.

The performance increase at the back of the room diminishes for each additional unit of ceiling length. Keeping cost in mind, 4 m was chosen as the length for the reference case, but increasing the reflective ceiling length reaps substantial dividends at the back of the room.

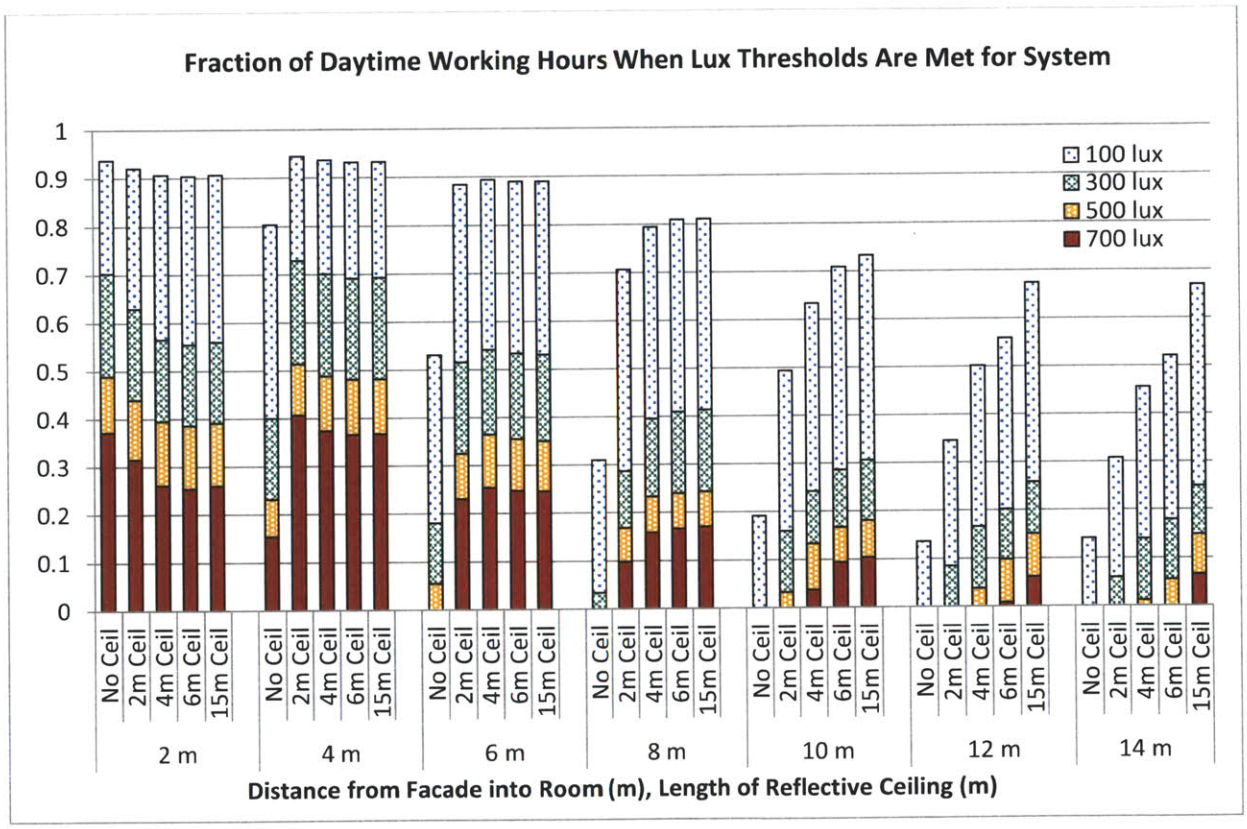


Figure 5.20 Effect of Reflective Ceiling Length on System Daytime Daylight Autonomy

### g) Effect of Refractive Rod Array Position

The final design trade concerned whether the refractive rods should be located inboard or outboard of the louvers. In other words, should the light pass through the louvers first or the rods? The simulation results in Figure 5.21 show that there is little difference between the two configurations in terms of lighting performance.

However, there is an aesthetic benefit to locating the rods inboard of the louvers. On the louvers' mirrored surfaces, imperfections such as dust, scratches, and fingerprints are easily seen and can mar the overall appearance of the system. When the rods are located between the louvers and the observer, these types of imperfections are not detectable and the overall look of the system is enhanced. As a result, the rods were placed inboard of the louvers in the final design. This effect and the appearance of the window unit from outside the building are both discussed further in Section 6.2.2.

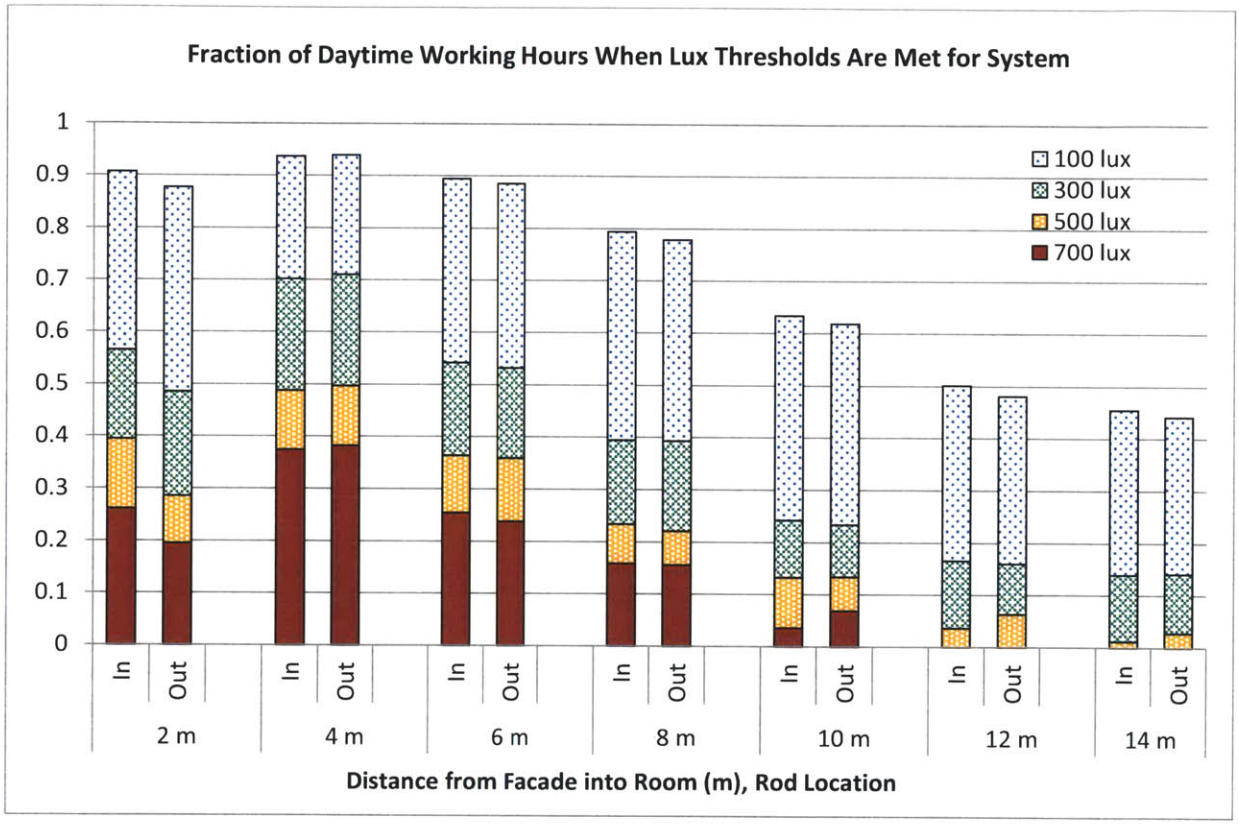


Figure 5.21: Effect of Refractive Rod Position on System Daytime Daylight Autonomy

## 5.5 Relative Energy Impact (REI) Estimate

Illuminance levels in the room only provide part of the picture when evaluating a daylighting system's impact on building energy consumption. In addition to the thermal dissipation of the electric lighting system, heat gains from solar radiation and conduction through the facade affect the overall energy balance as well. Depending on environmental conditions, a daylighting system's effect on solar heat gains and heat conduction can have a larger effect on the total energy consumption of a building than its

effect on the energy used for electric lighting. A new methodology proposed by Dave and Andersen provides a way to evaluate the total energy effects of complex fenestration systems, like the Soralux system, with a metric called the Relative Energy Impact (2011).

To allow some simplifying assumptions, the Relative Energy Impact (REI) is reported as a relative change from an easily understandable generic base case, and is therefore a unitless number. The base case description is similar to the one used throughout this chapter: a double-pane unshaded glazing covering the same size facade area as the complex fenestration system (Dave & Andersen, 2011). The REI of a system is defined as the net building energy load attributable to the evaluated system ($L_{sys}$) minus the net building energy load attributable to the base case ($L_{BC}$), divided by the absolute value of the net building energy load attributable to the base case, as shown in Equation 5.1.

$$REI = \frac{(L_{sys} - L_{BC})}{|L_{BC}|} \qquad \text{Equation 5.1}$$

By this definition, the base case has an REI of zero. The thermal model used to calculate REI accounts for solar heat gains due to direct and diffuse daylight, electric lighting, and conduction through the portion of the facade equipped with the system being tested. These energy loads are combined to determine, at each time step, the rate at which energy needs to be added or removed from the room by the HVAC system to maintain thermal equilibrium at 20°C, taking into account local weather conditions from a weather file. For solar heat gains, electric lighting, and conduction through the facade, energy savings are represented as positive numbers and energy expenditures are represented as negative numbers. Therefore, a negative REI indicates a system which results in higher energy consumption than the base case and a positive REI indicates a reduction in energy consumption relative to the base case.

For the REI calculation, the exterior balance point temperature was set to 10°C. When the exterior temperature was above this value, the building was assumed to be in cooling mode. When the exterior temperature was below this value the building was assumed to be in heating mode. For a real building, the exterior balance point temperature will depend on factors such as amount of insulation, amount of thermal dissipation resulting from occupants and electronics, etc. Whether the building was determined to be in heating or cooling mode defined whether particular heat flows were beneficial or detrimental to maintaining the energy balance of the test space. It was assumed that the heat flows resulting from the fenestration systems being tested would not be large enough in magnitude to shift the exterior balance point temperature of the building.

The following is an example of how REI is calculated. The units of the following factors are watts per square meter of fenestration system. A particular fenestration system might result in an average rate of electric lighting expenditure of -400 $W/m^2$, an average rate of energy savings of 1400 $W/m^2$ due to solar thermal heat gains, and an average rate of energy expenditure of -500 $W/m^2$ due to conduction across the facade. These three factors can then be added together for a positive net rate of energy savings of 500 $W/m^2$. If the base case resulted in a net rate of energy savings of 100 $W/m^2$, the REI of the system would be 4 ((500-100)/100 = 4). Admittedly, in its current form, REI is difficult to grasp intuitively. Development of the REI metric is still in progress and the methodology described above should be considered interim in nature. Future work by Dave & Andersen may further refine the metric.

The Soralux system, the base case, and a third case consisting of closed interior venetian blinds were all evaluated using the current REI methodology. The closed blinds were located inside the building space and were assigned a visible reflectance of 50%. These two cases were chosen as reference cases because they are both commonly occurring facade configurations in deep-plan office spaces with glazed curtain walls. The facade orientation evaluated was south and there were no sky obstructions.

The size of the glazed area, illuminance thresholds, and electric lighting dissipation were altered from the levels proposed in Dave & Andersen to match the specifics of the Soralux system and a typical Japanese office space (2011). Key assumptions are listed below and Figure 5.22 shows the model space used for the lighting calculations in Radiance.

- Tokyo weather data was used for sky conditions, exterior temperature, and wind speed.
- The double-glazed window transmittance is 81%.
- The facade area tested extends from 2.29 m to 3 m from the floor.
- The facade below 2.29 m is an opaque wall.
- The thermal dissipation of the electric lighting is 30 $W/m^2$ when fully on, and 20 $W/m^2$ when dimmed.
- The room is divided into three lighting zones of equal area. The first zone extends from the facade to a depth of 3 m. The second zone extends from 3 m to 6 m from the facade. The third zone extends from 6 m from the facade to the back of the space at 9 m.
- The workplane height in all zones is .76 m from the floor.
- If all sensors in a zone register at least 300 lux, the lights in that zone are dimmed.
- If all sensors in a zone register over 700 lux the lights in that zone are turned off.

- Surfaces' total spectral reflectances and transmittances are assumed to be equal to their visible reflectances and transmittances.
- Cloud cover is assumed to be 50% for all hours.
- Indoor convective heat transfer coefficient: 5 $W/m^2K$.
- Outdoor convective heat transfer coefficient: $16.21*(\text{wind speed})^{0.452}$ $W/m^2K$.

To evaluate conduction through the Soralux system, a simplified version of the window unit was modeled as a triple-glazing consisting of a glass pane, an acrylic pane, and a second glass pane. Because of the complex geometry of the louver section of the window unit, the rate of heat transfer was difficult to determine. Two simplified cases were modeled and their U-values (in $W/m^2K$) were calculated to establish upper and lower bounds for the insulating properties of the window unit. The U-values were calculated using standard National Fenestration Rating Council (NFRC) test conditions (interior temperature = 21°C, exterior temperature = -18°C, wind speed = 5.5 m/s).

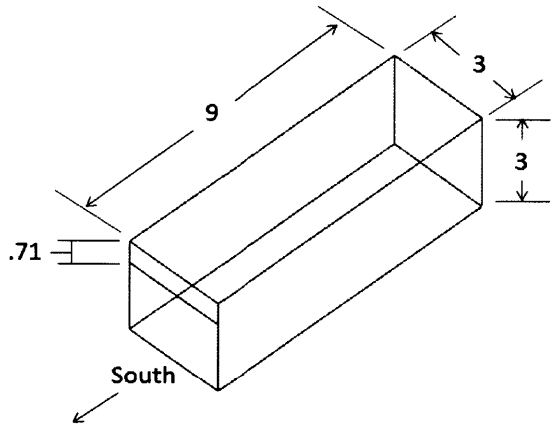


Figure 5.22: REI Radiance Model (Dimensions in Meters)

The lower bound for the U-value was found by modeling the section of the system containing the louvers as quiescent air. Still air is a relatively good insulator and so the resulting U-value for the system was 1.82 $W/m^2K$. The U-value calculated for the clear double-pane base case was 1.97 $W/m^2K$. An upper bound for the window unit was found by replacing the louver section of the window unit with a solid block of aluminum. In this case, the louver section offers almost no resistance to heat flow because of aluminum's high thermal conductivity (approximately 250 W/mK). Using this assumption, the U-value of the window unit was found to be 2.58 $W/m^2K$. This U-value is actually higher than the base case because the total thickness of the air gaps in the system is only 3 mm, compared to 6.4 mm for the base case.

The actual U-value of the Soralux window unit will likely fall in between these upper and lower bounds, although it is difficult to determine exactly where in that range without more sophisticated modeling.

The 10 mm diameter acrylic rods were modeled as a solid sheet of acrylic of equal volume to the actual rod array (sheet thickness: 7.9 mm). As with the louver approximations, this assumption was made to simplify the heat transfer model.

The results of the analysis showed that the Soralux system has an estimated REI between 1.9 and 10.1 compared to the clear double-paned base case. This range is defined by the results from the lower and upper bound U-values described above. As with the U-value, it is not possible to pinpoint where the system's REI would fall in the range between 1.9 and 10.1 without a more sophisticated model. However, this range does show that the system is expected to reduce the annual energy demands of a building compared to the base case. The actual REI value of the system is expected to be somewhere in the middle of the predicted range between 3 and 9.

The closed interior venetian blind case had an REI of 2.7, meaning that it would also reduce a building's energy annual demands, compared to the base case. Although the closed blinds reduce the solar heat gain factor, this is offset in part by the increase in electric lighting required. For the case tested, relative energy impact of the Soralux system is on par with or better than the closed interior venetian blinds, depending on where the REI of the system falls between its lower and upper bounds.

The primary reason for the Soralux system's superior performance compared to the unshaded window base case is due to decreased solar heat gains, not decreased lighting loads. The Soralux window unit causes lower solar heat gains than either of the two cases tested primarily because the louver surfaces absorb approximately 25-30% of the light that is incident on the window unit. The absorbed light turns to heat inside the window unit. Within the window unit, the heat is preferentially transferred back to the outdoors, due to the typically higher convective heat transfer coefficients found outdoors compared to indoors. The total amount of solar heat gain is further reduced for the Soralux window unit because the louvers reject low-angle light at their inlet. For a south-facing facade, this eliminates direct sunlight from entering the building early in the morning or late in the afternoon for certain parts of the year.

The other two cases allow all the light that is not reflected by the double-glazing into the room (since there is nothing inside of the window unit to absorb or reflect light), where the light is absorbed by interior room surfaces and remitted as long-wave infrared radiation. Since glass reflects, rather than transmits, long-wave infrared radiation, this energy cannot escape back through the glazing and adds to

the thermal load on the room (assuming the room is in cooling mode). Even the closed interior blind case suffers from this problem since half of the incident light is absorbed by the blinds before being reflected. The same effect happens with the Soralux system, but the amount of sunlight that passes through the facade is reduced because of the absorption and reflection in the window unit.

The estimated total solar heat gains are similar for the Soralux system and the closed interior venetian blinds, while the unshaded window allows significantly higher solar heat gains. This reduction in solar heat gains by the Soralux system will be less of an advantage in a consistently cold climate because the heat from the sun could be used to reduce building energy demands for a larger portion of the year. However for the climate tested here, Tokyo, reducing solar heat gains proved to be more beneficial.

# 6 Experimental Results

## 6.1 MIT Mockup

Once the initial design of the system was determined, a small physical prototype of the louver/ceiling system was built as a proof-of-concept to test for glare problems and to obtain a qualitative understanding of what the system would look like.

### 6.1.1 Mockup Fabrication

To produce the louver prototype, the louver was modeled in the Computer Aided Design (CAD) program SolidWorks. The edges of the individual louvers were designed so that they would stack together with the proper spacing. The parts were then exported as STL files that could be read by the 3D printer in the Edgerton Student Shop at MIT. Three-dimensional printing allows complex shapes to be formed by depositing one layer of liquid plastic at a time, analogous to the way a paper printer creates a page of text by marking one line at a time. Figure 6.1 shows a completed louver viewed edge-on.

Figure 6.1: Edge-On View of Louver Prototype

Once the louvers were complete, the surfaces were covered by a thin sheet of reflective metallized film, similar to Mylar™ made by DuPont. Although the material was highly reflective, the exact reflectance of the material is unknown because the equipment needed to test reflectance was not available. Strips of film were cut to the correct size and attached to the plastic louver using double-sided tape. The film

conformed to the profile of the louver, resulting in a louver with the correct shape and surface reflectance. The individual louvers were then assembled into a single unit, seven louver channels tall. The louver assembly was enclosed in a glazing unit with clear glass on both sides.

Because of the dimensional limitations of the 3D printer, as well as assembly time and cost considerations, the louver assembly prototype built was a small subset of the real size of the louver assembly. The louver's cross-section was built to scale (51 mm wide), but length and total number of louvers were reduced. The dimensions of the completed unit were .27 m wide and .15 m tall, not including the frame. The number of louver channels was limited to seven for the prototype, whereas the Tokyo mockup, described in Section 6.2, used 29 louver channels to fill the .71 m facade height allowed. Figure 6.2(a) shows the completed prototype louver unit.

The refractive rod assembly was created by cutting commercially-available acrylic rods to the correct length and gluing their ends to common top and bottom supports (see Figure 6.2(b)). The assembled rods were placed at the outlet of the window unit. The rods were not located between the panes of glass in this mockup because they were not a part of the original design.

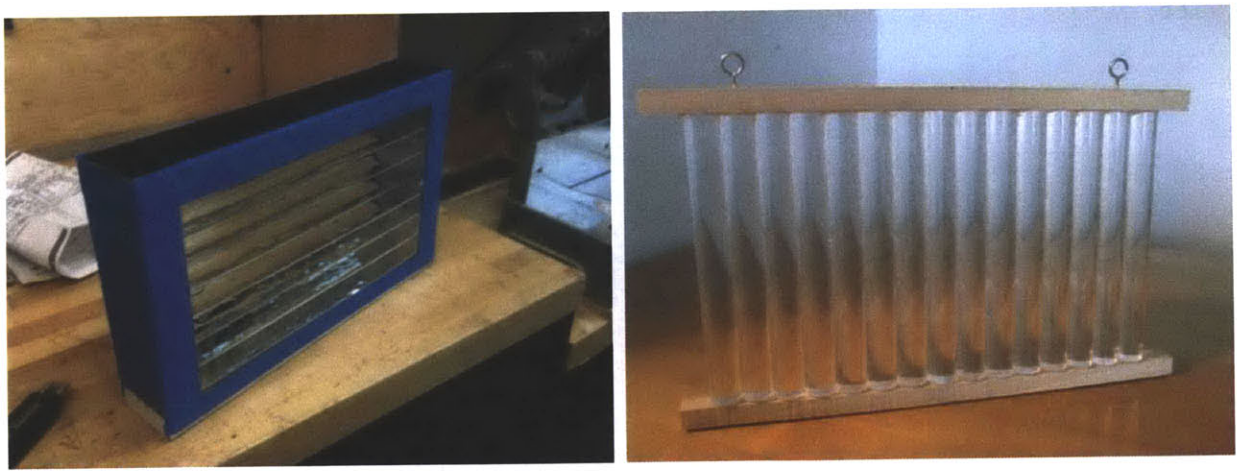

(a) (b)

Figure 6.2: Completed Louver Prototype Assembly (a); Completed Rod Prototype Assembly (b)

To create the reflective ceiling, sheets of bumpy reflective material (Cinegel #3803: Roscoflex S, made by Rosco) were glued to the underside of a large board measuring 2' x 6' (.61 x 1.83 m). Legs 5'6" (1.68 m) tall were attached to the corners of the board to provide sufficient vertical clearance to the ground. As with the louver material, the exact reflectance of the ceiling material is not known. A high strength Velcro strip was added to the underside of the board as well as the top of the glazing unit and rod

assembly so that they could be easily attached and removed from the ceiling assembly. The completed mockup, shown in Figure 6.3, was assembled and tested on a community baseball field in Cambridge, Massachusetts.

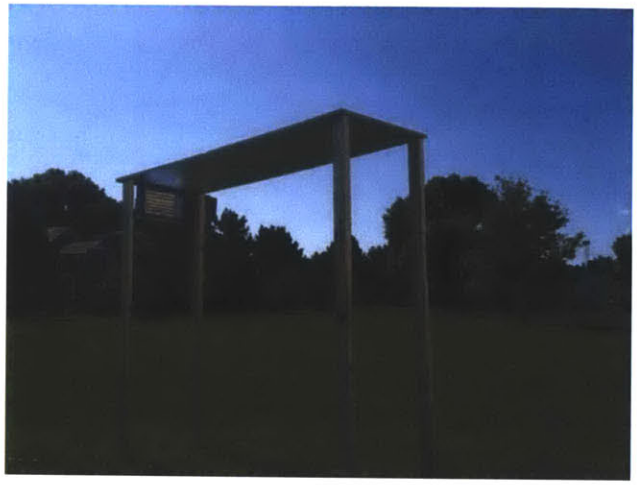

Figure 6.3: Test Mockup Fully Assembled

### 6.1.2 Mockup Test Results

The potential for glare was evaluated using point luminance readings as well as qualitative assessments and, while it was not considered to be a major concern, glare was identified as an issue that required further testing. At its brightest, the reflective ceiling did not cause visual discomfort, provided the reflection of the window unit off the ceiling was not in the center of the field of view. However, the ceiling was observed to cause visual discomfort if the reflection was in the center of the field of view. The addition of the refractive rods to the system reduced the peak luminance of the ceiling while increasing the ceiling's luminance in directions not parallel to the direct sun rays, as shown in Figure 6.4.

The data presented in Figure 6.4 was recorded on a clear November day in Cambridge, Massachusetts, near 10:45am at a constant distance of 3.5 m from the window unit and .75 m below the ceiling. The luminance meter used was a Minolta LS110. The prototype was aligned so that the azimuth angle of the incoming direct sunlight was 0°.

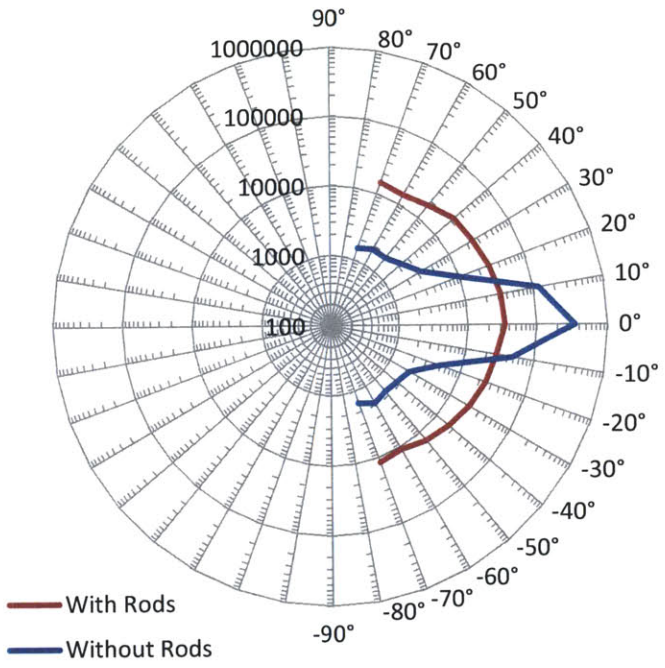


Figure 6.4: Prototype Ceiling Maximum Luminance (cd/m$^2$) as a Function of Azimuth Angle to Facade

Figure 6.5 illustrates how adding the refractive rods reduces the peak luminance of the ceiling. Figure 6.6 shows how the ceiling's brightness is elevated even for viewing angles not aligned with direct sunlight, due to the refractive rods. Additional MIT Mockup test results are found in Appendix C.

The most valuable benefit of the MIT mockup was that it allowed the system to be studied in the real world, rather than solely on the computer screen. Through evaluation of this mockup, it was determined that the amount of light diffusion resulting from the combined effect of louvers and ceiling was not sufficient to protect from glare resulting from direct sunlight. This conclusion led to the incorporation of the refractive rods, which were also tested on this mockup. Ultimately, the mockup gave confidence that the approach was reasonable and that the system would behave as expected. Obtaining this knowledge before designing and building the full-scale Tokyo mockup was invaluable. The MIT mockup effort illustrates the importance of iteration and testing in the product development process.

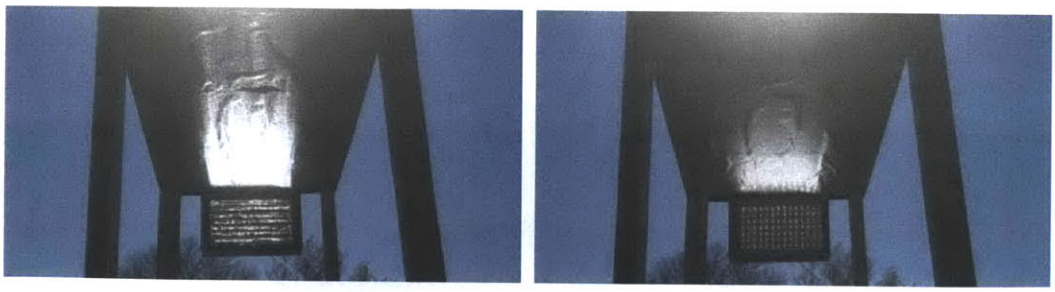

(a) (b)

Figure 6.5: Peak Brightness of Prototype Under Direct Sun Without Rods (a) and with Rods (b)

Figure 6.6: Ceiling Brightness Elevated for Angles Not Aligned With Direct Sunlight

## 6.2 Tokyo Mockup

In order to validate the Radiance simulation results, as well as test for glare problems more explicitly, a full-scale mockup of the daylighting system was erected in a Tokyo office building for two weeks in late February and early March 2011.

### 6.2.1 Mockup Fabrication

The louvers were the most complicated system element produced. After the profile of the louver was finalized, CAD drawings were sent out for fabrication. The louvers were produced through an aluminum extrusion process. Aluminum alloy 6063-T5, a common material for extrusion, was used. A section of the finished louver is shown in Figure 6.7.

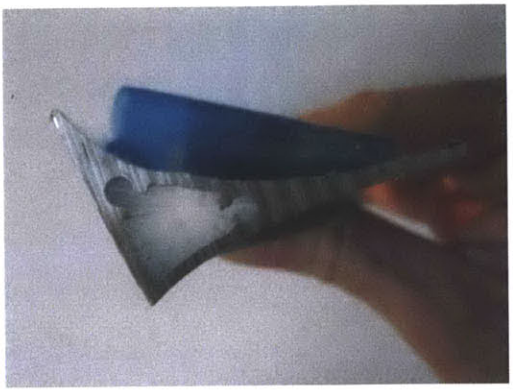

Figure 6.7: Tokyo Mockup Louver Viewed Edge-On

Although aluminum was chosen for this prototype, future versions could potentially use a polymer instead, as discussed in Section 4.2.7. Aluminum was selected in large part to maintain flexibility in the method by which the surface would be made reflective. Because of the concurrent nature of the mockup development, it was not clear until relatively late in the process whether the outer surfaces of the louvers would be made reflective by a) fine polishing, b) metal vapor deposition, or c) applying an adhesive-backed reflective film. Choosing plastic as the substrate material would have eliminated fine polishing as an option. Ultimately, the adhesive-backed reflective film was chosen for the mockup and after the louvers were produced, they were machine-wrapped with an adhesive-backed reflective film. The louvers were then assembled into an array by affixing them to endplates. Thru-holes were drilled into the endplates at the correct locations and screws were inserted into tapped holes in the louvers, as shown in Figure 6.8.

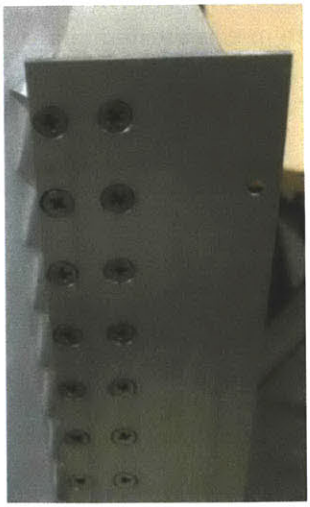

Figure 6.8: Louver Alignment and Support Method

Production of the acrylic rod assemblies was considerably simpler than the louvers. The rods were commercially available, so a quantity of 10 mm diameter acrylic rod was purchased and cut to the proper length. Sets of rods were then combined into .6 m wide assemblies by gluing their top and bottom ends to common endplates.

The louver and rod assemblies were then installed into a frame structure, which also included a pane of glass on the room side of the frame (Figure 6.9(a)). An exterior-side glazing was unnecessary because the mockup was to be installed behind the existing single pane window in the test office. The dimensions of each completed daylighting window module, including its frame, were 1.8 m (width) x .71 m (height) x .085 m (depth). Thirty individual louvers with a pitch of 22.1 mm were used to fill the height of each module.

(a) (b)

Figure 6.9: The Soralux Window Unit (a) and Reflective Ceiling (b) as Installed in the Tokyo Mockup

The reflective ceiling material was also commercially available. The particular material used for this mockup was the anodized version of Alanod's Miro Stucco G aluminum sheet. This material has the high reflectance and specularity and rough texture called for by the system's design. Sheets of the material were temporarily affixed to the existing acoustical tile ceiling, as shown in Figure 6.9(b).

### 6.2.2 Mockup Details

Since the project's sponsor organization, Hulic, is a commercial real-estate development company located in Tokyo, Japan, a number of potentially suitable company-owned mockup locations were identified. Based on availability and site characteristics, a seven-story office building in the Chuo ward of Tokyo was chosen (see Figure 6.10). The building has a southwest-facing facade (27° west of south) and a deep-plan office layout. The test office was located on the sixth floor.

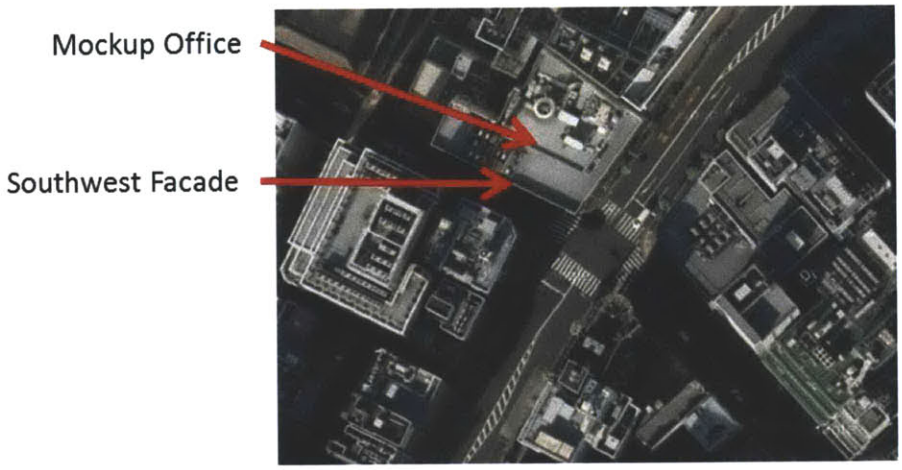


Figure 6.10: Plan View of Mockup Office and Its Surroundings

Three 1.8 m wide Soralux window modules were installed on the facade, inboard of the building's existing view window, making the mockup's total width 5.4 m. The dimensions of the installed reflective ceiling were 5.4 m in width and 4 m in depth from the facade. Opaque white curtains were installed along the full length of the glazed southern and eastern facades in order to block out exterior light. One limitation of the space was that the ceiling height was significantly lower than the height the system was designed for (2.8 m). The height of the ceiling in the office was 2.53 m, but the height dropped to 2.4 m at the facade, due to a structural beam. The window modules were installed directly underneath this beam so their maximum height was limited to 2.4 m. Because of the lower ceiling height, the window units appear lower and cover a larger portion of the facade than they will in the permanent installation. Figure 6.11 displays images of the system from different distances into the room.

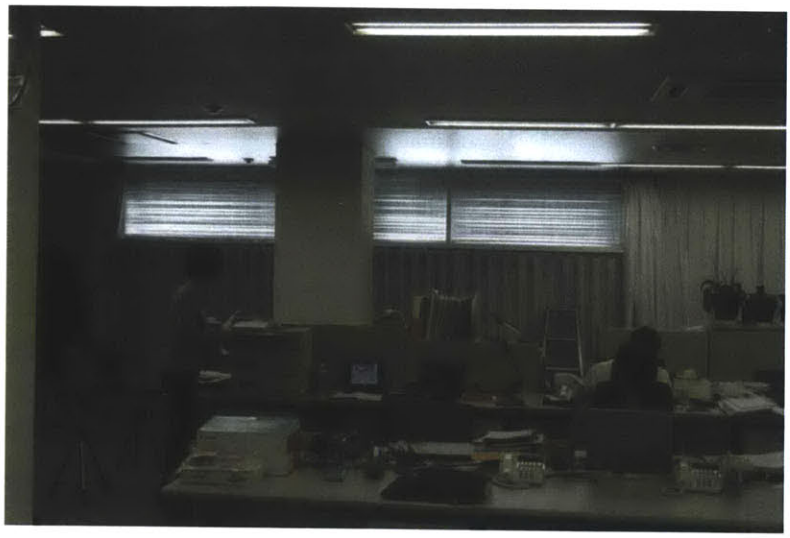

(a)

(b)

(c)

Figure 6.11: Views of the System at 12 m (a), 10 m (b), and 6 m (c) from Facade

Figure 6.12 shows the layout of the Soralux system and the geometry of the room near the facade. Figure 6.13 shows a close-up view of sunlight passing through the louvers without the refractive rods installed. The light patterns seen in this figure can be compared qualitatively with the ray tracing simulations shown in Figure 4.11 on page 43.

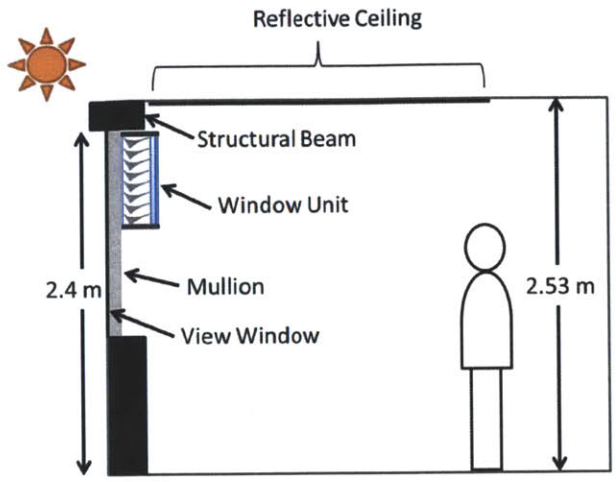


Figure 6.12: Cross-Sectional Diagram of Tokyo Mockup Installation at the Front of the Room

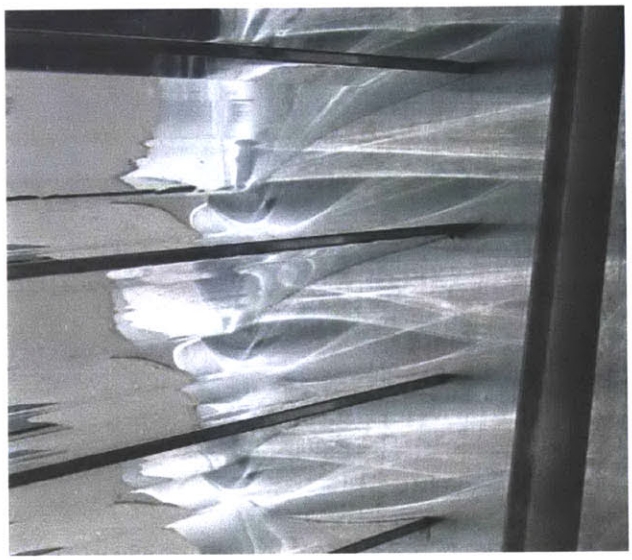

Figure 6.13: Light Rays Passing Through Louvers Without Rods Installed

Figure 6.14 shows window unit's appearance from close to the facade. In addition to the glare control function, the array of rods also provides several aesthetic effects. First, since they are located inboard of the louvers, the rods hide the imperfections in the louvers' surfaces. When the louvers are viewed without the rods installed, imperfections on the louver's specular surfaces are noticed easily. The imperfections include small air bubbles underneath the reflective surface from the wrapping process and stray fingerprints from handling. The bending of the light passing through the rods obscures the image of what is behind the rods and so the imperfections are not noticeable. This gives the window unit a much cleaner look.

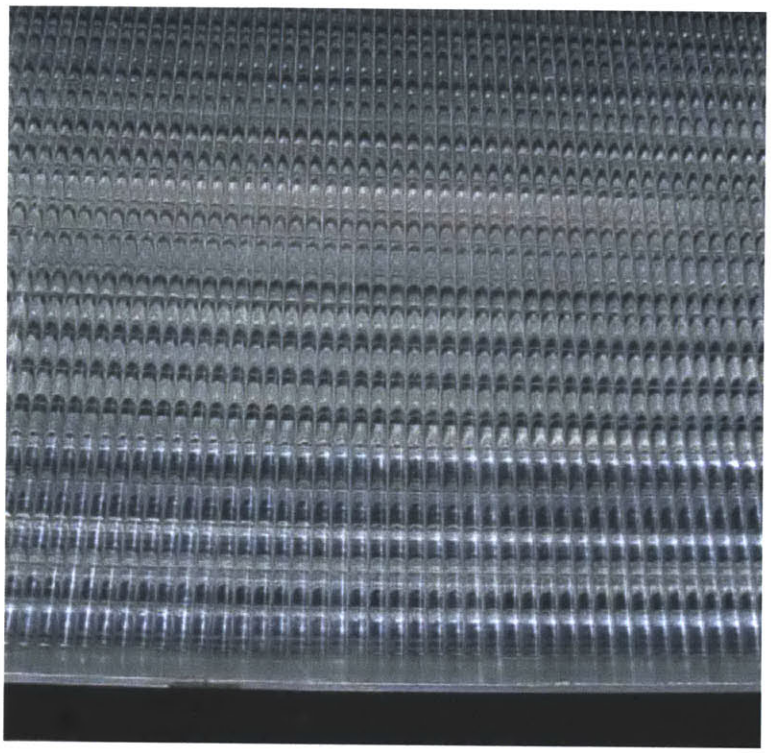

Figure 6.14: View of Window Unit from Below

The effect of light reflected off the interior surfaces of the window unit, discussed in Section 4.4, also improves the unit's visual appearance. Some of this internally reflected light exits the window unit at a downward angle in a diffuse manner, giving the unit a soft glow. The glow effect improves the visual appearance of the unit compared to if the unit was completely dark (resulting from zero downwardly directed light). Additional close-up views of the window unit are provided in Figures 6.26 and 6.27.

Figure 6.15 shows the appearance of the system from street level. Two significant effects can be seen in the images. First, most of the window unit appears relatively dark and is not greatly different in visual appearance from the windows on the neighboring floors above and below. Second, the leftmost section of the window unit has a different appearance from the rest, as it exhibits a light brown color. Both of these effects occur because the flat exterior-facing louver surface reflects light from below the horizon back down towards ground level, as shown in Figure 6.16. The light brown reflection on the left side of the louvers results from early morning sunlight reflected off an adjacent brown building, which can be seen at the left edge of Figure 6.15(a). The dark areas of the louvers are reflecting light from street level, which is not as brightly lit.

(a)

(b)

Figure 6.15: View of Window Unit from Street Level: Wide View (a), Close Up (b)

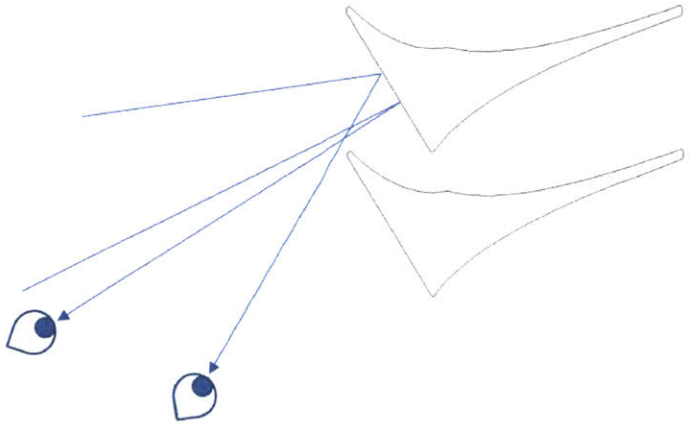

Figure 6.16: Reflection of Light from Below the Horizon by Louvers

This property of the Soralux system has the potential to provide visual interest to the exterior facade of a building by reflecting its surroundings. The patterns of light seen on the louvers will change depending on the surroundings and time of day. There is some potential for direct sunlight to be reflected by the outside of the louvers into the urban surroundings. However, this impact of this potential problem is expected to be limited for the reasons discussed in Section 4.2.4.

Although the mockup building's urban surroundings were typical of a dense city, they were not ideal for testing because the sun passed behind neighboring buildings in the afternoons, starting at about 2:30pm. Taking accurate sky condition measurements from the roof of the building was impossible after this time of day. Monitoring began each day at 9:00am. This start time was based on when the test operators had access to the building, rather than based on the sun course. Sun obstructions from the urban surroundings were not an issue in the morning. The view out from the mockup facade is shown as a composite image in Figure 6.17.

Figure 6.17: Southwestern Sky Obstructions as Seen from Mockup Space

### 6.2.3 Mockup Testing Procedure

Monitoring equipment consisted of a fixed line of illuminance sensors, a mobile illuminance sensor apparatus functioning as a manual pyrheliometer and pyrometer, and a luminance meter. The fixed illuminance sensors were lined up in a row normal to the facade and spaced in 1 m intervals, as shown in Figure 6.18.

Figure 6.18: Illuminance Sensor Line

There were eight sensors in total, resulting in measurement points at 1, 2, 3, 4, 5, 6, 7, and 8 m from the facade. The sensors were oriented to record horizontal illuminance at a workplane height of .75 m from the floor. Their measurement range was between 0 and 20,000 lux, with a resolution of 10 lux. The Hioki 3640 illuminance sensors contain onboard memory, so after synching all their internal clocks, the sensors were set to record illuminance values every 2 seconds throughout the monitoring day. At the end of each monitoring day, the data from each sensor were downloaded onto a computer and the sensors were set up for the next day's testing. The Hioki sensors have a ±4% accuracy rating, but the sensors used in the mockup did not have calibration documentation, so the error could have been higher (Tequipment, 2011).

An additional illuminance sensor of the same type as the fixed sensors was used to take sky measurements. The measurement range for this sensor was set to between 0 and 200,000 lux with a resolution of 100 lux. Figure 6.21 shows the sky condition measurement apparatus.

Finally, a luminance meter was used to take spot measurements of the luminance of the reflective ceiling throughout the day. The sensor used was a Minolta LS110. The monitoring campaign lasted for two weeks, beginning on February 21, 2011 and ending on March 4, 2011 with testing occurring during the two workweeks.

### a) Limitations of the Mockup Space

It is important to list the major limitations of the mockup setting as they have the potential to significantly impact the quality of the measured and simulated test results. These limitations were a result of constraints imposed by the existing mockup space and available budget.

First, and most significant, is that the available space and monitoring equipment did not allow for a separate set of control measurements to be taken. Ideally, an identical office space would have been set up adjacent to the system mockup space so that the base lighting conditions without the daylighting system could be measured. However, this was not an option, which increased both the difficulty and the importance of comparing the measured system results to the simulated results in order to validate the performance of the system.

The geometry of the office space also introduced some difficulties. As previously mentioned, the ceiling was only 2.53 m in the main space and 2.4 m at the facade. This affected the light distribution on the sensors. The lower ceiling also gave an inaccurate initial visual impression to visitors who had not yet been informed of this discrepancy. A large (.75 m x .75m) column, seen in Figure 6.20, was located along the centerline of the mockup. The presence of the column forced the line of illuminance sensors to be located off center from the daylighting window units. The column also blocked a nontrivial portion of the light emitted by the system from reaching the sensors. This effect was accounted for in the Radiance model by including the column in the room's geometry. Third, the outboard edge of the window unit had to be located several centimeters inboard of the office's existing window. In addition, there was an overhang on the exterior of the building (shown in Figure 6.19). As a result, the window unit had an effective overhang of .23 m which blocked a significant portion of the louvers area from receiving direct sunlight throughout the day. The overhang was modeled in Radiance to account for this effect.

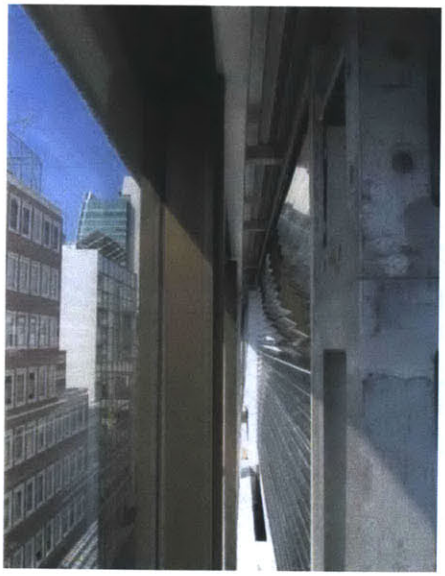

Figure 6.19: View of the Shading Caused by the Building Overhang

Because the space was being actively used as an office while testing was ongoing, the test space could not be isolated from the daily activities of the office. This meant that the space around the sensors could not be curtained off to simplify the room geometry of the model. As a result, the full office space had to be modeled in Radiance, which added potential sources of error. Additionally, because the row of sensors were located in a walkway between desks and office equipment, individual sensors were regularly blocked for a few seconds at a time as office workers moved past the sensors. This created a problem in a few cases where it was clear by looking at the measured data that someone or something was blocking one or more sensors during an important measurement interval. When this occurred, the problem was compensated for by selecting a time step a few seconds earlier or later where the blocking effect was not present.

A final limitation was that neither a pyrometer nor a pyrheliometer were available for use in taking direct normal and diffuse horizontal sky measurements. These values were captured manually using an illuminance meter and additional equipment.

### b) Static Data Acquisition Procedure

The majority of the data gathered during the test campaign was from the row of illuminance sensors inside the mockup space. The sensors were set up to continuously capture illuminance at 2 second intervals during the test day. Because the electric light fixtures remained on during the test period so that the office workers could function normally, the baseline light levels incident on the illuminance sensors resulting from the office's electric lighting had to be determined. To accomplish this, a curtain in addition to those which blocked the office's view windows, was drawn over the Soralux window units so that all light from outside the building was blocked out, as shown in Figure 6.20.

Figure 6.20: View of Mockup Office with All Curtains Drawn to Take Baseline Illuminance Measurements

In this state, illuminance values were recorded for all sensors. This procedure was repeated at the beginning and end of each test day. The two results for each day were averaged together to create a baseline illuminance level for each day, which was subtracted from the total illuminance measured to obtain the contribution resulting from the daylighting system. The baseline illuminance varied at most by about 10 to 20 lux across each day.

### c) Sky Measurement Procedure

Since the equipment necessary to take continuous sky condition measurements was not available, the data had to be captured manually as frequently as practical. Sky measurements were taken every 30 to 45 minutes during the test day on the roof of the mockup building. The two values measured were direct normal illuminance and diffuse horizontal illuminance. These two values were measured because they are required by the Gendaylit program in Radiance to create the simulated sky. Because the mockup building was not as tall as some of the surrounding buildings, part of the sky dome near the horizon was obstructed, which would tend to cause a small underestimate in the diffuse horizontal measurement. The direct normal measurement, however, was unaffected by these obstructions during the test interval.

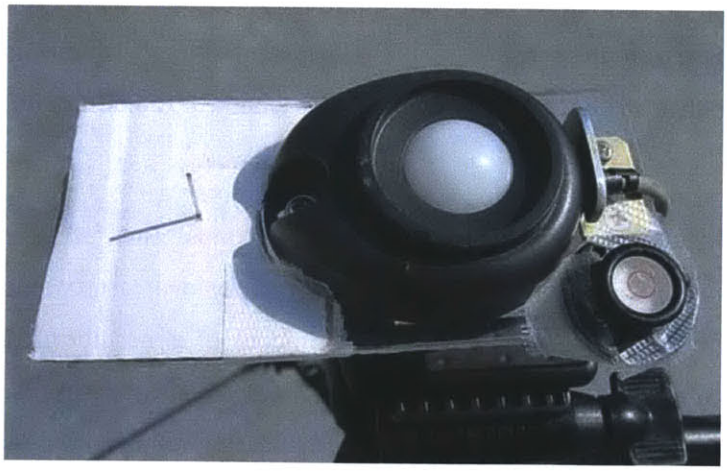

Figure 6.21: Sky Measurement Apparatus

Figure 6.21 shows the measurement apparatus used to determine direct normal and diffuse horizontal illuminance. The main element is an illuminance sensor, of the same type used for the static measurements in the mockup space, mounted on a tripod. Adjacent to the illuminance sensor is a simple sundial with a normal vector parallel to the normal vector of the illuminance sensor. The sundial

was used to find the orientation normal to the sun. Finally, a bull's eye (two-axis) spirit level, used to find the horizontal orientation, was mounted on a plane parallel to the mounting plane of the illuminance sensor. A separate sun shading disk mounted on a thin rod is used to block the sky within 3° of the sun, when necessary. Using this setup, the data acquisition procedure was as follows:

1) Align the illuminance sensor with the sun by adjusting the tripod mount until the shadow of the sundial's gnomon (shaft) disappears.
2) Record the current time.
3) Block direct sun using the shading disk by holding it between the sensor and the sun at a distance of .18 m from the sensor.
4) Record the illuminance value shown by the sensor. This corresponds to the diffuse normal illuminance of the sky.
5) Remove shading disk.
6) Record new illuminance value shown. This value corresponds to the global normal illuminance of the sky. The difference between this measurement and the one taken in step four is the direct normal illuminance.
7) Adjust mount so that the sensor's normal vector is vertical, using the spirit level.
8) Block direct sun using the shading disk by holding it between the sensor and the sun at a distance of .18 m from the sensor.
9) Record illuminance value shown. This value corresponds to the diffuse horizontal illuminance of the sky.

The process from steps two to nine takes about 15 seconds. The fact that the process is not instantaneous is not a problem for either fully clear or fully overcast time periods. However, for intermediate (partly cloudy) time periods, when the amount of direct normal and diffuse horizontal illuminance can change rapidly, the time interval for taking sky measurements can introduce significant error. Upon reviewing the collected data, it was determined that the results taken during intermediate sky conditions were too prone to error and were removed from the final data set. For each sky measurement time step, the corresponding set of office illuminance results were pulled from the data recorded by the workplane illuminance sensors.

After removing measurements taken under intermediate skies, there remained 35 measured Tokyo mockup time steps, taken over the course of eight separate days. The resolution of the sensors was 10 lux. Errors between measured and simulated results would be expected to increase as the measured

results decrease towards 10 lux. Consequently, in comparing measured and simulated results, only data points with measured values of 80 lux or higher were used to determine the bias and relative difference errors in order to limit the effect of sensor resolution on estimated error.

### 6.2.4 Tokyo Mockup Radiance Model

Since comparing the simulated results to the test results for the mockup was an important goal, it was critical that the Radiance model of the space be as accurate as possible. In order to create the Radiance model of the mockup space, the geometry and material properties of the office were defined using both blueprints and on-site measurements. Figure 6.22 shows details of the Tokyo mockup office space model and Table 6.1 provides the major material properties.

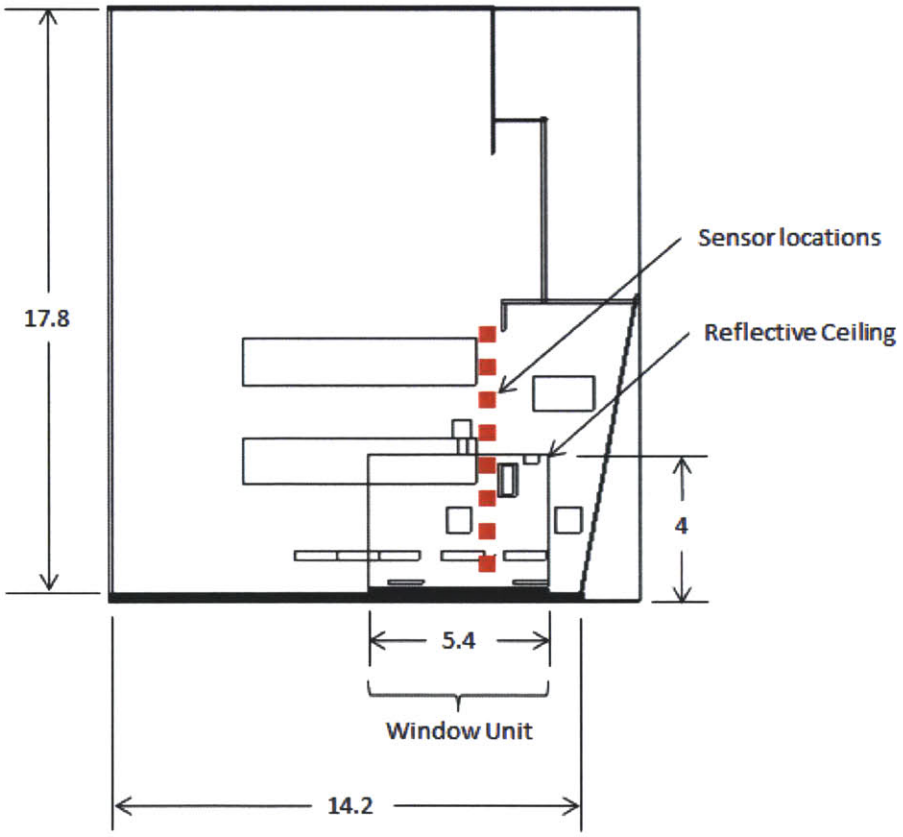


Figure 6.22: Plan View of Tokyo Mockup Office Radiance Model (Dimensions in Meters)

Table 6.1: Tokyo Mockup Radiance Model Parameters

| Name | Value | Notes |
|---|---|---|
| Refractive Rod Absorbtance over 1 m | 0.146 | .004 over 1 inch |
| Refractive Rod Index of Refraction | 1.49 | |
| Louver Reflectance | 0.87 | |
| Louver Specularity | 1.00 | Mirror material type |
| Louver Roughness | 0.00 | |
| Reflective Ceiling Reflectance | 0.856 | |
| Reflective Ceiling Specularity | 0.95 | |
| Reflective Ceiling Roughness | 0.125 | |
| **Wall Reflectance** | **0.48** | |
| Structural Column Reflectance | 0.80 | |
| Curtain Reflectance | 0.65 | Lowered from .72 measured value, because of self-shading |
| **Floor Reflectance** | **0.14** | |
| **Standard Ceiling Reflectance** | **0.71** | |
| Window Unit Frame Reflectance | 0.60 | |
| **Mullion Reflectance** | **0.07** | |
| **Existing Glass Transmittance (single pane)** | **0.893** | |
| **Window Unit Interior Glass Transmittance** | **0.92** | |
| Furniture Reflectance | 0.40 | |
| Exterior Ground Reflectance | 0.08 | |
| Southwest Building Reflectance | 0.12 | |
| Southeast Building Reflectance | 0.08 | |

*Rows in bold are different from the equivalent generic model parameters.

### a) Surroundings Properties

The building's orientation and surroundings were modeled using information from Google Earth. The surrounding building's heights, their dimensions, and the distances between buildings were all measured using the 3D representations of the area found in Google Earth. While the accuracy of this method is somewhat limited, it was the best option available and it allowed the model to be constructed before the trip to Tokyo. Figure 6.23 compares the view out from the facade of the test space in both the Radiance model and as photographed in the real space.

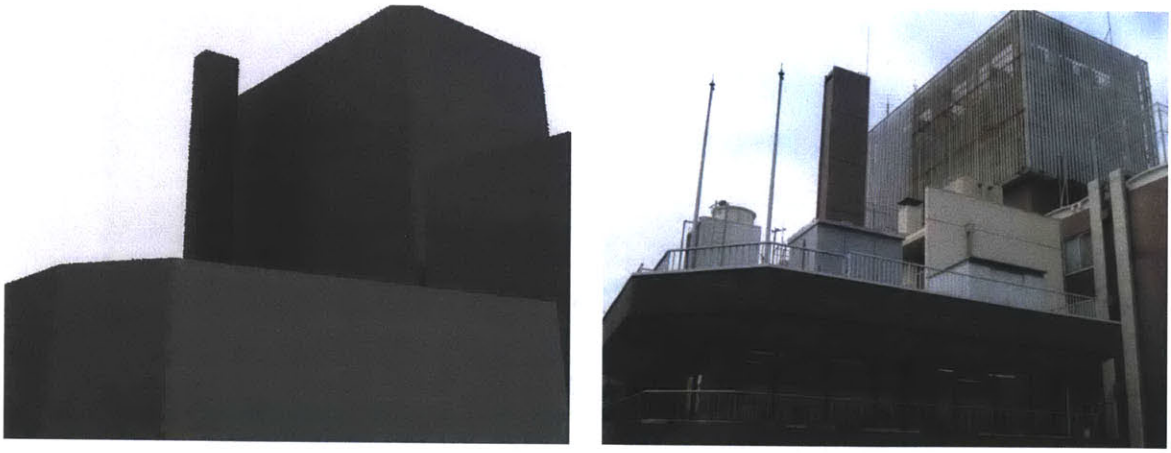

(a) (b)

Figure 6.23: View from the Mockup Facade Looking Out for Model (a) and Actual Space (b)

The surfaces that make up the sky obstructions in Figure 6.23(a) can be seen in the upper-right quadrant of the model in Figure 6.24. The white shape in the middle of the image is the test space. The surrounding buildings were modeled as triangular shapes to reduce model construction time, which could be done because the missing surfaces are not visible from inside the mockup space, as shown in Figure 6.23(a).

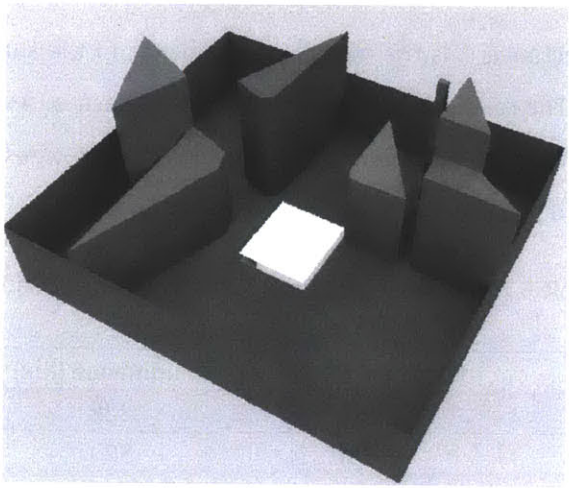

Figure 6.24: View of the Entire Model Scene Including Surroundings

### b) Office Space Properties

Figure 6.25 shows the Radiance model and actual mockup space from a viewpoint 6 m from the facade. The window unit and reflective ceiling, as well as major room geometry such as the vertical column and desks can be seen in the images.

(a) (b)

Figure 6.25: Comparison of Model (a) to Actual (b) Office Space

The reflectance of major room surfaces was measured on-site and calculated using the equation:

$$\rho = \frac{L\pi}{E} \qquad \text{Equation 6.1}$$

where ρ is the surface reflectance, L is the measured luminance of the surface, and E is the measured illuminance on the surface. The relationship assumes that the surface is Lambertian (perfectly diffusing): a reasonable approximation for the surfaces measured. Table 6.2 provides the measured data and the resulting reflectances used in the Radiance model.

Table 6.2: Measured Data Used for Reflectance Calculations

| Surface | Luminance ($cd/m^2$) | Illuminance (lux) | Reflectance |
|---|---|---|---|
| Walls | 50 | 328 | .48 |
| Columns | 150 | 590 | .80 |
| Curtains | 166 | 725 | .72 |
| Floor | 32 | 724 | .14 |
| Ceiling | 35 | 154 | .71 |
| Desks | 113 | 896 | .40 |
| Street | 270 | 10980 | .08 |
| South Building | 130 | 3460 | .12 |
| Southeast Building | 124 | 4950 | .08 |

The transmittance of the existing office glazing was measured using a luminance meter on a clear day when exterior light levels were relatively constant. A target for the luminance meter, consisting of a large white diffuse wall of a distant building, was identified. The window was partially opened and the luminance meter was focused on the target. The luminance of the target was first measured with the luminance meter located behind the open section of the window and then behind the closed section. The luminance meter was placed against the glass for the closed case to minimize errors due to interior light reflections off the glass. The ratio of these two measurements provides the window's transmittance. Table 6.3 shows the recorded values and the window transmittance used in the model.

Table 6.3: Measured Data Used for Existing Window Transmittance Calculation

| Open ($cd/m^2$) | Closed ($cd/m^2$) | Transmittance |
|---|---|---|
| 2290 | 2000 | .873 |
| 2060 | 1850 | .898 |
| 2070 | 1860 | .899 |
| 2070 | 1860 | .899 |
| 2130 | 1900 | .892 |
| 1800 | 1640 | .911 |
| 1780 | 1560 | .876 |
| | Average | .893 |

### c) Soralux Daylighting System Properties

Figure 6.26 shows images of the window unit taken from approximately .5 m away and above the bottom of the unit. This view would not normally be visible to the office's occupants because the viewpoint is significantly higher than typical eye level and a ladder was needed to take the photograph. These images are quite similar to one another.

An instructive effect is seen in both images. Near the top of the image, the window unit transitions from bright to dark. The transition point is at the same height as the camera location. This rapid transition from light to dark is a manifestation of the 0° cut-off angle designed into the louver profile. The louver channels at or below eye level are bright because the viewpoint is within the channels' range of output angles. The louvers that are above eye level remain dark because the light they are emitting does not travel downward to the viewpoint. The same effect occurs for high viewing angles as well. If an image was shown looking down on the window unit from above a 40° angle, the louvers would be seen transitioning back to dark again because they do not emit light at higher than a 40° angle.

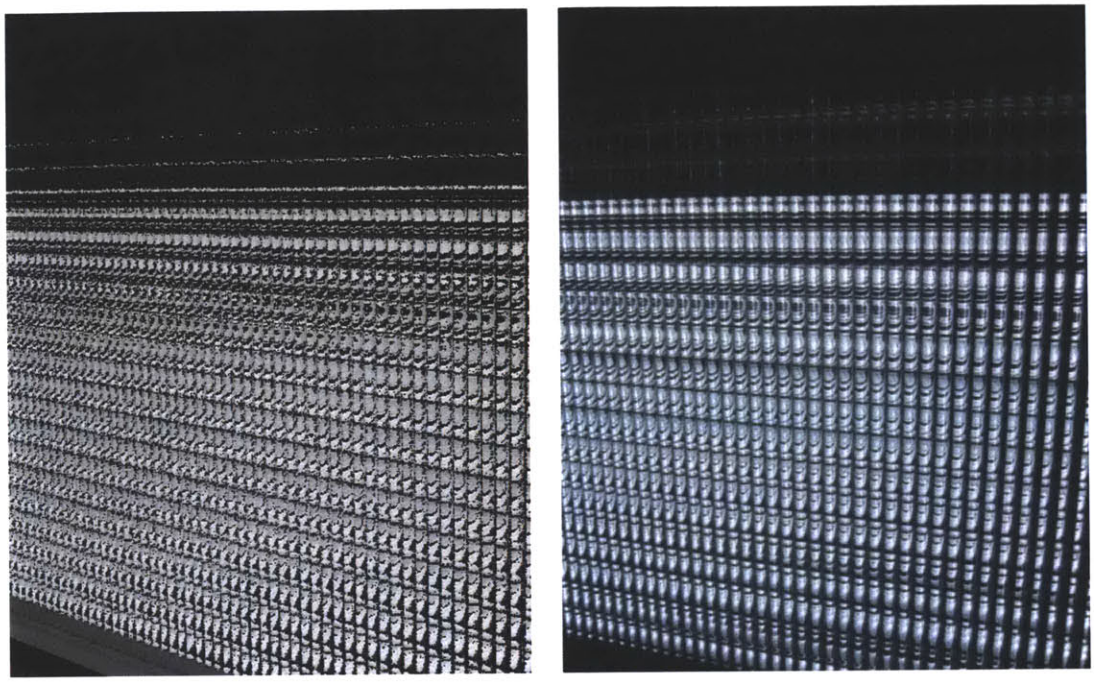

(a) (b)

Figure 6.26: Comparison of Model (a) to Actual (b) Window Unit

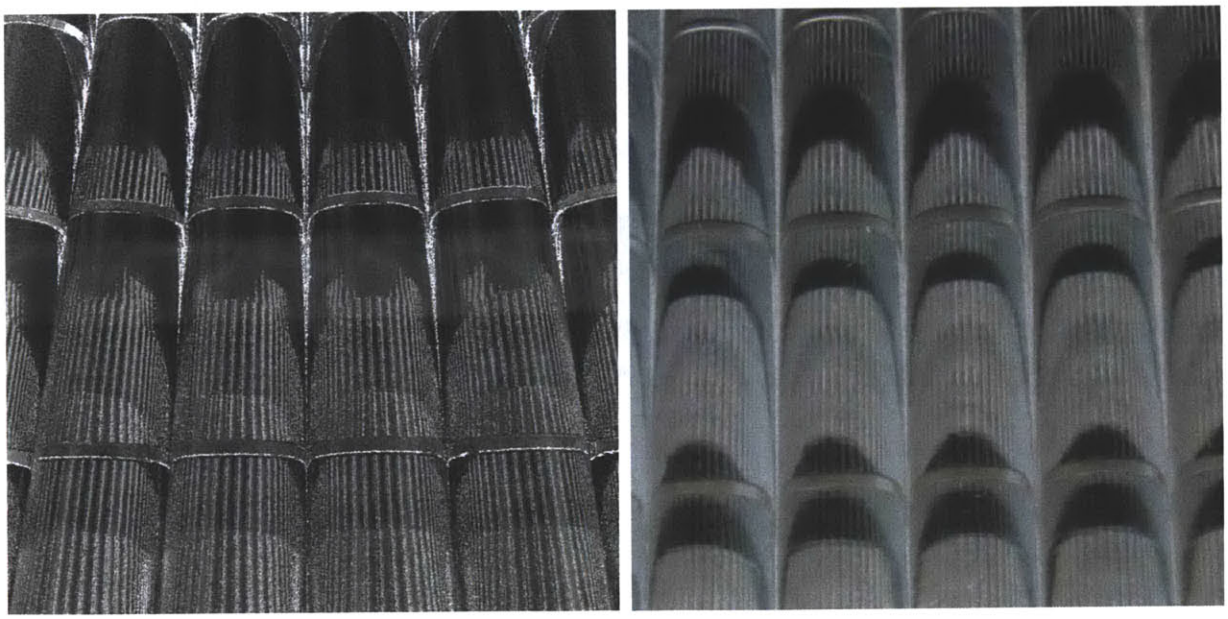

(a) (b)

Figure 6.27: Close-Up Comparison of Model (Left) to Actual (Right) Window Unit Interior Surface

Figure 6.27 shows a close-up view of the interior surface of the window unit. The vertical rods can be seen clearly. The curved horizontal lines seen in the images are the interior edge of the louvers. The interior edge of the louvers is a straight line but the image of the edge has been distorted into a series of curved lines by passing through the refractive rods. Many thin vertical lines are visible on each vertical rod. These lines are the reflection of the surrounding rod array off the surface of the interior pane of glass. This light is part of the internally reflected light discussed in Section 4.4.

The reflectance of the louver and metallic ceiling materials was measured using a Minolta CM-600D spectrophotometer. The spectrophotometer was not available during the Tokyo trip for testing the on-site reflectances. Published reflectance values for the louver and ceiling materials were not available. Measurements of other reflective materials with known reflectances were taken to help verify the results. The measured values are shown in Table 6.4 and Figure 6.28.

Table 6.4: Measured Reflectance Data Used to Determine System Reflectance

| # | Louver Material | Miro 2 4200 GP | Miro 4 4400 GP | Miro Stucco G | Anodized Stucco G |
|---|---|---|---|---|---|
| 1 | .8700 | .9480 | .9521 | .9106 | .8058 |
| 2 | .8708 | .9486 | .9508 | .9076 | .8182 |
| 3 | .8698 | .9488 | .9459 | .9235 | .8207 |
| 4 | .8697 | .9478 | .9504 | .9142 | .7957 |
| 5 | .8703 | .9472 | .9513 | .8427 | .7880 |
| 6 | .8699 | .9475 | .9505 | .9011 | .8081 |
| 7 | .8700 | .9478 | .9508 | .9010 | .8114 |
| 8 | .8702 | .9487 | .9508 | .8893 | .8117 |
| 9 | .8695 | .9465 | .9480 | .8952 | .8171 |
| 10 | .8696 | .9457 | .9504 | .8746 | .8154 |
| 11 | | | | .9179 | .8191 |
| 12 | | | | .9067 | .8084 |
| 13 | | | | .8884 | .8037 |
| 14 | | | | .8781 | .7923 |
| 15 | | | | .8895 | .7939 |
| Average | .8700 | .9477 | .9501 | .8960 | .8073 |
| Std Dev | .0004 | .0010 | .0018 | .0204 | .0106 |

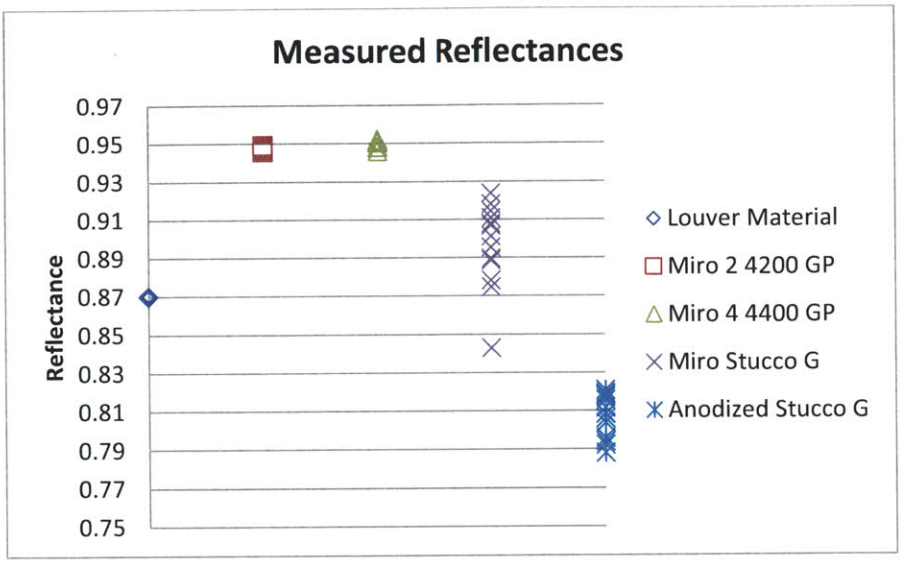


Figure 6.28: Measured Reflectances of System and Test Materials

The results for the bumpy ceiling material were less straightforward. In addition to the Anodized Stucco G material used in the actual mockup, a higher reflectance version of the same material called Miro Stucco G was also tested. The reflectance of Miro Stucco G is .95, according to data provided by Alanod, the manufacturer. However, testing showed a lower value of .896. The standard deviation for the measured results was much higher than for the smooth materials tested. Because the measured data matched the same manufacturer's data very well for the smooth materials, it was surmised that the bumpy nature of the ceiling material posed some problem for the spectrophotometer that caused it to underestimate the total reflectance. This conclusion is further supported by the fact that the standard deviation for the Anodized Stucco G is much larger than for the flat reflective materials as well. For modeling the reflectance of the ceiling material in Radiance, the decision was made to apply a correction factor to the measured reflectance value. The ratio of the measured reflectance of the Miro Stucco G material and the published value is .943 (.896/.950 = .943) and this value was applied to the measured Anodized Stucco G reflectance to arrive at the final value of .856 (.807/.943 = .856).

The spreading effect of the bumpiness of the ceiling material on light is modeled in Radiance through the roughness parameter of the metal material type. The roughness parameter is defined in Radiance as the root-mean-square slope of the surface facets (Ward Larson & Shakespeare, 1997). Roughness can vary from 0 to 1, but published guidelines indicate that values above .2 are uncommon in the real world (Ward Larson & Shakespeare, 1997). Roughness is not a value that can be measured directly from the

physical material, so an experiment was conducted in an attempt to match the luminance distributions of the physical material with the material in Radiance.

The experimental setup is shown in Figure 6.29. The space used for this test was a darkroom, with very low levels of stray light. A sample of the Anodized Stucco G material was placed on a rotating stand and a collimated light source was directed at the sample at grazing angles (angles between beam and surface) of 15°, 30°, and 45°. Measurement angles at 15° increments radiating outward from the sample stand were marked on the floor. A luminance meter was then mounted on a tripod and luminance measurements were taken of the sample's surface at varying angles. The height off the ground for the material sample, the light source, and the luminance meter was the same, so the emitted light and luminance results are all in a single plane.

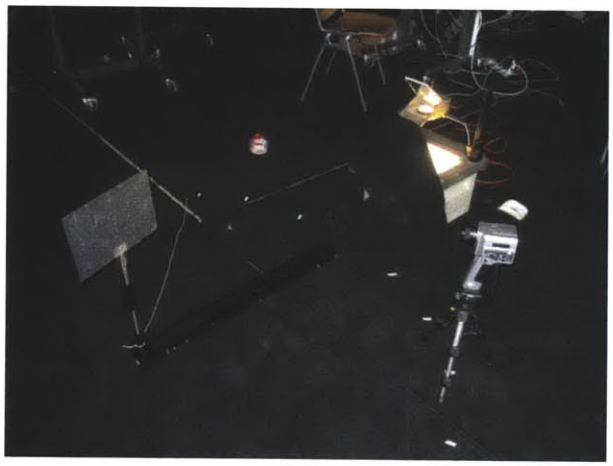

Figure 6.29: Test Setup for Measuring the Ceiling Material's Reflection Distribution

This setup was replicated in Radiance with a collimated light source, an area of the reflective material, and sensor points. The resulting luminance profiles were compared with the measured results and the roughness parameter was varied iteratively in order to arrive at the best possible agreement between the two sets of data. Figure 6.30 shows the final results using the roughness value of .125. Since the intensities of the physical and simulated light sources were not the same, the figures show the relative luminance at each point as a fraction of the peak luminance. The surface of the sample material is aligned with the 0° and 180° points in the figures.

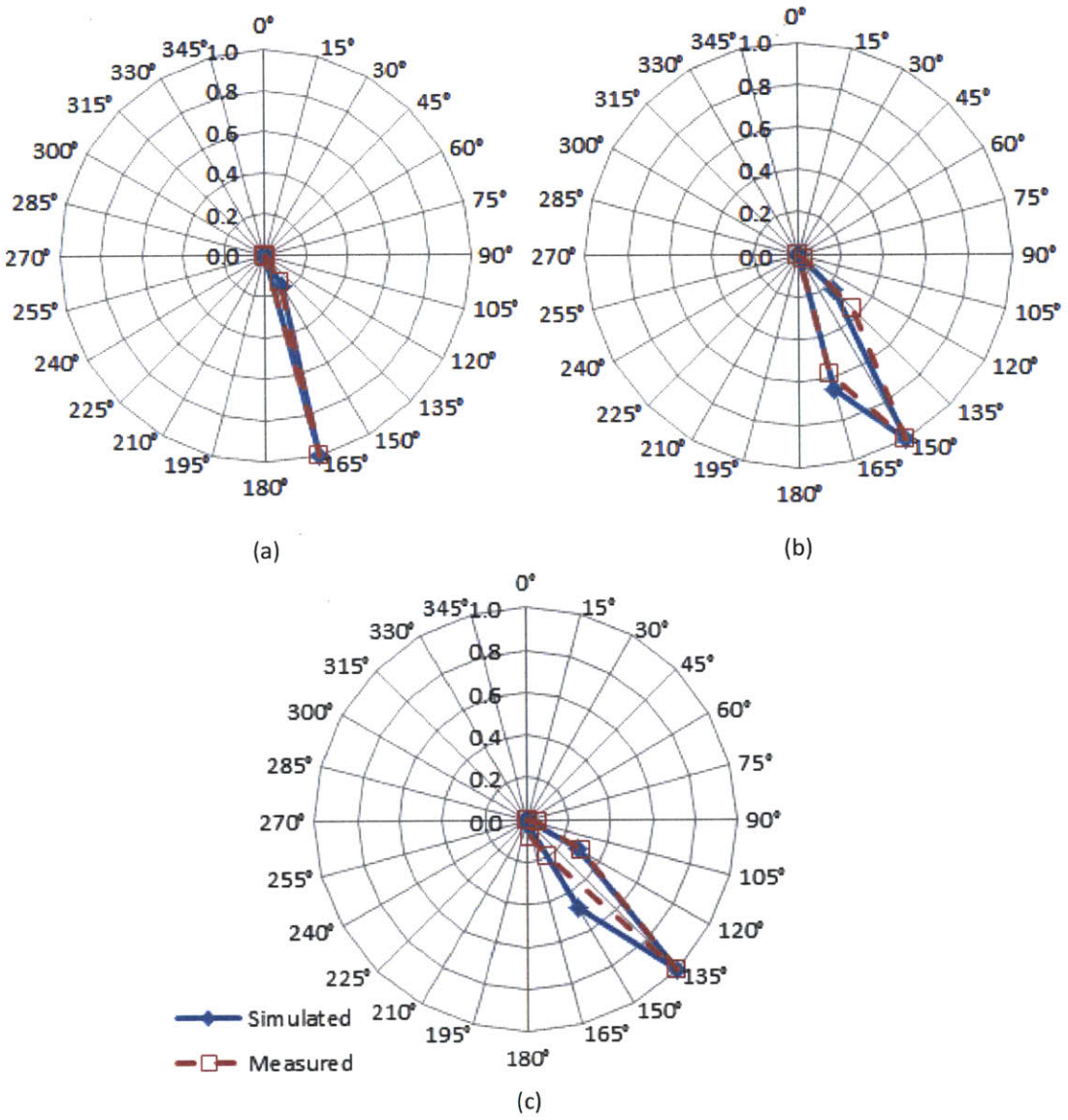


Figure 6.30: Luminance Distribution at 15° (a), 30° (b), and 45° (c) Grazing Angles

The results show reasonably good agreement between measured and simulated values. However, the measured results showed wide variation during testing. Due to the bumpy nature of the reflective material, the level of luminance measured was dependent on the specific contours of the small surface area being measured. Table 6.5 documents the measured values reported above as well as the percent variation above and below the reported values observed. Many of the measurement points have variations of ±50% or more.

Table 6.5: Representative Luminance Measurements and Percent Variation for 15° (a), 30° (b), and 45° (c) Grazing Angles

(a)

| Meas. Angle | Representative Luminance (cd/m2) | Low | High |
|---|---|---|---|
| 15° | N/A | - | - |
| 30° | 0.8 | -25% | 25% |
| 45° | 0.9 | -44% | 122% |
| 60° | 1 | 0% | 100% |
| 75° | 1 | -30% | 2400% |
| 90° | 4 | -75% | 900% |
| 105° | 40 | -73% | 125% |
| 120° | 26 | -58% | 169% |
| 135° | 200 | -63% | 100% |
| 150° | 2100 | -62% | 90% |
| 165° | 13500 | -41% | 5% |

(b)

| Meas. Angle | Representative Luminance (cd/m2) | Low | High |
|---|---|---|---|
| 15° | 1.3 | -8% | 8% |
| 30° | N/A | - | - |
| 45° | 1.1 | -9% | 9% |
| 60° | 1.2 | -17% | 17% |
| 75° | 1.1 | -18% | 9% |
| 90° | 9 | -33% | 33% |
| 105° | 30 | -67% | 133% |
| 120° | 150 | -40% | 33% |
| 135° | 1500 | -13% | 13% |
| 150° | 4200 | -52% | 86% |
| 165° | 2430 | -30% | 23% |

(c)

| Meas. Angle | Representative Luminance (cd/m2) | Low | High |
|---|---|---|---|
| 15° | 1.6 | 0% | 6% |
| 30° | 1.6 | -13% | 13% |
| 45° | N/A | - | - |
| 60° | 3 | -67% | 200% |
| 75° | 8 | -63% | 38% |
| 90° | 30 | -70% | 283% |
| 105° | 200 | -50% | 75% |
| 120° | 1100 | -73% | 100% |
| 135° | 3700 | -54% | 35% |
| 150° | 750 | -33% | 27% |
| 165° | 320 | -22% | 25% |

Varying the roughness coefficient in the generic Radiance model showed that it has a significant influence on the illuminance levels in the front of the room. The difficulty of measuring and modeling this property accurately and the nontrivial effect it has on illuminance levels makes this aspect of the model a significant potential source of error.

### 6.2.5 Measured Results Compared to Simulated Results

The following section describes the behavior of the mockup simulation model and how well it matches the measured results in the actual mockup space.

#### a) Mockup Model Behavior

Figure 6.31 shows workplane illuminance simulation results for the entire mockup office space for four time steps over the course of a single day. The weather was clear and sunny throughout the day. The illuminance contour lines in the room are more complicated for the mockup case than for the generic case, seen in Section 5.3, because of the additional details included in the mockup model. In the graphs, the southwest-facing facade on which the Soralux system is installed is located along the bottom edge. The extent of the system installation runs from about 7.3 m to 12.7 m on the x-axis, not the full width of the facade. Three dark marks are apparent on these graphs. The dark areas at coordinates [10,2] and [13,2] are interior structural columns. The dark spot at [10,5] is a printer station that extends above workplane height.

The four graphs help explain how the light contribution from the system changes throughout the day. Light levels increase from the morning to mid-day as the shading caused by the building overhang is reduced and the sun moves closer to normal to the facade. The images also illustrate how the distribution of light in the azimuth direction changes with sun location. Even though the incoming light is spread in azimuth by the refractive rods, the spread light still peaks around the direction parallel to the sun's rays. This can be seen in the graphs, as in the morning there is more light on the left side of the building column located at [10,2]. By 12:38pm, when the sun is nearly normal to the facade in azimuth, light levels are roughly even on either side of the column. As the day progresses, higher illumination is seen on the right side of the column. As shown in the generic model results, this time of day effect would be less apparent in a room with the system installed on the full width of the facade, rather than just a portion of the facade.

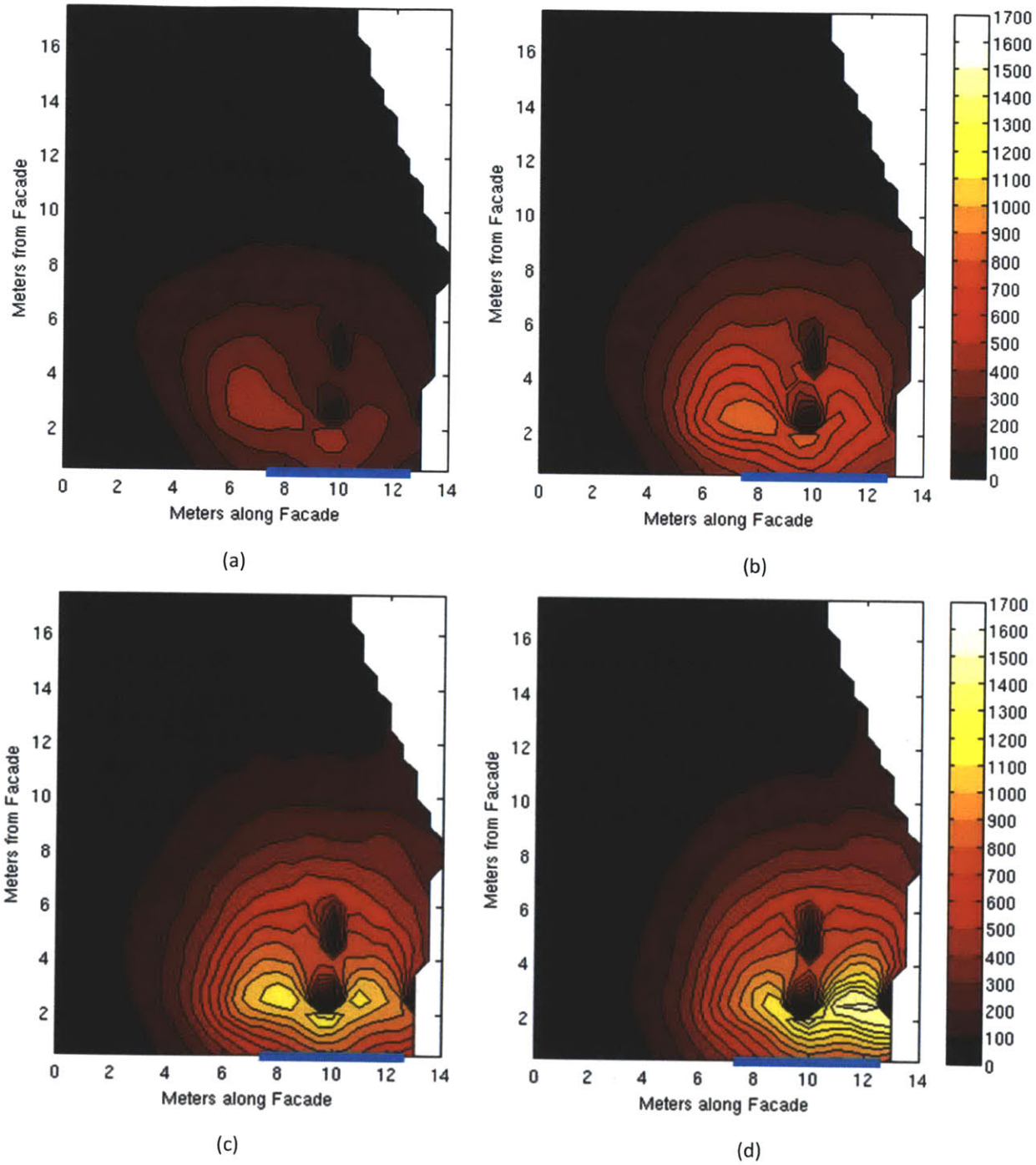


Figure 6.31: Tokyo Mockup Radiance Model Workplane Illuminance Under Sunny Conditions at 10:23am (a), 11:48am (b), 12:38pm (c), and 2:17pm (d). Extent of Soralux Window Unit on Facade Indicated with a Blue Line.

### b) Individual Time Step Comparisons

Figure 6.32 compares the measured illuminance results from the physical mockup with simulated results from the mockup's Radiance model for three of the time steps shown in Figure 6.31. The differences between the measured and simulated illuminance profiles shown here are representative of the behavior of the larger data set. There is relatively good agreement between the measured and simulated results over the range of sun positions.

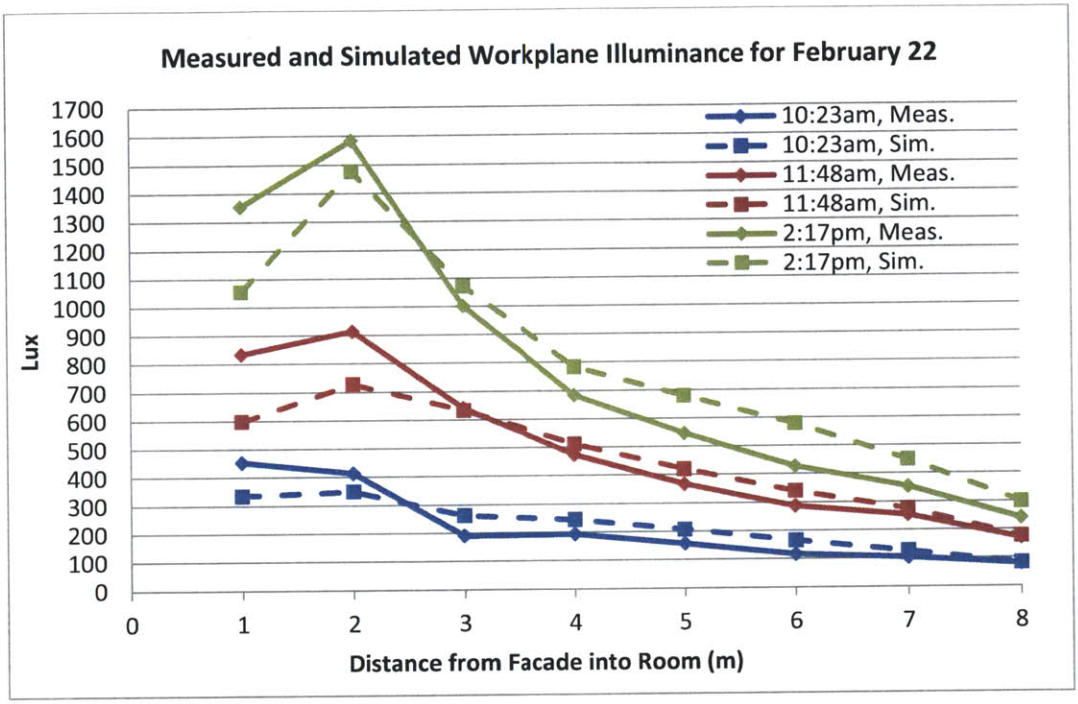


Figure 6.32: Comparing Measured and Simulated Workplane Illuminance for the Tokyo Mockup

However, there are some systematic differences between the two profiles. The simulated results are observed to consistently underestimate light levels at the front of the room by 10% to 20% and overestimate light levels deeper in the room by 10% to 25%. It appears this error is systematic and not random since the same behavior is seen over the full range of time steps. Attempts were made to uncover the cause of the disparity, so as to potentially correct it through a compensation factor, but the task was made more difficult by the increased model complexity required to match the less than ideal testing conditions.

The sky model produced by Radiance's Gendaylit program was tested to ensure that the simulated illuminance results matched the measured data at points that were independent of any of the scene

geometry. To accomplish this, illuminance measurements were simulated at a height above the tops of all the buildings in the scene, so that the full sky dome was unobstructed. Tables 6.6 and 6.7 show the results for overcast and sunny skies, respectively. For the time steps tested, the sky model was able to reproduce the measured results with less than 2% error, meaning that the sky definition was not a significant source of the observed error.

Table 6.6: Error Between Measured and Simulated Overcast Sky Conditions

| Mockup Time Step | Measured Global Horizontal Illuminance (Lux) | Simulated Global Horizontal Illuminance (Lux) | Error (%) |
|---|---|---|---|
| 15 | 27,500 | 27,089 | -1.5% |
| 16 | 31,400 | 30,932 | -1.5% |
| 17 | 26,300 | 25,891 | -1.6% |

Table 6.7: Error Between Measured and Simulated Sunny Sky Conditions

| Mockup Time Step | Measured Global Normal Illuminance (Lux) | Simulated Global Normal Illuminance (Lux) | Error (%) |
|---|---|---|---|
| 5 | 109,000 | 109,332 | .3% |
| 24 | 96,400 | 97,564 | 1.2% |

Ultimately, it could not be determined whether the systematic error was the result of the inherent simulation process or differences between the scene, as modeled, and reality. Since the source of the error could not be determined, we felt that applying a correction factor to simulated results would not be appropriate.

A study conducted by Mardaljevic comparing Radiance results with a physical mockup provides a useful comparison point for the source of the error (1995). The illuminance profile for a room equipped with a specular light shelf is shown in Figure 6.33. Although the sign of error is not necessarily in the same direction, the magnitude of the simulated results' bias is similar to the bias seen in the figures above: on the order of ±15%. These results suggest that at least some of the observed error is intrinsic to the calculation software, rather than model parameter inaccuracies.

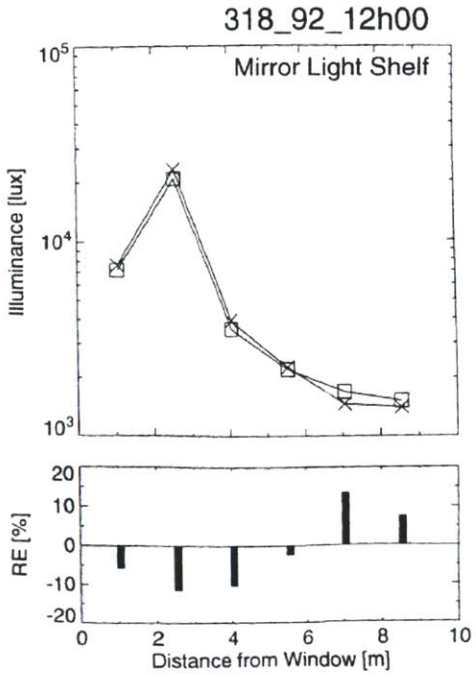


Figure 6.33: Comparing Measured and Simulated Results for a Room Equipped with a Specular Light Shelf (Reprinted from Mardaljevic, 1995, p. 186, Fig. 4). Square Markers Indicate Measured Values and Xs Mark Simulated Values.

### c) Model Bias Error

For all measured data points that met the screening requirements (no intermediate skies, minimum 80 lux measured) the percentage that the simulated results differed from the measured results was plotted for each sensor point. Figure 6.34 shows the simulation bias error at each sensor point as well as the average and standard deviation of the error.

The bias is observed to begin in the negative range and increase up to the 6 m sensor, where it begins to decrease again. The data points are broken down by sky type and time of day, in an attempt to identify any trends that would expose the cause of the bias. Aside from the overcast data points being less accurate than the sunny data points, no clear trends in the error were apparent. Increased error under overcast skies can be explained by the fact that absolute illuminance levels were much lower and thus closer to the resolution of the illuminance sensors. Smaller illuminance numbers also magnify the impression of small absolute errors. With a measured illuminance of 80 lux, for example, a simulated result of 100 lux would be reported as a 25% simulation error, even though those two results are in relatively good agreement in absolute terms.

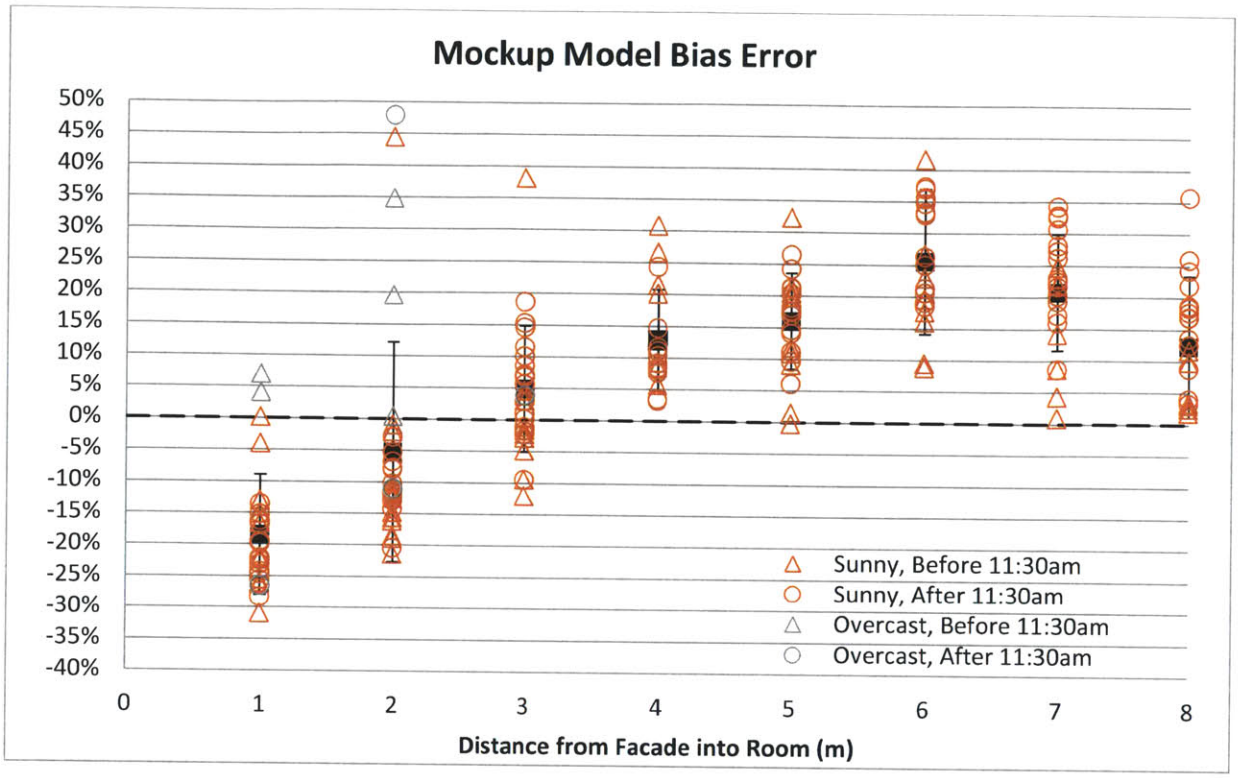


Figure 6.34: Bias Error of Mockup Model with Respect to Measured Data

### d) Model Absolute Difference Error

Looking at the average bias error does not give a complete picture of the data because large positive and negative errors can, in effect, cancel each other out when looking at the average. The standard deviation of the bias error is one way to look at the spread of data, but another is to look at the absolute values of all the errors. Figure 6.35 provides the error data in this form. It illustrates how far off the simulated result was from the measured result without regard for whether the error was positive or negative.

The average of the absolute difference errors at individual sensor locations range from 8% at 3 m to 26% at 6 m. The average of all the individual sensor averages is 16%. While an even closer agreement between measured and simulated results would of course have been preferred, given the limitations of the mockup space and time allotted for setup and data collection, the agreement between the two is acceptable and in line with our a priori expectations.

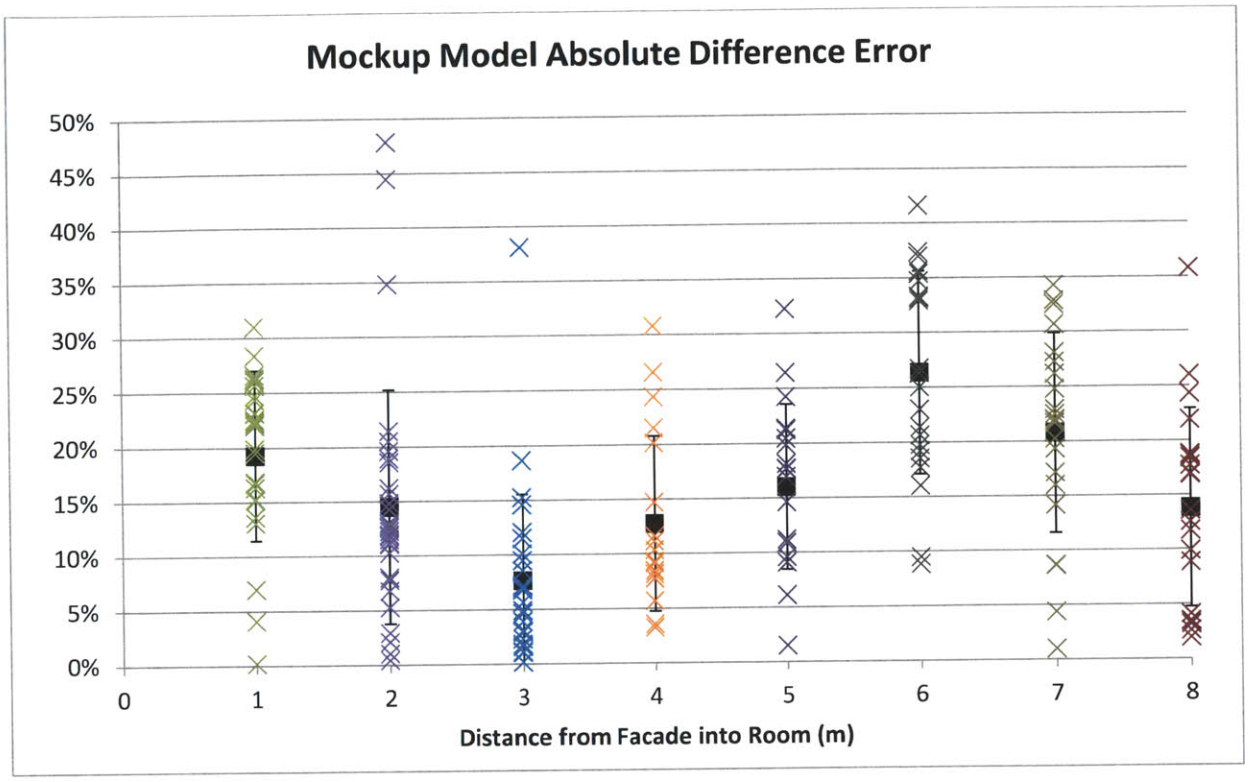


Figure 6.35: Absolute Difference Error of Mockup Model Results with Respect to Measured Data

### 6.2.6 Ceiling Luminance

Another aspect of the daylighting system evaluated during the test campaign was how the luminance of the ceiling varied over the course of the day. Since the system works with direct sunlight, the potential for glare has to be addressed.

The ceiling started out on the morning with a low level of brightness that increased steadily to the middle of the day. At its brightest, the ceiling generally ranged from 15,000 to 30,000 cd/m$^2$, with the higher end of that range located in the direction of the sun from the observer's eye. The highest value recorded at any point was 34,000 cd/m$^2$. Figure 6.36 shows luminance readings for a point in time when the ceiling was near its maximum brightness. The light fixtures in the room had a measured luminance of about 17,000 cd/m$^2$. However, because the eye's response to luminance is logarithmic, rather than linear, the brightest point on the ceiling appeared only marginally brighter than the room's light fixtures.


Figure 6.36: Spot Luminance (cd/m$^2$) Values Taken on March 3 at 1:56pm

Even so, due to both the level of luminance and the size of the bright ceiling area, the system has the potential to be glary for some situations. Based on observations of the system, we drew the following conclusions.

1) At its brightest, the view of the ceiling causes minor visual discomfort when staring directly at the ceiling.
2) At standing height, looking straight ahead towards the daylighting system at the front of the room, as one would do while moving around the room, the ceiling is high enough in one's field of view that it does not cause visual discomfort.
3) At seated height looking towards the front of the room, the situation is even better as the ceiling is farther removed from the center of the field of view.
4) For locations farther back in the room, the reflective ceiling strip appears closer to the center of the field of view. However, this tends to be offset by the fact that the projected area of the reflective ceiling is smaller and its brightness is lower than when it is viewed closer to the facade.

5) Veiling reflections on computer monitors were easily avoided, even when the screen was directly facing the reflective ceiling. A small adjustment to the tilt angle of the screen was all that was needed to keep the reflection off the screen.

The overall consensus among the team members was that the ceiling was bright but not excessively so. The fundamental problem is that to make the system effective while also keeping it passive, at its brightest, the system needs to go up to the edge of acceptability. If the ceiling's brightness was limited to a much lower level under very bright sky conditions, it would dramatically reduce the system's ability to provide workplane illuminance under all sky conditions. User studies will be needed to confirm that the system will be accepted by office occupants.

Problems due to the brightness of the ceiling can also be mitigated by orienting desks so that the center of the occupant's field of view is at a right angle to the daylit facade, rather than directly facing it. This is good daylighting design practice regardless of whether the system is installed or not. Orienting the desks in this way is not sufficient as a glare control strategy on its own, since the desks may be rearranged at a later time, but it does help. Orienting the desks at a right angle to the facade also improves workplane illuminance because the occupant's body does not obstruct the incoming light.

Figure 6.37 shows measured luminance results over the course of a clear sunny day (March 4) for two fixed locations on the ceiling. The locations of the two measurement spots are identified as well as the measurement location, 6 m from the facade.

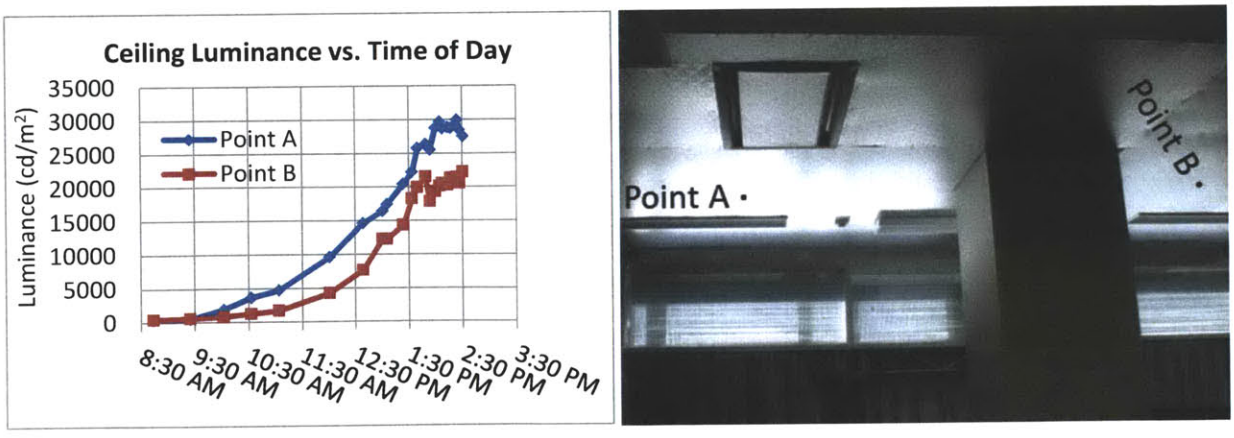


(a) (b)

Figure 6.37: Ceiling Luminance Variation by Time of Day for Measurement Points (a); Point Locations and View Location (b)

Luminance rose throughout the morning and peaks for Point A at 29,900 cd/$m^2$ and Point B at 22,200 cd/$m^2$. The graph ends at 2:32pm because at that point the sun began to pass behind a neighboring building. Interestingly, the peak luminance for both locations occurred after the sun has passed the plane normal to the facade. The sun was normal to the facade in azimuth at about 1:10pm on this measurement day, yet the luminance peaked between 2:00pm and 2:30pm. This effect was seen in a more limited fashion in the illuminance results. The peak in illuminance in the room occurred around 1:45pm, after the sun has passed the normal plane.

The explanation for this behavior is not obvious. It may have to do with the sun's changing elevation angle. For example, as the sun drops lower in the sky fewer and fewer of the louver channels are obstructed by the building's overhang, resulting in more light being emitted into the space. This explanation does not seem entirely sufficient, however, because the sun's elevation angle only changes from about 45° to about 35° between 1:10pm and 2:30pm, yet the ceiling brightness almost doubles. The effect may be a function of sun azimuth and elevation angle, direct normal illuminance, glass reflectance, overhang shading, the number of bounces off the louvers, light incident angle on the refractive rods, ceiling measurement point, and observation location. More testing is required to fully determine and explain the behavior.

The major concern resulting from this uncertainty is that the illuminance levels and ceiling luminance might be significantly higher for some time of the day and/or year not tested by the mockup. This concern is allayed somewhat by an additional simulation that was run.

The mockup space with the surrounding environment removed was run using the full Tokyo annual weather file. The highest illuminance values for the entire year occurred on February 1 at 1:30pm. When compared to the mockup time step with the highest illuminance, the annual mockup maximum was at most 14% higher than the actual mockup model, leading to the conclusion that the ceiling luminance observed was likely to be near the annual maximum.

### 6.2.7 Technical Issues with the Tokyo Mockup

Three significant technical issues with the mockup were observed. They are presented here in order of importance.

First, the straightness of the louver profile resulting from the extrusion process was inadequate. Although their locations were fixed at either end of the 1.8 m span, the louvers tended to bow slightly in

different directions in the unsupported area between the end supports. Differences in the distance between adjacent louvers varied by as much as 4 mm. The result was that the louver array allowed some reflected sunlight to spill below the horizontal, resulting in unacceptable levels of glare from the window units. In the next system prototype, the extrusion process will have to be controlled more tightly, or a different production method will be needed. Die casting (for aluminum) or injection molding (for polymers) offers the potential for tighter tolerances, but the louvers would then need to be made in short segments, on the order of .3 m long, and then fitted together to form longer spans.

Second, light exiting at a slight downward angle of 1 or 2° is not a serious problem because, even for the lowest louver channel, the light will travel 15 to 30 m into the room before descending to standing eye level. Light from higher louvers would travel even farther before becoming a problem. Even if the space's dimensions allowed the light to reach eye level before hitting a wall, at those distances the louvers would not present much of a glare source.

If changes to the manufacturing process cannot completely eliminate the downward light problem, as a final fall back measure the design of the louvers can be altered to increase the minimum output angle from 0° to a slightly higher value. This will impact the effectiveness of the system so it will only be done if other solutions are not found.

The manufacturer chosen to produce the louvers did not have the capability to produce the parabolic curves the louver cross-section was modeled with. Instead, the manufacturer approximated the parabolic curves as a series of tangent circular arcs. Due to time constraints, it was not possible to avoid this limitation. Although the differences in the resulting profile are seemingly small, they do have an impact on the light distribution of the louvers, resulting in light exiting below the horizontal for most incident angles. An example of such an incident angle is shown in Figure 6.38.

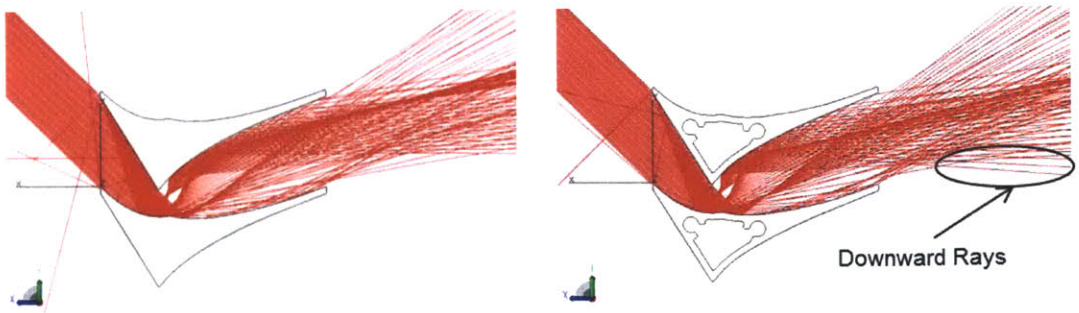


(a) (b)

Figure 6.38: Ray Tracing Through Louver Profile as Designed (a) and as Produced (b)

Third, there were some complaints about the aesthetics of the reflective ceiling material. Opinion was not universally negative, but the feeling was that the bumpiness of the ceiling had an old-fashioned or simply unattractive look to it. A solution to this problem is readily apparent. The bumpiness of the material acts to spread the specular reflection out. This effect is not dependent on the average size of the bumps, but their average slope. If the scale of the bumps is reduced from macroscopic to microscopic, but the same level of roughness is maintained, the ceiling will have a much smoother appearance without affecting is functionality. The task remains to find an existing material with these properties.

# 7 Discussion

As awareness of the Soralux system spreads, interested parties will want to know if the system is suitable for their particular situations. Providing general guidelines is difficult, because in addition to all the site-specific factors that will affect performance, the client's available budget, schedule of working hours, and illuminance requirements for the space will also play a role. In addition, the perceived performance of the system will be different depending on whether the goal is to increase light levels compared to a base case or meet absolute illuminance targets. For example, as the level of sky obstruction increases, the performance of the system improves relative to the unshaded window, but the absolute illuminance levels fall for both.

It would be helpful to have metrics with established benchmarks to define good, moderate, and poor daylighting performance. Not only would these benchmarks assist in evaluating the differences between daylighting systems, they would also help set realistic expectations for what can be accomplished with daylight. Although research is ongoing in this area, no set of widely accepted daylighting benchmarks has been developed to date (Reinhart et al., 2006). Establishing daylighting benchmarks is a difficult task for at least three reasons. First there are a large number of factors which effect the performance of a building space which would have to be captured in an effective benchmark. Second, simply defining high quality daylighting is difficult because there are many different aspects to daylighting: workplane illuminance, visual comfort, lighting uniformity, etc. Any successful benchmark would have to take these factors into account, but their relative importance is subjective. Third, the development of widely applicable benchmarks is further complicated by the fact that emphasis will be placed on different daylighting aspects for different spaces. In one space maximizing available daylight may be the preeminent goal, while glare control and minimizing solar thermal heat gains may take precedence in another space.

Despite this lack of formally agreed upon benchmarks, and starting from the assumption that simply outperforming a base case would not be sufficient justification for installing the system, absolute illuminance benchmarks were selected based on our opinion of reasonable performance expectations. Benchmark locations were defined at 4, 6, and 8 m from the facade, along the centerline of the room. These locations were chosen because they represent a range of depths to which daylighting systems are typically tested (Ruck et al., 2000). The performance of the system is categorized in Table 7.1, based on

the percentage of daytime working hours (hours between 8am and 7pm, with an exterior unobstructed diffuse horizontal illuminance of at least 1000 lux) when the system provides at least 300 lux at the specified depth into the room. Three hundred lux was chosen as the illuminance threshold because this level is on the low end of commonly recommended illuminance levels for office work (Mardaljevic et al., 2009). To achieve the performance rating shown (Good, Moderate, or Poor), at least two of the three benchmark locations had to meet the requirements for the designated rating. This stipulation was added because, in some cases, one of the locations would miss the cut off for a category by a small margin while the other two would fall into that category.

Table 7.1: Daytime Daylight Autonomy Performance Category Definition

| Depth | Good | Moderate | Poor |
|---|---|---|---|
| 4 m | > 50% | 50-30% | < 30% |
| 6 m | > 40% | 40-20% | < 20% |
| 8 m | > 25% | 25-10% | < 10% |

Table 7.2: Performance Ratings for the Large Generic Office Using Tokyo Weather Data

| | 0° | 15° | 30° | 45° | 60° |
|---|---|---|---|---|---|
| South | G | G | G | M | P |
| West | M | M | M | P | P |
| East | M | M | M | P | P |
| North | P | P | P | P | P |

Table 7.3: Performance Ratings for the Small Generic Office Using Tokyo Weather Data

| | 0° | 15° | 30° | 45° | 60° |
|---|---|---|---|---|---|
| South | G | G | M | P | P |
| West | M | M | P | P | P |
| East | M | P | P | P | P |
| North | P | P | P | P | P |

More detailed illuminance information for each case is provide in Section 5.4.2. These performance tables should be taken as rough guidelines only, due to the variability in individual projects and performance goals. The Soralux system needs access to direct sunlight to be most effective and this is the primary driver of the differences in performance between the various cases. A facade facing south has the most exposure to direct sunlight and, consequently, shows the best performance. The performance of east and west is similar, but with working hours defined as between 8am and 7pm, there is slightly more sun exposure on the west than east. Both west and east meet the benchmark illuminance levels roughly half as frequently as south. North-facing facades are not good candidates for installing the system because they receive very little direct sunlight.

The Soralux system is largely unaffected by sky obstruction angles up to 30° from the horizon. Between 30° and 45° the performance of the system begins to drop sharply due to increasing blockage of the annual sun course, or solar window. By 60°, enough of the annual sun course is obstructed that it does not make sense to install the system. One thing to consider in evaluating a site is the potential for future sky obstructions. An empty field across the street can turn into a high-rise building during the life span of the system.

Rooms that are wide with respect to their depth will see better performance because, in a narrow room, the light tends to hit the diffuse side walls near the front of the room before it can travel deeply into the space. For shallower spaces in the range of 3 to 5 m, the length of the reflective ceiling can be reduced to around .75 to 2 m, in order to reduce cost.

The Soralux system exhibited relatively constant performance for three of the four geographic locations evaluated: Austin, Boston, and Tokyo. The fourth, Stockholm, showed decreased performance due to its very high latitude. The days are short and the sun does not rise very high in the winter. The poor winter conditions are not counterbalanced during the summer months because, while the days are long, the sun's course does not allow any single facade orientation to take advantage of the full day, as shown in Figure 2.2 on page 19. With regard to climate, locations which are consistently overcast are not good candidates for implementation.

There are a number of variables which affect workplane illuminance beyond those considered above. The following parameter changes will also improve lighting levels compared with the generic office case considered:

- Increase ceiling height
- Increase window transmittance
- Increase room surface reflectances
- Decrease depth of room (due to reflectance off the rear wall)

The system is well-suited for both new construction and as a retrofit to existing buildings. In the case of new construction, the Soralux system should be integrated into the building design at the earliest possible stage in order to prevent avoidable problems from factors such as facade orientation and shading of the system by the building. For a retrofit situation, the window unit can be installed behind an existing facade. Some additional support structure may need to be added to secure the window unit against the facade. The reflective ceiling tiles could replace the existing ceiling tiles relatively easily. In this manner, the system could be installed with a minimal impact on the existing building.

Development of the Soralux Daylighting System has progressed rapidly during the relatively short period of this thesis effort. However, a substantial amount of work remains to be done before this system can be considered a validated commercial product. Final material and manufacturing process selections are needed. The technical problems with the Tokyo mockup outlined in Section 6.2.7 need to be solved. An array of system tests in areas such as thermal, condensation, fire safety, and life-cycle need to be conducted, as they would for any new building product. These steps need to be completed before the system is installed into occupied building spaces.

# 8 Conclusion

The goal of this thesis effort was to identify and evaluate advanced passive daylighting systems that would be appropriate for deep-plan urban building spaces. A review of existing systems found that, although some were more effective than others, all had significant shortcomings. Major problems included:

- Significant spans of the day and year when the system was ineffective
- Glare resulting from direct sunlight transmission
- Large volumetric requirements
- Ineffectiveness due to under-operated shading systems

Upon reaching this conclusion, the decision was made to embark on a new product development effort. Building on the existing knowledge base of nonimaging and imaging optics, the Soralux Daylighting System was created. Throughout the design process, the performance of the system was evaluated through computer simulations as well as testing of progressively more sophisticated mockups.

Annual performance simulations were conducted using Radiance. The results show that the system is effective in pushing light deeper into a building space when direct sunlight is incident on the system. For the main reference case tested (a south-facing facade with a 15° sky obstruction), the Soralux system was able to provide a workplane illuminance of at least 300 lux for 40% of annual daytime working hours at 8 m from the facade, whereas the unshaded window base case never met the 300 lux threshold at this location. With ideal conditions, the system was able to provide 450 to 500 lux 14 m from the facade. For overcast conditions, although the system increases light levels by a factor of three over the base case results for the back half of the space, the absolute light levels are low (on the order of 50 to 100 lux).

Sky obstructions of 30° or less were not found to significantly degrade the performance of the system. Obstruction angles of 45° or more had a severe impact on the system's effectiveness because obstructions of this size block direct sunlight for a significant part of the year. Room width was found to have a modest impact on the depth of light penetration, with wider rooms being better suited for the system. Geographic location had a moderate effect on workplane illuminance levels for the cities tested.

The better performing cities had sunnier climates and were located within 50° from the equator in latitude.

Mockup testing confirmed that the reported simulation results were acceptably accurate (within 16% of the measured results, on average) and also provided the opportunity to evaluate the glare potential and aesthetics of the system. Mockup observations found glare to be a possible concern, but one that would not prohibit the system from being used successfully. The architectural aesthetic was found to have several positive aspects. The texture of the window unit resulting from the array of refractive rods, as seen from inside the space, was both interesting and attractive. The glow given off by the window unit was also a pleasant effect. The reflection of the louvers, as seen from outside the building, has the potential to add visual interest to the building. There was one negative to the system's aesthetics. The texture of the reflective ceiling was generally thought to be unattractive. To remedy this, the ceiling material used in the Tokyo mockup will be replaced with a similar material with a smaller grain pattern so that the bumpy surface is not as apparent.

Overall, the development effort was a success. Efforts are underway to solve the manufacturing issues identified in Section 6.2.7, in order to ready the system for permanent installation. The project's sponsor organization is proceeding with plans to install the Soralux system into its new headquarters building, scheduled for completion in 2012. The system will be installed on several of the building's top floors, although the exact number has not been determined yet. The southwest facade of the building (shown in Figure 5.1(c) on page 67) was chosen for installation due to its access to direct sunlight. Patent protection for the system is also being pursued and a US provisional patent application has been filed (serial number 61/413,804).

## 8.1 Future Work

The work in this thesis lays the foundation for a new daylighting system for use in deep-plan building spaces. There is a large worldwide market of existing and future buildings that could benefit from the Soralux Daylighting System and we hope that, over time, the system will find widespread use. There are a number of new approaches future research could take to further describe or improve the performance of the system:

- Once the system is installed into buildings on a permanent basis, user surveys should be completed to evaluate occupant impressions. In addition to surveys, quantitative glare analysis using HDR imaging could also be completed.

- For the Soralux system to achieve widespread use, the costs of the system must be seen as reasonable. While a detailed cost analysis has not been completed for the production of this system, cost reductions are always welcome. Future efforts to reduce the cost of materials, manufacturing processes, assembly, and installation would enhance the appeal of the system.
- To improve the system's performance for overcast skies and skies with high sun angles, a new version of the window unit may be designed so that it is tilted out at an angle from the vertical facade of the building, like an awning. Tilting the unit would allow it to capture light from the top portion of the sky dome. However, this approach would complicate the design of the facade more than the vertical approach used in this thesis. The design of the louvers, rods, and window unit would all have to reconsidered to make the tilted approach work.

## 8.2 Final Remarks

Daylight is an important resource for both energy and human health. Whether it is in designing the layout of a building, installing an advanced daylighting system like the one discussed here, or simply remembering to turn off the lights in a room when there is sufficient daylight, there are many ways we can tap into this abundant resource. After all, it is literally right outside our windows. The sooner we can change the status quo, the better, because as things stand now, we are burning daylight.

# Appendix A: Detailed Simulation Method

There are two different types of ray tracers: forward and backward. In a forward ray tracer, rays are emitted from light sources and their paths are tracked as they move from the sources' locations. A backward ray tracer takes the opposite approach: rays are emitted at the view or sensor point and traced back to the light sources. TracePro is a forward ray tracer and Radiance is a backward ray tracer.

What advantage does a backwards ray tracer have, since following the ray paths in reverse makes less intuitive sense? If the desired result is a rendering or a luminance/illuminance measurement at a point, backward ray tracing can save a large amount of computing time. This is because in a forward ray tracer, generally only a tiny percentage of rays emitted from light sources actually end up at the point of interest (Ward Larson & Shakespeare, 1997).

Radiance is a powerful tool for daylighting simulation. It is capable of modeling complex lighting situations and has been validated against physical model results (Mardaljevic, 1995; Ward Larson & Shakespeare, 1997). However, the program is not without limitations. The type of daylighting system proposed in this thesis exposes one of the weak spots of the program. Fortunately, there is a way around this difficulty.

To understand the problem, it is first necessary to explain a few aspects of how ray tracing in Radiance works. To save computation time, Radiance divides its efforts into a Direct Calculation and an Indirect Calculation. Concentrated light sources, such as the sun or a light fixture, are handled in the Direct Calculation. The Direct Calculation makes use of the facts that a) concentrated light sources have a major impact on the illumination in a scene and b) the locations of the light sources can be identified in advance, rather than having to search for them with Monte Carlo sampling.

The Indirect Calculation accounts for all sources of illumination that were not found as part of the Direct Calculation. This calculation includes diffuse light bouncing between surfaces as well as specular reflections. In order to calculate the diffuse interreflection component, Radiance sends out a number of rays in different directions to sample the scene. The ambient settings of the simulation control the quantity of rays needed for this calculation, and hence they influence the simulation time.

Complications with the program arise when curved specular surfaces need to be modeled in a scene and evaluated using the Direct Calculation. Reflections off specular surfaces are not included in the Direct

Calculation by default. In other words, the sun spot resulting from sunlight reflecting off a mirror onto a wall will not be accurately modeled in Radiance under its default settings. However, there is an option which accounts for this: the Virtual Light Source Calculation (VLSC). The VLSC creates new light sources which correspond to the mirrored reflections of the concentrated light sources in the Direct Calculation. This option is activated in Radiance by setting the –dr option to the desired number of reflections allowed. For example, setting –dr equal to 1 would allow the sun spot on the wall to be rendered correct for the scenario described above. However, if the rays reflect off multiple specular surfaces, virtual-virtual sources, virtual-virtual-virtual sources, etc. must be created. The total calculation time required to render a scene increases approximately linearly in relationship to the number of light sources (Ward Larson & Shakespeare, 1997). The Soralux louvers are modeled as hundreds of thin flat surfaces in Radiance in order to maintain a highly accurate profile. In the Direct Calculation, each of these facets would create new virtual sources as sunlight bounces between louvers. There can be hundreds of louver channels in a given scene so the number of virtual light sources can quickly soar into the tens of thousands. The result is that the simulation runs very slowly and ultimately crashes due to the number of light sources in the scene.

A solution to this problem lies in the use of the Daylight Coefficient Method for calculating illuminance. This approach also has the major advantage that it allows annual simulations using hourly time steps to be completed quickly. The following process description assumes that the final result is a set of illuminance values, but the process to obtain rendering is largely the same.

Instead of simulating results for approximately 4400 different sky conditions, the scene is simulated for a single sky condition. In Radiance, this process is carried out by the Rtcontrib program (Jacobs, 2010). In this simulation, the sky has a uniform radiance of 1 $W/m^2/sr$. The sky is then subdivided into discrete patches (145 in the case of the Tregenza sky subdivision) and the contribution from each sky patch to the illuminance at each sensor point is computed separately. These contributions are known as Daylight Coefficients (Tregenza & Waters, 1983). The result of the process is an $m \times n$ matrix containing all the Daylight Coefficients, where $m$ is number of sky patches and $n$ is the number of sensor points. This method requires the time intensive Indirect Calculation to be performed only once, rather than for each time step (Mardaljevic, 2000). Once the Daylight Coefficients for a scene have been calculated, the actual sensor illuminances can be calculated by a simple linear combination with the Sky Matrix (Jacobs, 2010).

The Sky Matrix is the other set of data needed to arrive at time series illuminance values. The Radiance programs Gendaylit and Genskyvec perform the calculations necessary for this process. For each time step, a representative sky is simulated using detailed weather data, time of day/year, and location. These inputs are taken from weather data files available through the *Energy Plus* website, among other places (U.S. Department of Energy, 2010). The weather data are most often given as averages over one hour increments of local legal time, so for each time step in the simulation the sun position is modeled at the mid-point of each hour (eg. 8:30am, 9:30am, etc.).

Gendaylit utilizes the Perez All Weather Model, to create the sky distribution (Perez et al., 1993). The sky is then sampled to estimate the radiance of each of the sky patches used in the Daylight Coefficient calculation. The sun's energy is allocated to the three nearest sky patches. The result of this calculation is an *m x n* matrix, where *m* is the total number of time steps and *n* is the number of sky patches. This process is relatively quick, requiring only a few minutes to generate an entire year's worth of sky conditions (Jacobs, 2010). When the Sky Matrix and the Daylight Coefficient Matrix are multiplied together, the resulting Sensor Illuminance Matrix contains illuminance values at each sensor point for each time step. Equation A.1 shows the matrix operation involved and Equation A.2 shows the dimensions of each matrix.

$$Sky\ Matrix \times Daylight\ Coefficient\ Matrix = Sensor\ Illuminance\ Matrix \qquad \text{Equation A.1}$$

$$[\#\ of\ Time\ Steps \times \#\ of\ Sky\ Patches] \times [\#\ of\ Sky\ Patches \times \#\ of\ Sensors] = [\#\ of\ Time\ Steps \times \#\ of\ Sensors] \qquad \text{Equation A.2}$$

The size of the Sky Matrix is generally around 4380 x 146 (145 sky patches + 1 ground patch) and the size of the Daylight Coefficient Matrix is 146 x ~300 (depending on the number of sensors). The resulting data provide a much more complete picture of the system's performance over the full year compared to only simulating results for a few key times during the year. Furthermore, because the Daylight Coefficient Method can use real weather data as an input, the results can be made climate-specific.

With this understanding in hand, it is possible to return to the initial problem faced when trying to model curved specular surfaces in Radiance. The Daylight Coefficient method does not make use of the Direct Calculation in Radiance. There is no sun in the uniform sky used to calculate the Daylight Coefficients and the sky only participates in the Indirect Calculation. Since there is no Direct Calculation, the problem of dealing with thousands of light sources is eliminated. There is a price to pay for this benefit, however, in the form of dramatically increased ambient settings. Because the Indirect

Calculation cannot predetermine where the important light sources will come from, the sampling pattern must be very fine to ensure that the light contribution from the daylighting system (and any other light source) is accurately accounted for. The finer settings increase calculation time such that generating results for more than a few hundred sensor points becomes time prohibitive (for the simulations done with the model described in Section 5.3 and ambient settings shown in Table 5.2 on page 72, the Daylight Coefficient calculation took about 40 seconds for each sensor).

With the very high settings needed to ensure highly repeatable results, rendering times for image creation were excessive, and the simulation crashed before the rendering was complete. However, for simpler cases, such as a room with an open window, is it possible to create renderings using the Daylight Coefficient Method (Jacobs, 2010). The renderings of the system shown in Chapters 4, 5, and 0 were created with much lower settings than those shown in Table 5.2, allowing images to be created in a reasonable amount of time with a corresponding loss in accuracy.

For those familiar with the Radiance program, the following is a description of the Daylight Coefficient Method as implemented. After reading in sensor locations, Rtcontrib starts Rtrace which sends out a very large number of rays due to the high ambient settings. The rays that pass through the daylighting system arrive at the diffuse sky made of the glow material. There is no sun in the sky definition and the glow material can only participate in the Indirect Calculation. Rtcontrib samples this uniform sky at each sky patch to determine the irradiance on each sensor for a constant sky patch radiance of 1 W/m2/sr. This result is then converted from irradiance to illuminance. Appendix B provides the scripts used to run these commands.

If renderings of specific viewpoints are the desired result, photon maps offer another option. The photon map adds a forward ray tracing pass to the Radiance process and can dramatically reduce rendering times compared to Radiance's standard backward ray tracing process (Schregle, 2004). By tracing rays forward from light sources to the viewpoint, the photon map process is able to accurately and quickly model the behavior of specular and refractive materials. However, photon maps cannot be used in conjunction with the Daylight Coefficient Method because, as explained previously, there are no direct light sources in the scene for rays to be traced from. Consequently, photon maps can be used to produce individual renderings but the process is not suited for the rapid production of annual illuminance results. Another issue with photon maps is that, in order to keep the simulation time efficient, windows and other exterior openings are usually defined as photon ports. These ports are the source of the emitted photons and no interreflection is calculated outside of these ports. Therefore, sky

obstructions due to the surrounding environment cannot be considered without significant further complication to the model. Because annual results and sky obstructions were central to the analysis completed in this research effort, the photon map approach was not pursued.

# Appendix B: Radiance Files and Scripts

The following files provide the material and scene descriptions for the Radiance models. The Bash scripts used to run the annual simulations are also included. Bash is a Linux programming language.

## B.1 Generic Office Space Material File

```
#generic materials file
#this goes with generic model

#.996^39.37 = .854
void dielectric splitter
0
0
5 .854 .854 .854 1.49 0

void mirror ref_mat
0
0
3 .87 .87 .87

void metal ceil_diff2
0
0
5 .856 .856 .856 .95 .125

void plastic walls
0
0
5 .5 .5 .5 0 0

void plastic floor
0
0
5 .15 .15 .15 0 0

void plastic ceiling
0
0
5 .7 .7 .7 0 0

void plastic frame
0
0
5 .6 .6 .6 0 0

void plastic mullion_white
0
0
5 .5 .5 .5 0 0
```

```
void plastic block
0
0
5 .04 .04 .04 0 0

void plastic blinds
0
0
5 .4 .4 .4 0 0

void plastic ground
0
0
5 .08 .08 .08 0 0

#.859 transmittance = .935 transmissivity, .859^2 = .738 for double #glazing,
.656 xmit = .715 xmitivity

void glass win_gen
0
0
3 .935 .935 .935

void plastic facade
0
0
5 .1 .1 .1 0 0
```

## B.2 Generic Office Space Model

```
##########Toggle

#system = off, base = on, lower = on
#inner glazing

#win_gen polygon window1_in
#0
#0
#12
#     37    14.994      0
#     37    14.994      2.8
#     0     14.994      2.8
#     0     14.994      0

#system = on, base = off, lower = off
#window unit (1 pane) w/ louvers

!xform -n window_unit -rz 180 -t 1.8 14.999 2.09 -a 20 -t 1.85263 0 0
th_window_unit_gen.rad

#system = on, base = off, lower = off
```

```
#reflective ceiling section

ceil_diff2 polygon ceil_mir
0
0
12
      0     15    2.799
      37    15    2.799
      37    11    2.799
      0     11    2.799

#system = on, base = on, lower = off
#lower wall block

block polygon cover_low
0
0
12
      37    14.997      2.09
      0     14.997      2.09
      0     14.997      0
      37    14.997      0

#system = off, base = off, lower = on
#upper wall block

#block polygon cover_high
#0
#0
#12
#     37    14.997      2.8
#     0     14.997      2.8
#     0     14.997      2.09
#     37    14.997      2.09

#small = on, big = off
#small room wall, left

#walls polygon left_wall
#0
#0
#12
#     14.821      15    0
#     14.821      15    2.8
#     14.821      0     2.8
#     14.821      0     0

#small = on, big = off
#small room wall, right

#walls polygon right_wall
#0
#0
#12
#     22.179      15    0
#     22.179      15    2.8
#     22.179      0     2.8
```

```
#     22.179      0     0

##########End Toggle

#walls, ceiling, floor
!genrbox walls wall1 .2 15.2 3.2 | xform -t -.2 -.2 -.2
!genrbox walls wall2 .2 15.2 3.2 | xform -t 37 -.2 -.2
!genrbox walls wall_back 37.4 .2 3.2 | xform -t -.2 -.2 -.2
!genrbox ceiling ceil1 37.4 15.2 .2 | xform -t -.2 -.2 2.8
!genrbox floor floor1 37.4 15.2 .2 | xform -t -.2 -.2 -.2

#blinds
!genblinds blinds b1 .0495 37 2.09 47 65 | xform -rz -90 -t 0 14.96 .004

#outer glazing
win_gen polygon window1_out
0
0
12
      37    15    0
      37    15    2.8
      0     15    2.8
      0     15    0

#mullions
!genrbox mullion_white m_all .05263 .064 2.8 | xform -t 1.8 14.935 0 -a 19 -t
1.85263 0 0
```

## B.3 Top Level Generic Assembly

```
#top level scene

!xform -n gen_office -t -18.5 -15 20 -rz 180 gen_master.rad
!xform -n surround -rz 180 gen_surround_00.rad
```

## B.4 Tokyo Mockup Materials File

```
#materials file
#this goes with mockup model

#.996^39.37 = .854
void dielectric splitter
0
0
5 .854 .854 .854 1.49 0

void mirror ref_mat
0
0
3 .87 .87 .87
```

```
void metal ceil_diff2
0
0
5 .856 .856 .856 .95 .125

void plastic walls
0
0
5 .48 .48 .48 0 0

void plastic floor
0
0
5 .14 .14 .14 0 0

void plastic ceiling
0
0
5 .71 .71 .71 0 0

void plastic black
0
0
5 0 0 0 0 0

void plastic frame
0
0
5 .6 .6 .6 0 0

void plastic mullion
0
0
5 .07 .07 .07 0 0

void plastic mullion_white
0
0
5 .5 .5 .5 0 0

void plastic brown
0
0
5 .8 .5 .3 0 0

void plastic blue
0
0
5 .1 .14 .6 0 0

void plastic block
0
0
5 .04 .04 .04 0 0
```

```
#measured 72% but effectively less bc of light trapped in curtain #waves,
assume .65
void plastic curtain
0
0
5 .65 .65 .65 0 0

void plastic overhang
0
0
5 .25 .25 .25 0 0

void plastic blinds
0
0
5 .4 .4 .4 0 0

void plastic ground
0
0
5 .08 .08 .08 0 0



void plastic blind_bot
0
0
5 .4 .4 .4 0 0

void plastic furniture
0
0
5 .4 .4 .4 0 0

void plastic test
0
0
5 0 1 0 0 0

#.738 transmittance = .80 transmissivity
void glass window
0
0
3 .80 .80 .80

#.892 = .972 transmissivity

void glass win_tok
0
0
3 .972 .972 .972

#.859 transmittance = .935 transmissivity, .859^2 = .738 for double-glazing,
.656 xmit = .715 xmitivity

void glass win_gen
0
```

```
0
3 .935 .935 .935

void glass win_sing
0
0
3 1.001 1.001 1.001

void plastic column
0
0
5 .8 .8 .8 0 0

void plastic brn_bldg
0
0
5 .12 .12 .12 0 0

void plastic blk_bldg
0
0
5 .08 .08 .08 0 0

void plastic facade
0
0
5 .1 .1 .1 0 0
```

## B.5 Tokyo Mockup Office Model

```
#room geometry

!genrbox curtain south_facade_lower 14.24 .161 1.69  | xform -t 26.26 .089 0

!genrbox curtain east_facade_all .05 9.2 2.53  | xform -rz -10.6 -t 40.380
.226 0
!genrbox walls interior1 4.08 .1 2.53  | xform -t 38.1 8.96 0
!genrbox walls interior1b .1 .81 2.53  | xform -t 38.1 8.15 0
!genrbox walls int2 .1 5.55 2.53  | xform -t 39.3 8.96 0
!genrbox walls int3 1.65 .1 2.53  | xform -t 37.78 14.4 0
!genrbox walls int4 .1 4.42 2.53  | xform -t 37.78 13.44 0
!genrbox walls int5 11.62 .1 2.53  | xform -t 26.26 17.76 0
!genrbox walls int6 .1 17.86 2.53  | xform -t 26.26 0 0

!genrbox curtain south_facade_left 1.04 .01 2.53  | xform -t 39.46 .24 0
!genrbox curtain south_facade_right 7.8 .01 2.53  | xform -t 26.26 .24 0

!genrbox floor floor1 15.92 17.76 .1 | xform -t 26.26 0 -.1
!genrbox ceiling ceil1 15.92 17.76 .1 | xform -t 26.26 .069 2.53


!genrbox overhang ceiling_step 14.24 .161 .13 | xform -t 26.26 .069 2.4

!genrbox column col_left .75 .75 2.53 | xform -t 39.67 2.10 0
```

```
!genrbox column col_right .75 .75 2.53 | xform -t 36.42 2.10 0

##########furniture
!genrbox furniture desk_block1 7.00 1.40 .70 | xform -t 30.31 3.53 0
!genrbox furniture desk_block2 7.00 1.40 .70 | xform -t 30.31 6.5 0
!genrbox furniture printer .559 .559 1.111 | xform -t 36.58 4.93 0
!genrbox furniture binders .3 .5 .35 | xform -t 36.75 4.4 .7
!genrbox furniture table 1.83 1 .70 | xform -t 39 5.75 0

###############window unit w/ louvers

!xform -n window_unit -t 37.66 .298 1.69 -a 3 -t -1.8 0 0 th_window_unit.rad

################mullions
!genrbox mullion m1 .051 .07 .7 | xform -t 38.133 .18 1.7
!genrbox mullion m2 .051 .07 .7 | xform -t 36.895 .18 1.7
!genrbox walls m3 .324 .07 .7 | xform -t 36.571 .18 1.7
!genrbox mullion m4 .051 .07 .7 | xform -t 36.520 .18 1.7
!genrbox mullion m5 .051 .07 .7 | xform -t 35.368 .18 1.7
!genrbox mullion m6 .1 .07 .7 | xform -t 39.45 .18 1.7

#############ceiling features
!genrbox walls vent1_left 1.019 .105 .1 | xform -t 38.403 .557 2.52
!genrbox walls vent1_right 1.019 .105 .1 | xform -t 34.682 .557 2.52
!genrbox walls light_left 1.251 .248 .013 | xform -t 38.145 1.257 2.517
!genrbox walls light_mid 1.251 .248 .074 | xform -t 36.272 1.257 2.456
!genrbox walls light_right 1.251 .248 .013 | xform -t 34.392 1.257 2.517 -a 3
-t -1.251 0 0
!genrbox walls vent_out .584 1.029 .002 | xform -t 37.949 3.142 2.528
!genrbox ceil_diff2 vent_in .356 .897 .003 | xform -t 38.063 3.206 2.527
!genrbox walls cut .464 .279 .002 | xform -t 38.704 4.147 2.528

walls cylinder alarm
0
0
7
      37.834      1.381 2.53
      37.834      1.381 2.479
      .051

#######block around louvers
walls polygon block_left
0
0
12
      39.46 .363  2.429
      39.46 .16   2.429
      39.46 .16   1.69
      39.46 .363  1.69

walls polygon block_right
0
0
12
      34.06 .363  2.429
      34.06 .16   2.429
      34.06 .16   1.69
```

```
      34.06 .363  1.69

walls polygon block_bot
0
0
12
      39.46 .363  1.69
      39.46 .16   1.69
      34.06 .16   1.69
      34.06 .363  1.69

##################
#windows: single pane
#outer glazing
win_tok polygon window1_out
0
0
12
      40.5  .18   1.7
      40.5  .18   2.4
      26.26 .18   2.4
      26.26   .18 1.7

#######################################

ceil_diff2 polygon ceil_mir
0
0
12
      39.46 .425  2.529
      34.06 .425  2.529
      34.06 4.425 2.529
      39.46 4.425 2.529
```

## B.6 Tokyo Mockup Top Assembly

```
!xform -n office -t 0 0 19.1 -rz -26.66 th_office.rad
!xform -n surround -rz -26.66 th_surround.rad
```

## B.7 Rtcontrib Script for Calculating Daylight Coefficients

```
#!/bin/bash
#run rtcontrib for all cases
rm log_file

while read sensor_name model; do
sensors="pts/final_gen/$sensor_name"
octree="DC_$model"
DC_vec="DC_vec/$octree.vec"

mkdir test/$octree
```

```
#rm test/$octree/*.*
rm DC_vec/$octree.vec

echo -e "$octree"
echo -e "$octree" >> log_file
date
date >> log_file

#for mockup office
oconv -f mat_gen.rad $model.rad sky_white.rad > white.oct

####################rtc_gen.opt
date
date >> log_file

cat $sensors.pts | rtcontrib -h -I+ -fo @rtc_gen.opt -e MF:1 -f tregenza.cal
-b tbin -o test/$octree/p%03d.dat -m sky_glow -w white.oct
date
date >> log_file

#needs to be updated based on number of sky patches (577 or 145)
for i in {000..145}; do
#     set to folder with DCs
      cat test/$octree/p$i.dat |rcalc -e '$1=179*($1*0.265+$2*0.67+$3*0.065)'
\
            |tr '\n' '\t' >> $DC_vec
    # Append a line break
    echo >> $DC_vec
done

done < model_info.dat
```

## B.8 Sky Distribution Script

```
#!/bin/bash
#reads weather file data, if diffuse horizontal > 0 runs gendaylit and
#genskyvec. Outputs patch radiance file for each time step

#specify what folder to put files in
fol="tregenza"
divisions=1
output="sky_dist_tokyo_ann.dat"

#clears out files begining w/ sky_dist
rm -f $fol/sky_dist_*
count=1

#Tokyo
# -a 35.68 -o -139.78 -m -135
#Stockholm
#-a 59.35 -o -18.07 -m -15
#Austin
# -a 30.25 -o 97.75 -m 90
#Boston
```

```
# -a 42.35 -o 71.07 -m 75

while read M D H DN DH; do
if [[ $count -ge 9 && $count -le 19 && $DH -gt 1000 ]]; then
                  echo -e "$M\t$D\t$H"
            #-W for irradiance -L for illuminance
            gendaylit $M $D $H -L $DN $DH -a 59.35 -o -18.07 -m -15 |
genskyvec -m $divisions \
                  -c 1 1 1 | rcalc -e '$1=$1*0.265+$2*0.67+$3*0.065' >
tmp/sky_tmp.dat
                  #^combines rgb into 1 weighted average
            #writes timesteps headers that are valid to file
            if [[ -s tmp/sky_tmp.dat ]]; then
                  echo -e "$M\t$D\t$H\t$DN\t$DH" >>
$fol/sky_dist_tokyo_timestep.dat
                  #formats output to 3 decimal places
                  while read line; do
                        printf "%.3f\n" $line |tr '\n' '\t' >>
$fol/sky_dist_ann.dat

                  done < "tmp/sky_tmp.dat"

      fi
 # Append a line break
            echo >> $fol/sky_dist_ann.dat
      fi

#setting time of day
count=$count+1
if [[ $count -ge 25 ]]; then
      count=1
fi

#change to data source
done < tokyo_lux.dat

#eliminate blank lines
sed '/^$/d' $fol/sky_dist_ann.dat > $fol/$output

#check for empty files
ls ~/Desktop/thesis/$fol | while read file; do
if [[ ! -s $file ]]; then
    echo "$file is empty" > $fol/empty_files.dat
fi
done
```

# Appendix C: Additional MIT Mockup Test Results

Additional mockup test results are provided here, based on an early version of the design which did not include the refractive rods. The preliminary results revealed that the ceiling was excessively bright under direct sunlight, which prompted the subsequent inclusion of the refractive rods as a glare control measure.

The initial mockup was tested near MIT's campus in Cambridge under clear sunny conditions at two different times: 8/7/10 between 10:25am and 11:00am Eastern Daylight Time (EDT) (referred to as Day 1) and 8/11/10 between 5:20pm and 5:30pm EDT (referred to as Day 2). The mockup was repositioned throughout testing so that the window unit directly faced the sun at all times, ensuring that the maximum brightness of the system was being evaluated. For Day 1, the sun's elevation angle was about 55° and for Day 2 it was about 25°. Although 25° is below the cut-off angle of 27.8°, a check of the mockup during testing showed that direct sunlight was not yet being rejected by the louvers. Therefore, the actual angle between sun and louver was still greater than 27°, which is understandable because of the uncertainty in the alignment of the mockup with respect to horizontal. Luminance measurements of the mockup were recorded using both a luminance meter as well as High Dynamic Range (HDR) imaging. The luminance meter used was a Minolta LS110 and the camera used for HDR imaging was a Canon EOS-20D.

Although luminance meter readings tend to be more accurate, HDR images provide several advantages. HDR images can be used to produce luminance maps that show the luminance of every pixel in the picture, whereas the luminance meter gives only spot readings of a small area. Also, the equipment required to produce HDR images is more easily attained, as a standard DSLR camera can be used, rather than a more expensive luminance meter. HDR images are created by taking several images of the same scene at different exposure levels. The images are then combined into a single image using a computer program such as hdrgen.

One important limitation was found by comparing the results of the HDR images to the direct luminance readings. With the camera's f-number set to 5.6 and the shortest possible exposure setting of 1/8000 seconds, the brightest points on the ceiling were still overexposed. As a result, the HDR images were not able to resolve the highest peaks in luminance. It may be possible to fix this problem during future testing by adjusting the f-number or by using a camera with a faster shutter speed.

## C.1 Results for Direct Sun

Figures C.1 through C.3 show the system's appearance and brightness under direct sun at increasing distances from the window unit. The increasing distance from which the photos were taken corresponds to the view from deeper and deeper into a real office space. As mentioned in the previous section, the luminance maps do not accurately display the peak luminance of the system. For this reason, the peak luminance, as measured by the luminance meter, is shown underneath each figure.


(a) 6' (1.83 m) from Facade, Peak Luminance: 300,000 cd/m²


(b) 12' (3.66 m) from Facade, Peak Luminance: 260,000 cd/m²

Figure C.1: Luminance Maps (Left) and HDR Images (Right) at Increasing Distance to the Facade on Day 1


(a) 18' (5.49 m) from Facade, Peak Luminance: 270,000 cd/m²


(b) 24' (7.32 m) from Facade, Peak Luminance: 220,000 cd/m²

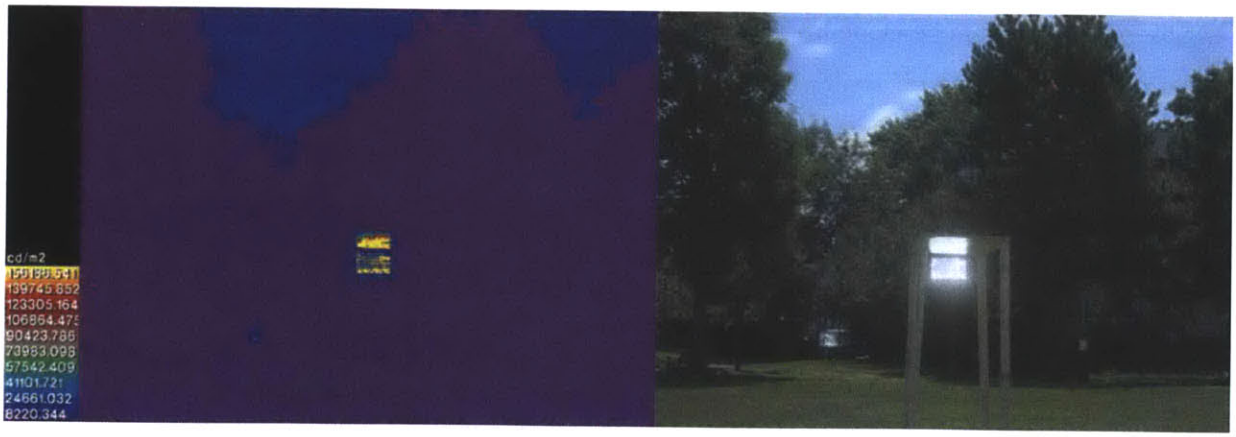


(c) 36' (10.98 m) from Facade, Peak Luminance: 150,000 cd/m²

Figure C.2: Luminance Maps (Left) and HDR Images (Right) at Increasing Distance to the Facade on Day 1

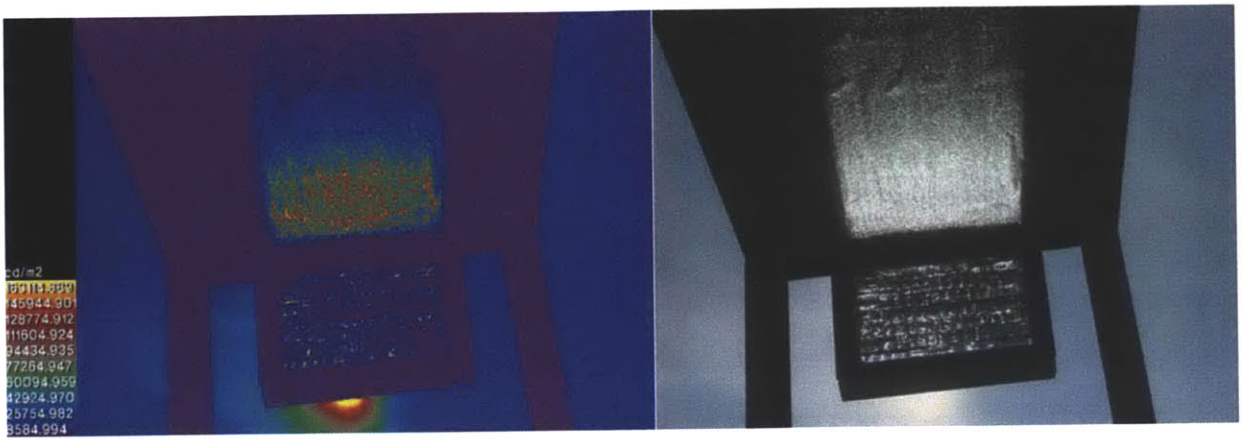


(a) 6' (1.83 m) from Facade, Peak Luminance: 300,000 cd/m²

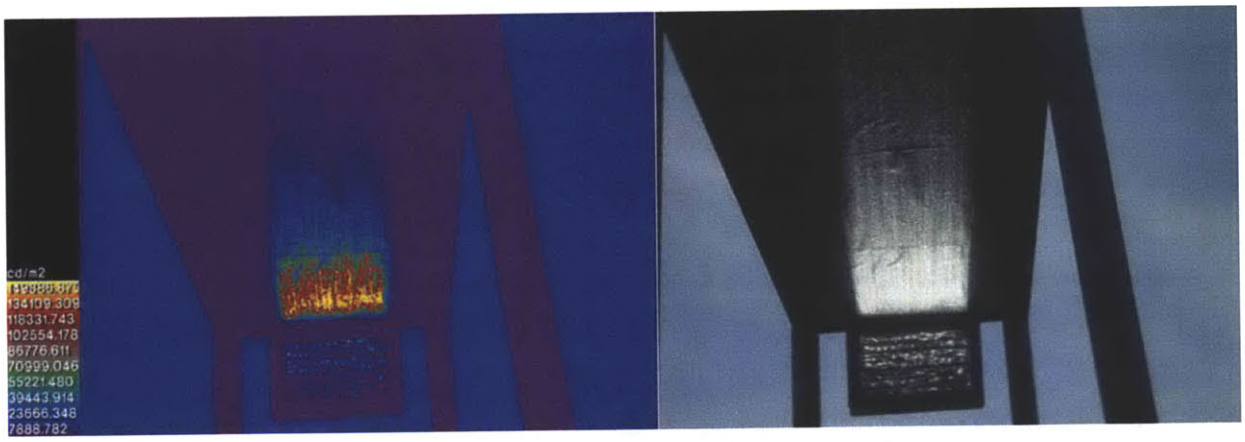


(b) 12' (3.66 m) from Facade, Peak Luminance: 300,000 cd/m²

Figure C.3: Luminance Maps (Left) and HDR Images (Right) at Increasing Distance to the Facade on Day 2

An observation that can be made from viewing these images is that the prototype louvers allowed some light to exit at a downward angle. This effect is especially apparent in the images taken at a greater distance from the facade, beginning with Figure 6.2(a). Rays would have to leave the louver at a downward angle of about 5° to reach this location.

The existence of these downward traveling rays was attributed to two manufacturing issues. First, the 3D printer was unable to produce the sharp edges found at either end of the louver profile. As a result, the location of the louvers with respect to one another was slightly off. Second, it was very difficult to make the reflective film material lay completely flat on the louver profile. Slight ripples in the film inevitably formed when it was attached to the louver via double-sided tape.

## C.2 Results at an Angle to Direct Sun

As part of the testing completed on Day 1, the mockup was imaged at an angle to the direct sun rays to determine how wide the brightest area on the ceiling would be in the full scale version (without the refracted rods included in the design). The results showed that the peak brightness fell very quickly as the camera or luminance meter was moved laterally with respect to the facade (see Figure C.4).

These results show that under sunny conditions, the ceiling's peak brightness associated with the direct sun rays will drop quickly in the direction parallel to the facade. This effect will limit the overall size of the bright patch which is desirable from a glare standpoint.

## C.3 Results for Clear Sky with No Direct Sun

On Day 2, the mockup was tested to gain an understanding of the system's brightness under clear skies without exposure to direct sun (see Figure C.5). The mockup was oriented so that no direct sun impinged on the louver unit. The results confirmed the expectation that the brightness of the system would be much lower without direct sunlight. Because the maximum brightness level was much lower, readings from the luminance meter were not needed.

## C.4 Individual Louver Channel Contributions

The physical mockup provided one more important insight into how the louver array functions. Figure C.6 shows how each channel contributes to the overall light pattern on the ceiling. The images were created by covering all the louver channels with an opaque material and then uncovering them one-by-one, until all the channels were uncovered. These images are not HDR images. Instead they are single exposure images taken with the fastest possible shutter speed (1/8000 sec). Because the exposure was so short, the level of contrast seen between the bright and dim spaces is much higher than perceived by a human eye. The images are intended to illustrate the pattern of light on the ceiling only. The channels are numbered from one (closest to the ceiling) to seven (furthest from the ceiling). These images show that the different louver channels tend to light up different parts of the ceiling, although there is some overlap.


(a) 12' (3.66 m) from Facade, 1' (.30 m) from Centerline, Peak Luminance on Ceiling Centerline: 30,000 cd/m²


(b) 12' (3.66 m) from Facade, 2' (.61 m) from Centerline, Peak Luminance on Ceiling Centerline: 14,000 cd/m²


(c) Day 1, 12' (3.66 m) from Facade, 3' (.91 m) from Centerline, Peak Luminance on Ceiling Centerline: 6,000 cd/m²

Figure C.4: Luminance Maps (Left) and HDR Images (Right) at Increasing Distance from the Facade Centerline on Day 2

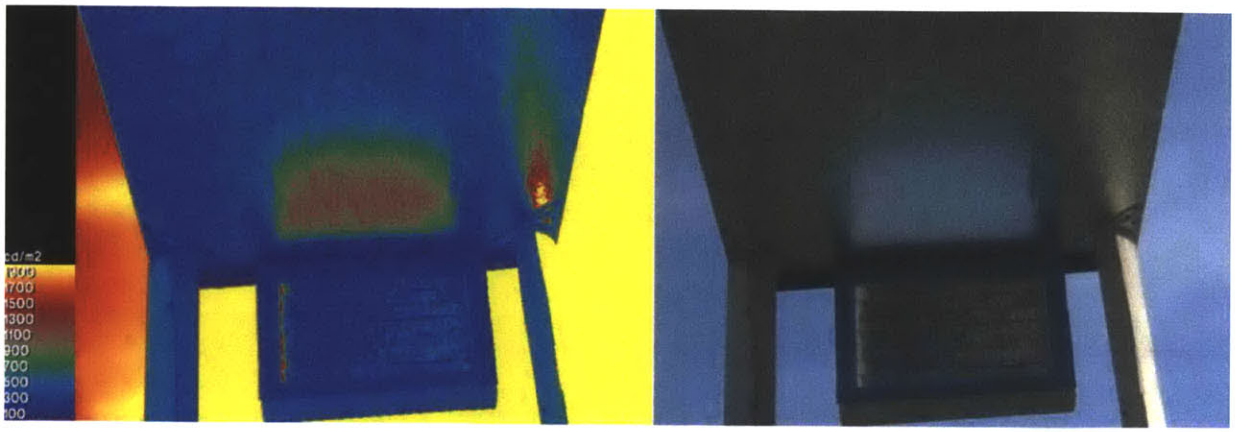

(a) 6' (1.83 m) from Facade

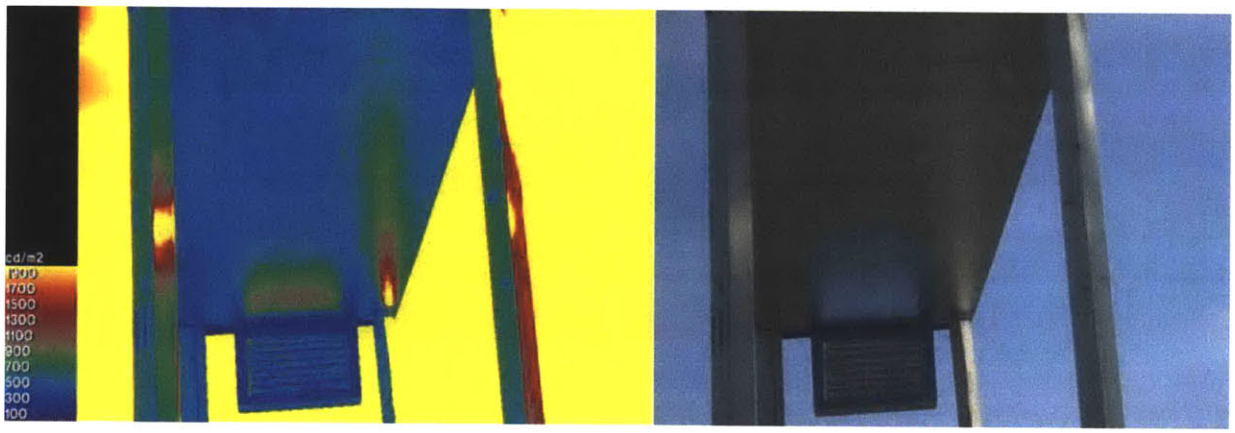

(b) 12' (3.66 m) from Facade

Figure C.5: Luminance Maps (Left) and HDR Images (Right) at Increasing Distance to the Facade on Day 2 Without Direct Sunlight

Based on the results in this appendix, it was determined that the ceiling's luminance under direct sun was too high for an office setting. As discussed in Section 6.1.2, the refractive rods were included in the design to address this problem. The rods reduced the peak ceiling luminance by an order of magnitude from about 350,000 cd/m$^2$ to about 35,000 cd/m$^2$.

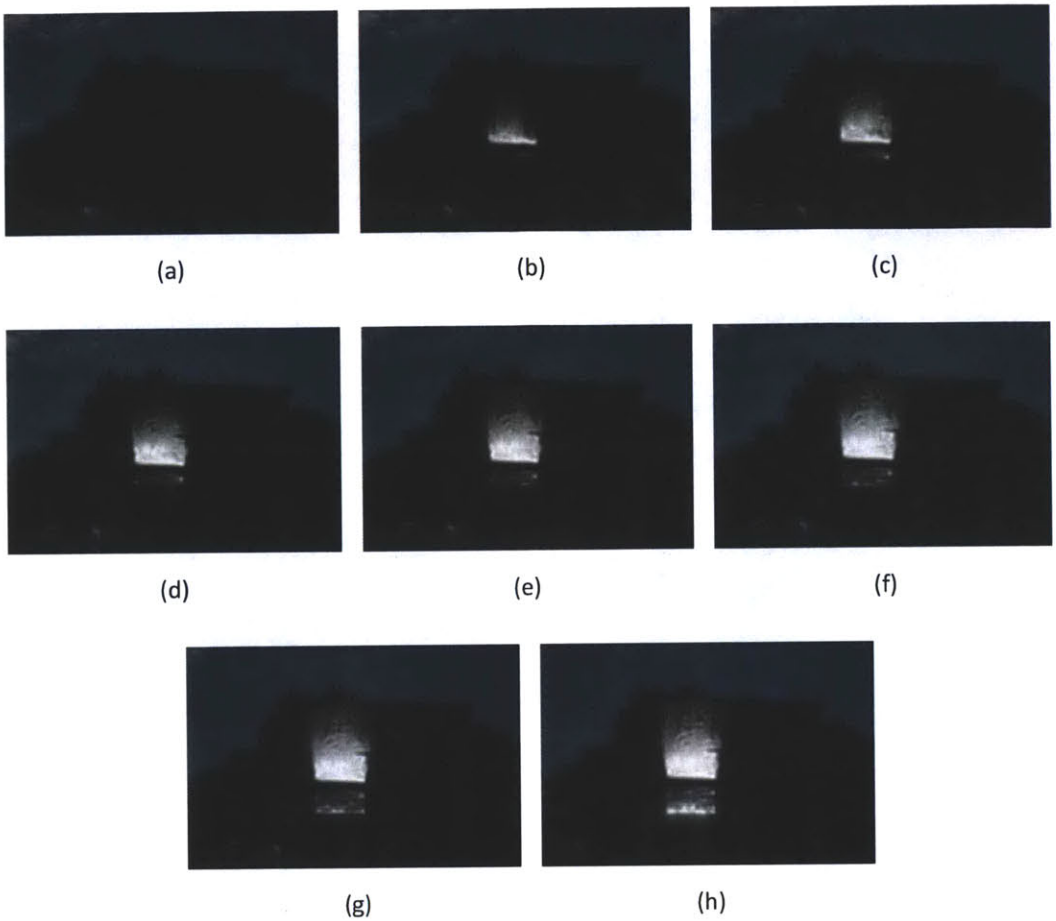


Figure C.6: Day 1, 12' (3.66 m) from Facade, with No (a), 1 (b), 2 (c), 3 (d), 4 (e), 5 (f), 6 (g), and 7 (h) Channels Exposed

# Appendix D: Tokyo Mockup Time Step Results

The full data set of measured and simulated results for the Tokyo mockup are provided below in Tables D.1 through D.3. The shading of each row indicates information about the sky condition for that time step. Light shading corresponds to sunny skies, while dark shading refers to overcast skies. Blue coloring indicates that the time step was before 11:30am, red coloring indicates times after 11:30am. The time of 11:30am was chosen to break the test day into two roughly equal halves.

Table D.3 shows the average baseline illuminance measured with all the curtains closed for each day. All exterior light, including light from the Soralux system, was blocked out. The values are an average of two measurements, taken at the beginning and ending of each test day (February 22 is an exception, with three measurements). These values were subtracted from the raw illuminance data to obtain the contribution from the daylighting system reported in Table D.2.

Table D.1: Full Sky Measurement Data Set from Tokyo Mockup

| Time Step | Month | Day | Hour | Dir Norm Illum (Lux) | Diff Horiz Illum (Lux) |
|---|---|---|---|---|---|
| 1 | 2 | 22 | 10.383 | 78300 | 21900 |
| 2 | 2 | 22 | 11.317 | 77000 | 24200 |
| 3 | 2 | 22 | 11.800 | 77700 | 22600 |
| 4 | 2 | 22 | 12.633 | 80800 | 22800 |
| 5 | 2 | 22 | 13.050 | 84100 | 21600 |
| 6 | 2 | 22 | 13.850 | 79800 | 20100 |
| 7 | 2 | 22 | 14.283 | 70600 | 19800 |
| 8 | 2 | 23 | 9.267 | 70300 | 18100 |
| 9 | 2 | 23 | 9.900 | 75900 | 20000 |
| 10 | 2 | 23 | 11.217 | 78400 | 23500 |
| 11 | 2 | 23 | 11.983 | 74600 | 25200 |
| 12 | 2 | 23 | 12.600 | 84400 | 21600 |
| 13 | 2 | 23 | 13.783 | 84100 | 18700 |
| 14 | 2 | 23 | 14.367 | 73700 | 17700 |
| 15 | 2 | 24 | 11.150 | 0 | 27500 |
| 16 | 2 | 24 | 11.675 | 0 | 31400 |
| 17 | 2 | 24 | 13.725 | 0 | 26300 |
| 18 | 2 | 25 | 9.208 | 65300 | 18700 |
| 19 | 2 | 25 | 9.892 | 88200 | 18500 |
| 20 | 2 | 25 | 10.500 | 90900 | 17000 |
| 21 | 2 | 25 | 11.317 | 93200 | 17600 |
| 22 | 2 | 25 | 11.950 | 93700 | 18900 |
| 23 | 2 | 25 | 13.425 | 73000 | 24000 |
| 24 | 2 | 25 | 14.000 | 68000 | 25800 |
| 25 | 2 | 28 | 11.025 | 0 | 9200 |
| 26 | 2 | 28 | 11.763 | 0 | 7000 |
| 27 | 3 | 1 | 9.125 | 0 | 14900 |
| 28 | 3 | 1 | 9.583 | 0 | 28200 |
| 29 | 3 | 2 | 9.117 | 0 | 30100 |
| 30 | 3 | 3 | 9.233 | 90600 | 17100 |
| 31 | 3 | 3 | 9.933 | 94900 | 14000 |
| 32 | 3 | 3 | 11.018 | 99000 | 14500 |
| 33 | 3 | 3 | 11.704 | 99300 | 15100 |
| 34 | 3 | 3 | 12.729 | 96200 | 19800 |
| 35 | 3 | 3 | 13.883 | 91100 | 20800 |

Table D.2: Full Measured and Simulated Data Set for Tokyo Mockup

| | Distance from Facade (m), Measured | | | | | | | | | Distance from Facade (m), Simulated | | | | | | | |
|---|---|---|---|---|---|---|---|---|---|---|---|---|---|---|---|---|---|
| Time Step | 1 | 2 | 3 | 4 | 5 | 6 | 7 | 8 | | 1 | 2 | 3 | 4 | 5 | 6 | 7 | 8 |
| 1 | 453 | 413 | 190 | 193 | 157 | 117 | 103 | 80 | | 335 | 349 | 262 | 245 | 207 | 165 | 126 | 83 |
| 2 | 703 | 723 | 500 | 373 | 297 | 227 | 193 | 140 | | 485 | 568 | 476 | 405 | 329 | 263 | 210 | 135 |
| 3 | 833 | 913 | 640 | 473 | 367 | 287 | 253 | 170 | | 597 | 726 | 633 | 512 | 420 | 340 | 275 | 176 |
| 4 | 1133 | 1293 | 930 | 683 | 537 | 417 | 353 | 250 | | 881 | 1125 | 993 | 759 | 650 | 572 | 430 | 294 |
| 5 | 1323 | 1543 | 1080 | 783 | 627 | 477 | 403 | 280 | | 1018 | 1354 | 1141 | 874 | 737 | 635 | 485 | 327 |
| 6 | 1453 | 1703 | 1120 | 773 | 617 | 487 | 413 | 280 | | 1081 | 1489 | 1121 | 853 | 726 | 615 | 479 | 332 |
| 7 | 1353 | 1583 | 1000 | 683 | 547 | 427 | 353 | 240 | | 1053 | 1476 | 1070 | 784 | 679 | 579 | 450 | 298 |
| 8 | 130 | 135 | 95 | 75 | 65 | 55 | 45 | 45 | | 113 | 120 | 84 | 64 | 57 | 48 | 36 | 25 |
| 9 | 250 | 245 | 165 | 135 | 115 | 95 | 85 | 55 | | 240 | 240 | 173 | 162 | 140 | 112 | 86 | 56 |
| 10 | 650 | 685 | 475 | 375 | 295 | 235 | 195 | 135 | | 479 | 555 | 461 | 396 | 322 | 256 | 203 | 132 |
| 11 | 850 | 955 | 665 | 525 | 405 | 315 | 255 | 195 | | 659 | 819 | 722 | 569 | 474 | 394 | 312 | 203 |
| 12 | 1130 | 1305 | 925 | 715 | 565 | 435 | 345 | 255 | | 906 | 1155 | 1018 | 780 | 667 | 586 | 442 | 302 |
| 13 | 1480 | 1735 | 1145 | 855 | 675 | 525 | 425 | 295 | | 1115 | 1531 | 1157 | 882 | 750 | 637 | 498 | 345 |
| 14 | 1410 | 1645 | 1025 | 745 | 575 | 435 | 345 | 225 | | 1084 | 1517 | 1099 | 803 | 697 | 596 | 463 | 306 |
| 15 | 80 | 85 | 50 | 30 | 30 | 15 | 10 | 10 | | 86 | 115 | 86 | 64 | 53 | 44 | 34 | 22 |
| 16 | 140 | 155 | 100 | 70 | 50 | 45 | 30 | 20 | | 103 | 138 | 104 | 77 | 64 | 53 | 41 | 27 |
| 17 | 70 | 85 | 50 | 40 | 20 | 15 | 10 | 10 | | 92 | 126 | 94 | 69 | 57 | 47 | 36 | 24 |
| 18 | 105 | 115 | 65 | 35 | 40 | 30 | 35 | 35 | | 105 | 114 | 80 | 61 | 54 | 45 | 34 | 23 |
| 19 | 235 | 225 | 145 | 105 | 100 | 90 | 75 | 65 | | 174 | 183 | 131 | 115 | 101 | 81 | 63 | 41 |
| 20 | 415 | 405 | 275 | 195 | 180 | 140 | 115 | 95 | | 346 | 357 | 269 | 255 | 217 | 172 | 131 | 86 |
| 21 | 675 | 715 | 495 | 365 | 300 | 240 | 185 | 145 | | 527 | 609 | 514 | 443 | 360 | 287 | 231 | 148 |
| 22 | 895 | 1005 | 715 | 525 | 430 | 340 | 275 | 215 | | 749 | 924 | 824 | 653 | 544 | 453 | 359 | 234 |
| 23 | 1215 | 1475 | 1015 | 745 | 620 | 480 | 375 | 275 | | 978 | 1310 | 1045 | 802 | 679 | 579 | 447 | 309 |
| 24 | 1275 | 1505 | 995 | 705 | 590 | 460 | 355 | 255 | | 965 | 1312 | 977 | 730 | 626 | 548 | 436 | 290 |
| 25 | 30 | 30 | 25 | 25 | 20 | 15 | 10 | 10 | | 26 | 35 | 26 | 19 | 16 | 13 | 10 | 7 |
| 26 | 20 | 20 | 15 | 15 | 10 | 15 | 0 | 0 | | 20 | 26 | 19 | 14 | 12 | 10 | 8 | 5 |
| 27 | 20 | 40 | 30 | 20 | 20 | 10 | 10 | -10 | | 43 | 57 | 43 | 31 | 26 | 21 | 17 | 11 |
| 28 | 80 | 110 | 70 | 50 | 40 | 30 | 10 | 0 | | 83 | 110 | 83 | 62 | 52 | 42 | 33 | 22 |
| 29 | 75 | 95 | 65 | 45 | 25 | 20 | 25 | 15 | | 86 | 114 | 85 | 64 | 53 | 44 | 34 | 22 |
| 30 | 70 | 80 | 50 | 0* | 35 | 25 | 25 | 5 | | 109 | 116 | 80 | 61 | 55 | 46 | 35 | 24 |
| 31 | 190 | 190 | 120 | 0* | 95 | 65 | 55 | 35 | | 161 | 166 | 118 | 106 | 95 | 75 | 58 | 38 |
| 32 | 510 | 520 | 340 | 0* | 235 | 165 | 135 | 95 | | 396 | 436 | 350 | 324 | 263 | 209 | 165 | 106 |
| 33 | 750 | 830 | 570 | 0* | 365 | 265 | 215 | 155 | | 624 | 745 | 653 | 536 | 439 | 353 | 285 | 184 |
| 34 | 1110 | 1310 | 900 | 0* | 585 | 445 | 365 | 255 | | 959 | 1241 | 1067 | 813 | 687 | 602 | 460 | 311 |
| 35 | 1370 | 1610 | 1050 | 0* | 665 | 505 | 405 | 285 | | 1161 | 1563 | 1171 | 884 | 759 | 671 | 538 | 359 |

*Measurements for sensor 4 on 3/3 were accidently overwritten and lost

Table D.3: Baseline Illuminance Readings for Each Day

| | Distance from Facade | | | | | | | |
|---|---|---|---|---|---|---|---|---|
| **Day** | **1** | **2** | **3** | **4** | **5** | **6** | **7** | **8** |
| 22-Feb | 207 | 367 | 700 | 967 | 973 | 793 | 897 | 820 |
| 23-Feb | 200 | 355 | 705 | 975 | 975 | 785 | 885 | 815 |
| 24-Feb | 200 | 365 | 700 | 990 | 970 | 785 | 880 | 800 |
| 25-Feb | 205 | 355 | 685 | 955 | 940 | 770 | 865 | 805 |
| 28-Feb | 200 | 370 | 715 | 1045 | 950 | 775 | 880 | 810 |
| 1-Mar | 210 | 370 | 710 | 1050 | 970 | 790 | 880 | 840 |
| 2-Mar | 205 | 375 | 715 | 1055 | 975 | 790 | 875 | 815 |
| 3-Mar | 210 | 370 | 720 | 1060 | 965 | 785 | 875 | 825 |

# Bibliography


Aizlewood, M.E., 1993. Innovative Daylighting Systems: An Experimental Evaluation. *Lighting Research and Technology*, 25(4), pp.141-52.

Ander, G.D., 2003. *Daylighting Performance and Design*. Hoboken: John Wiley & Sons, Inc.

Bartenbach, C., Moeller, M. & Lanzenberger, R., 1987. *Arrangement for Illuminating a Room with Daylight*. US Patent 4,699,467.

Bodart, M. & De Herde, A., 2002. Global Energy Savings on Offices [sic] Buildings by the Use of Daylighting. *Energy and Buildings*, 34(5), pp.421-29.

Butti, K. & Perlin, J., 1980. *A Golden Thread: 2500 Years of Solar Architecture and Technology*. Palo Alto: Van Nostrand Reinhold Company.

Compagnon, R., 1994. *Simulations Numeriques de Systemes D'Eclairage Naturel a Penetration Laterale*. PhD Thesis. Lausanne: Ecole Polytechnique Federale de Lausanne.

Courret, G., Paule, B. & Scartezzini, J.-L., 1994. Application de l'Optique Anidolique a l'Eclairage Naturel Lateral d'un Nouveau Baitment. In *Wärmeschutz Conference*. Zurich, 1994.

Courret, G., Scartezzini, J.-L., Francioli, D. & Meyer, J.-J., 1998. Design and Assessment of an Anidolic Light-Duct. *Energy and Buildings*, 28, pp.79-99.

Dave, S. & Andersen, M., 2011. A Comprehensive Method to Determine Performance Metrics for Complex Fenestration Systems. In Bodart, M. & Arnaud, E., eds. *International Conference on Passive and Low Energy Architecture*. Louvain-la-Neuve, 2011.

Eames, P. & Norton, B., 1994. A Window Blind Reflector System for the Deeper Penetration of Daylight into Room Without Glare. *International Journal of Ambient Energy*, 15(2), pp.73-77.

Edmonds, I., 1993. Performance of Laser Cut Light Deflecting Panels in Daylighting Applications. *Solar Energy Materials and Solar Cells*, 29, pp.1-26.

Edmonds, I., 2005. Daylighting High-Density Residential Buildings with Light Redirecting Panels. *Lighting Research and Technology*, 37(1), pp.73-87.

Edwards, L. & Torcellini, P., 2002. *A Literature Review of the Effects of Natural Light on Building Occupants*. Technical Report. Golden: National Renewable Energy Laboratory.

Ekirch, A.R., 2005. *At Day's Close: Night in Times Past*. New York: W. W. Norton & Company.

Greenup, P.J. & Edmonds, I.R., 2003. Test Room Measurements and Computer Simulations of the Micro-Light Guiding Shade Daylight Redirecting Device. *Solar Energy*, 76, pp.99-109.

Heschong, L., Wright, R.L. & Okura, S., 2002. Daylighting Impacts on Human Performance in School. *Journal of the Illuminating Engineering Society*, Summer, pp.101-14.

Ihm, P., Nemri, A. & Krarti, M., 2009. Estimation of Lighting Energy Savings from Daylighting. *Building and Environment*, 44, pp.509-14.

Jacobs, A., 2008. *Basic Radiance Tutorial.* London: London Metropolitan University.

Jacobs, A., 2010. *rtcontrib Lesson*. [Online] Available at: http://www.jaloxa.eu/resources/radiance/documentation/index.shtml [Accessed 25 February 2010].

Kalpakjian, S. & Schmid, S., 2001. *Manufacturing Engineering and Technology*. 4th ed. Upper Saddle River: Prentice-Hall, Inc.

Köster Lichtplanung, n.d. *Highly efficient sun-protection louvres*. [Online] Available at: http://www.detail.de/artikel_koester-lichtplanung-sun-protection-louvres_23759_En.htm [Accessed 8 April 2011].

Kristensen, P., 1991. Efficient Use of Daylight in Commercial Buildings. In *Right Light 1*. Stockholm, 1991. International Association for Energy-Efficient Lighting.

Laar, M. & Grimme, F.W., 2002. German Developments in Daylight Guidance Systems: An Overview. *Building Research & Information*, 30(4), pp.282-301.

Lambert, G.W. et al., 2002. Effect of Sunlight and Season on Serotonin Turnover in the Brain. *Lancet*, 360, pp.1840-42.

LightLouver, 2010. *Slat Ray Tracing Diagram*. [Online] Available at: http://lightlouver.com/performance-information/slat-ray-tracing-diagram/ [Accessed 9 April 2011].

Littlefair, P.J., Aizlewood, M.E. & Birtles, A.B., 1994. The Performance of Innovative Daylighting Systems. *Renewable Energy*, 5(2), pp.920-34.

Lorenz, W., 2001. A Glazing Unit for Solar Control, Daylighting and Energy Conservation. *Solar Energy*, 70(2), pp.109-30.

Mardaljevic, J., 1995. Validation of a Lighting Simulation Program Under Real Sky Conditions. *Lighting Research and Technology*, 27(4), pp.181-88.

Mardaljevic, J., 2000. Simulation of Annual Daylighting Profiles for Internal Illuminance. *Lighting Research and Technology*, 32(3), pp.111-18.

Mardaljevic, J., Heschong, L. & Lee, E., 2009. Daylighting Metrics and Energy Savings. *Lighting Research and Technology*, 41, pp.261-83.

Markus, T.A., 1967. The Significance of Sunshine and View for Office Workers. In *Sunlight in Buildings*. Rotterdam: Boewcentrum International.

Maunder, R., n.d. *Lighting Design Toolkit*. [Online] Available at: http://www.vuw.ac.nz/architecture-onlineteaching/toolkit/tutorials/7redirecta.html [Accessed 9 April 2011].

MIT OpenCourseWare, 2004. *Types of Reflection*. [Online] Available at: http://www.flickr.com/photos/mitopencourseware/4815499473/in/set-72157624551994570/ [Accessed 5 March 2011].

National Research Council Canada, 2010. *Cost-effective Open-Plan Environments (COPE) Project*. [Online] Available at: http://www.nrc-cnrc.gc.ca/eng/projects/irc/cope.html [Accessed 9 April 2011].

Perez, R., Seals, R. & Michalsky, J., 1993. All-Weather Model for Sky Luminance Distribution - Preliminary Configuration and Validation. *Solar Energy*, 50(3), pp.235-45.

Rashid, M. & Zimring, C., 2008. A Review of the Empirical Literature on the Relationships Between Indoor Environment and Stress in Health Care and Office Settings: Problems and Prospects of Sharing Evidence. *Environment and Behavior*, 40(2), pp.151-90.

Rea, M.S., 1984. Window Blind Occlusion: A Pilot Study. *Building & Environment*, 19(2), pp.133-37.

Rea, M.S., Figueiro, M.G. & Bullough, J.D., 2002. Circadian Photobiology: An Emerging Framework for Lighting Practice and Research. *Lighting Research and Technology*, 34(3), pp.177-90.

Reinhart, C.F., 2005. A Simulation-Based Review of the Ubiquitous Window-Head-Height to Daylight Zone Depth Rule-of-Thumb. In *Buildings Simulation*. Montreal, 2005.

Reinhart, C.F. & Herkel, S., 2000. The Simulation of Annual Daylight Illuminance Distributions - A State-of-the-Art Comparison of Six RADIANCE-Based Methods. *Energy and Buildings*, 32, pp.167-87.

Reinhart, C.F., Mardaljevic, J. & Rogers, Z., 2006. Dynamic Daylight Performance Metrics for Sustainable Building Design. *Leukos*, 3(1), pp.7-31.

Reinhart, C.F. & Voss, K., 2003. Monitoring Manual Control of Electric Lighting and Blinds. *Lighting Research & Technology*, 35(3), pp.243-60.

Rogers, Z.L., Holtz, M.J., Clevenger, C.M. & Digert, N.E., 2004. *Mini-Optical Light Shelf Daylighting System*. US Patent 6,714,352.

Ruck, N. et al., 2000. *Daylight in Buildings: A Source Book on Daylighting Systems and Components*. Berkeley: Lawrence Berkeley National Laboratory.

Scartezzini, J.-L., 2010. *Anidolic systems: Non-imaging transmission of daylight into darker parts of buildings*. [Online] Available at: http://leso.epfl.ch/page-35535-en.html [Accessed 14 July 2010].

Scartezzini, J.-L. & Courret, G., 2002. Anidolic Daylighting Systems. *Solar Energy*, 73(2), pp.123-35.

Scartezzini, J.-L. & Courret, G., 2004. Experimental Performance of Daylighting Systems Based on Non-Imaging Optics. In Winston, R., ed. *Nonimaging Optics: Maximum Efficiency Light Transfer VII*. Bellingham, 2004. Society of Professional Illumination Engineers.

Schregle, R., 2004. *Daylight Simulation with Photon Maps*. PhD Thesis. Saarbrücken: Universität des Saarlandes.

Solar Radiation Montoring Laboratory, U.o.O., 2008. *Polar sun path chart program*. [Online] Available at: http://solardat.uoregon.edu/PolarSunChartProgram.html [Accessed 8 April 2011].

Talman, C.F. & Keally, F., 1930. Now the Windowless Building with Its Own Climate. *The New York Times*, 10 August.

Tequipment, 2011. *Hioki 3640-20 Lux Logger*. [Online] Available at: http://www.tequipment.net/Hioki3640-20.html [Accessed 8 January 2011].

Thuot, K. & Andersen, M., 2011. A Novel Louver System for Increasing Daylight Usage in Buildings. In Bodart, M. & Arnaud, E., eds. *International Conference on Passive and Low Energy Architecture*. Louvain-la-Neuve, 2011.

Tregenza, P. & Waters, I., 1983. Daylight Coefficients. *Lighting Research and Technology*, 15(2), pp.65-71.

U.S. Department of Energy, 2009. *2008 Commercial Energy End-Use Expenditure Splits, by Fuel Type*. [Online] Available at: http://buildingsdatabook.eren.doe.gov/TableView.aspx?table=3.3.4 [Accessed 2 April 2011].

U.S. Department of Energy, 2010. *Weather Data*. [Online] Available at: http://apps1.eere.energy.gov/buildings/energyplus/cfm/weather_data.cfm [Accessed 2 February 2010].

Ward Larson, G. & Shakespeare, R., 1997. *Rendering with Radiance: The Art and Science of Lighting Visualization*. San Francisco: Morgan Kaufmann Publishers.

Wienold, J. & Christoffersen, J., 2006. Evaluation Methods and Development of a New Glare Prediction Model for Daylight Environments with the Use of CCD Cameras. *Energy and Buildings*, 38, pp.743-57.

Winston, R., Minano, J.C. & Benitez, P., 2005. *Nonimaging Optics*. Burlington: Elsevier Academic Press.